SLIPLINE FIELD ANALYSIS OF DEFORMATION IN METAL MACHINING WITH WORN TOOL WITH ADHESION FRICTION IN CONTACT REGIONS

A THESIS SUBMITTED TO

NATIONAL INSTITUTE OF TECHNOLOGY, ROURKELA
(Deemed University)

FOR THE DEGREE OF

DOCTOR OF PHILOSOPHY

IN

MECHANICAL ENGINEERING

BY

SURESH TOTAPPA DUNDUR

(University Registration No. 7/2001/ Mech. Engg., Ph.D.)

DEPARTMENT OF MECHANICAL ENGINEERING
NATIONAL INSTITUTE OF TECHNOLOGY, ROURKELA

APRIL 2005

Dedicated to
all my Teachers...

CERTIFICATE

This is to certify that the thesis titled "Slipline Field Analysis of Deformation in Metal Machining with Worn Tool with Adhesion Friction in Contact Regions" being submitted by Mr. Suresh Totappa Dundur to the National Institute of Technology, Rourkela for the award of the degree of DOCTOR OF PHILOSOPHY is a record of bonafide research carried out by him under my guidance and supervision.

Mr. Dundur has worked for more than five years on the above problem and the work has reached the standard fulfilling the requirements and the regulations relating to the degree. To the best of my knowledge the work incorporated in this thesis has not been submitted to any other University or Institute for the award of any other degree or diploma.

Date:

Dr. N. S. Das
Professor Emeritus
Mechanical Engineering Department
National Institute of Technology
Rourkela 769008
India

ACKNOWLEDGEMENT

The author expresses his deep sense of gratitude and heartfelt regards to his supervisor Professor N S Das for his invaluable help and guidance throughout the entire course of this work.

He is extremely grateful to Dr. S C Haldar and Mr. Alok Satpathy who were always eager to extend all help to him and shall remain ever grateful to them for their good company during these years.

He thanks Prof. N. Kavi, present Head of the Department and Q. I. P. Coordinator and former Heads and Q. I. P. Coordinators Prof. A. K. Behera and Prof. P. K. Kar, of Mechanical Engineering Department for providing facilities for smooth conduct of this work.

The author would also like to thank Prof. Sunil Kumar Sarangi, former Director, NIT Rourkela and A. K. Mohanty, former Principal, R E C, Rourkela for creating good working environment at NIT campus and for the timely help he received from them.

He remains obliged to Prof. K. R. Patel, Dr. S. K. Acharya, Dr. C. K. Biswas, Dr. K. P. Maity, Mr. N. P. Barik and all other staff members of the Mechanical Engineering Department for their useful suggestions and for the help rendered to him in carrying out this work.

He is immensely grateful to Dr. U. K. Mohanty, former Head, Central Workshop and his staff for their encouragement and support in conducting the metal cutting experiments.

The author is also indebted to Dr. S. Adak, and Dr. J. Bera, of the Department of Ceramic Engineering for the cooperation and help extended to him during the time of experimentation.

He will carry in his memory the company of Mr. B. S. Chawla, Mr. Naresh Prasad and Mr. S. D. Patle, all Q I P Research Scholars at NIT Rourkela and all “brothers” in the same “boat”.

Thanks are also due to his colleagues in the Department of Industrial and Production Engineering, Basaveshwar Engineering College, Bagalkot for their whole hearted support and cooperation during the course of this work.

He is extremely grateful to his wife Vijaya, daughter Aishwarya and son Kushal for their sacrifice, endless inspiration and patience without which this work would not have been completed.

Finally, the author wishes to acknowledge the financial support given to him by the Ministry of Human Resources Development, Government of India during his tenure of stay at National Institute of Technology, Rourkela and the leave of absence granted to him by the Management of Basaveshwar Engineering College, Bagalkot to carry out this research work at N. I. T. Rourkela.

(Suresh T. Dundur)

ABSTRACT

The subject of friction is important in all engineering applications wherever solid surfaces are in sliding contact with each other. This is particularly true in metal working processes where the sliding pair of surfaces are metals and where plastic deformation of the softer of the two metals usually takes place under conditions of high normal pressure. In orthogonal metal cutting processes frictional drag apparently is encountered on the rake face between chip and tool and as the tool wears, additional frictional drag also occurs between flank of the tool and the work piece. Friction at these contact regions affects the chip formation process, power consumption, metal removal rate, quality of machined surface and active life of the cutting tools.

Although, friction in cutting is of interest for fundamental studies of wear and chemical reaction, under conditions of high temperature and high pressure, there seems to be a lack of agreement as to how to represent this interface friction characteristics in steady state machining. According to Oxely and Hastings, the frictional conditions along the tool rake face in machining can best be represented by a constant interfacial shear stress ($\tau = mk$). This assumption has been made by Dewhurst, Childs and Shi and Ramalingam in formulating slipline field solutions for metal machining. Yet, others such as Ernst and Merchant, Lee and Shaffer and Kudo have indicated that the tool-chip interface friction is governed by Coulomb's law ($\tau = \mu p$). It has also been suggested that tool-chip natural contact length consists of a zone of slipping contact on which the classical Coulomb's law of friction applies and a zone of sticking contact on which the friction stress attains the limiting value of yield stress k in shear of chip material. Slipline field solutions assuming this "modified" Coulomb's law has also been proposed.

It is now generally recognized that Coulomb-Amonton's law is not applicable at the tool-chip contact area where high pressure / high traction condition leads to an extreme friction situation. Measurement of contact stress distributions at this interface using split tool dynamometers or photo-elastic tools are in general found to be in agreement with this observation. As for friction characteristics at the tool-chip interface, it is likely that adhesion is predominant over abrasion, where the friction force stems from the shear fracture of the bonded asperities. The empirical equation that is known to describe this friction condition may be stated as,

$$\tau = k\left[1 - e^{-\left\{\frac{\mu\sigma_n}{k}\right\}^{n_p}}\right]^{\frac{1}{n_p}} \tag{1}$$

where, τ is the friction stress, σ_n is the normal stress, μ is the low stress level friction coefficient, and n_p is a constant whose value depends on tool-work material combination. Equation (1) reduces to that proposed by Finnie and Shaw for $n_p = 1$. It is easily verified that in a lightly loaded condition ($\tau, \sigma \to 0$) equation (1) reduces to Coulomb's law. On the other hand when σ_n becomes large the friction stress τ approaches the shear flow stress k of the chip material. As suggested by Wanheim, equation (1) provides a smooth transition between two regimes predicted by the modified coulomb's law ($\tau = \mu\sigma_n$, $\mu\sigma_n \le k$, $\tau = k$, $\mu\sigma_n \ge k$).

In the present study an exhaustive analysis of the chip forming process involving sharp and worn tools has been carried out using rigid-plastic slipline field theory. The fields are similar to those suggested earlier by Dewhurst, Kudo and Lee and Shaffer and are analyzed by the matrix operational procedure developed by Dewhurst and Collins and Dewhurst by assuming adhesion friction at tool-chip and tool-work piece

contact regions. Limit of validity of the proposed fields are examined using Hill's overstressing criteria.

For all fields the field parameters have been determined from static admissibility condition by considering the force and moment equilibrium of the chip. In some cases this has required the assumption of an elastic contact zone such that the elastic forces and the forces at the rigid-plastic chip boundary keep the chip in static equilibrium. As the equations involving the forces and the field parameters are non-linear these have been solved by an algorithm developed by Powell for solution to non-linear algebraic equations with unknown derivatives. For worn tools the field parameters on the flank side have been determined from the friction condition at tool flank and a geometric condition deduced from the hodograph.

It is seen that the rake angle and rake friction are the two most important variables in metal machining that influence the machining parameters such as the cutting ratio, cutting forces, chip curvature and contact length. It is further observed that the peak tool-tip pressure for a worn tool is considerably lower than that for a sharp tool even though the cutting forces for this case are higher. Also the peak pressure is found to be very little affected by rake angle and the size of the wear land.

It is also seen that the force ratio and tool-chip interface Coulomb coefficient of friction for a sharp tool decrease with rake angle. But presence of even a small flank wear land may reverse the trend.

Results from the theoretical analysis show excellent agreement with experimental observations reported in literature and also with those obtained by the author from orthogonal cutting tests especially at lower rake angles.

CONTENT

List of figures

List of Tables

Nomenclature

AF	Adhesion friction operator
F_c	Cutting force
F_t	Thrust force
FX, FY	Traction components along Cartesian coordinate directions
$F\overline{X}, F\overline{Y}$	Traction components along moving coordinate directions
H_E, V_E, M_E	Forces and moment at elastic contact region
H_P, V_P, M_P	Forces and moment at chip boundary
I	Unit matrix
$P, Q, R, S...$	Un-starred standard matrix operators
$P^*, Q^*, ..$	Starred standard matrix operators
R	Reversion operator
S	Shift operator
X	Ratio of elastic to plastic contact length
$\overline{c}$	Column vector representing an unit circle
d	Thickness of subsurface deformation zone
k	Yield stress in shear of chip material
l_c	Natural contact length
l_e	Elastic contact length
l_p	Plastic contact length
l_f	Size of the flank wear land

n_e	Exponent of normal pressure distribution in the elastic region
n_p	Constant defining the relationship between normal and shear stresses in the plastic contact region according to adhesion friction law
p_R	Hydrostatic pressure at point *R*
t_0	Uncut chip thickness
t_1	Chip thickness
t_1/t_0	Cutting ratio
$\alpha, \beta, \psi, \theta, \ldots$	Slipline angles
φ	Inclination of free-surface with the horizontal in the pre-deformation zone
λ	Shear plane angle/ average shear plane angle
δ	Slope of the flank wear land with the horizontal
ϕ_R	Friction angle at point *R*
γ	Tool rake angle
η_1	Rigid vertex angles at point *O*
η_2	Rigid vertex angles at point *O* or *I*
μ	Low stress level friction coefficient
ρ_1, ρ_2	Velocity discontinuities along the initial and final boundaries respectively of the primary shear zone.
τ , σ_n	Shear and Normal stresses on rake face
ω	Angular velocity of chip curl

n_p	Constant defining the relationship between normal and shear stresses in the plastic contact region according to adhesion friction law
p_R	Hydrostatic pressure at point *R*
t_0	Uncut chip thickness
t_1	Chip thickness
t_1/t_0	Cutting ratio
$\alpha, \beta, \psi, \theta, \ldots$	Slipline angles
φ	Inclination of free-surface with the horizontal in the pre-deformation zone
λ	Shear plane angle/ average shear plane angle
δ	Slope of the flank wear land with the horizontal
ϕ_R	Friction angle at point *R*
γ	Tool rake angle
η_1	Rigid vertex angles at point *O*
η_2	Rigid vertex angles at point *O* or *I*
μ	Low stress level friction coefficient
ρ_1, ρ_2	Velocity discontinuities along the initial and final boundaries respectively of the primary shear zone.
τ , σ_n	Shear and Normal stresses on rake face
ω	Angular velocity of chip curl

Chapter 1

CHAPTER 1

INTRODUCTION

In recent times manufacturing industries have striven to reduce operating costs while at the same time improve product quality. In manufacturing, cost cutting and improved product quality are necessary measures to take in an increasingly competitive world, where investors demand a better return on their investment. This drive for cost savings has culminated in a reduction in the number of manned equipments and operations, with increase in productivity expected. Many manufacturing processes involve some aspects of metal cutting operations, where there is a need for quantitatively estimating the technological performance of machining operations such as tool life, force, power and surface finish. This performance information is required for the selection and design of machine tools and cutting tools as well as optimization of cutting conditions for the efficient and effective use of machining operations. The most crucial factor determining successful continuation of the manufacturing activity in any typical metal cutting operation is tool wear.

Tool wear may be defined as the gradual erosion of cutting tool due to the rubbing action of the chip and the work piece in the presence of friction. After the tool has been in use for some time, wear land appears at the flank of the tool below the cutting edge developing a small negative clearance angle. This form of wear, known as *flank wear*, is due to the rubbing of tool flank with the work piece. Wear also appears on the tool face due to the sliding action of the chip, forming the characteristic cavity known as *crater*. The tool tip also wears out giving rise to a nose

radius. This form of wear is known as *nose wear*. These three forms of wear are shown in Fig. 1.1(a). The useful life of a tool is limited by the amount of tool wear and the cutting operation is discontinued when the wear growth is excessive.

The following mechanisms are believed to be responsible for gradual loss of tool material during cutting operations:

i. Mechanical processes like abrasion and adhesion involving macro-transfer of tool material

ii. Thermo-chemical processes like diffusion involving micro-transfer of tool material

iii. Electro-chemical processes like corrosion and oxidation.

When rubbing surfaces are free from any active chemical environment and the deteriorative action of electricity is absent, the mechanical wear process contributes the major share in total wear volume particularly at low cutting speeds. Such mechanical wear takes place in two predominant ways:

a) Abrasion due to ploughing into softer matrix by hard constituents such as segregated carbides, inclusions etc.

b) Adhesion and the formation of metallic bonds over the rubbing surfaces under load and subsequent rupture of these bonds followed by transfer of the elementary particles.

If the mechanical process involved in adhesion is capable of increasing the localized temperature of the real area of contact, interstitial diffusion occurs, wherein micro-transfer of the material from the tool to the chip and from the chip to the tool takes place in the direction of the concentration gradient. The process of diffusion induces a two fold wear process, *viz*. direct metal transfer through diffusion and macroscopic metal removal by the adhering effluent chip through breaking away of the surface

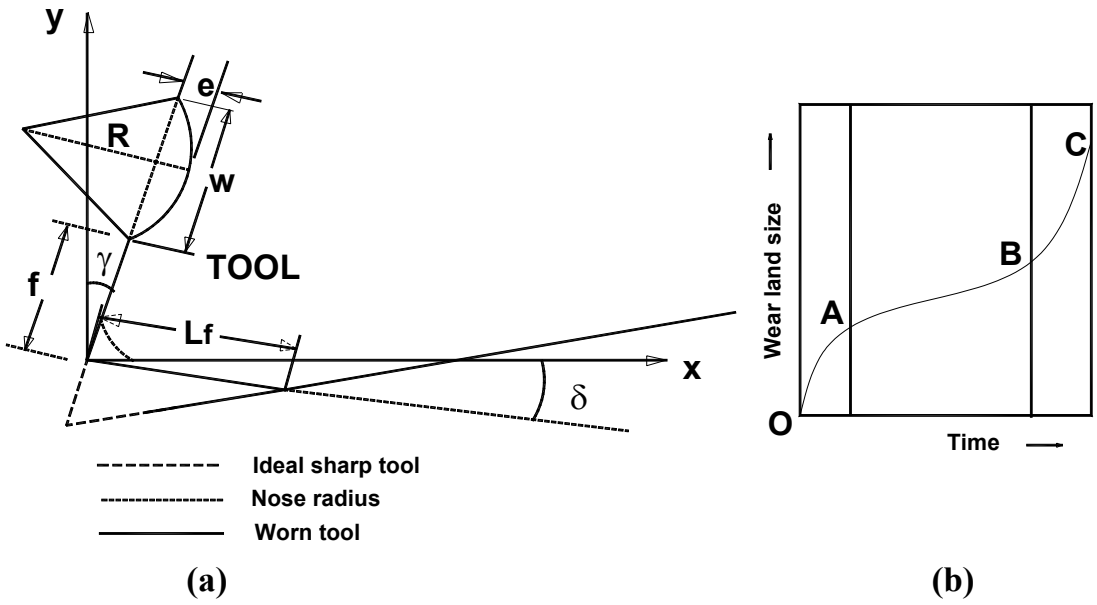

Fig. 1.1 : (a) Worn tool (b) Characteristic curve for flank wear growth.

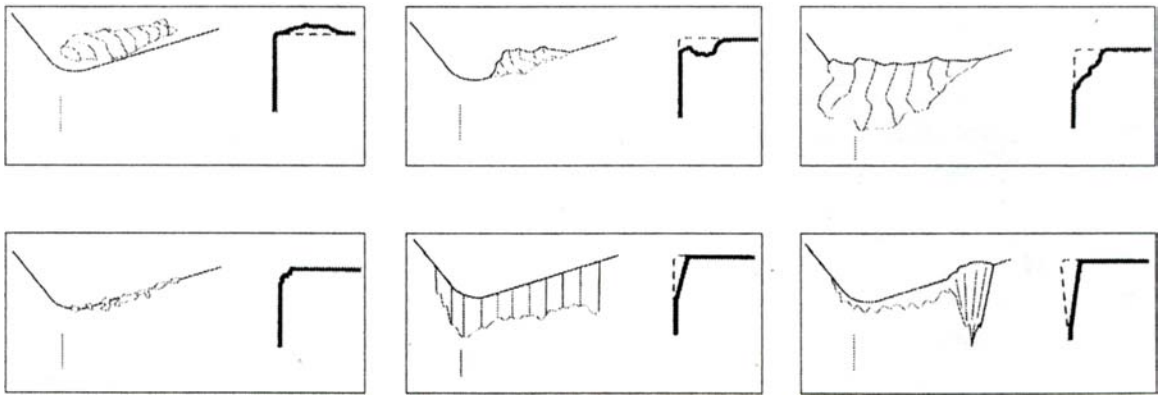

Fig. 1.2 : Types of tool wear [Ref. 3]

layers already weakened by the structural transformation undergone at the interface due to diffusion of various constituents of tool material and reverse diffusion of iron into carbide. Diffusion wear is a time and temperature dependent process and also depends on bonding affinity of the tool/work-piece pair and degree of atomic agitation.

Chemical wear is due to interaction between tool and the work material in the cutting fluid environment. If the fluid is active to the tool, wear may be greatly accelerated by chemical reaction or galvanic corrosion. If the tool-chip interface temperature is very high, oxidation of the tool material may take place giving rise to oxidation wear.

However, it is very difficult to pin down the exact cause and nature of tool wear, the phenomenon being very complex and dependent on many aspects such as the tool/work pair, the environment, the temperature of the interfaces, etc. The magnitude of the temperature at the interfaces may cause a shift from abrasion to adhesion or adhesion to the diffusion wear process.

The flank wear is characterized by the wear land l_f, while the crater wear is indicated by the width w, depth e and radius of curvature R of the crater (Fig. 1.1(a)). As cutting progresses, these parameters grow in the manner as shown in Fig. 1.1(b) and Fig. 1.2 [1,2,3]. Certain characteristic features of the growth of the flank wear land l_f may be observed from Fig. 1.1(b) and Fig. 1.2. Up to point '*A*' the region denotes the zone of initial *break-in*. After point '*A*' the wear proceeds in a more or less uniform manner till point '*B*'. The region '*A-B*' is the mechanical wear region under temperature insensitive conditions. Longer duration of this type of gradual wear is vital to the performance of cutting tools, because during this phase, machining

parameters remain stable. Beyond point '*B*' the rate of wear becomes *rapid* or *catastrophic* and cutting tool fails very soon after reaching this point.

For crater wear the *criterion of wear* is the ratio $\left(\frac{e}{(w/2)+f}\right)$. When this reaches a critical limit machining is discontinued. Catastrophic failure of the cutting tools (edge breaking due to cracking etc.) of course, may not be due to wear only. This may be the result of the impact or excessive loading, thermal shocks and chatter [1].

The useful life of the cutting tool is decided by the time period for the *catastrophic failure* to set in. Depending on the cutting velocity and the tool/work-piece combination, this failure may be due to the flank wear or crater wear.

The condition of the tool exerts a strong influence on the surface finish and dimensional integrity of the work piece, cutting forces and vibration levels of machine tools. Tool wear formed at the different tool faces also alters the original tool configuration/geometry, which, in turn greatly influences chip forming patterns and chip breakability [4].

A number of techniques have been employed to assess the extent of wear suffered by the cutting tools engaged in the cutting operations. Principally these techniques are classified into two groups: whether if they measure tool wear directly at the cutting edge of the worn tool (direct measurement technique) or if the parameters or signals of the cutting process allow to draw conclusions upon the degree of tool wear (indirect measurement technique). The flank wear land l_f can be directly measured by examining the flank of the worn tool under a Tool Maker's Microscope. The crater wear can be evaluated by topographic or spectroscopic analysis or by direct measurement of a sectioned tool at several cross sections [1,2]. Volumetric wear can be assessed from the loss of weight of a tool in an operation

either by radioactive methods or by electron microprobe analysis [5]. However, such *off-line* direct methods cause loss of productivity and hence have not found much application in industries.

In estimating tool wear, *on-line* methods are generally preferred, as these do not interrupt the production process. Such on-line direct methods of measurement using optical [6-8], wear particle and radioactivity [9,10], tool-work junction resistance [9] and tool work distance (dimensional deviation) [11,12] have been developed in the past. But none of these have achieved significant use in industries. *On-line* indirect methods based on the measurement of cutting forces [13-16], acoustic emission [17-19], vibration signal [20,21], temperature [22-25], cutting power [26], roughness of the machined surface [27], motor current and spindle speed [28] have also been used for estimation of tool wear and tool breakage. In place of tracking the force components independently, the use of force ratio has been preferred by some investigators [29-31] as this minimizes the noise factor arising out of the material property variations. More recently machine vision has also been used for reliable tool wear monitoring [32-33]. Trends show that monitoring one or more of the above parameters sensitive to the tool wear growth is rather easy when used with a computer interface. However, it is reported that the signal-processing methods based on force and acoustic emission are more reliable and sensitive compared to other methods of monitoring the tool condition [28].

In recent times *sensor fusion* has gained wider acceptance in tool condition monitoring (TCM) because of its ability to provide information on the state of the tool more reliably under varying process conditions. The advantage of this method is that the loss of sensitivity in one sensor domain is compensated by information from other sensors, enabling successful decision making over a wider range of operating

conditions. In this method the signals from a number of sensors placed at specific locations are used simultaneously to recognize the process abnormalities and to initiate corrective action. The integration of these signals essentially requires fast computation using suitable statistical tools such as time series modeling, regression analysis or self organization methods like group method of data handling [28]. However, *fusion* of sensor data has most successfully been accomplished by the introduction and use of *Artificial Neural Networks* (ANN) and this has continued to develop to date with vigorous diversity [28, 34-37].

Neural networks provide a new approach to solve a complicated problem through the way of learning by being shown and synthesizing knowledge from the observed input and output variables of the process under consideration. These have a mathematical background and theory with their development and their refinement stemming from basic mathematical principles, modeled on biological neurons and the nervous system.

It must, however be emphasized that successful tool condition monitoring by *indirect methods* depends on the quality of information generated by the monitoring sensors and the techniques used to process this information in order to make decisions. Thus the accuracy of prediction depends upon the accuracy of signal processing and analysis. Normally these methods are based upon the comparison of a reference signal of a *controlled* cutting process with the actual processing signal. In practice obtaining a suitable reference signal from an undisturbed cutting process requires a lot of efforts and skills. Even if this is done, the comparison of the reference signal with the actual process signal may in itself entail errors since the process signals obtained from manufacturing processes characterized by unpredictable shop-floor environments may be marked by a high noise/signal ratio. Hence indirect

methods of tool wear measurement may reflect far more than the tool wear alone and parameters associated with the tool wear must be extracted from them and correlated to give a measure of extent of the tool wear [34]. Further, it is reported that these measuring techniques are useful for monitoring the production of large batches, where identical cutting operations are repeated many times [34].

Empirical approaches have also been followed to establish the equations or models for quantitative prediction of the technological performance. Pioneering work in this direction was first initiated by Taylor [1,2] who proposed an empirical relation between cutting velocity and tool life. This equation known as Taylor's tool life equation is written as,

$$V_c T^n = c \tag{1.1}$$

where, V_c is the cutting velocity, T is the tool life and n and c are constants. The above equation was subsequently extended and modified to incorporate the effects of feed and the depth of cut. Empirical equation relating cutting forces with machining parameters has also been suggested by Kronenberg [38].

In the empirical approach experimentally measured machining characteristic values such as forces and tool life are related to the cutting variables by regression analysis. This approach involves considerable testing to determine the constants in the empirical equations and the results apply only to the machining operations tested. Given the significantly large and unmanageable number of tool-work material combinations, cutting and tool variables and different practical machining operations, empirical approach is clearly undesirable in practice.

It therefore appears that there is a need for fundamental study of machining process and for establishing cutting models for machining when tool wear is present. Such a study, apart from helping in the deeper understanding of the

mechanics of the process will also help the practicing engineers in their tool changing strategies. At the present time such an analysis can only be carried out on the geometrically simple orthogonal cutting process involving two-dimensional plastic deformation. But as argued by Oxley et al [39], although practical machining operations use geometrically more complex tools than the wedge shaped cutting tools used in orthogonal cutting, the basic material removal process in the two cases essentially remains the same.

In all metal machining processes such as turning, milling, drilling, shaping etc, removal of unwanted material is carried out in a number of steps and through each step a thin layer of work material is removed using a wedge shaped cutting tool. When the cutting tool penetrates the work material, the metal ahead of the tool deforms plastically before forming into chip. Large plastic deformation in this region was recognized by French scientist H. Tresca [40] as far back as in 1873. He measured the length of the chip and concluded that the chip length is only one third to half of the distance traveled by the tool. Subsequent, researchers like Coker and Chakko [41], Piispanen [42], Rosenberg and Eremin [43] etc also studied the plastic behavior of work material in the process of chip formation. Coker and Chakko's research on plastic models proved the existence of shear plane that extended from the tip of the tool to the surface of the work-piece [41]. The work material on crossing this plane transforms into the chip. The whole course of chip formation and reason for significant increase in chip thickness relative to uncut chip thickness was better grasped through the *card heap analogy model* conceptualized by Piispanen [42]. According to this model, thin lamellae of work material, on striking the cutting tool, moved over the tool face one after the other, similar to the displacement of cards in an inclined deck (shear plane) when they strike a solid surface (inclined plane of tool

face). However, across the shear plane the gradient of stress and velocity become infinite. Hence, Rosenberg and Eremin [43] proposed a model in which these authors argued that a shear zone must separate the chip from the work material within which the material is progressively deformed. Kececioglu [44] measured the average shear zone thickness experimentally while cutting *SAE 1015*. For orthogonal machining with a tool with rake angle of 33^0, uncut chip thickness of 0.10 millimeter and cutting velocity of 227 meters per minute, he found that the average shear zone thickness was as small as 17 microns. He studied the variation of average shear zone thickness under varied cutting conditions and noticed that in some cases it measured up to 170 microns. Hill [45] on the other hand, viewed that, for an ideal rigid-perfectly plastic material a single shear plane involving a narrow zone of intense shear is theoretically viable, the phenomenon being similar to that of flow of gases through a nozzle where, shock plane exists, across which the pressure and velocity undergo finite change. For strain hardening materials, however, this shear plane *opens up* giving rise to a shear zone. More recently Chawla, Biswas and Das [46] analytically determined the shear strains in the primary and secondary deformation zones and concluded that the primary deformation zone (shear plane) accounts for approximately 90% of the total strain suffered by the material, the rest 10% being attributed to the secondary shear zone. This observation seems to justify the assumption usually made in the slipline field analysis that the material is rigid-perfectly plastic. Stresses and strains in metal machining has been examined more critically in a recent paper by Astakhov and Shvets [36].

The chip-tool contact region is also equally important as normal and frictional stresses developed in this zone have profound effect on the chip formation process, cutting forces, chip-curling, interface temperature and tool wear.

Experimental observations using photo-elastic tool [47-49], split tool dynamometers [50-53], or a composite tool [54] indicate that these contact stresses have unique distributions in the contact region: *the normal stress increasing monotonically from the chip releasing point to the cutting edge, where as the frictional stress remains constant over certain portion of the contact area nearest to the cutting edge and then decreases gradually to zero at the chip releasing point*. Further, the peak normal stress is found to be as high as 1.9 to 3.6 times the shear flow stress of the work material at the cutting edge. Under such high normal pressures the conventional Amonton's law of friction, fails to explain the friction phenomenon between the chip and the tool. Different schools of thought have evolved over the years to stipulate the appropriate friction condition that governs the chip-tool and tool-work contact regions. Most analysts looking into the mechanics of chip formation have preferred the linear friction law given by

$$\tau = mk \tag{1.2}$$

where, τ is the interface friction stress, m is the friction factor and k is the shear flow stress of work material. Oxely and Hastings [39] have indicated that the above friction law best represents the frictional conditions along the tool rake face in metal machining. However, Merchant [55], Lee and Shaffer [56], Zorev [57], Childs [52], Kudo [58] and many others have advocated that the rake friction may be adequately represented by a modified Coulomb friction law which may be stated as,

$$\tau = \mu\sigma \text{ at low normal pressure } (\mu\sigma \le k) \tag{1.3.a}$$

and $$\tau = k \text{ at very high normal pressure } (\mu\sigma \ge k) \tag{1.3.b}$$

where, τ and σ are the interface shear stress and the normal stress respectively and μ is the coefficient of friction. But these friction laws fail to explain two apparent anomalies observed in metal machining. They are:

1. If only the rake angle is changed during cutting, a wide range of friction coefficients is obtained and,
2. The tendency towards complete adhesion of chip to tool increases as coefficient of friction decreases

This has lead several investigators such as Burwell and Strang [59], Chao and Trigger [60], Bowden and Tabor [61], Trent [62,63], Finnie and Shaw [64], Maekawa et al [65], Kobayashi and Thomsen [66], Wright and Tangaraj [67] to postulate that under the given circumstances, when a clean and chemically active chip passes swiftly over the tool face under a very high normal pressure, metallic bonding is likely to take place between the asperities of the contacting surfaces. Thus it is viewed that continuous formation and breakage of the welds between these asperities at the chip-tool and tool- work contact surfaces is mainly responsible for the frictional resistance. Of course other mechanisms like ionic exchange between tool and work material, asperity interlocking, ploughing of asperities of harder material into softer material, electrochemical processes like localized galvanic action and oxidation may also coexist along with asperity encounter. But asperity welding (adhesion) and ion exchange (diffusion) are considered the dominant factors contributing to friction and wear in metal machining.

The adhesion theory was doubted by some, especially by Challen and Oxely [68] in view of the most common understanding that no relative motion could take place between the surfaces when complete adhesion occurred. But an extensive micrographic study undertaken by Trent [62,63] for various combinations of tool and work material indicated that adhesion in metal machining is possible and is distinguished from common type of adhesion due to the fact that in machining, i) the contact area is very small, ii) the power available is sufficient to break the welded

portion to make advancement, iii) the tool is sufficiently strong to resist the fracture and iv) work material fractures in a controlled manner. Vieregge [69] studied the contribution of various wear mechanisms in the growth of flank wear and showed that metallic bonding is the dominant factor that causes resistance to flow of material at low cutting speeds though diffusion as a consequence of increased temperature may become dominant at high cutting speeds.

Under adhesion friction condition the relation between the frictional stress τ and the normal stress σ is written as,

$$\tau = k\left[1 - e^{-\frac{\mu\sigma_n}{k}}\right] \tag{1.4}$$

where, μ is the low stress level friction coefficient between the chip and the tool. The above empirical equation was proposed by Finnie and Shaw [64], Usui and Shirkashi [70] and was constituted from the observation that the frictional resistance relies on the real area of contact, which is the gross sum of contact areas of all the asperities in contact with each other. Real contact area constitutes a fraction (K) of the apparent contact area, and the value of this fraction varies from 0 to 1 depending on the normal pressure. Near the chip releasing point, the magnitude of the normal pressure is very small and the contact between chip and tool takes place through a small number of asperities so that, the real contact area approaches zero ($K \rightarrow 0$). Conversely, near the cutting edge, where the normal pressure is very high, contact occurs through large number of asperities making the real contact area to approach the apparent contact area ($K \rightarrow 1$). Thus it is postulated that both sliding ($K \approx 0$) and adherence ($K \approx 1$) are simultaneously present in the chip-tool contact region in metal machining [64,70].

More recently the contact stress distribution at the tool-chip interface was studied by Maekawa, Kitagawa and Childs [65] using a split-tool dynamometer when

machining steel with TiN cemented, P20 and K20 carbide tools in dry conditions. These authors observed that the friction stress τ in the contact zone shows a trapezoidal distribution that increases from the chip leaving point to the cutting edge and saturates at the shear flow stress of the chip, where as the normal stress σ_n has an exponential distribution that increases rapidly towards the cutting edge. Based upon their experimental observations, they proposed a modified empirical equation for the governing (adhesion) friction condition, which is stated as,

$$\tau = k\left[1 - e^{-\left\{\frac{\mu\sigma_n}{k}\right\}^{n_p}}\right]^{\frac{1}{n_p}} \qquad (1.5)$$

where, n_p is a constant, whose value depends on the tool-work material combination.

Despite the rapid growth in the applications of metal machining in manufacturing, a comprehensive analysis of machining processes has always been a difficult task. This is because incorporating the effect of a shear yield stress varying with strain, strain rate and temperature into an analytical model is not so easy. Consequently, the problem of prediction of different machining parameters has been approached using empirical relations, machinability data banks and analytical methods based on simplified assumptions. Large industrial companies in particular have developed banks of machining data over many years. One of the earliest data banks was established by 'Metcut Research Associates', who carried out extensive practical conventional and non-conventional cutting tests for American space programme. Data banks established in the recent years incorporate information from in-practice machining rather than from machining tests. The strength of data banks lie in their ability to provide information concerning the machining of new components based on previous experience of machining similar components. This approach

overcomes the main flaw of empirical approach, which does not provide any mechanism to learn from previous machining experiences. In contrast to these approaches investigators dealing with analytical models look for patterns of behavior at a higher level by invoking known relationships borrowed from Physics, Mechanics and Material Science.

One of the earliest analytical models in metal machining was due to Merchant and Ernst [55]. These authors proposed a shear plane model based on the assumption that continuous chip is formed by plastic deformation in a narrow zone that runs from the tool cutting edge to the free surface of the work piece. The model proposed by them is shown in Fig. 1.3(a), where OQ represents the shear plane. Across this plane the work velocity V_C (the tool is assumed stationary) is instantaneously changed to the chip velocity $V_{chip.}$ This requires discontinuity (jump) in the tangential component of velocity across OQ equal to V_S as shown in the velocity diagram (Fig. 1.3(b)). Two cardinal principles that were established by these authors are as follows,

1. Chip equilibrium (the chip can be considered as a rigid body in translational equilibrium under the external forces acting on it).
2. Force velocity co-linearity (the shear and frictional forces at the shear plane and the tool-chip contact face are co-linear and opposite to the shear and sliding velocities at the two faces respectively).

The solution proposed by Merchant is now accepted as an upper bound solution provided the work material could be considered as perfectly plastic. Because of poor agreement of this solution with some of the experimental observations, Merchant introduced the effect of dependency of the shear stress on the normal stress on the shear plane [71]. Lee and Shaffer [56] applied the slipline field theory and

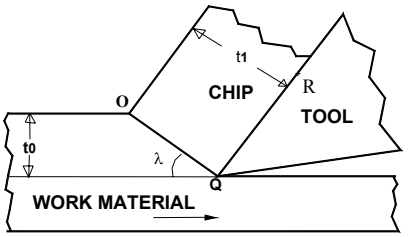

Fig. 1.3 (a): Shear plane model

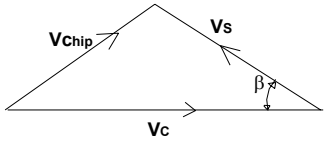

Fig. 1.3 (b): Velocity field

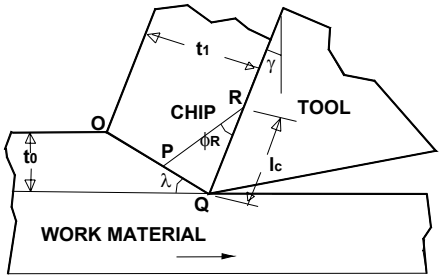

Fig. 1.4: Lee and Shaffer's model

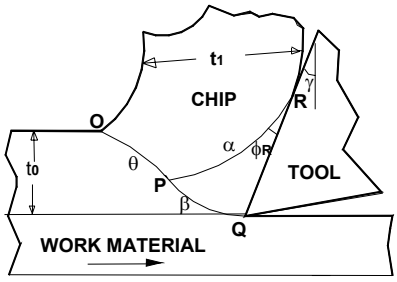

Fig. 1.5: Kudo's field I

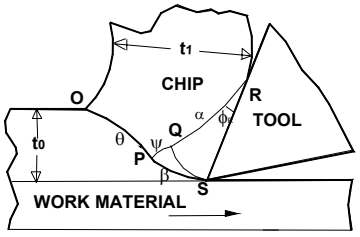

Fig. 1.6: Dewhurst's field

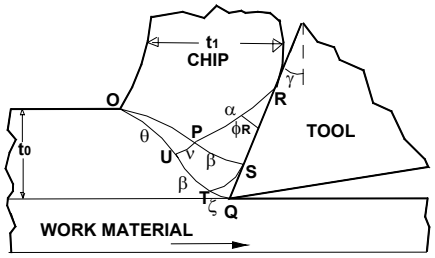

Fig. 1.7: Kudo's field II

assumed a plastic zone in contact with the tool face with uniform stress distribution at the chip-tool interface. They constructed a slipline field as shown in Fig. 1.4 with straight boundaries *OP*, *PR* and *PQ*. Taking *OP* and *PR* as sliplines of equal length, equilibrium of the chip is ensured. Hence, the hydrostatic pressure, equal to the yield stress k in shear, is uniform throughout the field. For any given rake angle γ, the field angle ϕ_R (friction angle at R) is determined by the rake face friction stress ratio τ/k assumed to be constant along QR ($\tau/\kappa = \cos 2\phi_R$). Thus for this field each of the non-dimensional machining parameters l_c/t_0 , t_1/t_0 and shear angle λ is uniquely determined by τ/k and γ. The admissibility of the above solution has been examined by Hill [72]. It may be seen that under high friction condition (low value of ϕ_R) and with a negative rake tool the shear angle λ may be zero or negative which is physically not tenable. Even with low positive rake angle the cutting forces calculated from the above field becomes extremely high. This led Lee and Shaffer [56] to conclude that under such conditions a small permanent built up edge exists. They assumed that this would be stable in character and could be likened to a cap of dead metal, which was formed early in cutting and remains constant in shape and size. Kudo [58] suggested a slipline field solution for the case of chip curling by replacing straight sliplines of Lee and Shaffer by curved sliplines (Fig. 1.5**)**. The field suggested by him satisfies the kinematic requirements of chip flow but the solution becomes inadmissible for free machining, as the static force equilibrium is not realized. Kudo [58] also suggested another slipline field by replacing the concave slipline *PR* by a convex slipline identical to the circular arc *OP* to satisfy the static force equilibrium of the chip. With a convex slipline *PR* however the normal stress at

the chip-tool interface decreases from the chip releasing point to the tool tip, which is in contrast with the experimental observations.

Dewhurst [73] proposed a non-unique solution (Fig. (1.6)) for free machining operation for the case of chip curling. Initially, Dewhurst [73] had proposed a unique solution with a small triangular pre-deformation region with a curved stress-free surface. But with this field he could find no solution which satisfied the force and moment equilibrium conditions imposed by a force free chip. He speculated that possibly in cases where the chip is not free as when machining with a chip breaker such solutions might be found. Noting that neither the uniqueness theorem nor the limit theorem (on which the upper bound method is based) given by Hill [45] can apply to a process such as machining with its undefined boundaries, Dewhurst[73], following Hill [72], determined a permissible range of solutions such that the rigid vertices in the chip or the work-piece are not overstressed. Dewhurst showed that his field degenerated to Lee and Shaffer field (Fig. 1.4) with a straight shear plane when the hydrostatic pressure at 'O' equaled k. Dewhurst made a number of comparisons between his predicted results and experimental results of other investigators. He obtained excellent agreement between his predicted values with the experimental results reported by Ota et al. [74] and Low et al. [75]. He further concluded that since the machining process is not uniquely defined it would be expected that the final steady state for particular cutting conditions would depend to some extent upon the initial conditions.

Dewhurst [76] also analyzed the same field for the case of machining with a ramp type chip breaker and found the solution to be non-unique in nature. For a

particular position of the chip breaker the solutions were found to lie between two limiting conditions: one with largest chip thickness, largest contact length and hence largest cutting forces and another corresponding to the field with smallest chip thickness and contact length. This lower limit was referred to as *Kudo limit*. Petryk [77] developed a stress free boundary operator and analyzed Dewhurst's field with a pre-deformation region. The analysis of the mechanics of machining as carried out by the various investigators and also by the author along with the assumed boundary conditions is summarized in table 1.1.

Investigators concerned with the distribution of stresses at the chip-tool interface[47-49] had concluded that the contact length obtained experimentally was much greater than the theoretical plastic contact length. Zorev [57] looking into this disparity postulated the existence of an elastic contact region at the chip tool interface beyond the length of plastic contact. He also proposed that the normal stress distribution in the elastic contact region followed a power law given by the relation,

$$\sigma = \sigma_0 \left(\frac{l}{l_e} \right)^{n_e} \tag{1.6}$$

where, σ is normal stress at any reference point at a distance l from the chip releasing point, l_e is elastic contact length, σ_0 is the normal stress at the elastic/plastic transition zone and n_e is the power index. Later Childs [78] proposed an approximate analysis with elastic contact using Dewhurst's[73] slipline field model for free machining replacing curved slipline elements by circular arcs. He reported that theoretical results are closer to the experimental results when elastic zone is considered.

Maity and Das [79] showed that the stress boundary conditions can also be satisfied by assuming an exponential distribution of normal stress in the elastic region as,

$$\sigma = \frac{\sigma_0}{1-e^{n_e}}\left(1-e^{\left(\frac{n_e l}{l_e}\right)}\right) \tag{1.7}$$

They showed that the force and the moment equilibrium of the chip is realized by considering normal and shear forces at the elastic zone and the forces at the rigid-plastic chip boundary.

The finite element method (FEM) has been applied to analyze machining process in the last two decades by various investigators. A comprehensive survey of major contributions in this regard is presented in [80]. The advantage of FEM modeling is that, the realistic material properties including the effect of large strain, strain rate and temperature can be incorporated in the analysis. However, despite the increasing application of finite element techniques in analyzing plasticity problems and the limitations of slipline field theory with respect to strain hardening, strain rate and temperature effects, the later method is still very important in the analysis of metal working processes. This is because of the relative simplicity of slipline fields and the clarity with which they can be made to reflect deformation modes.

From the foregoing discussion it may be seen that considerable attention has been paid in the past to the analysis of metal machining involving a sharp tool. However, there seems to be a distinct dearth of study on the cutting phenomenon and establishing cutting models for machining when tool wear occurs. Friction condition

on the flank face of the tool has been investigated in depth by McAdoms and Rosenthal [81], Kobayashi and Thomsen [66], Thomsen et al. [82], Okashi and Sata [83] , Zorev [84] and Shi and Ramalingam [85]. Kobayashi and Thomsen [66] and Thomsen et al. [82] observed that material immediately beneath the flank contact surface is in a state of plastic flow. Interestingly they also observed that deformations in the primary and the secondary shear zones are not influenced by the size of the flank wear land.

The first slipline field solution for orthogonal cutting with a chip breaker and flank wear was proposed by Shi and Ramlingam [85]. For a worn tool with a finite flank wear land l_f , this slipline field featured a primary deformation zone, a pre-deformation zone and two secondary shear zones: one along the rake face and the other along the flank face. The chip, in static equilibrium under the action of the chip breaker force and the forces at rigid plastic chip boundary was assumed to leave the deformation zone with a constant curvature (*chip curl*). It was shown that the cutting geometry was completely determined by specifying the tool rake angle, tool-chip interface friction and the chip breaker constraint. The chip radius of curvature, chip thickness and the stresses and velocities within the plastic region were computed by these authors for the above field. The grid deformation patterns calculated from the velocity field were found to be in accordance with experimental observations. Incidentally, a pre-deformation zone of finite width between the chip and the work material was first noticed by Armago and Brown [86]. Shi and Ramlingam, however, correlated it to the presence of flank wear.

Shi and Ramalingam [85] in their proposed field assumed the flank wear land to be at non-zero inclination with the cutting direction and not parallel to the machined surface. This assumption was based on the experimental observations made earlier by Thomsen et al [82] and on the theoretical consideration that for a rigid-perfectly plastic material the material beneath the flank surface would not be plastic if the worn surface was parallel to the machined surface. In fact, Thomsen et al [82] had found that when flank wear land was parallel to the cutting direction, the cutting force components were virtually constant and did not vary with the size of the flank wear land. Since the cutting force components measured during machining are found to increase linearly with the size of the flank wear land [66,82-85], it is reasonable to assume that the wear land cannot be parallel to the cutting direction.

More recently, the effect of tool flank wear on the orthogonal cutting process was examined by Wang et al [87] using *thin shear zone* model of chip formation proposed by Ernst and Merchant [55]. The experimental investigations carried out by these authors showed that the flank wear does not affect the basic cutting quantities such as shear angle and shear stress both qualitatively and quantitatively, but results in additional rubbing or ploughing force on the wear land. The wear land was found to result in substantial increase in cutting forces and that the thrust force was found to be more sensitive to flank wear.

The major shortcoming of the slipline field solutions discussed in the earlier sections is that the rake face friction stress in these solutions is assumed either constant ($\tau = mk$) [73,85] or is distributed according to Coulomb's law ($\tau = \mu p$) [56,58,78]. This is obviously incorrect since experimental evidence now suggests that

the nature of friction at the tool-chip interface is adhesion rather than sliding and the relation between the contact normal and shear stress is more appropriately given by equation (1.5). Also, except for the solution by Childs [78] and Maity and Das [88], none of these solutions take account of the influence of elastic contact length on the machining parameters such as contact length, cutting and thrust forces and cutting ratio. It is, therefore, expected that the analysis of the chip formation process assuming adhesion friction and the existence of an elastic contact length will be of value to scientists and practicing engineers and this is the concern of the present investigation.

In this study an exhaustive analysis of the chip forming process involving chip curling and chip streaming has been carried out using the rigid plastic slipline field theory with the assumption of adhesion friction at the contact regions at tool face and flank. The slipline fields analyzed are similar to those suggested earlier by Lee and Shaffer [56], Kudo [58] and Dewhurst [73] and results are computed both for a sharp tool and a worn tool with and without the assumption of an elastic contact region. It is shown that n_e (equation (1.7)) has only marginal influence on the machining parameters such as cutting and thrust forces and cutting ratio, though the natural contact length is greatly affected by its value.

In Chapter 2 a brief account of plain-strain slipline field theory is presented and the power series and the matrix method of analysis [89-91] is explained in detail. The structure of the fundamental matrix operators is discussed and the equations are presented for the calculation of traction and moment for any slipline curve. The Coulomb friction operator [92,93] to deal with non-linear boundary value

problems such as those involving adhesion friction or curved boundaries is also discussed.

In Chapter 3 slipline field solutions for free-chip machining are presented considering adhesion friction at chip-tool interface. The field is similar to that suggested earlier by Dewhurst[73] and is analyzed by the matrix method suggested by Dewhurst and Collins [89] and Dewhurst [92,93]. The limits of the solution range are examined from the consideration of overstressing of rigid vertices in the assumed rigid regions [45]. Variation of cutting forces, cutting ratio, chip curvature and contact length with rake angle and friction parameters is investigated.

In chapter 4 slipline field solutions for orthogonal machining are proposed considering the influence of elastic effects in chip formation. The slipline fields are similar to those suggested earlier by Kudo [58]. It is assumed that the total contact length is composed of a plastic contact length and an elastic part. Within the plastic contact zone the normal stress is assumed to vary according to Hencky's equations. In the elastic zone it is assumed that the normal pressure σ_n increases exponentially from zero at the chip releasing point to it's maximum value at the elastic-plastic boundary. It is postulated that the chip is in a state of static equilibrium under the action of the forces in the elastic contact zone and those at the rigid-plastic chip boundary as suggested by Childs [78]. Machining parameters such as cutting forces, cutting ratio, chip curl radius and contact length are estimated for different values of friction parameters and rake angles. It is shown that a unique value of the exponent of normal pressure distribution in the elastic range can be obtained if it is assumed that the slopes of normal stress distribution curves in the elastic and plastic contact

zones have the same value at the elastic/plastic boundary. The fields are analyzed by the matrix method. The range of validity of the proposed fields is established using Hill's overstressing criteria [45]. Results from the theoretical analysis are compared with those from experiments available in literature.

In chapter 5 slipline field solutions are proposed for machining with a tool with a finite flank wear land. Slipline fields are constructed in a manner similar to that suggested by Shi and Ramalingam [85]. Force and moment equilibrium of the chip is ensured by considering the forces in the elastic and plastic contact zones. Variation of cutting and thrust forces with tool wear is studied for different tool rake angles and friction conditions. It is shown that even a small amount of wear in the tool flank has significant effect on 'tool-chip interface average Coulomb coefficient of friction' as reported by Albrecht [94]. Computed results indicate that though the cutting and thrust forces increase the peak normal stress on the rake face for a worn tool is less than that for a sharp tool.

In chapter 6 slipline field solutions for free machining are proposed for cutting with a worn tool with finite flank wear land. The proposed solutions take account of both *chip streaming* and *chip curling*. Results are computed when the interfacial friction at the tool flank is assumed to be governed by adhesion friction. Range of validity of the proposed solutions is examined using Hill's overstressing criteria [45]. Variation of cutting and thrust forces with tool wear and interface friction is studied. The theoretical findings are also compared with experimental results reported in literature.

Chapter 7 describes in detail the experimental investigation carried out to validate the present theoretical models. For this purpose cutting tests were carried out on mild steel bars of diameters 40 and 67-mm. The bars were machined using HSS tools with 10% cobalt. The tool rake angle was varied from 0 to 25 degrees. Tests were conducted for a number of cutting speeds and feed rates. To study the effect of flank wear on machining parameters, finite flank wear lands were ground on the cutting tools using a surface grinding machine. Cutting and thrust forces were measured using a strain gauge type tool dynamometer and chip thickness by a reflected light microscope. The shear plane angle was calculated from the cutting ratio. The shear stress in the shear plane was estimated following the procedure suggested by Kobayashi and Thomsen [66]. Non-dimensional cutting and thrust forces were calculated and compared with the theoretical results.

Conclusions from the present investigation are finally presented in chapter 8.

-ooOoo-

Table 1.1 Summery of the past and the present investigations

Name of the investigator	Ref. no.	Chip shape	Tool condition	Friction condition	Free/Forced chip	Remark
Merchant	55,71	Straight	Sharp tool	Coulomb friction	Free chip	Upper bound
Lee and Shaffer	56	Straight	Sharp tool	Coulomb friction	Free chip	Unique solution
Kudo	58	Straight as well as curled	Sharp tool	Coulomb friction	Free chip	Unique solutions for curled chip with normal pressure decreases from chip separation point to tool tip.
Dewhurst	73,76	Curled	Sharp tool	Constant friction	Free chip	Non-unique solutions
Childs	78	Curled	Sharp tool	Constant friction	Constrained due to elastic contact	Non-unique solutions
Shi and Ramlingam	85	Curled	Worn tool	Constant friction	Constrained due to chip breaker	Unique solutions
Maity and Das	79,88	Curled	Sharp tool	Coulomb friction	Free and forced chip	Non-unique solutions
Fang	102,103	Curled	Worn tool	Constant friction	Constrained due to chip breaker	Unique solutions
Author		Straight as well as curled	Sharp as well as worn	Adhesion	Free as well as constrained due to elastic contact	Unique as well as non-unique

Chapter 2

CHAPTER 2

MATHEMATICAL FORMULATION OF SLIPLINE FIELDS BY MATRIX METHOD

2.1 Introduction

In the absence of body forces the state of stress in a body deforming under conditions of plain strain satisfy the equilibrium equations,

$$\frac{\partial \sigma_x}{\partial x} + \frac{\partial \tau_{xy}}{\partial y} = 0$$

$$\frac{\partial \tau_{xy}}{\partial x} + \frac{\partial \sigma_y}{\partial y} = 0 \qquad (2.1)$$

and the yield criterion

$$(\sigma_x - \sigma_y)^2 + 4\tau^2{}_{xy} = 4k^2 \qquad (2.2)$$

The stresses in the Cartesian coordinate directions that satisfy the yield criterion are given by

$$\sigma_x = -p - k\sin(2\phi)$$

$$\sigma_y = -p + k\sin(2\phi)$$

and $$\tau = k\cos(2\phi) \qquad (2.3)$$

where, $-p = \frac{1}{2}(\sigma_x + \sigma_y)$ is the hydrostatic part of the stress tensor and $\left(\phi + \frac{\pi}{4}\right)$ is the anti-clockwise rotation of the direction of the algebraically greatest principal stress from the positive direction of the x-axis as shown in Fig. 2.1. Substitution of equation (2.3) in equation (2.1) gives

$$\frac{-\partial p}{\partial x} - 2k\cos 2\phi\left(\frac{\partial \phi}{\partial x}\right) - 2k\sin 2\phi\left(\frac{\partial \phi}{\partial y}\right) = 0$$

and $$-\frac{\partial p}{\partial y} - 2k\sin 2\phi\left(\frac{\partial \phi}{\partial x}\right) + 2k\cos 2\phi\left(\frac{\partial \phi}{\partial y}\right) = 0 \qquad (2.4)$$

Equations 2.4 are hyperbolic and yield two families of characteristics inclined to the x -axis at angles ϕ and $\left(\phi + \frac{\pi}{2}\right)$ respectively, thus forming an orthogonal network known as sliplines. The members of the family given by the parameter ϕ are by convention called the α -lines and those given by the parameter $\left(\phi + \frac{\pi}{2}\right)$ the β -lines. Evidently, the α-and β -lines coincide with the trajectories of maximum shear stress.

The hydrostatic pressures along the sliplines satisfy Hencky's equations which in the absence of work-hardening may be expressed as:

$p + 2k\phi = const.$ along an α - line

and $p - 2k\phi = const.$ along a β - line. (2.5)

The velocities along the sliplines are related by Geiringer's equations written as,

$du - v.d\phi = 0$ on an α - line

and $dv + u.d\phi = 0$ on a β - line (2.6)

where, *u* and *v* are the velocity components in the α - and β - directions respectively.

A field of sliplines possesses several geometrical properties, which are enunciated in the two theorems due to Hencky [95-97]. Hencky's first theorem states that the

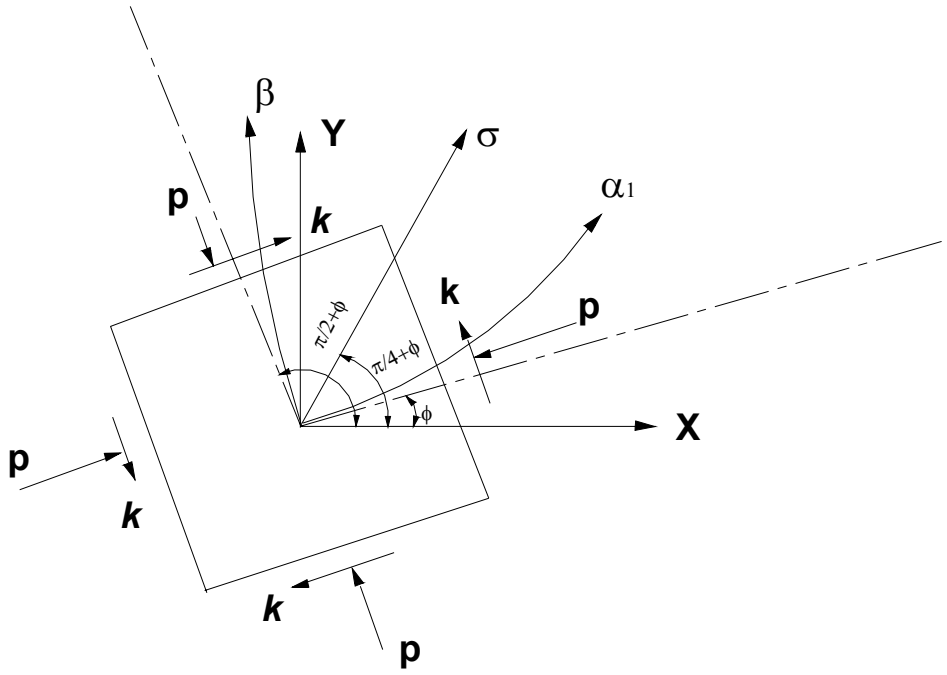

Fig. 2.1: Physical plane showing stress system in plane plastic flow.

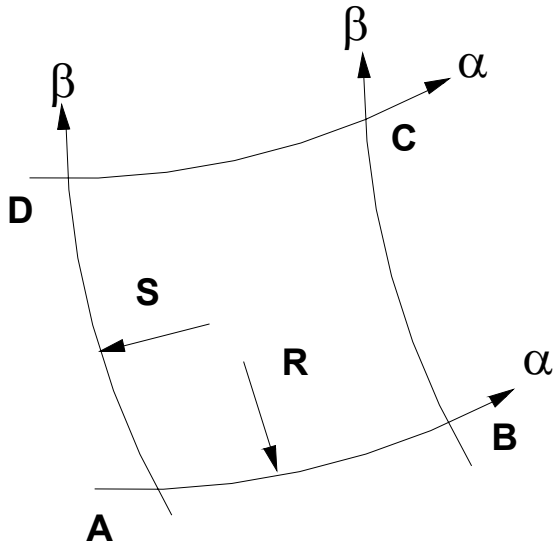

Fig. 2.2: A slipline field net for demonstrating Hencky's theorems.

angle between two sliplines of one family, where they are intersected by a pair of sliplines of the other family is constant along their length. Thus referring to Fig. 2.2, we have

$$\phi_D - \phi_A = \phi_C - \phi_B$$

or
$$\phi_C - \phi_D = \phi_B - \phi_A \tag{2.7}$$

Hencky's second theorem states that as we move along a slipline, the radii of curvature of the sliplines of the other family change by the distance traveled. Thus, referring to Fig. 2.2, we have,

$$dS + Rd\phi = 0, \quad \text{along an } \alpha\text{-line}$$

and
$$dR - Sd\phi = 0, \text{ along a } \beta\text{-line.} \tag{2.8}$$

Solutions to boundary value problems by analytic integration of the plain strain equations is possible only in a few simple cases. Hence, construction of the slipline network is usually carried out by the graphical procedure suggested by Hill [95] or Prager [96,97]. When applied to indirect or mixed boundary value problems, however, this method of analysis becomes very cumbersome. Such problems are more readily solved by the matrix method, where the construction of the slipline field is achieved through the use of some standard matrix operators and superposition principle [90, 98].

2.2 Series representation for radius of curvature of sliplines

The sign convention for the series representation of the radius of curvature of the slipline curves is same as that adopted by Dewhurst and Collins [89], so that the slipline field construction is independent of whether it is an α-line or a β-line. It states that,

a) The inclination of a slipline is always reckoned from the tangent to the slipline at its base point and is always taken as positive irrespective of the sense of rotation.

b) The radius of curvature ρ of a slipline is defined by $\frac{1}{\rho} = \pm \frac{d\psi}{ds}$

where, ψ is the inclination of the local tangent to that at the base point and ds is the differential arc length. The plus or minus sign is taken according as whether ψ increases in an anti-clockwise or clockwise sense along the slipline. With this sign convention, Hencky's second theorem for the slipline network shown in Fig. 2.3 is given as:

$$\frac{\partial R}{\partial \beta} = -S$$

and $$\frac{\partial S}{\partial \alpha} = -R$$

Referring to Fig. 2.3 (a), if the radii of curvature of the two given sliplines *OA* and *OB* are expanded in a power series in terms of the angular coordinates such that

$$R_0(\alpha) = \sum_{n=0}^{\infty} a_n \frac{\alpha^n}{n!}$$

and $$S_0(\beta) = \sum_{n=0}^{\infty} b_n \frac{\beta^n}{n!} \tag{2.9}$$

Then, the radii of curvature at the general point $P(\alpha, \beta)$ are given by [99]

$$R(\alpha, \beta) = \sum_{m,n=0}^{\infty} \left(a_n \frac{\alpha^{m+n}}{(m+n)} \frac{\beta^m}{m!} - b_n \frac{\alpha^m}{m!} \frac{\beta^{m+n+1}}{(m+n+1)!} \right) \tag{2.10}$$

$$S(\alpha, \beta) = \sum_{m,n=0}^{\infty} \left(-a_n \frac{\alpha^{m+n+1}}{(m+n+1)!} \frac{\beta^m}{m!} + b_n \frac{\alpha^m}{m!} \frac{\beta^{m+n}}{(m+n)!} \right) \tag{2.11}$$

It may be seen with reference to equations (2.10), (2.11) that the radii of curvature of α -and β -lines through $P(\alpha, \beta)$ are obtained by algebraic addition of two terms, which in essence is the mathematical formulation of superposition principle.

2.3 Matrix representation of slipline fields

The series solutions given by Ewing [99] were developed into the matrix formulation by Dewhurst and Collins [89] and Collins[98] using principles of linear algebra. Referring to Fig. 2.3(b), let the radius of curvature of the base sliplines *OA* and *OB* through *O* be represented by the column vectors σ_1 and σ_2 respectively where, the elements of the column vectors are the coefficients in the power series expansion of the radius of curvature of the sliplines (equation 2.9). Then, as shown by Dewhurst and Collins [89], the column vectors σ_3 and σ_4 representing the radius of curvature of the sliplines *BP* and *AP* are given by the relations.

$$\sigma_3 = P_\beta^* \sigma_1 + Q_\beta^* \sigma_2$$

$$\sigma_4 = P_\alpha^* \sigma_2 + Q_\alpha^* \sigma_1 \tag{2.12}$$

where,

$$P_\phi^* = \begin{vmatrix} \phi_0 & 0 & 0 & -- \\ \phi_1 & \phi_0 & 0 & -- \\ \phi_2 & \phi_1 & \phi_0 & -- \\ -- & -- & -- & -- \\ -- & -- & -- & -- \end{vmatrix}$$

and

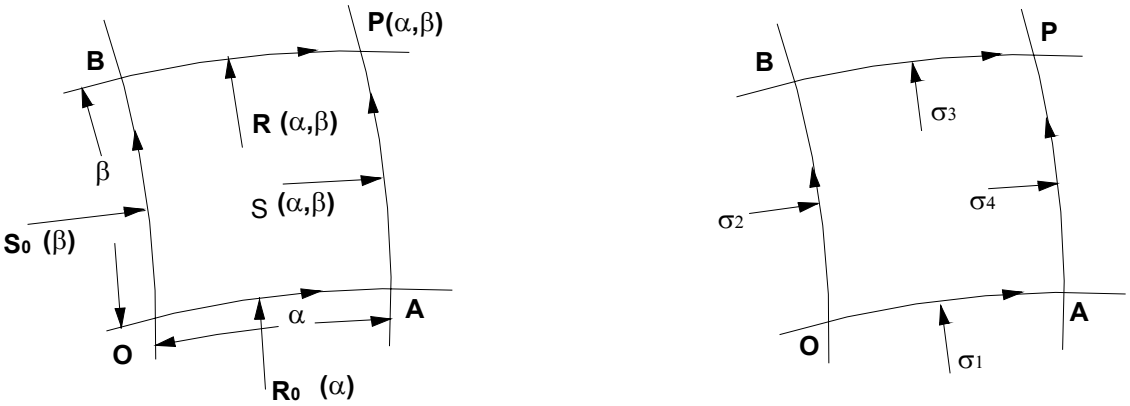

(a) **(b)**

Fig. 2.3: A slipline field net for (a) Series representation of radius of curvature (b) Matrix representation of slipline curves.

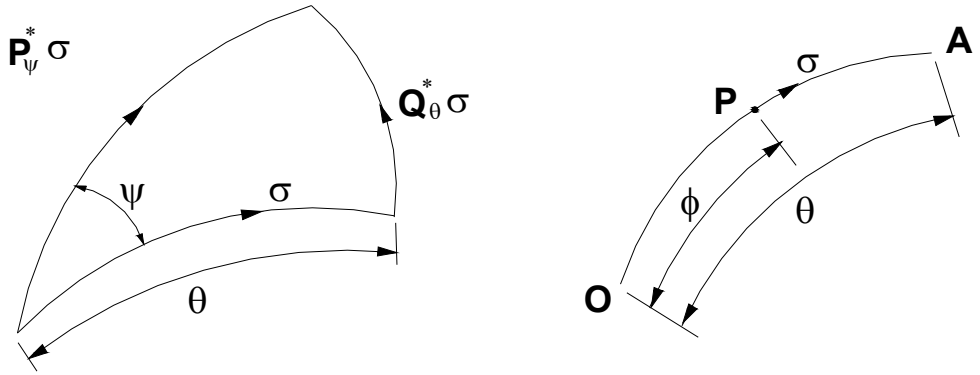

(a) **(b)**

Fig. 2.4: Matrix operators for (a) Generating singular field on the convex side of a slipline curve (b) Shifting of the origin of a slipline curve.

$$Q_{\phi}^{*} = -\begin{vmatrix} \phi_1 & \phi_2 & \phi_3 & -- \\ \phi_2 & \phi_3 & \phi_4 & -- \\ \phi_3 & \phi_4 & \phi_5 & -- \\ -- & -- & -- & -- \\ -- & -- & -- & -- \end{vmatrix} \tag{2.13}$$

and $\phi_m = \dfrac{\phi^m}{m!}$ is the reduced power of ϕ. In equation (2.12) $P^{\star}$ and $Q^{\star}$ are the matrix operators that generate the singular fields on the convex side of a given slipline (Fig. 2.4(a)).

The reversion matrix operator R_{ϕ} reverses the intrinsic direction of a given slipline with angular span ϕ. Thus, referring to Fig. (2.4(b)) if slipline curve *OA* is represented by σ , the curve *AO* is given as

$$AO = R_{\theta}\sigma \tag{2.14}$$

where the reversion operator R_{ϕ} is given by the square matrix

$$R_{\phi} = -\begin{vmatrix} \phi_0 & \phi_1 & \phi_2 & -- \\ 0 & -\phi_0 & -\phi_1 & -- \\ 0 & 0 & \phi_0 & -- \\ -- & -- & -- & -- \\ -- & -- & -- & -- \end{vmatrix} \tag{2.15}$$

The shift operator S_ϕ shifts the origin of a slipline through an angular distance ϕ in the intrinsic direction (Fig. 2.4(b)). Thus, if *OA* is represented by σ, *PA* is given as

$$PA = S_\phi \sigma \tag{2.16}$$

where the shift operator is written in the matrix form as,

$$S_\phi = \begin{vmatrix} \phi_0 & \phi_1 & \phi_2 & -- \\ 0 & \phi_0 & \phi_1 & -- \\ 0 & 0 & \phi_0 & -- \\ -- & -- & -- & -- \\ -- & -- & -- & -- \end{vmatrix} \tag{2.17}$$

The un-starred *P* and *Q* operators are defined using the reversion operator as ,

$$P_{\theta\psi} = R_\theta P^*_\psi \text{ and } Q_{\theta\psi} = R_\psi Q^*_\theta \tag{2.18}$$

Using the reversion operators, the relation between the radius of curvatures of the sliplines σ_1, σ_2, σ_3, and σ_4 may be written as (Fig. 2.5)

$$\sigma_3 = P_{\theta\psi}\sigma_1 + Q_{\psi\theta}\sigma_2$$

$$\sigma_4 = P_{\psi\theta}\sigma_2 + Q_{\theta\psi}\sigma_1 \tag{2.19}$$

By taking $\sigma_3(PB)$ and $\sigma_4(PA)$ as base sliplines, the relations for σ_1 and σ_2 may be expressed as,

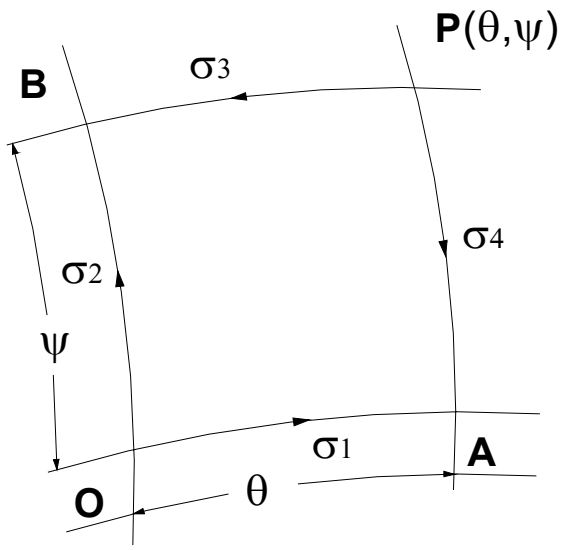

Fig. 2.5: A slipline field net for showing relation between radius of curvatures of slipline curves.

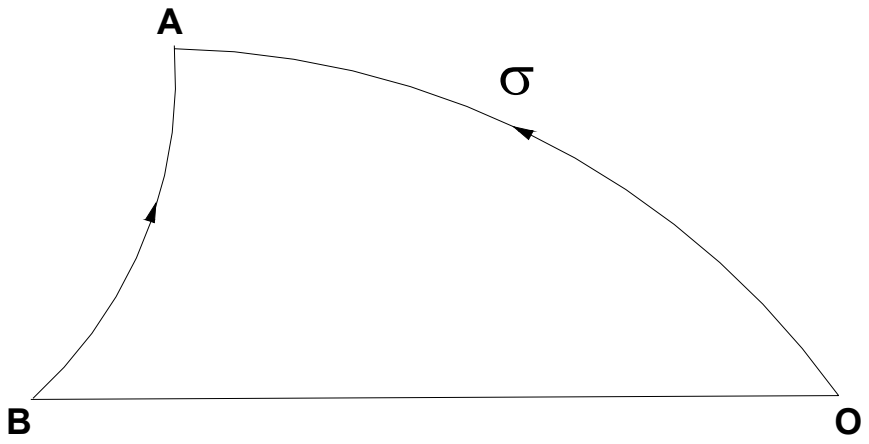

Fig. 2.6: Smooth boundary operator generating field between a slipline curve and a straight frictionless boundary.

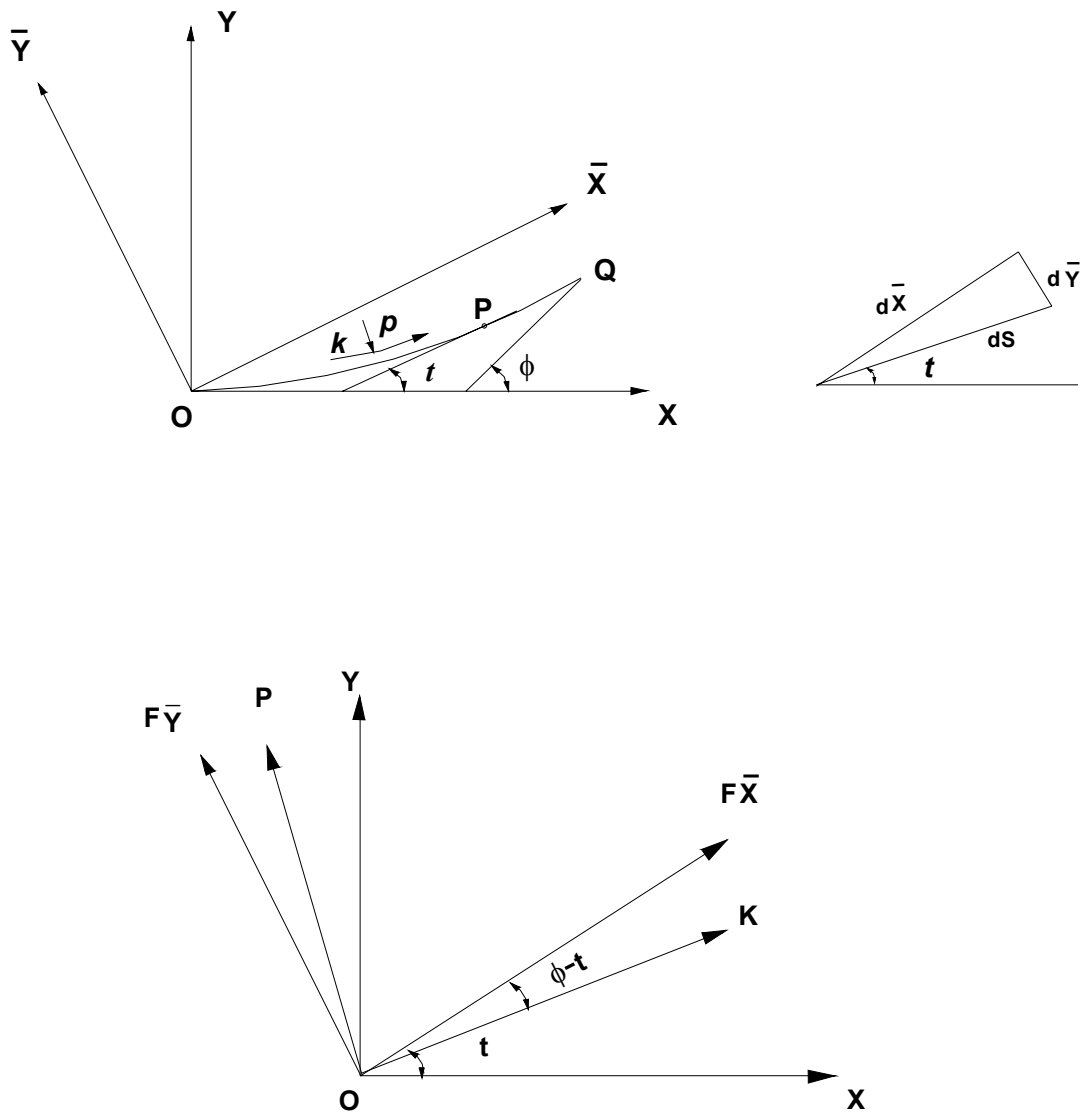

Fig. 2.7: Calculation of coordinates, traction and moment.

$$\sigma_1 = P_{\theta\psi}\sigma_3 - Q_{\psi\theta}\sigma_4$$

$$\sigma_2 = P_{\psi\theta}\sigma_4 - Q_{\theta\psi}\sigma_3 \tag{2.20}$$

The smooth boundary operator T_ϕ generates the field between a given slipline and a straight frictionless boundary (Fig. 2.6). T_ϕ constructs the field on the concave side of the given slipline, while it's inverse T_ϕ^{-1} yields the field on convex side.

Thus, $BA = T_\phi \ OA$ and $OA = T_\phi^{-1} \ BA$ where,

$$T_\phi = -P_{\phi\phi} - Q_{\phi\phi}$$

$$T_\phi^{-1} = -P_{\phi\phi} + Q_{\phi\phi} \tag{2.21}$$

2.4 Calculation of coordinates, traction and moment

Coordinates:

Referring to Fig. 2.7, *OQ* is a slipline with range ϕ and *OX* and *OY* are the Cartesian co-ordinate axes. $O\overline{X}$ and $O\overline{Y}$ are the moving or Mikhlin coordinate axes. At any point *P* with angular coordinate *t*, the differential arc length *ds* can be expressed in terms of its components as,

$$d\bar{X} = ds\cos(\phi - t)$$

and $$d\bar{Y} = -ds\sin(\phi - t) \tag{2.22}$$

The coordinates of the point *Q* are, therefore, given by,

$$\bar{X} = \int_0^\phi ds\cos(\phi - t) = \int_0^\phi R(t)\cos(\phi - t)dt$$

$$\bar{Y} = -\int_0^\phi ds\sin(\phi - t) = -\int_0^\phi R(t)\sin(\phi - t)dt \tag{2.23}$$

where, $ds = R(t)dt$. If R(t) is expanded as a power series such that

$$R(t) = \sum_{n=0}^{\infty} \frac{r_n t^n}{n!} \tag{2.24}$$

Then $\bar{X}$ and $\bar{Y}$ are given by [99]

$$\bar{X} = \sum_{n=0}^{\infty} \frac{t_n \phi^n}{n!}$$

$$\bar{Y} = \mp \sum_{n=0}^{\infty} \frac{t_n \phi^{n+1}}{(n+1)!} \ . \tag{2.25}$$

where t_n's are given by the recurrence relation,

$$t_{n+1} - t_{n-1} = \left| r_n \right| , \ t_0 = 0 \text{ and } t_1 = \left| r_0 \right|$$

The minus or plus sign is taken according as whether R(t) is positive or negative. Once the moving coordinates of the point Q are known, the Cartesian coordinates can be calculated from the relationships,

$$x = \bar{X} \cos\phi - \bar{Y} \sin\phi$$

and $$y = \bar{X} \sin\phi + \bar{Y} \cos\phi \tag{2.26}$$

Traction

Referring to Fig. 2.7, if p_0 is the hydrostatic pressure at the origin O, the hydrostatic pressure at the point P is given by

$$p = p_0 \mp 2kt$$

The negative or positive sign being chosen according as whether the slipline is an α -line or a β -line and k is the yield stress in shear. The traction along the Mikhlin directions at the point P is given by,

$$dF\,\bar{X} = (p_0 \mp 2kt)ds\sin(\phi - t) \mp kds\cos(\phi - t)$$

$$dF\,\bar{Y} = (p_0 \mp 2kt)ds\cos(\phi - t) \mp kds\sin(\phi - t) \qquad (2.27)$$

where *ds* is the differential arc length.

Integrating equation (2.27) and substituting $ds = R(t)dt$, the total traction for the slipline is given by:

$$F\overline{X} = -p_0\,\bar{Y} \pm k\,\bar{X} \mp 2k\int_0^{\phi} t\sin(\phi - t)R(t)dt$$

and $$F\overline{Y} = p_0\,\bar{X} \mp k\,\bar{Y} \mp 2k\int_0^{\varphi} t\cos(\phi - t)R(t)dt \qquad (2.28)$$

Substituting for *R(t)* (equation 2(a)) the integration finally

$$\int_0^{\phi} t\cos(\phi - t)R(t)dt = \sum_{n=0}^{\infty}\frac{C_n\phi^n}{n!}$$

and $$\int_0^{\phi} t\sin(\phi - t)R(t)dt = \sum_{n=0}^{\infty}\frac{C_{n-1}\phi^n}{n!} \qquad (2.29)$$

where, the coefficients C_n's are given by the recurrence relation.

$$C_{n+1} = n|r_{n-1}| - C_{n-1}$$

and $$C_0 = C_{-1} = 0$$

Moment

Unfortunately, a series representation for the moment *M* does not lead to any simple recurrence relation and recourse must be made to numerical integration. However, the required integrand takes a particularly simple form when expressed in terms of the Mikhlin coordinates ($\bar{X}, \bar{Y}$).

For positive α -line shown in Fig. 2.7 the moment is given by [99]

$$\frac{M}{k} = \int_0^{\phi} \left[\left(\frac{p_0}{k} - 2t \right) \overline{X}(t) + \overline{Y}(t) \right] R(t)\, dt \tag{2.30}$$

2.5 Straight rough boundary operator

Let σ_1 and σ_2 be the vector representation of the bounding sliplines of deforming region *ABC* (Fig. 2.8). *AC* is a straight boundary with the constant shear stress $\tau = mk$ acting on it. Then the families of α -and β lines in *ABC* meet *CA* at constant angles of λ and $\frac{\pi}{2} - \lambda$ respectively, where $\lambda = \frac{1}{2}\cos^{-1}\left(\frac{\tau}{k}\right)$.

Then,

$$\sigma_2 = \left[Q_{\theta\theta} + P_{\theta\theta} (I\cos\lambda - J\sin\lambda)^{-1} (J\cos\lambda - I\sin\lambda) \right] \sigma_1 = G_{\lambda}\sigma_1 \tag{2.31a}$$

$$\sigma_1 = \left[-Q_{\theta\theta} - P_{\theta\theta} (I\sin\lambda + J\cos\lambda)^{-1} (J\cos\lambda + I\sin\lambda) \right] \sigma_2$$

$$= G^{-1}_{\frac{\pi}{2}-\lambda}\, \sigma_2 \tag{2.31 b}$$

where *I* is the unit matrix and *J* the integration operator, which is written as

$$J = \begin{vmatrix} 0 & 0 & 0 & 0 & -- \\ 1 & 0 & 0 & 0 & -- \\ 0 & 1 & 0 & 0 & -- \\ 0 & 0 & 1 & 0 & -- \end{vmatrix}$$

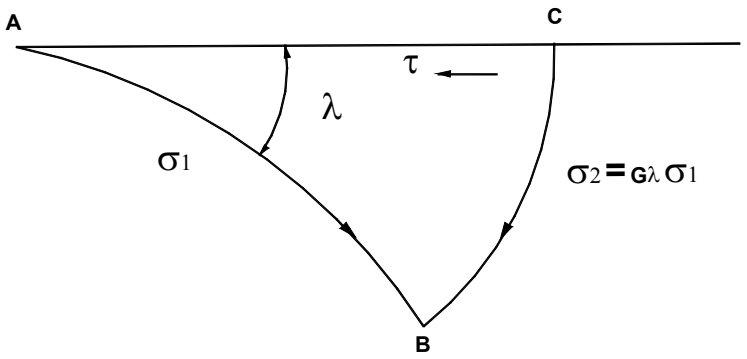

Fig. 2.8: Slipline field adjacent to a straight rough boundary.

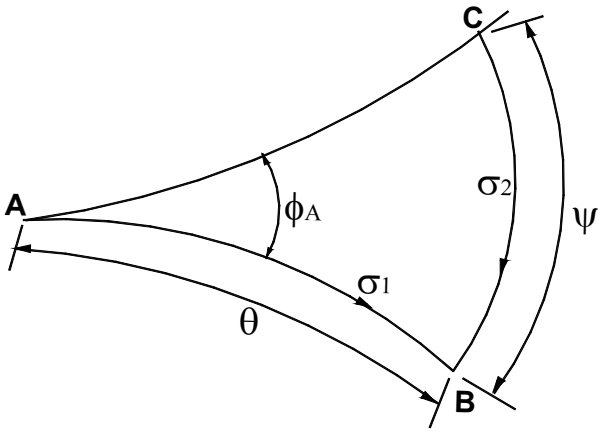

Fig. 2.9: Slipline field adjacent to a curved boundary.

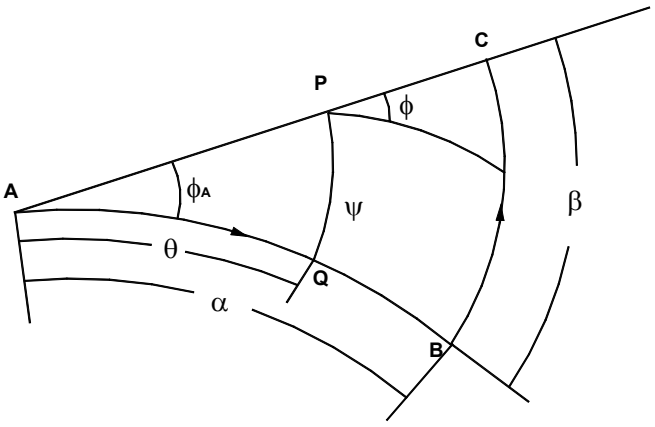

Fig. 2.10: Slipline field adjacent to a rough boundary with Coulomb friction

The two extreme cases are:

a) The boundary is perfectly smooth so that the sliplines meet the boundary at angles $\pm\frac{\pi}{4}$. The straight rough boundary operator then reduces to the smooth boundary operator given by $G_{\frac{\pi}{4}} = Q_{\theta\theta} - P_{\theta\theta}$

b) The boundary is perfectly rough so that the sliplines meet the boundary at *0* degree and $\frac{\pi}{2}$ thus, $G_{\theta} = Q_{\theta\theta} + P_{\theta\theta}J$.

2.6 Adhesion operator

Dewhurst [92,93] has proposed a more general form of matrix operator which generates the slipline field adjacent to an arbitrary curved surface with a constant interfacial shear stress τ acting on it or a flat surface with the interfacial shear stress governed by Coulomb's law of friction. In the present investigation the above matrix operator has been used to construct the field when interfacial shear stress follows the adhesion friction law.

Referring to Fig. 2.10, the boundary *AC* is defined by a linear relationship in the slipline coordinate system,

$$\psi = B_0\theta \tag{2.32}$$

and along the boundary, the angle of intersection of the sliplines with the boundary is given by:

$$\phi = \phi_A + B_1\theta \tag{2.33}$$

Coefficient B_0 and B_1 are constants and ϕ_A is the intersection angle at point *A*.

Slipline *AB* is defined by column vector $a = \{a_n\}$ such that the radius of curvature at any angular position θ from *A* is given by:

$$R(\theta) = \sum_{n=1}^{\infty} \frac{a_n \theta^n}{n!} \tag{2.34}$$

Then the radius curvature of line *CB* is given by:

$$S(\psi) = \sum_{n=1}^{\infty} \frac{b_n \psi^n}{n!} \tag{2.35}$$

where, vector $b = \{b_n\}$ is obtained from a simple matrix transformation:

$$b = AF \; a$$

Where, AF is the general matrix operator as established by Dewhurst [92] and is given as follows:

$$AF = Q_{\theta(B\theta)} + P_{(B\theta)\theta}(K_\phi MJ - m_0 k_{(\phi+\frac{\pi}{2})} M)^{-1} \quad (k_\phi - B_0 k_{(\phi+\frac{\pi}{2})} J) \tag{2.36}$$

where, P, Q are the unstarred matrix operators defined earlier (equation 2.18) and *J* and *M* are matrices given as,

$$J = \begin{vmatrix} 0 & 0 & 0 & -- & -- \\ 1 & 0 & 0 & -- & -- \\ 1 & 1 & 0 & -- & -- \\ 1 & 1 & 1 & 0 & -- \\ 1 & 1 & 1 & 1 & 0 \end{vmatrix} \tag{2.37}$$

$$M = \begin{vmatrix} 1 & 0 & 0 & -- & -- \\ 0 & B_0 & 0 & -- & -- \\ 0 & 0 & B_0^2 & 0 & -- \\ -- & -- & -- & -- & -- \end{vmatrix} \tag{2.38}$$

and k is a lower triangular matrix whose general term k_{ij} at row i and column j is given by:

$$k_{ij} = \sum_{p=0}^{\text{int}\left(\frac{i-j}{2}\right)} \binom{i}{j+2p} M_1^{(i-j-2p)} \sin^{(i-j-2p)} \phi_A \binom{j+2p)}{p} M_0^p \qquad \text{for } i \geq j$$

$$= 0 \quad \text{for } i<j \tag{2.39}$$

Subroutines:

The subroutines used for the present slipline field analysis are similar to those given in references [89,93,94].

-ooOoo-

Chapter 3

CHAPTER 3

A SLIPLINE FIELD ANALYSIS OF FREE-CHIP ORTHOGONAL MACHINING WITH ADHESION FRICTION AT RAKE FACE

3.1 Introduction

The subject of friction is important in all engineering applications wherever solid surfaces are in sliding contact with each other. This is particularly true in metal working processes where the sliding pair of surfaces are metals and where plastic deformation of the softer of the two metals usually takes place under conditions of high normal pressure. In orthogonal metal cutting process frictional drag apparently is encountered on the rake face of the tool between the chip and the tool and, as the tool wears, additional frictional drag also occurs between the flank of the tool and the work piece. Friction at these contact regions plays a decisive role in chip formation, determination of cutting forces, stresses, strains and flow of work material in the primary and secondary shear zones.

It is now known that the friction process in metal cutting is greatly different from that with the same metal pair undergoing conventional sliding [59-61]. This is because in metal cutting relatively large forces act over a small contact area between the tool and the chip which results in the *real* area of contact being nearly equal to the *apparent* area of contact over a portion of the *natural* contact length. In mechanical theories of chip formation such as the slipline field analysis, however, this complex nature of tool-chip interface friction is not taken into account and the analysis is carried out assuming the frictional shear traction in the *natural* contact length to be either constant [73,85,100-103] or is governed by Coulomb's law [55,58,71]. Slipline solutions

with *sticking* contact over a portion of the tool-chip contact length and *slipping* contact over the rest has also been proposed [79].

It is now generally recognized that friction characteristics at the tool-chip interface is adhesion where the friction force stems from shear fracture of the bonded asperities. Measurement of contact stress distribution at this interface using split tool dynamometers [50-53] or photo-elastic tools [47-49] are in general found to be in agreement with this observation. The empirical equation that is known to describe this friction condition may be stated as [65]

$$\tau = k\left[1 - e^{-\left(\frac{\mu\sigma_n}{k}\right)^{n_p}}\right]^{\frac{1}{n_p}} \tag{3.1}$$

where τ is the friction stress, σ_n is the normal stress, μ is the low stress level friction coefficient and n_p is a constant whose value depends on the tool-work material combination.

The fact that friction characteristics at the chip-tool interface is likely to be adhesion was proposed much earlier by Trent [62], Finnie and Shaw [64] and Usui and Shirakashi [70]. An exponential relation between τ and σ_n to describe this friction condition had also been suggested by Finnie et al [64] and Usui et al [70].

In the present investigation slipline solutions for the orthogonal machining process are proposed where the rake face friction is governed by the adhesion friction law as stated by equation (3.1). The field is similar to that suggested by Dewhurst [73] and is analyzed by the matrix operational procedure developed by Dewhurst and Collins [89] and Dewhurst [92,93]. A linear relation between the angular range of α- and β- lines in the secondary shear zone is assumed. The limit of validity of the proposed solutions is

determined with the help of Hill's overstressing criteria [45]. Machining parameters such as the cutting forces, cutting ratio, chip curl radius and contact lengths are estimated for different values of tool rake angle and friction conditions. Results from the theoretical analysis are also compared with experiments.

3.2 Slipline field solution

The slipline field satisfying the boundary condition on stress and velocity for the orthogonal machining problem under consideration is shown in Fig. 3.1 along with its associated hodograph. This field (henceforth to be referred to as Field I) was originally proposed by Dewhurst [73], but the chip formation in his study was assumed to take place under condition of constant shear stress ($\tau = mk$).

Referring to Fig. 3.1.(a) it may be seen that the field consists of the primary shear line *OPS*, the singular field *PSQ*, and the secondary shear zone *QRS*. The chip material slides on the rake face *RS* in accordance with the adhesion friction law given by equation (3.1). It is assumed that the chip material on leaving the plastically deforming zone undergoes rigid body rotation forming a chip of constant curvature.

Let the column vector in the power series expansion of the radius of curvature of the base slipline *RQ* be indicated by σ. Hence,

$$SQ = AF_{\alpha\phi_R}\sigma \tag{3.2}$$

and

$$PQ = Q_{\beta\psi}\, AF_{\alpha\phi_R}\sigma \tag{3.3}$$

where, *AF* is the adhesion friction operator that constructs the field between the slipline *RQ* and the tool face *RS* consistent with the friction law stated by equation (3.1), α is the angular range of the slipline RQ and ϕ_R is the friction angle at R.

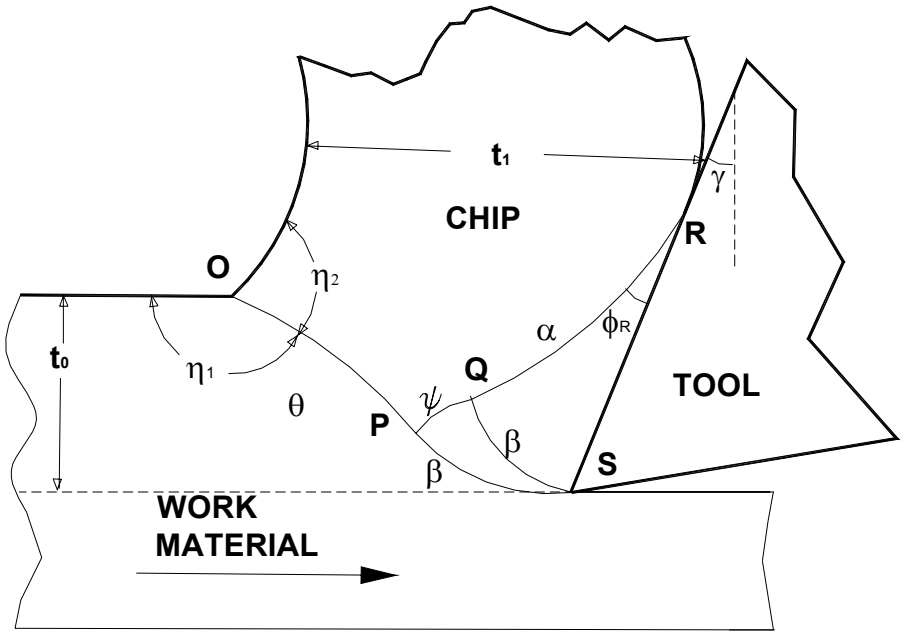

(a)

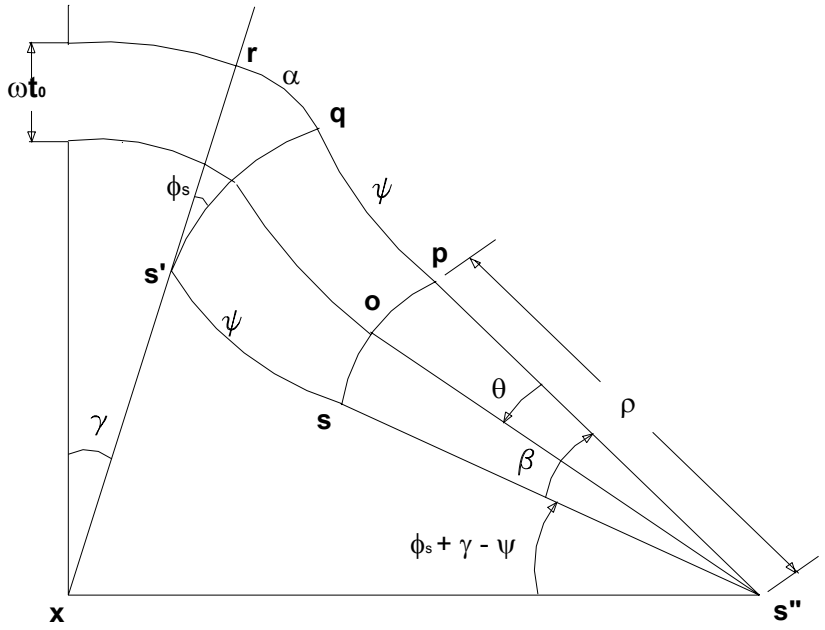

(b)

Fig. 3.1: Field I (a) Slipline field (b) Hodograph

The work material on crossing the primary shear line suffers a velocity discontinuity of magnitude ρ. Therefore, circular arc *sp* in the hodograph plane (Fig. 3.1 (b)) is expressed as,

$$ps = \rho \bar{c} \tag{3.4}$$

where, $\bar{c}$ is a column vector representing an unit circle.

The geometrical similarity between the sliplines *RQ*, *PQ* (Fig. 3.1(a)) and their hodograph images *rq*, *pq* (Fig. 3.1(b)) may be represented by the relations,

$$rq = \omega \sigma \tag{3.5}$$

and $$pq = \omega Q_{\beta\psi} AF_{\alpha\phi_R} \sigma \tag{3.6}$$

where, ω is the angular velocity of chip curl.

The curve *s'q* in the hodograph is calculated from the curves *ps* and *pq* using the relation [89]

$$s'q = P_{\beta\psi} \rho \bar{c} + \omega Q_{\psi\beta} Q_{\beta\psi} AF_{\alpha\phi_R} \sigma \tag{3.7}$$

Also, $$rq = AF_{\beta\phi_S} s'q \tag{3.8}$$

where, ϕ_S is the friction angle at S (Fig. 3.1(a)). Using (3.5), (3.7) and (3.8) the matrix equation yielding the column vector σ is finally written as,

$$\left(I - AF_{\beta\phi_S} Q_{\psi\beta} Q_{\beta\psi} AF_{\alpha\phi_R} \right) \sigma = \left(\frac{\rho}{\omega} \right) AF_{\beta\phi_S} P_{\beta\psi} \bar{c} \tag{3.9}$$

where, *I* is the unit matrix and *P*, *Q* are the standard matrix operators as defined in [89,98].

3.3 Method of solution

Field I shown in Fig. 3.1 is of "indirect" type as shapes of none of the slipline curves nor their hodograph images are known a priori. The field was therefore

analyzed by solution to equation (3.9) to determine the shape of the base slipline *RQ*. It may be seen that the angular coordinates α_i, β_i of any point on the rake face *RS* are related by equation (3.1) through equations

$$\frac{\sigma_n}{k} = p_R + 2(\alpha_i + \beta_i) + \sin(2(\phi_R + \alpha_i - \beta_i)) \qquad (3.10(a))$$

and

$$\frac{\tau}{k} = \cos(2(\phi_R + \alpha_i - \beta_i)) \qquad (3.10(b))$$

where, p_R and ϕ_R are the hydrostatic pressure and the friction angle at *R* respectively. With the assumption of adhesion friction this relation becomes non-linear. Following Dewhurst [92,93] this non-linear relation was approximated by the linear relation

$$\beta = m_0 \alpha \qquad (3.11)$$

m_0 in equation (3.11) was evaluated by linear regression analysis from angular coordinates of ten discrete points on *RS* using the equation (refer to Appendix I)

$$m_0 = \frac{\sum_{i=1}^{i=10} \alpha_i^2}{\sum_{i=1}^{i=10} \alpha_i \beta_i} \qquad (3.12)$$

The FORTRAN programme developed for solution to the above field required the input of friction parameters μ, n_p and an initial guess for the field angles θ and ψ and the hydrostatic pressure p_R. The programme first evaluated the friction angle ϕ_R by solution to equation (3.1) at *R* $\left(\tau = k\cos 2\phi_R, \sigma_n = p_R + k\sin 2\phi_R\right)$ and then determined m_0 with the help of equations (3.1), (3.10), (3.11) and (3.12). This value of m_0 along with those of the field angles α, β, θ and ψ were then used to construct the basic matrix operators *P* and *Q* [89,98], the adhesion friction operator *AF* [92,93] and determine the column vector σ for the base slipline *RQ* by solution to equation (3.9). Radius of curvatures of other slipline and hodograph curves were now calculated and the

resultant force and moment on the chip boundary *OPQR* evaluated. For any given value of α, the field angles θ and ψ and the hydrostatic pressure p_R at R should be such that the above force and moment are simultaneously equal to zero. This condition may be mathematically stated as

$$F(Z) = 0 \tag{3.13}$$

where, Z is the vector of field variables θ, ψ and p_R and F is the vector containing the resulting force system. Equation (3.13) was examined over a range of rake angles and friction parameters μ and n_p. As these equations are non-linear, they were solved by an algorithm developed by Powell [104]. The requirement of force free chip was assumed to be achieved when the values of θ, ψ and p_R were such that the following inequality was satisfied:

$$\left(\frac{F_1}{kt_0}\right)^2 + \left(\frac{F_2}{kt_0}\right)^2 + \left(\frac{F_3}{kt_0^2}\right)^2 \leq 10^{-10} \tag{3.14}$$

where, t_0 is the uncut chip thickness. The optimized field variables so obtained were then used to compute the machining parameters such as the cutting and thrust forces, chip curl radius and chip-tool contact length. The program incorporated flatness, traction and mass-flux checks to test the accuracy of solution [88]. It also contained checks to determine whether Hill's inequalities for overstressing [45] were violated at the rigid vertices at O. With reference to Fig. 3.1(a), these may be written as,

$$\frac{p_0}{k} \leq 1 - 2\cos\left(\eta_1 - \frac{\pi}{4}\right), \quad \eta_1 \leq \frac{3\pi}{4} \tag{3.15(a))}$$

$$\frac{p_0}{k} \leq 1 + 2\cos\left(\eta_1 - \frac{3\pi}{4}\right), \quad \eta_1 \geq \frac{3\pi}{4} \tag{3.15(b))}$$

$$1 + 2\left(\eta_2 - \frac{\pi}{4}\right) \geq \frac{p_0}{k} \geq -1 + 2\cos\left(\eta_2 - \frac{3\pi}{4}\right)$$

and $$\eta_2 \geq \frac{\pi}{4} \qquad (3.15(c))$$

where, η_1 and η_2 are the vertex angles and p_O is the hydrostatic pressure at O.

It may be seen that the above field has four degree of freedom given by the field angles α, ψ, θ and the hydrostatic pressure p_R. As there are only three boundary conditions to be satisfied for a force free chip, the field is non-unique in nature.

3.4 Results and discussion

The proposed solution range satisfying the free chip equilibrium condition for values of μ=1.0 and n_p=1.0, 2.0 is presented in Fig. 3.2. The figure shows the limits on the allowable values of field angle ψ for which the vertex angles η_1 and η_2 are not overstressed. Referring to this figure it may be seen that for any particular value of tool rake angle γ, the maximum permissible value of ψ must not be greater than that defined by the curve OSL-2. If the value of ψ exceeds this limit, the vertex angle η_2 is overstressed. It may also be seen that for cutting tools with rake angles less than 20 degrees the lower limit on ψ is zero. This is indicated by the straight line LSL in Fig. 3.2. For this case Field I reduces to that suggested by Lee and Shaffer [56]. For tools with rake angles greater than that defined by the Lee and Shaffer limit (LSL) the minimum value of ψ can not be less than that given by the curve OSL-1. If ψ has a value less than this, the vertex angle η_1 is overstressed. For higher values of μ or n_p the curves OSL-2 and OSL-1 shift to the right and for lower values they shift to the left.

The results of computation of machining parameters obtained from the present slipline field analysis are shown in figures 3.3-3.10 for values of μ equal to 1.0 and 2.0 and for n_p =1.0 and 2.0 where, these are compared with the experimental observations of Eggleston et al [105]. Referring to the above figures it may be seen that for any given value of tool rake angle γ, the solution is not uniquely defined but lie

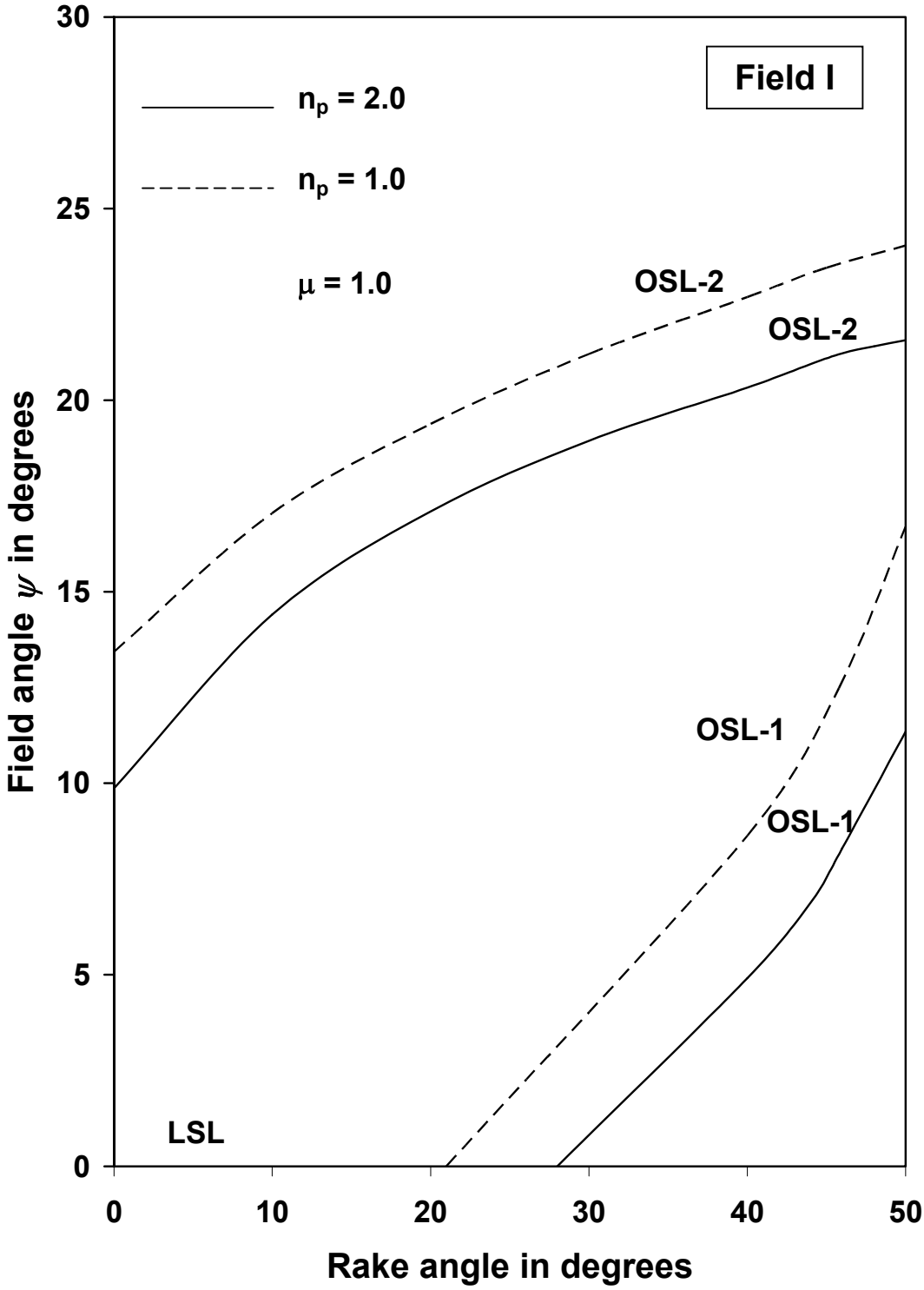

Fig. 3.2: Range of allowable values of field angle ψ for different friction parameters and rake angles.
(OSL-2: Overstressing at η_2, OSL-1: Overstressing at η_1, LSL: Lee and Shaffer's limit)

within a range bounded by the limits OSL-2 and LSL or limits OSL-2 and OSL-1 as discussed earlier. The difference in the two limits, however, decreases as the rake angle increases. Rake angle, rake friction and n_p are found to be the most important variables in metal machining that influence the cutting force, the cutting ratio and the chip curvature (figures 3.3-3.9). The cutting and thrust forces and the cutting ratio decrease as γ increases but increase as μ increases. Referring to Fig. 3.10, it may be seen that tool-chip contact length decreases as rake angle increases. Hence the average normal and shear stresses (total force / contact length) on the tool face increases as rake angle increases (figures 3.11 and 3.12) though, the cutting and thrust forces decrease. The variation of average Coulomb coefficient of friction on the rake face with rake angle as calculated from the contact stresses is shown in Fig. 3.13 for n_p=1.0, μ=1.0, 2.0 and in Fig. 3.14 for μ =1.0, n_p =1.0, 2.0. The figure indicates that the Coulomb friction coefficient is not uniquely determined by the rake angle γ, but may have a range of allowable values for any particular value of γ. The absolute value of the friction coefficient however is found to decrease with increase in the rake angle. It may also be seen that except in respect of contact length (Fig. 3.10), there is excellent agreement between theory and experiment. For the same rake angle, experimental results show wide scatter in the values of machining parameters and this may be due to the non-unique nature of the machining process as predicted by the present analysis.

For compression of a rigid-perfectly plastic strip between parallel dies, the average normal stress varies with aspect ratio (die width/strip thickness) [95]. A direct comparison between machining and compression is rather difficult to visualize, but aspect ratio in machining can be tentatively defined as the ratio of contact length to chip thickness (l_e / t_1). As rake angle increases the natural contact length decreases and so also the chip thickness, but their ratio for Lee and Shaffer's solution remains constant [see

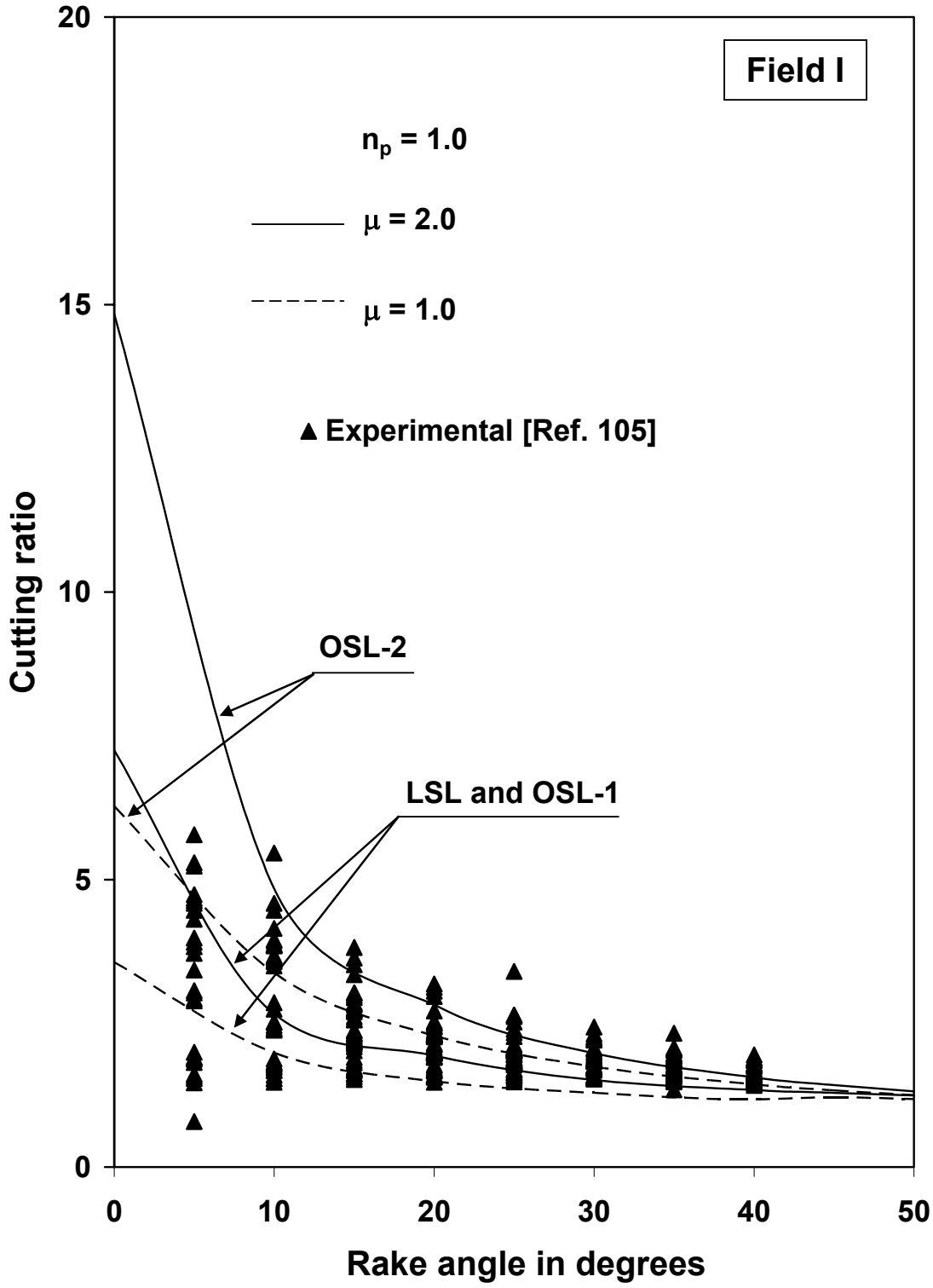

Fig. 3.3: Variation of cutting ratio with rake angle.

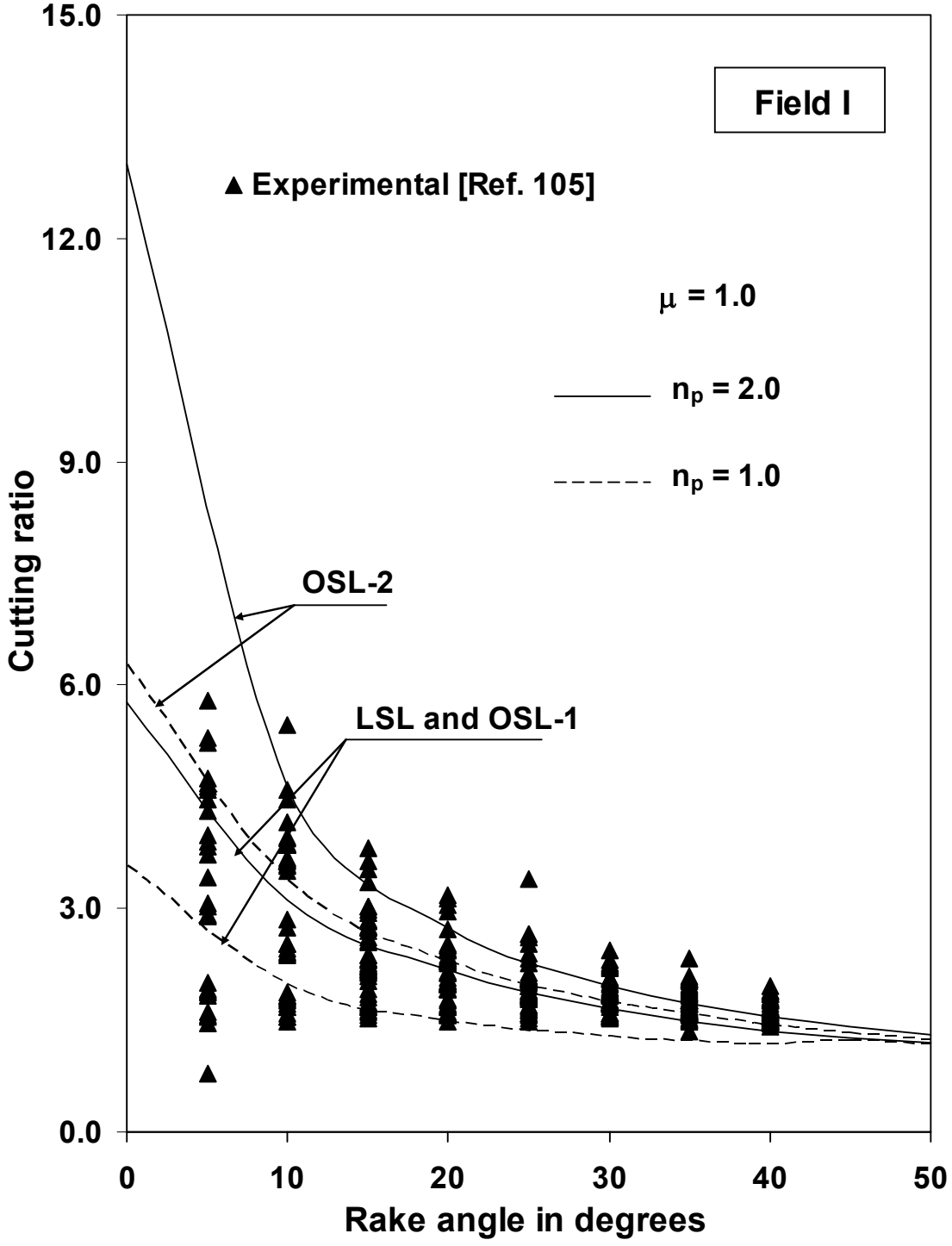

Fig. 3.4: Variation of cutting ratio with rake angle.

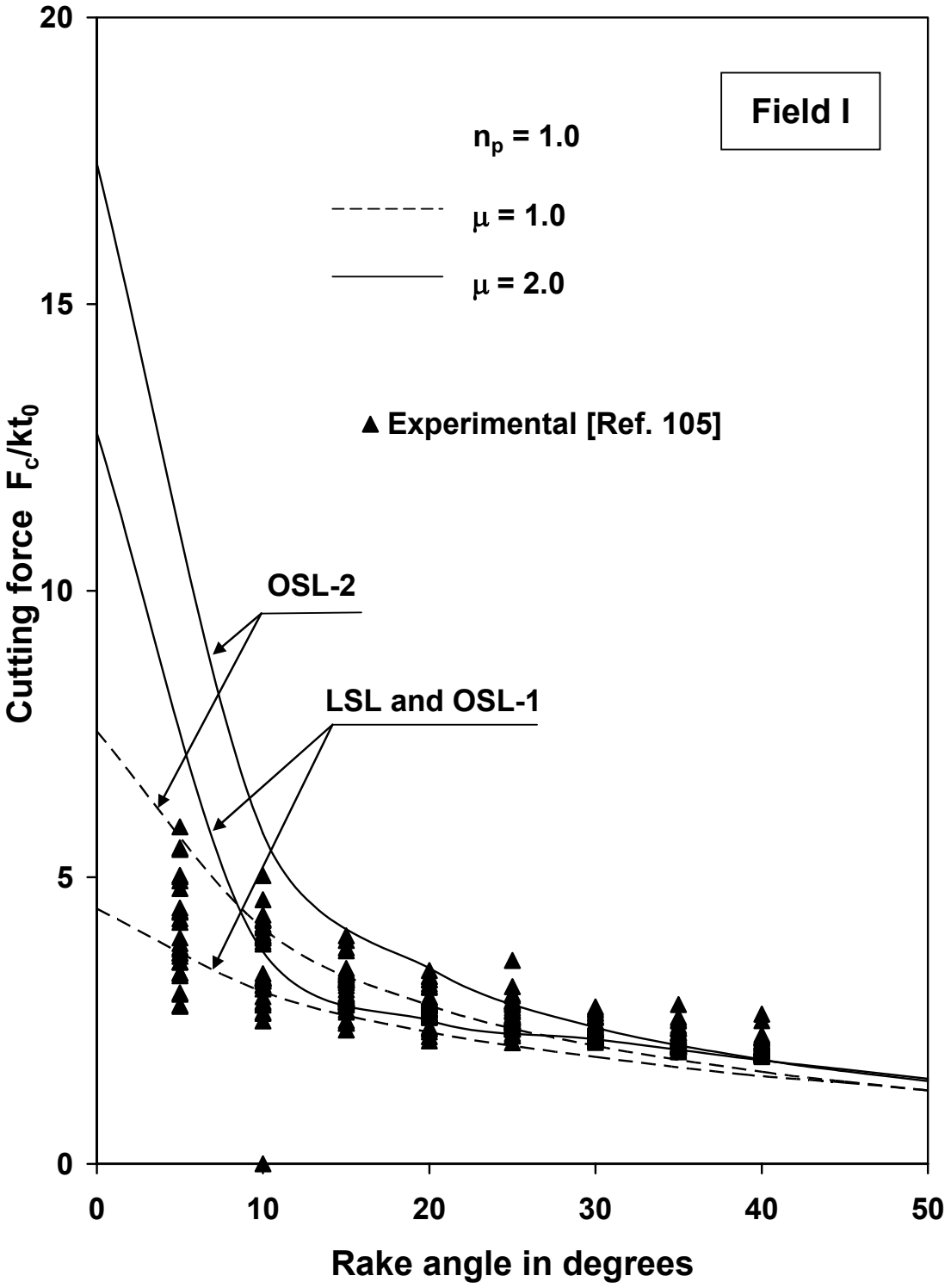

Fig. 3.5: Variation of cutting force with rake angle.

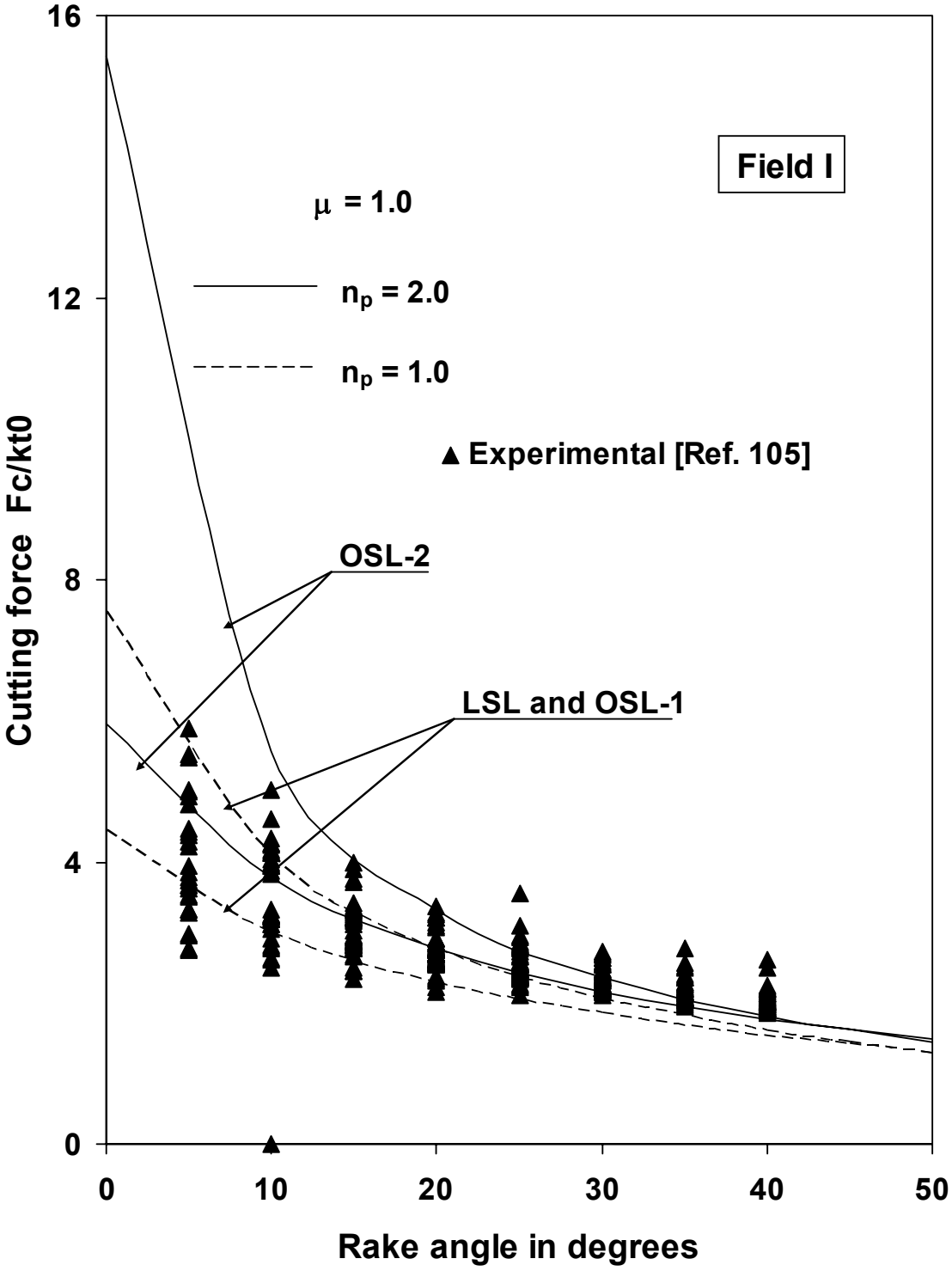

Fig. 3.6: Variation of cutting force with rake angle.

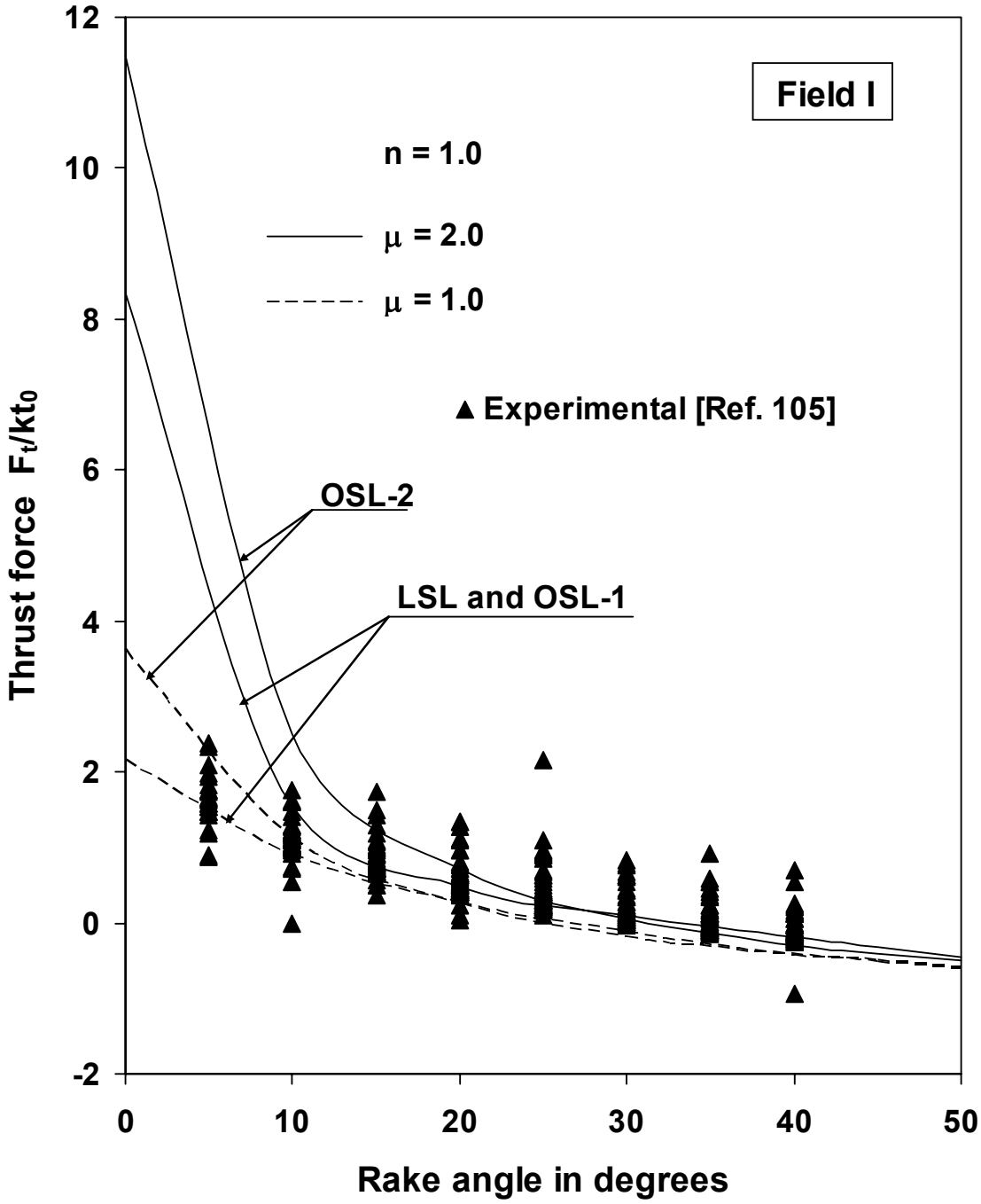

Fig. 3.7: Variation of thrust force with rake angle.

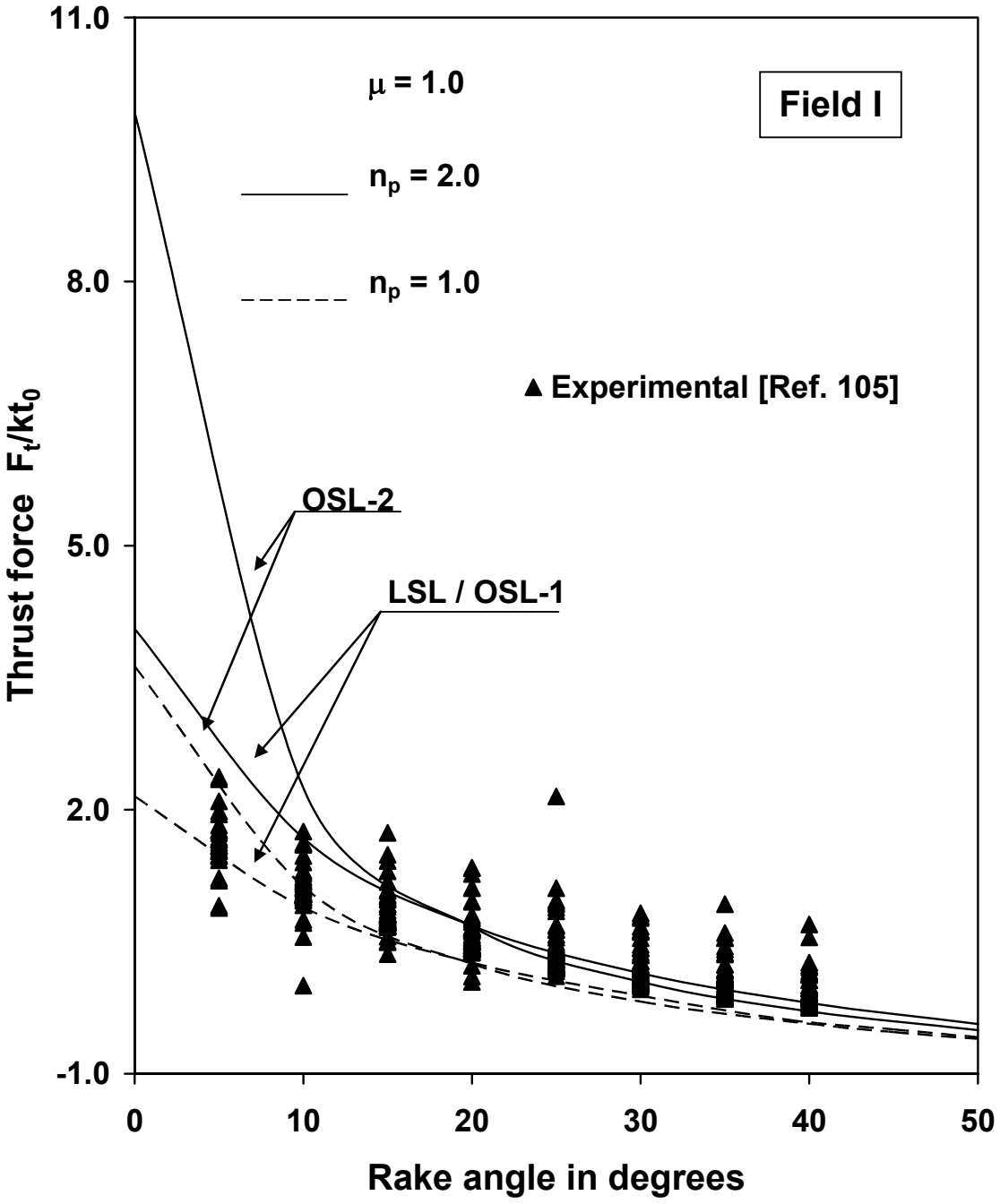

Fig. 3.8: Variation of thrust force with rake angle.

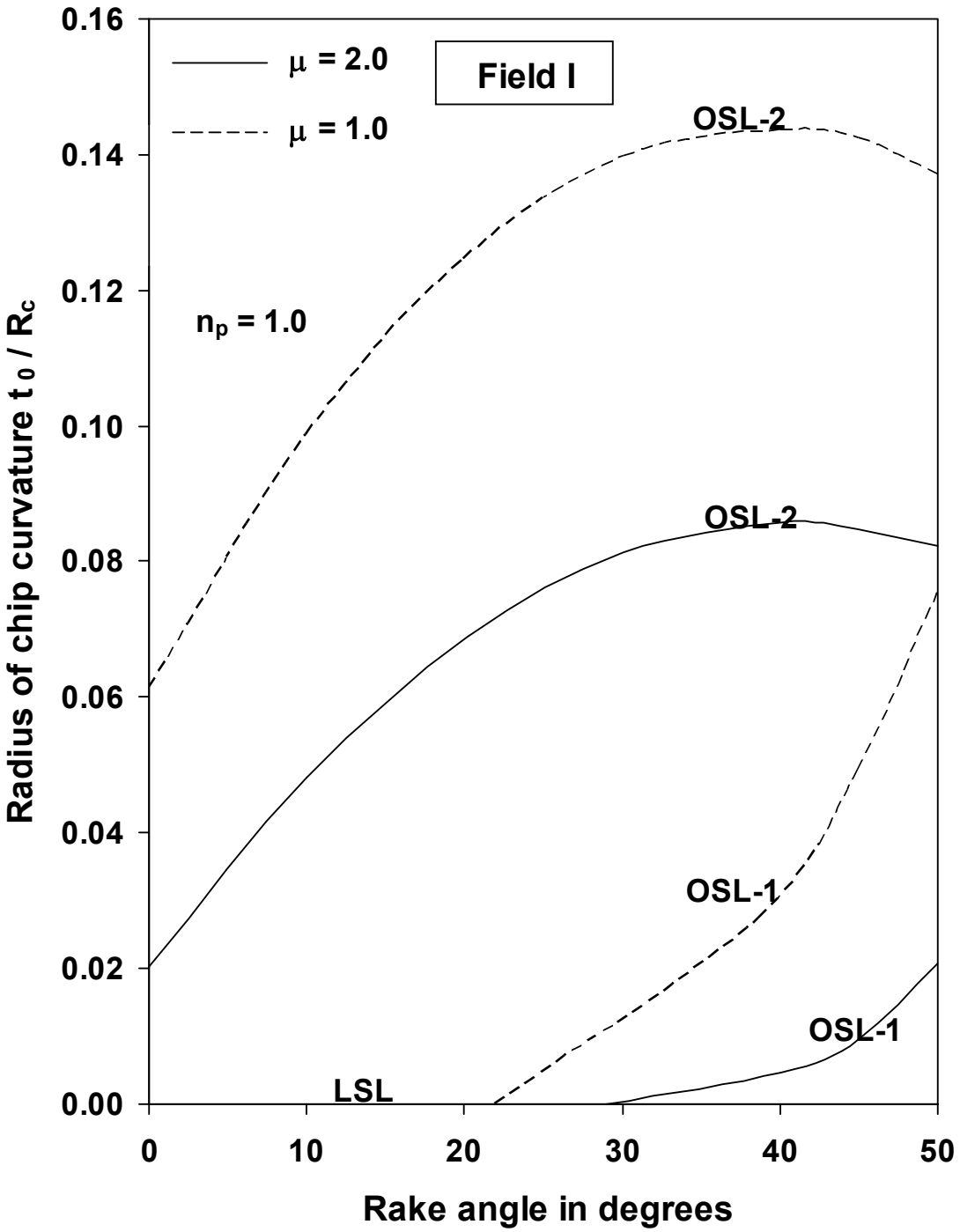

Fig. 3.9: Variation of radius of chip curvature with rake angle.

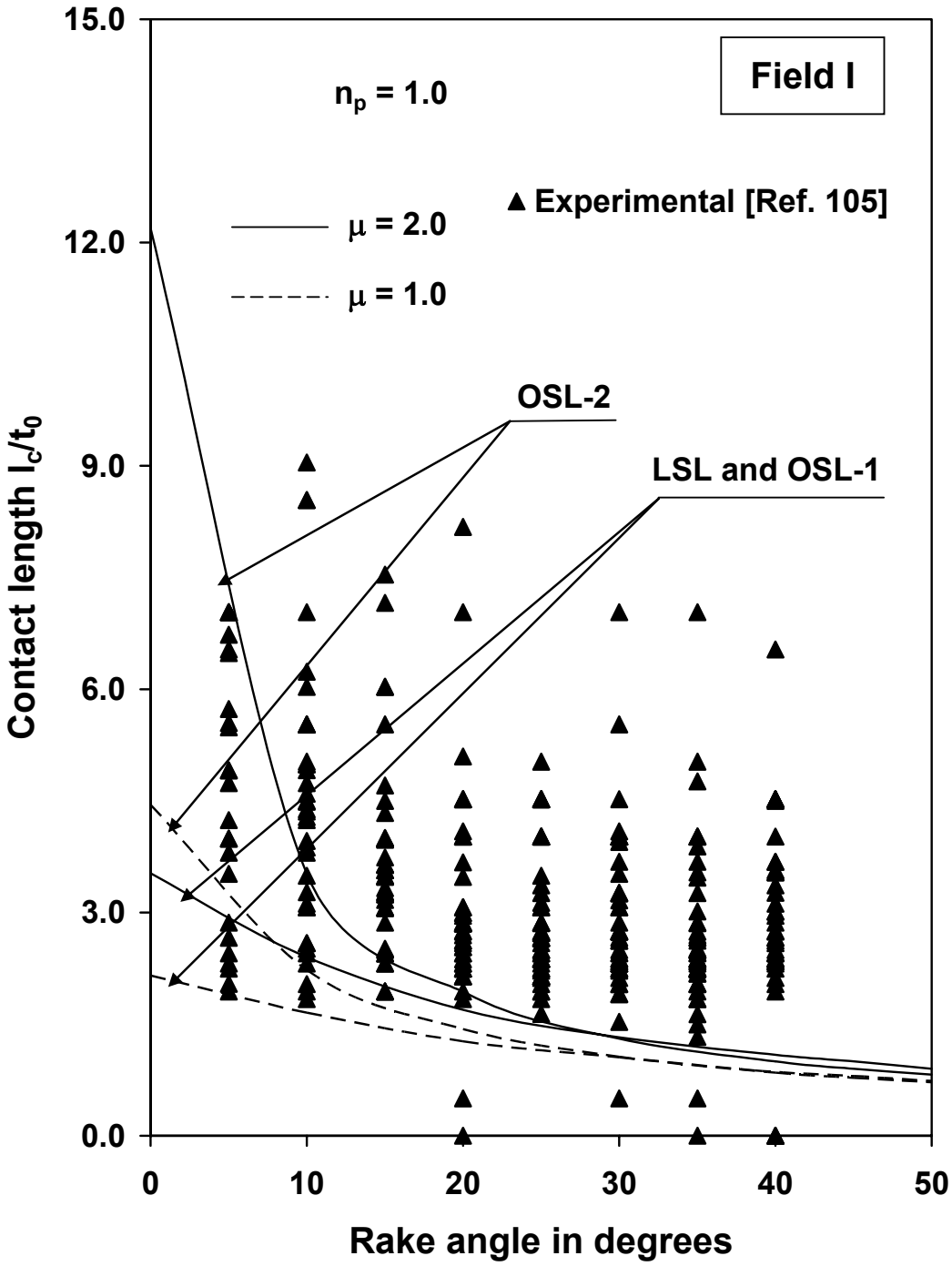

Fig. 3.10: Variation of contact length with rake angle.

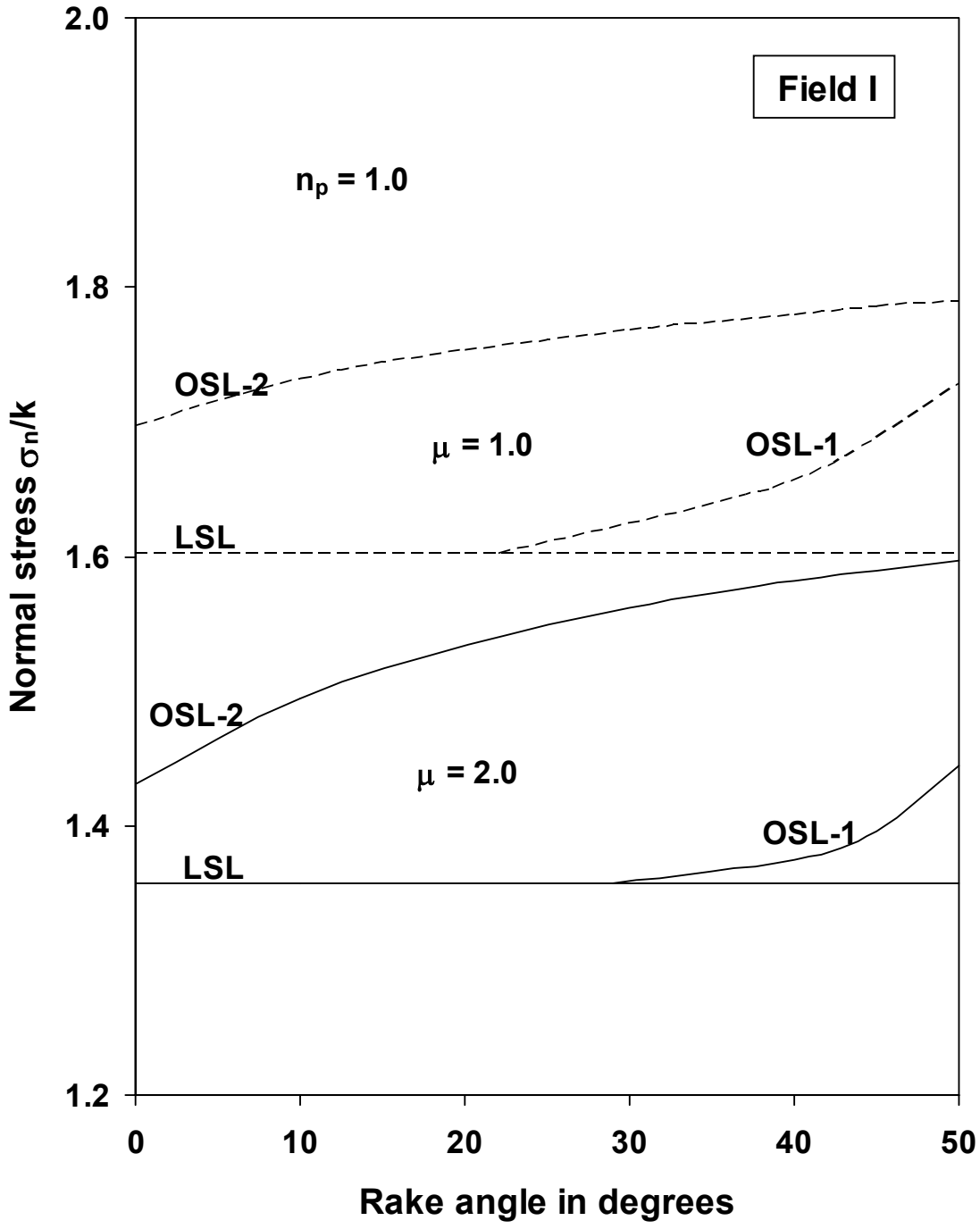

Fig. 3.11: Variation of average normal stress with rake angle.

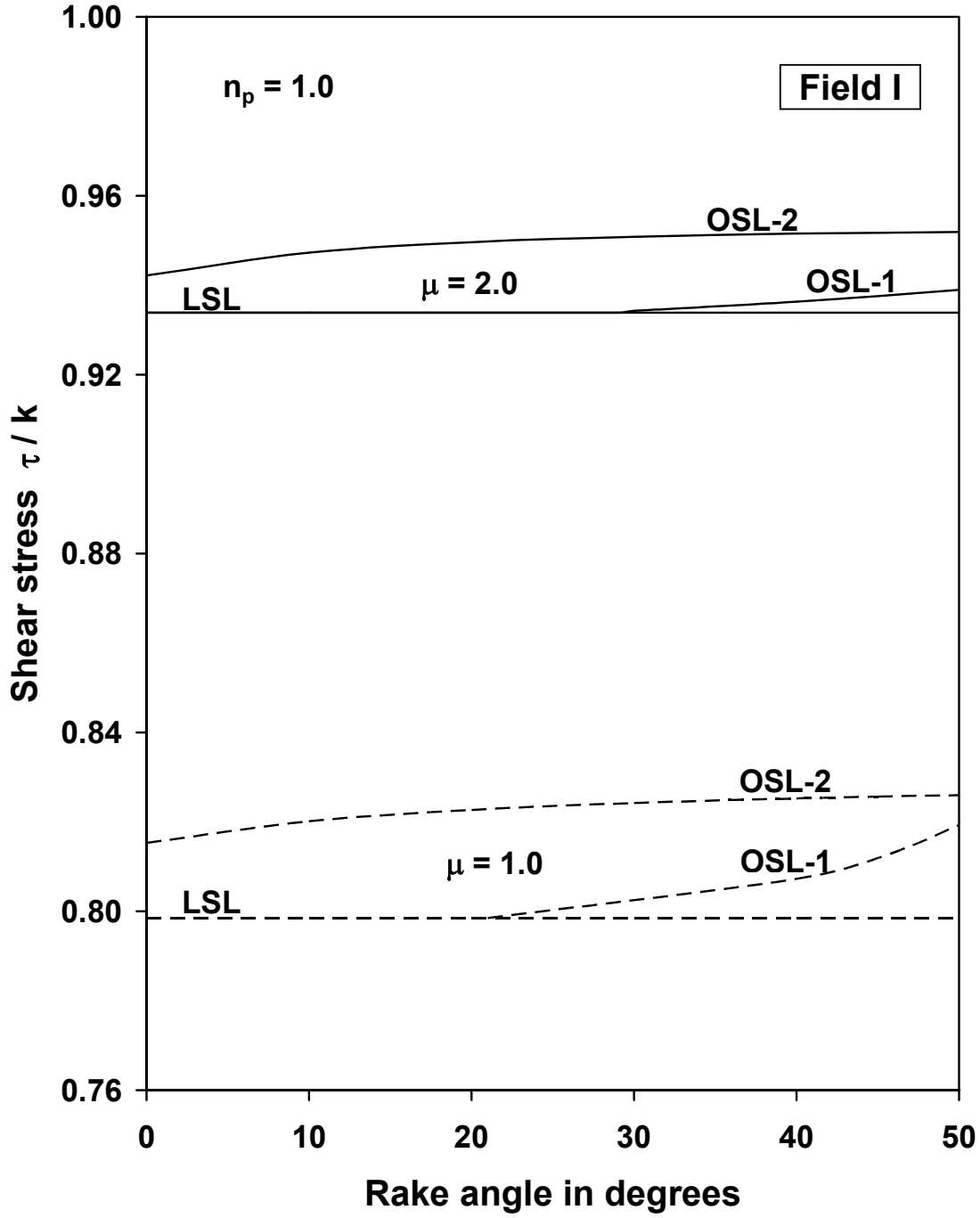

Fig. 3.12: Variation of average shear stress with rake angle.

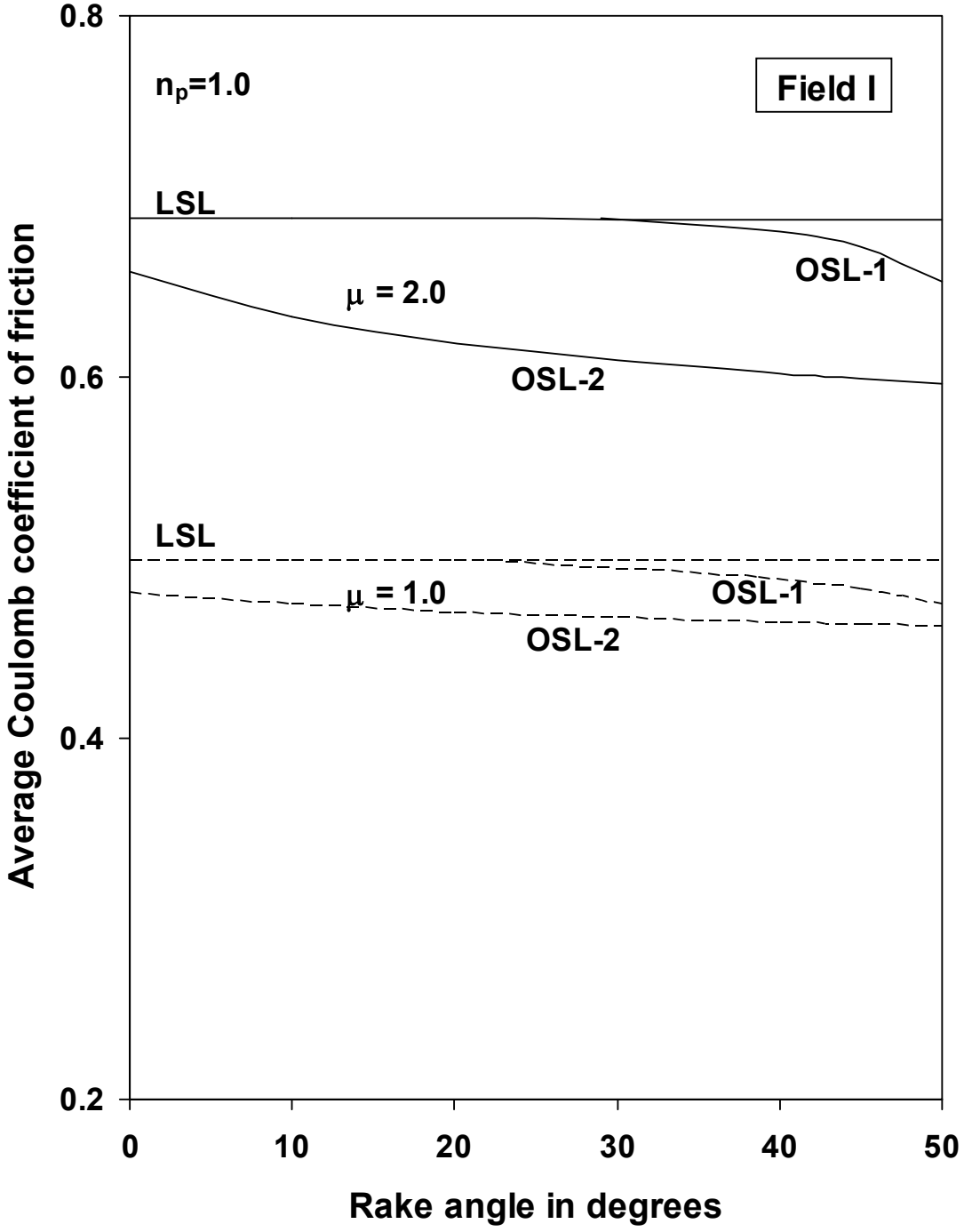

Fig. 3.13: Effect of rake angle on average Coulomb coefficient of friction.

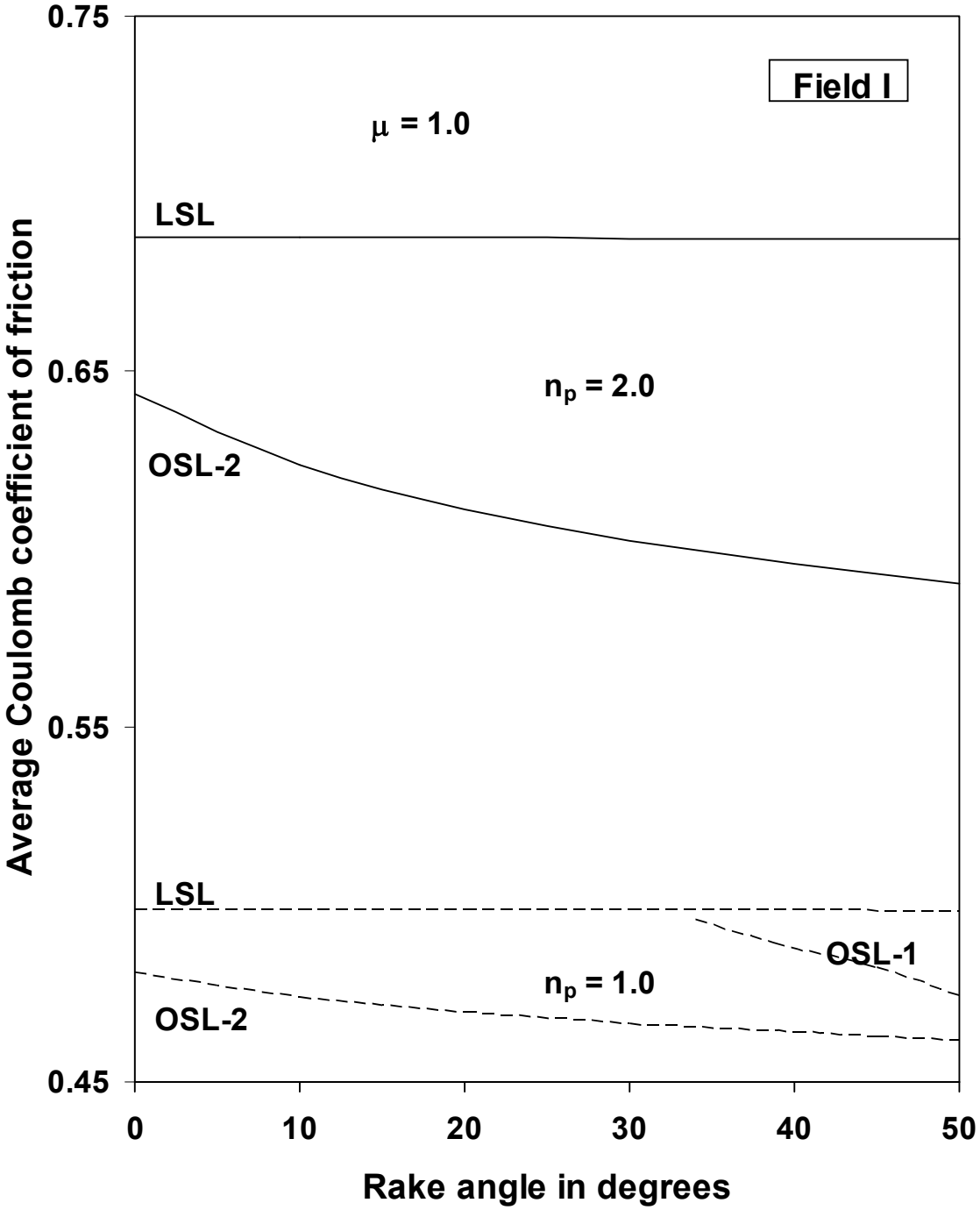

Fig. 3.14: Effect of rake angle on average Coulomb coefficient of friction.

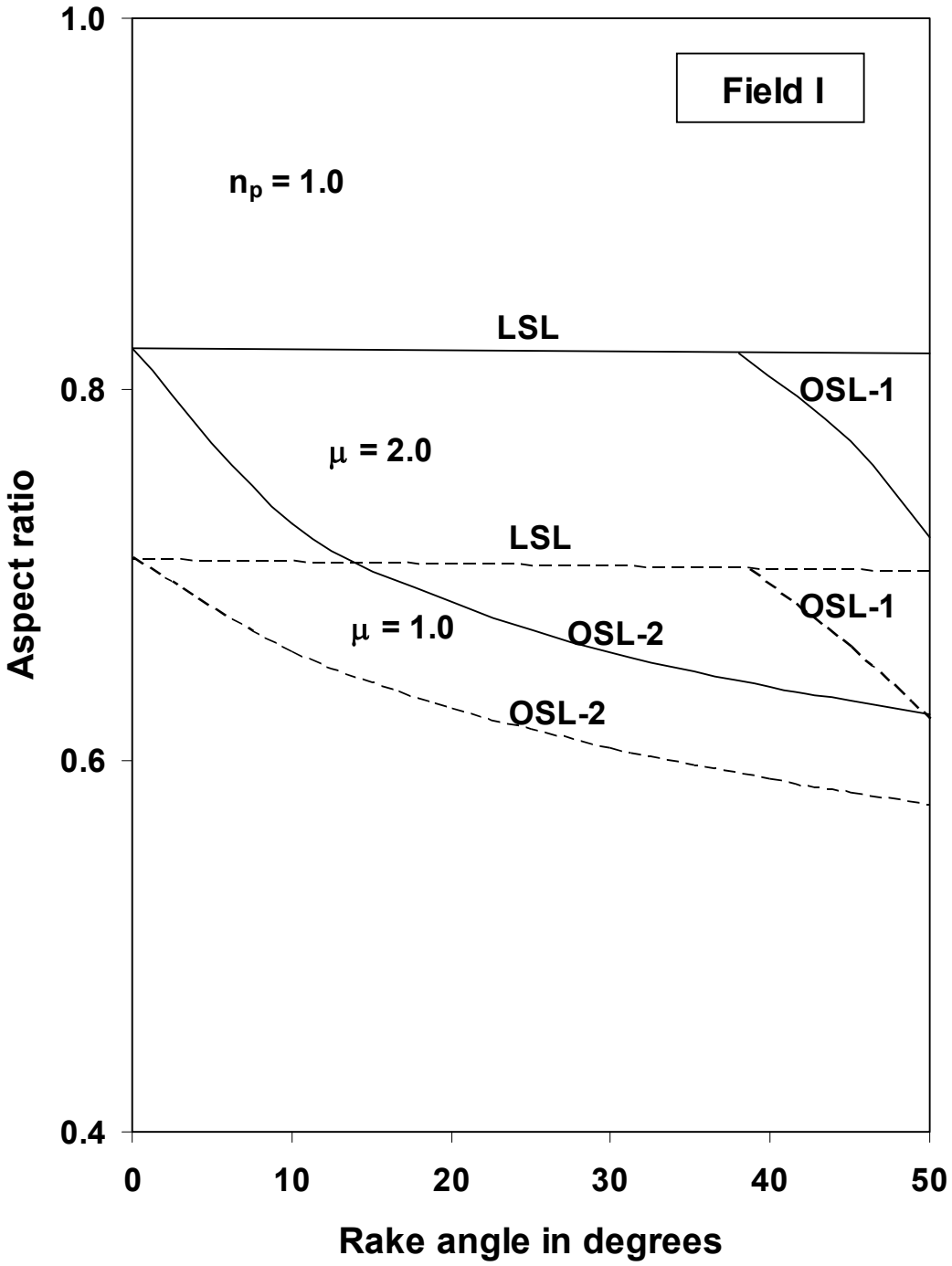

Fig. 3.15: Variation of aspect ratio with rake angle.

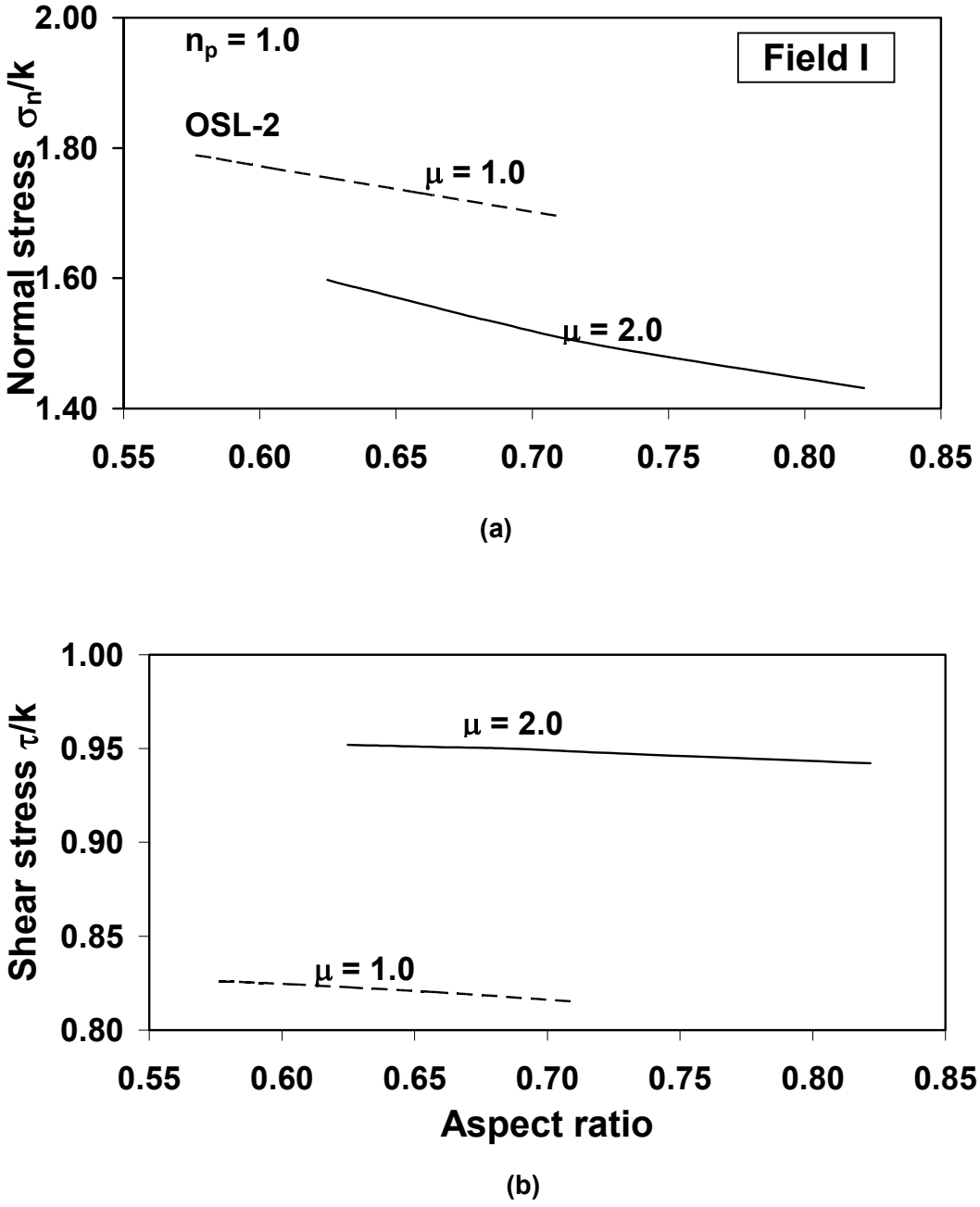

Fig. 3.16: Variation of normal and shear stresses with aspect ratio.

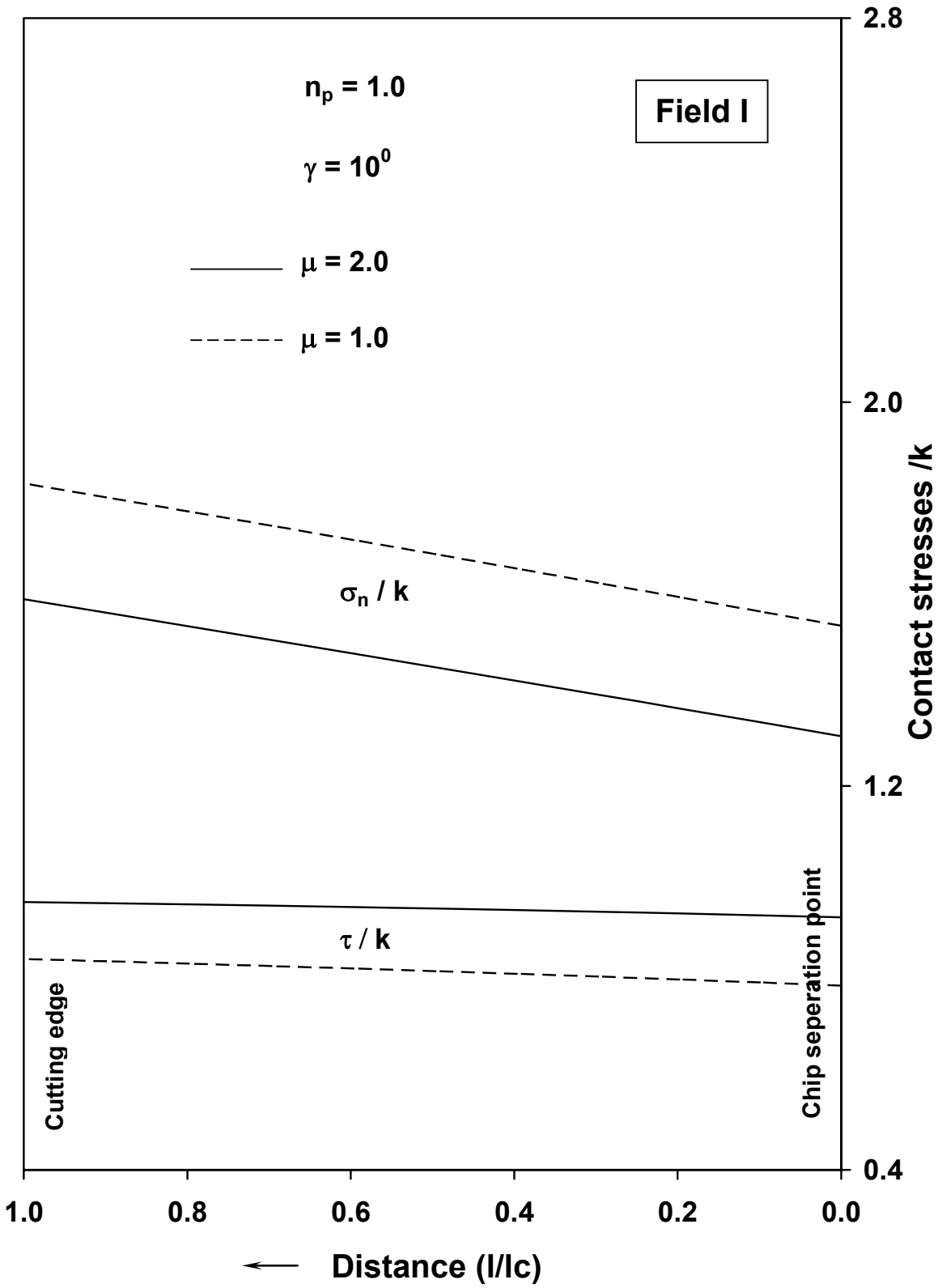

Fig. 3.17: Distribution of contact stresses at chip-tool interface.

Appendix II]. Hence, the normal stress and shear stress remains independent of the rake angle for this case. For other solutions, however, this ratio may vary with rake angles as is demonstrated in Fig. 3.15. Since the aspect ratio decreases with increase in the rake angle, the normal pressure and the shear stress increase as is indicated in figures. 3.16(a) and 3.16(b) respectively [1].

Finnie and Shaw [64] had stated that the average normal pressure decreases as rake angle increases. The present analysis and the related experimental results [105] seem to contradict this view.

The variation of normal and shear stresses along the tool-chip contact length is shown in Fig. 3.17 for a tool with γ=10 degrees. Both contact stresses are found to increase from their minimum value at the chip releasing point to their maximum value at the tool tip. Rake friction has a tendency to lower the contact stresses as may be seen with reference to the above figure.

3.5. Conclusions

Slipline field solutions for orthogonal machining are presented assuming adhesion friction at chip-tool interface. The friction law assumed was that suggested by Maekawa et al [65]. The field is of "indirect" type and is analyzed by the matrix method suggested by Dewhurst and Collins [89] and Dewhurst [92,93].

It is seen that for each value of the tool rake angle γ the solution zones are bounded by the limits imposed by Hill's overstressing criteria [45]. The extent of the solution range, however, decreases as the rake angle increases.

The rake angle, the rake friction and the exponent n_p are found to be the most important variables that influence the machining parameters. The cutting forces and the cutting ratio decrease as the rake angle increases but increase as μ increases. It is seen that the average normal and shear stresses on the tool face increases as rake angle increases. The

computed results show that the Coulomb coefficient of friction calculated from the average normal and shear stresses on the tool rake face is not uniquely determined but has a range of allowable values for any particular value of rake angle. The predicted values of machining parameters such as cutting ratio and cutting forces are found to have excellent agreement with the experimental observations by Eggleston et al. [105]. The agreement in respect of contact length, however is not found to be so good.

3.6. Plotting of some slipline fields and hodographs

The following sections present some slipline fields and the corresponding hodographs for specific field geometries and friction parameters. These slipline fields and their associated hodographs shown in figures 3.18–3.20 are plotted graphically from coordinates calculated from the FORTRAN programme described in section 3.3. The network is constructed by joining consecutive points by a smooth curve.

-ooOoo-

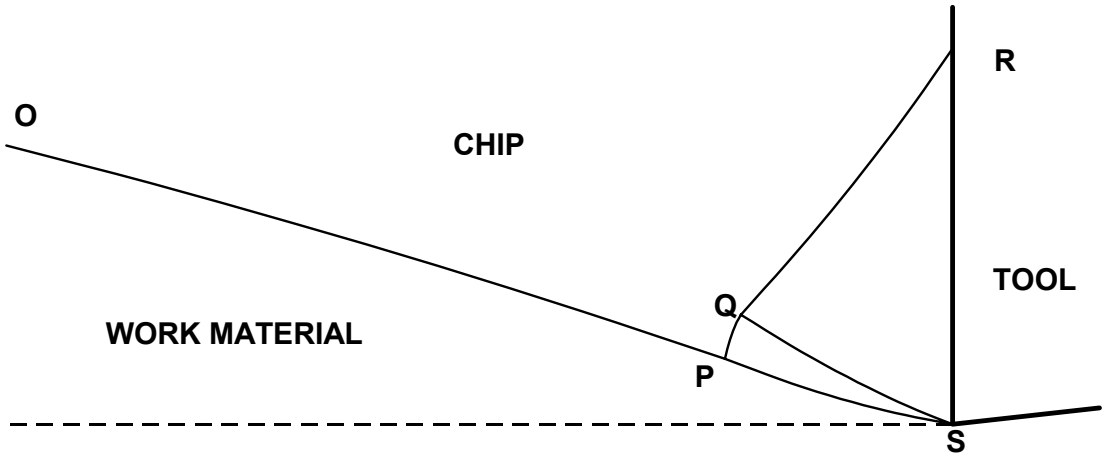

(a)

n_p	1.0
μ	1.0
γ	0^0
α	4.7^0
θ	3.8^0
ψ	13.4^0

(c)

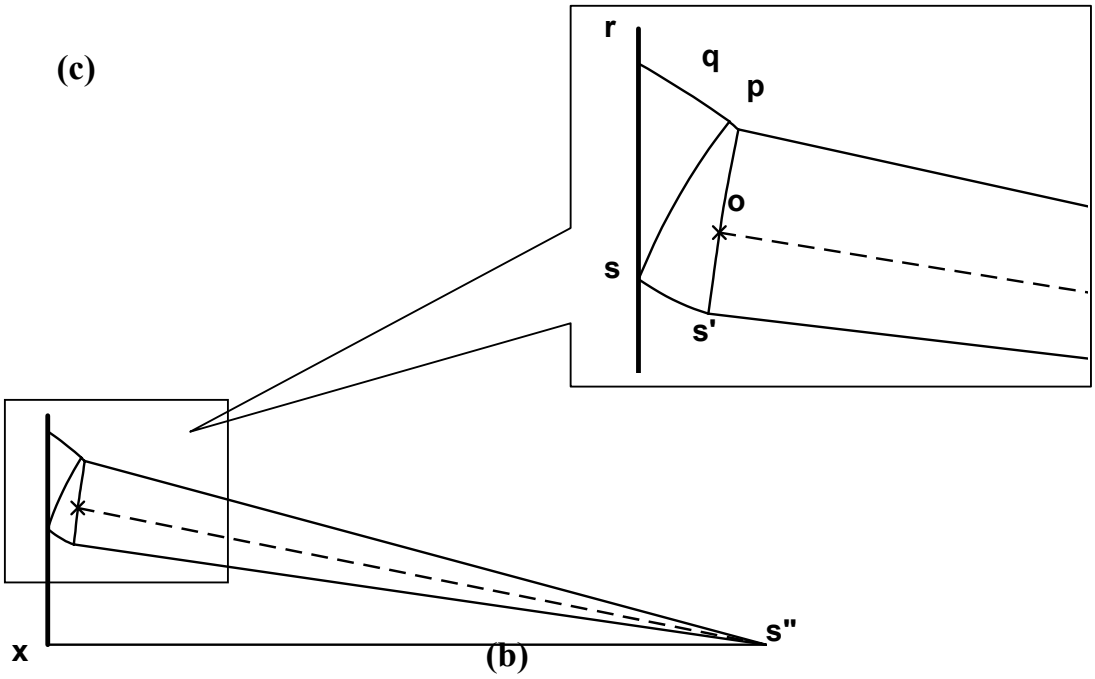

(b)

Fig. 3.18: Graphical plotting of Field I (a) Slipline field (b) Hodograph (c) Table of input/output values.

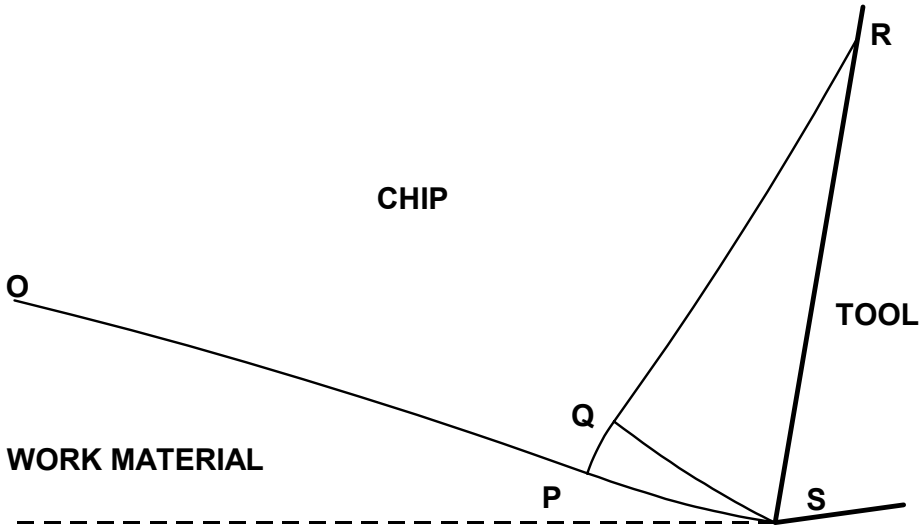

(a)

n_p	1.0
μ	1.0
γ	10^0
α	6.7^0
θ	5.2^0
ψ	15.8^0

(c)

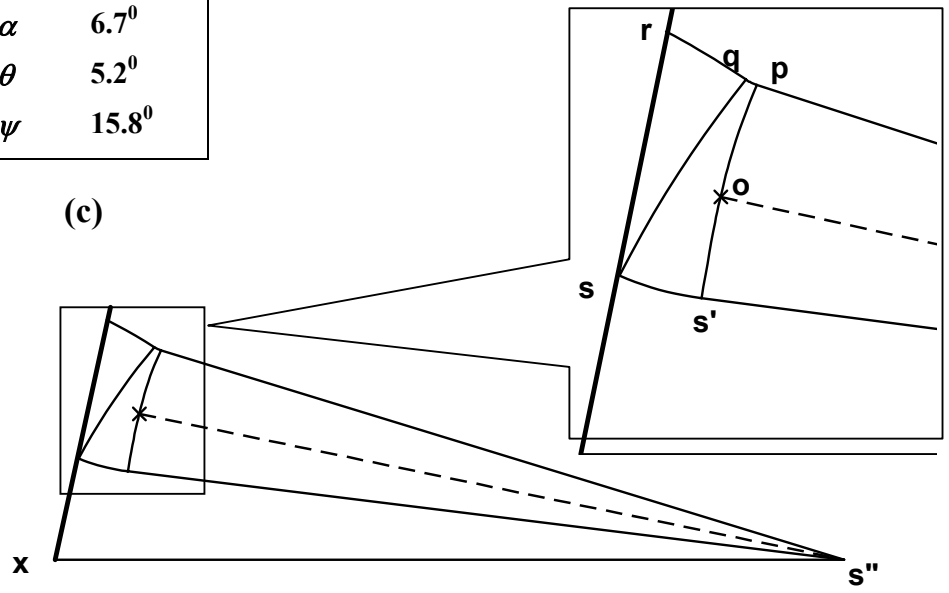

(b)

Fig. 3.19: Graphical plotting of Field I (a) Slipline field (b) Hodograph (c) Table of input/output values.

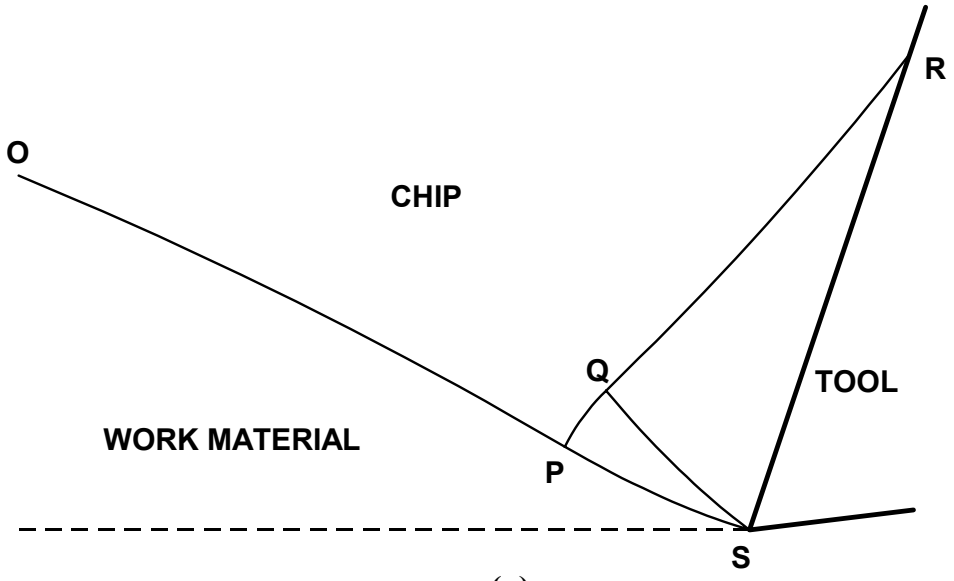

(a)

n_p	1.0
μ	1.0
γ	20^0
α	8^0
θ	7.7^0
ψ	19.4^0

(c)

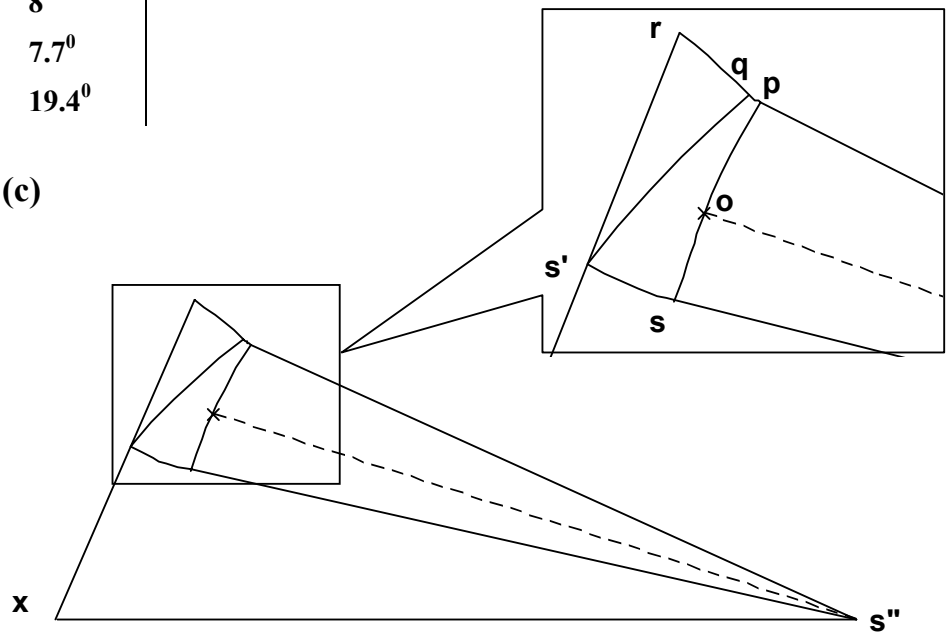

(b)

Fig. 3.20: Graphical plotting of Field I (a) Slipline field (b) Hodograph (c) Table of input/output values.

Chapter 4

CHAPTER 4

SLIPLINE FIELD SOLUTIONS FOR METAL MACHINING WITH ADHESION FRICTION AND ELASTIC EFFECTS AT CHIP-TOOL CONTACT REGION*

4.1 Introduction

In metal machining deformation process is greatly influenced by the friction phenomenon at the contact regions at tool face and flank. Friction at these contact regions affects the chip formation, power consumed, metal removal rate, quality of machined surface and active life of the cutting tools. Although friction in cutting is of interest for fundamental studies of wear and chemical reaction under conditions of high temperature and high pressure, there seems to be a lack of agreement as to how to represent this interface friction characteristics in steady state machining. According to Oxely and Hastings [39], the frictional conditions along the tool rake face in machining can best be represented by a constant interfacial shear stress ($\tau = mk$). This assumption has been made by Dewhurst [73], Childs [78] and Shi and Ramalingam [85] in formulating slipline field solutions for metal machining. Yet, others such as Ernst and Merchant [55], Lee and Shaffer [56] and Kudo [58] have indicated that the tool-chip interface friction is governed by Coulomb's law ($\tau = \mu p$). It has also been suggested that the tool-chip natural contact length consists of a zone of slipping contact on which the classical Coulomb's law of friction applies and a zone of sticking contact on which the friction stress attains the limiting value of yield stress k in shear of chip material [52]. Slipline field solutions assuming this "modified" Coulomb's law has also been proposed [79].

* This chapter is based on the paper titled "*Slipline solutions for metal machining with adhesion friction and elastic effects at the chip-tool contact region*", Das N. S. and Dundur S. T., Proc. IMechE, J. of Eng. Manufact. part B, Vol. 219, p 57-72, 2005.

The limitation of using a coefficient of friction to describe the friction characteristics at tool-chip interface has been discussed at length by Finnie and Shaw [64], Kobayashi and Thomsen [66] and Thomsen et al [82]. These authors have clearly stated that the coefficient of friction in metal cutting bears little relationship to the ordinary friction process and is inadequate to characterize the sliding between the chip and the tool. This is because if only the rake angle is changed during cutting a wide range of friction coefficients is obtained which are found to be greater and are often less than those obtained with the same metal combination in conventional sliding friction experiments. Another disturbing feature of the coefficient of friction is the increasing tendency for complete adhesion and formation of a built-up edge with decreased rake angle while the coefficient of friction is decreasing.

It is now generally recognized that Coulomb- Amonton's law of sliding friction do not hold on the tool-chip contact area where high-pressure/high-traction condition leads to an extreme friction situation. Measurement of contact stress distributions at this interface using split tool dynamometers [50-53] or photo-elastic tools [47-49] are in general found to be in agreement with this observation. As for the friction characteristics at the tool-chip interface, it is likely that adhesion is predominant over abrasion, where the friction force stems from the shear fracture of the bonded asperities. The empirical equation that is known to describe this friction condition may be stated as [65], (refer to equation (3.1))

$$\tau = k\left[1 - e^{-\left\{\frac{\mu\sigma_n}{k}\right\}^{n_p}}\right]^{\frac{1}{n_p}} \tag{4.1}$$

where, τ is the friction stress, σ_n is the normal stress, μ is the low stress level friction coefficient, and n_p is a constant whose value depends on tool/work material

combination. Equation (4.1) reduces to that proposed by Finnie and Shaw [64] for $n_p = 1$.

It is easily verified that in a lightly loaded condition ($\tau, \sigma_n \to 0$) equation (4.1) reduces to Coulomb's law. On the other hand when σ_n becomes large the friction stress τ approaches the shear flow stress k of the chip material. As suggested by Wanheim [106] equation (4.1) provides a smooth transition between two regimes predicted by the modified coulomb's law ($\tau = \mu\sigma_n$, $\mu\sigma_n \le k$, $\tau = k$, $\mu\sigma_n \ge k$)

In the present investigation slipline field solutions for orthogonal machining are proposed, where, the rake face friction is governed by the adhesion friction law as stated by equation (4.1). Another significant feature of the proposed solutions is that the influence of elastic effects on chip formation has been taken into account by considering an elastic contact zone beyond the region of plastic contact. The chip is assumed to leave the plastically stressed region with a constant curvature. The fields are analysed using the matrix operational procedure developed by Dewhurst and Collins [89] and Dewhurst [92,93]. The limit of validity of the proposed solutions is examined with the help of Hill's overstressing criteria [45]. Machining parameters such as cutting forces, cutting ratio, chip curl radius and contact length are estimated for different values of μ and n_p and for different tool rake angles. Results from the theoretical analysis are also compared with experiment.

4.2 Slipline field solutions

The two-slipline fields, Field II and Field III for the problem under consideration are shown in figures 4.1 and 4.2 along with their associated hodographs.

Referring to Fig. 4.1 (a) (Field II) it may be seen that the plastically stressed region consists of the primary shear line OPQ and the secondary shear zone PQR. The chip boundary is defined by OPR where, RP is the α-line and OP is the β-line. Within PQR, the deforming material slides on the rigid tool face QR in accordance with the adhesion friction law given by equation (4.1).

Referring to the hodograph shown in Fig. 4.1(b) it may be seen that the material suffers a velocity discontinuity of magnitude ρ on crossing the primary shear line OPQ. Thus, the velocity along OPQ is mapped into the circular arc qp of radius ρ in the hodograph diagram. Similarly, the velocity along the slipline curve PR is indicated by the hodograph curve pr. It is assumed that the material on leaving the deformation region undergoes rigid body rotation producing a curled chip of constant curvature. Hence, the curves PO and PR appear in the hodograph rotated through 90 degrees in the direction of the angular velocity ω and multiplied by the scale factor ω. Therefore, the slipline curves PR and PO are geometrically similar to the hodograph curves pr and po respectively. Thus, the slipline PO is a circular arc of radius (ρ/ω).

It is easily verified that the column vector σ in the power series expansion of the radius of curvature of the base slipline RP is calculated from the equation [89,92,93]

$$\sigma = -\left(\frac{\rho}{\omega}\right) AF_{\beta\phi_Q}\,\bar{c} \tag{4.2}$$

where, AF is the adhesion friction operator that constructs the field between the straight rough surface xqr and slipline curve qp consistent with the friction law stated in equation (4.1) and $\bar{c}$ is a column vector representing a circle of unit radius.

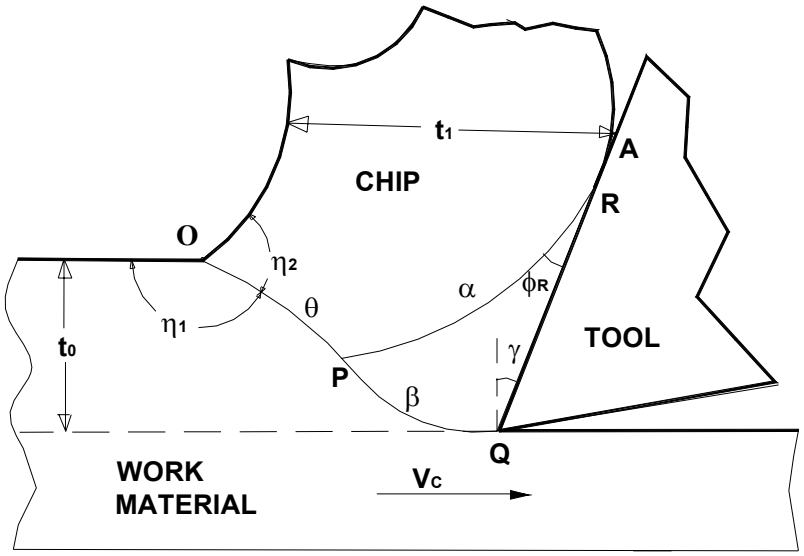

(a)

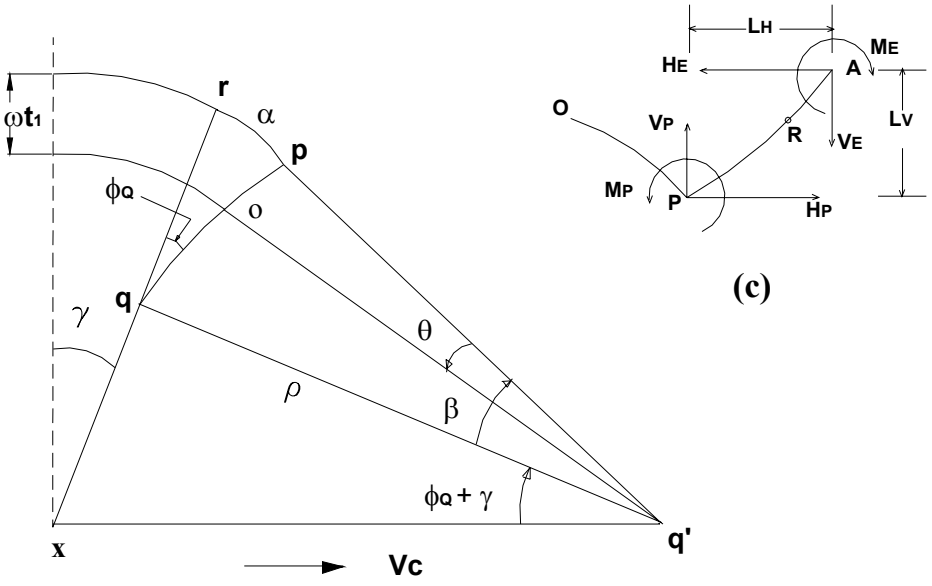

(c)

(b)

Fig. 4.1: Field II (a) Slipline field (b) Hodograph (c) Forces and moment on the chip.

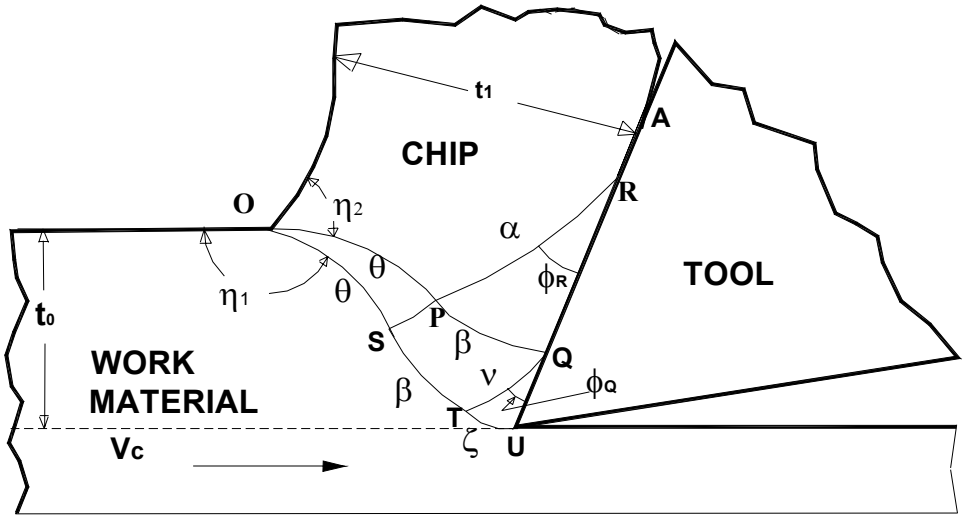

(a)

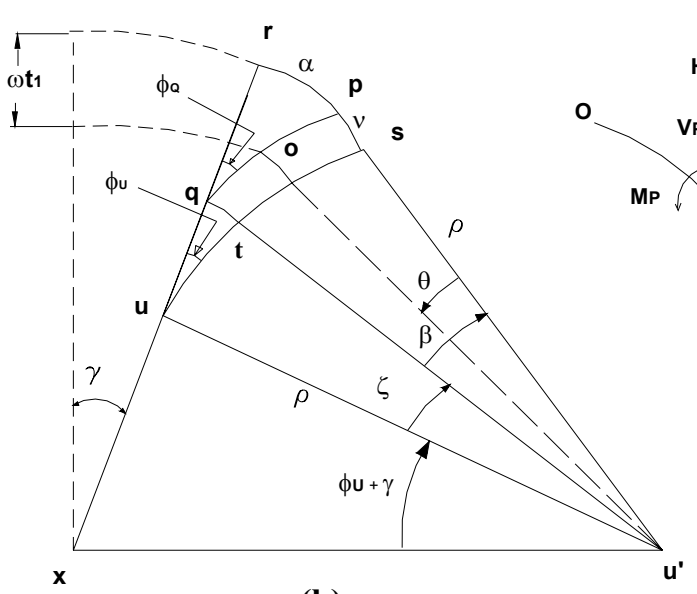

(b)

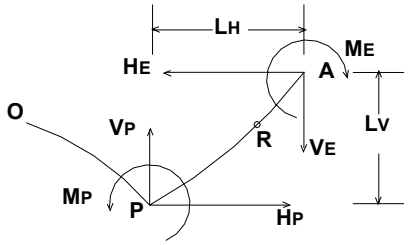

(c)

Fig. 4.2: Field III (a) Slipline field (b) Hodograph (c) Forces and moment on the chip.

In equation (4.2) ϕ_Q is the friction angle at which hodograph curve qp meets the tool face and β is its angular range.

Slipline Field III is an extension of Field II. In this case, a singular field OPS separates the rigid chip from the work material with another plastically deforming region QTU in contact with the tool face. Referring to its hodograph (Fig. 4.2(b)) it is also verified that all velocity boundary conditions are satisfied: namely *rigid body rotation of the chip and translation along the tool face*. Velocity compatibility further requires that uts is a circular arc of radius ρ and that the hodograph curves op and rp are geometrically similar to their slipline images OP and RP.

OP and RP are easily calculated from the circular arc uts $(=-\rho\bar{c})$ using the standard matrix operators [89,92,93]. Thus,

$$us = -\rho\bar{c} \tag{4.3}$$

Hence, $$qt = -\rho AF_{\zeta\phi_u}\bar{c} \tag{4.4}$$

And $$tq = -\rho R_\upsilon AF_{\zeta\phi_u}\bar{c} \tag{4.5}$$

qp is related to ts and tq by the equation

$$qp = P_\upsilon^* ts + Q_\upsilon^* tq \tag{4.6}$$

Using equations (4.3), (4.5) and (4.6), qp is finally given by the equation,

$$qp = -\rho\left(P_\upsilon^* + Q_\upsilon^* R_\upsilon AF_{\zeta\phi_u}\right)\bar{c} \tag{4.7}$$

Hence, $$op = -\rho S_\delta\left(P_\upsilon^* + Q_\upsilon^* R_\upsilon AF_{\zeta\phi_u}\right)\bar{c}$$

$$rp = -\rho AF_{\beta\phi_Q}\left(P_\upsilon^* + Q_\upsilon^* R_\upsilon AF_{\zeta\phi_u}\right)\bar{c}$$

Where, $\delta = \beta - \theta$

also $op = \omega\, OP$

and $rp = \omega\, RP$

Hence, $$OP = -\left(\frac{\rho}{\omega}\right) S_{\delta} \left(P_{\upsilon}^{*} + Q_{\upsilon}^{*} R_{\upsilon} AF_{\zeta\phi_Q}\right) \bar{c} \tag{4.8}$$

$$RP = -\left(\frac{\rho}{\omega}\right) AF_{\beta\phi_U} \left(P_{\upsilon}^{*} + Q_{\upsilon}^{*} R_{\upsilon} AF_{\zeta\phi_Q}\right) \bar{c} \tag{4.9}$$

In the above equations, P^{*}, Q^{*}, R … etc. are the standard matrix operators, and ϕ, β, a …etc. are the field angles as shown in Fig. 4.2.

4.3 Method of solution

It may be noticed that in both these fields the chip boundary is defined by a concave α-line and a convex β-line. As reported by Kudo [58], however, with this configuration it is impossible to ensure the force and moment equilibrium of the chip. Chip equilibrium in the present solutions was realised by introducing elastic effects into the analysis of chip formation as explained in [79]. It was assumed that the total contact length QA (UA for Field III) is composed of a plastic contact length QR (UR) and an elastic part RA. Within QR (UR) the normal stress was assumed to vary according to Hencky's equations. Within RA it was assumed that normal pressure σ_e decreased exponentially from its maximum value σ_R at R to zero at the chip releasing point A according to the equation,

$$\left(\frac{\sigma_e}{k}\right) = \left(\frac{\sigma_R}{k}\right) \frac{\left[1 - e^{n_e (l/l_e)}\right]}{1 - e^{n_e}} \tag{4.10}$$

where, $l_e (= RA)$ is the elastic contact length, l is the distance of any point within RA

as measured from A and n_e is a constant. Within RA the normal stress (σ_e / k) and the shear stress (τ / k) (as calculated from equation (4.1)) gave rise to the resultant forces H_E, V_E and moment M_E which together with the forces H_P, V_P and moment M_P calculated from the slipline curves OP and PR brought the chip into static equilibrium (Fig. 4.1(c) and Fig. 4.2(c)).

The FORTRAN programme developed for analysing these fields evaluated the above force components and the moments in terms of the angular range θ of the slipline OP, the hydrostatic pressure p_R at R and the ratio X of the elastic to the plastic contact lengths (RA / RQ or RA / RU). For inputs of friction coefficient μ, constants n_p, n_e and angular range α of the base slipline RP, the programme first evaluated the friction angle ϕ_R by solution to equation (4.1) $(\tau = k\cos 2\phi_R,\ \ \sigma_n = p_R + k\sin 2\phi_R)$ and then determined the relation between the angular range of α- and β-lines within PQR for points on the tool face QR. With the assumption of adhesion friction, this relation becomes nonlinear. Following Dewhurst [92,93] this nonlinear relation was approximated by a linear relation $\beta = m_0\alpha$. The linear coefficient m_0 was calculated by the method of regression analysis as explained in Appendix I. This value of m_0 together with the field angles ϕ_R, α and θ were then used to construct the adhesion and other matrix operators and compute the force components H_P, V_P and the moment M_P with the help of the subroutines given in [89, 92,93]. For the given p_R and X values the elastic forces H_E, V_E and moment M_E was calculated in a straightforward manner using equation (4.1) and (4.10). For equilibrium of the chip it is necessary that

$$F_1 = H_P - H_E = 0 \tag{4.11a}$$

$$F_2 = V_P - V_E = 0 \tag{4.11b}$$

$$F_3 = M_P - M_E + H_E L_V - V_E L_H = 0 \tag{4.11c}$$

where, L_H and L_V are the horizontal and the vertical distances of A from P respectively (Fig. 4.1(c) and Fig. 4.2(c)). The above equations were solved for the parameters θ, p_R and X with the help of an algorithm developed by Powell [104] for the optimization of nonlinear functions with unknown derivatives. The requirement of chip equilibrium was achieved when the computed values of θ, p_R and X satisfied the inequality,

$$\left(\frac{F_1}{kt_1}\right)^2 + \left(\frac{F_2}{kt_1}\right)^2 + \left(\frac{F_3}{kt_1^2}\right)^2 \leq 10^{-10} \tag{4.12}$$

The optimized field variables calculated in this manner were used to determine the machining parameters such as the cutting and the thrust forces, chip curl radius and the contact length etc. The programme incorporated flatness and mass-flux checks as explained in [88]. It also contained checks to determine whether Hill's overstressing criterion [45] was violated at the rigid vertices at O (Fig. 4.1 (a) and Fig. 4.2(a)) to test the range of validity of the proposed solutions (refer to equation 3.15)).

Introduction of elastic effects brought in additional variables n_e and X into the field apart from the existing ones, θ, α and p_R. Since, only three equations are to be satisfied for chip equilibrium (equation 4.11), the proposed fields are non-unique in nature.

The solutions to the present slipline fields can also be obtained without the assumption of an elastic contact length if the chip is constrained to move over a chip breaker as demonstrated by Dewhurst [76] and Shi and Ramlingam [85].

It must be emphasized that no attempt has been made in the present study to evaluate whether the assumed elastic contact conditions are compatible with the flow of the chip. It is further assumed that the distortion to the field brought about due to the assumption of an elastic contact length is only of a small order so that the assumptions made for the rigid-plastic slipline field analysis are still valid.

4.4 Results and discussion

The range of validity of the proposed solutions defined in terms of the angular span α of the base slipline RP is shown in Fig. 4.3 and Fig. 4.4 for slipline Field II and in Fig. 4.5 for slipline Field III for a tool with 10^0 rake angle. Referring to these figures it may be seen that for Field II the solution zone is bounded by Lee and Shaffer's limit (LSL) and the overstressing limit (OSL-1) and for Field III by the extension of Lee and Shaffer's solution as introduced by Kudo (KL) and the overstressing limit (OSL-1). The overstressing limit here refers to the overstressing of the vertex angle η_1 (Fig. 4.1(a) and Fig. 4.2(a)). For the whole range of solutions examined, the vertex angle η_2 was never found to be overstressed.

It was also noticed that increasing either n_e (Fig. 4.3) or υ (Fig. 4.5) or decreasing the value of μ (Fig. 4.4 and Fig 4.5) resulted in a decrease in the solution range. For solution III increasing either α or μ in general imposed restrictions on the permissible value of υ for which valid solutions could be obtained without overstressing the work-piece at O.

For both the fields extreme values of cutting (F_C / kt_0) and thrust (F_t / kt_0) forces and cutting ratio (t_1 / t_0) are found to be associated with the chip streaming solutions of either Lee and Shaffer [56] or Kudo [58] for which α = 0. Chip curvature (t_0 / R) and contact length (l_c / t_0), however, show the reverse trend.

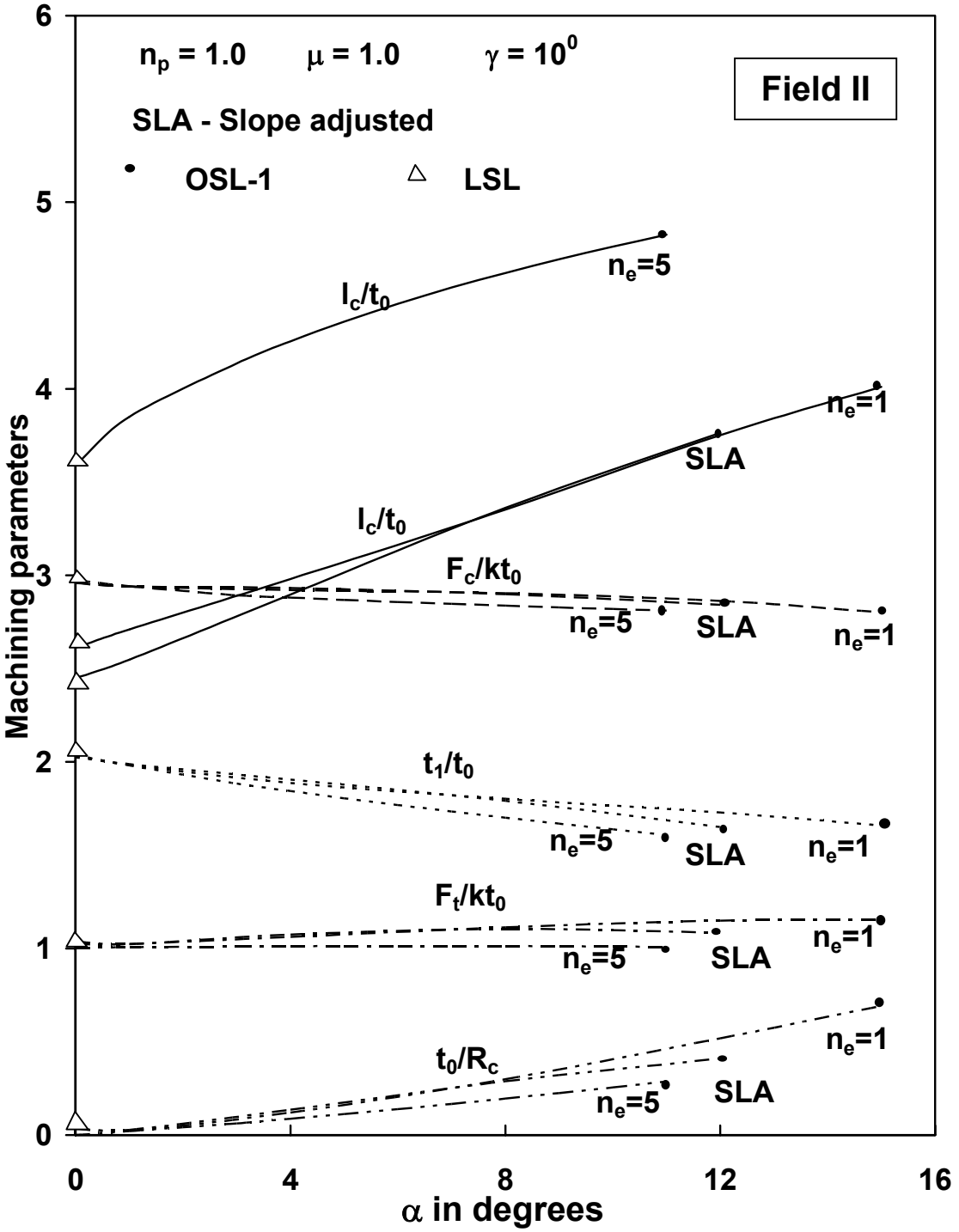

Fig. 4.3: Variation of machining parameters with field angle α for different values of n_e .
(OSL-1: Overstressing limit at η_1 , LSL- Lee and Shaffer limit)

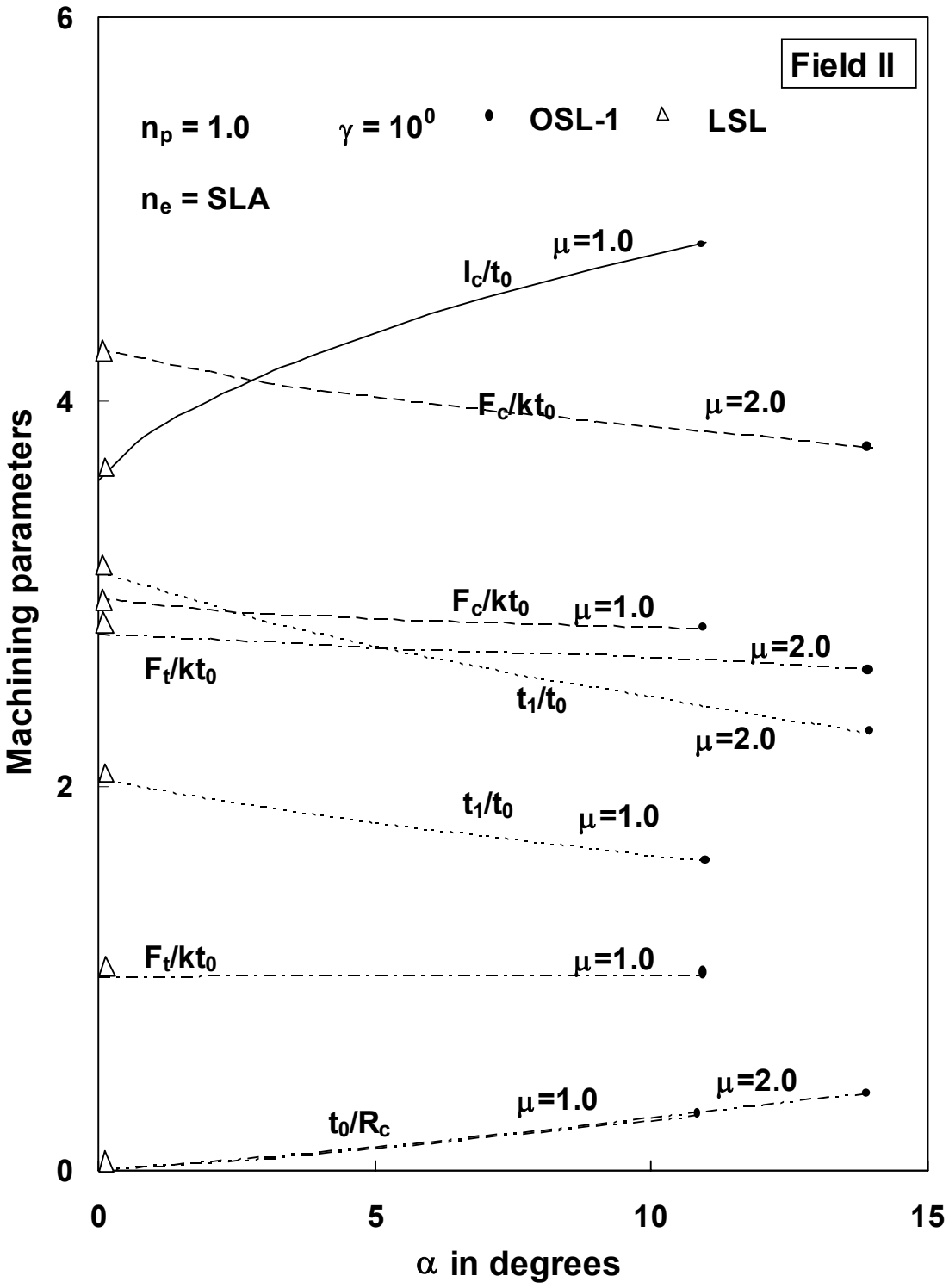

Fig. 4.4: Variation of machining parameters with field angle α for different values of friction coefficient μ..

Except for the contact length, the machining parameters are found to be only marginally influenced by n_e (Fig. 4.3) though these are affected significantly by the friction coefficient μ (Fig. 4.4 and Fig. 4.5).

It may be seen that for the calculation of the elastic forces the value of n_e could be chosen arbitrarily (equation (4.10)). An unique value of n_e however, is obtained if it is assumed that the slopes of normal stress distribution curves in the elastic and plastic contact zones have the same value at R (Fig. 4.1(a)) and Fig. 4.2(a)). For the elastic part, this slope was calculated by straightforward differentiation of equation (4.10). For the plastic part this was calculated by Lagrange interpolation. The variation of machining parameters corresponding to this value of n_e ($= SLA$) is also shown in Fig. 4.3. SLA in general varied with α, but results of machining parameters computed with this value of n_e was found to be close to those calculated with $n_e = 1$. In Fig. 4.4 and Fig. 4.5, the results presented correspond to those with $n_e = SLA$.

The predicted variation of machining parameters with rake angle are shown graphically in figures 4.6 - 4.11 for values of μ equal to 1 and 2 where these are compared with the experimental observations of Eggleston, Herzog and Thomsen [105] from orthogonal cutting tests on steel using H.S.S. tools. The average shear plane angle λ in Fig. 4.6 at the overstressing limit (OSL-1) was calculated from the equation

$$\lambda = \phi_Q + \gamma + \left(\frac{\beta}{2}\right) - \left(\frac{\theta}{2}\right) \tag{4.7}$$

where, γ is the rake angle, ϕ_Q is friction angle at Q, and β and θ are the angular ranges of sliplines PQ and OP respectively.

The figures indicate that for each value of the rake angle the range of possible solutions as computed from the slipline field analysis lie within LSL and OSL-1 (Field II) or KL and OSL-1 (Field III) as discussed earlier in the text. The difference in the two limits, however, narrows down as the rake angle increases and is found to be negligible beyond $\gamma = 20^0$ for Field II and beyond $\gamma = 10^0$ for Field III. This is in agreement with the observations reported earlier by Dewhurst [73].

It is also demonstrated that the rake angle and rake friction are the two most important variables in metal machining that influence machining parameters. Cutting ratio, cutting forces, and contact length increase as rake angle decreases and μ increases and this is in agreement with experimental observations. It may also be seen that for the same values of γ and μ Field III predicts lower values of cutting forces in comparison to Field II (Fig. 4.8 and Fig. 4.9).

Referring to the above figures it may be seen that there is excellent agreement between theory and experiment especially at lower rake angles. The agreement, however, is found to be not so good at $\gamma = 20^0$. For the same rake angle, experimental results show wide scatter in the values of machining parameters and this may be due to the non-unique nature of the machining process as predicted by the present analysis.

The variation of average contact normal and shear stresses as predicted by the present analysis are shown in Fig. 4.11, where these are compared with those from the experimental observations of Eggleston et al [103]. For Lee and Shaffer's solution the stresses are independent of rake angle and this is indicated by lines horizontal to the abscissa in the above figures. The stresses at the overstressing limit also, are found to be insensitive to increase in rake angle. Most of the experimental points, however, fall within LSL and OSL-1 for values of μ equal to 1 and 2.

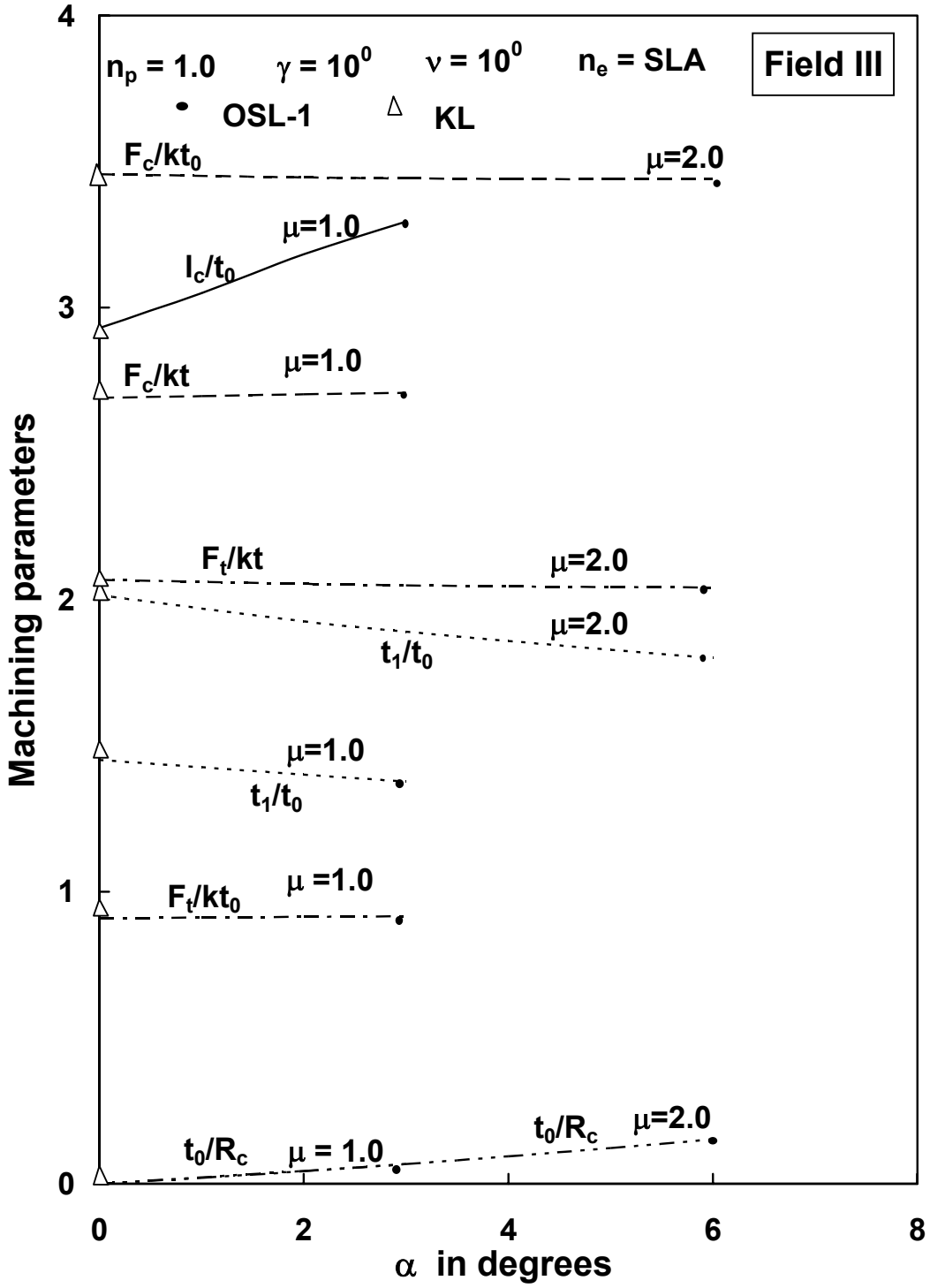

Fig. 4.5: Variation of machining parameters with field angle α for different values of friction coefficient μ.
(OSL-1: Overstressing limit at η_I, KL: Kudo limit)

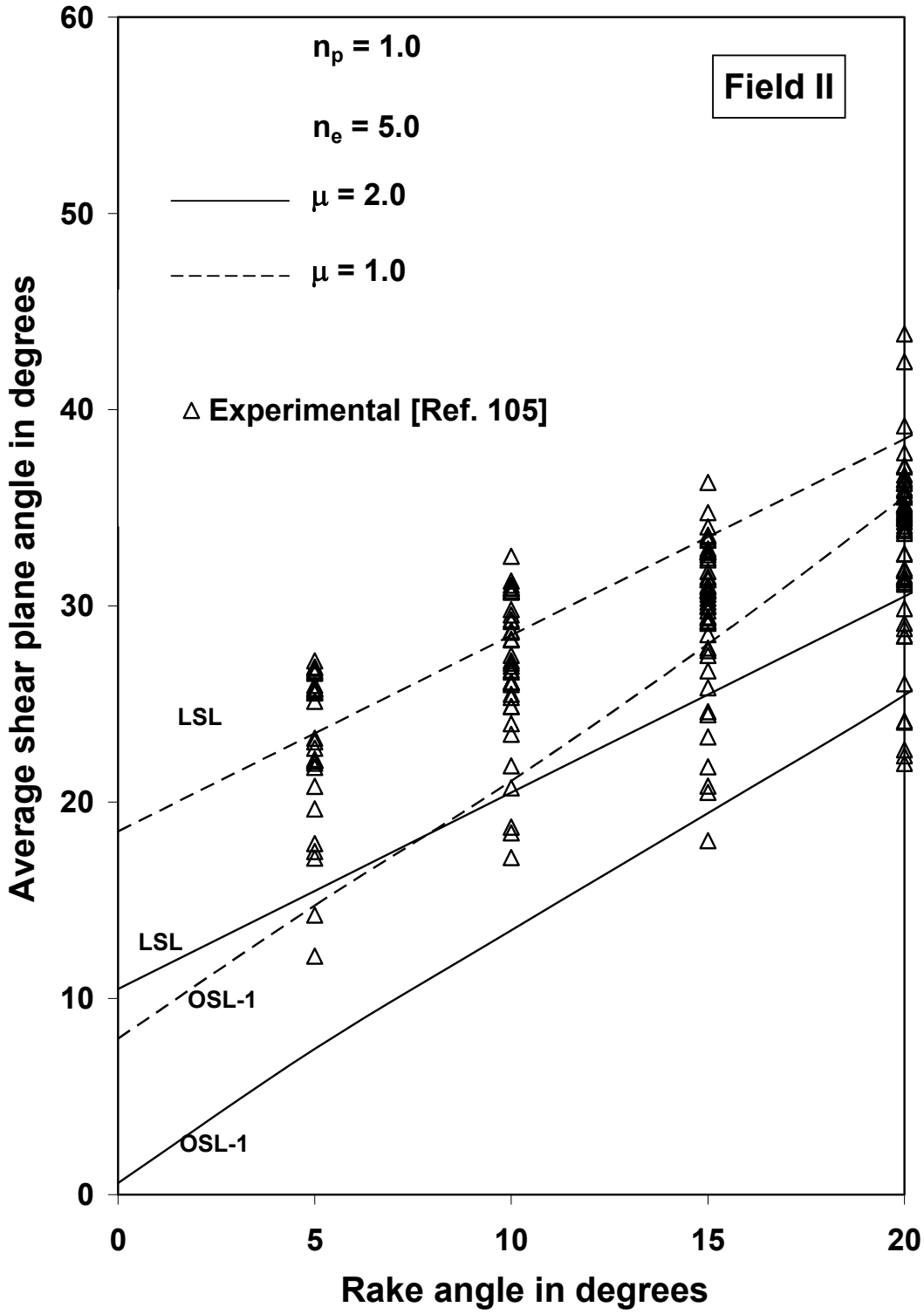

Fig. 4.6: Variation of average shear plane angle with rake angle.

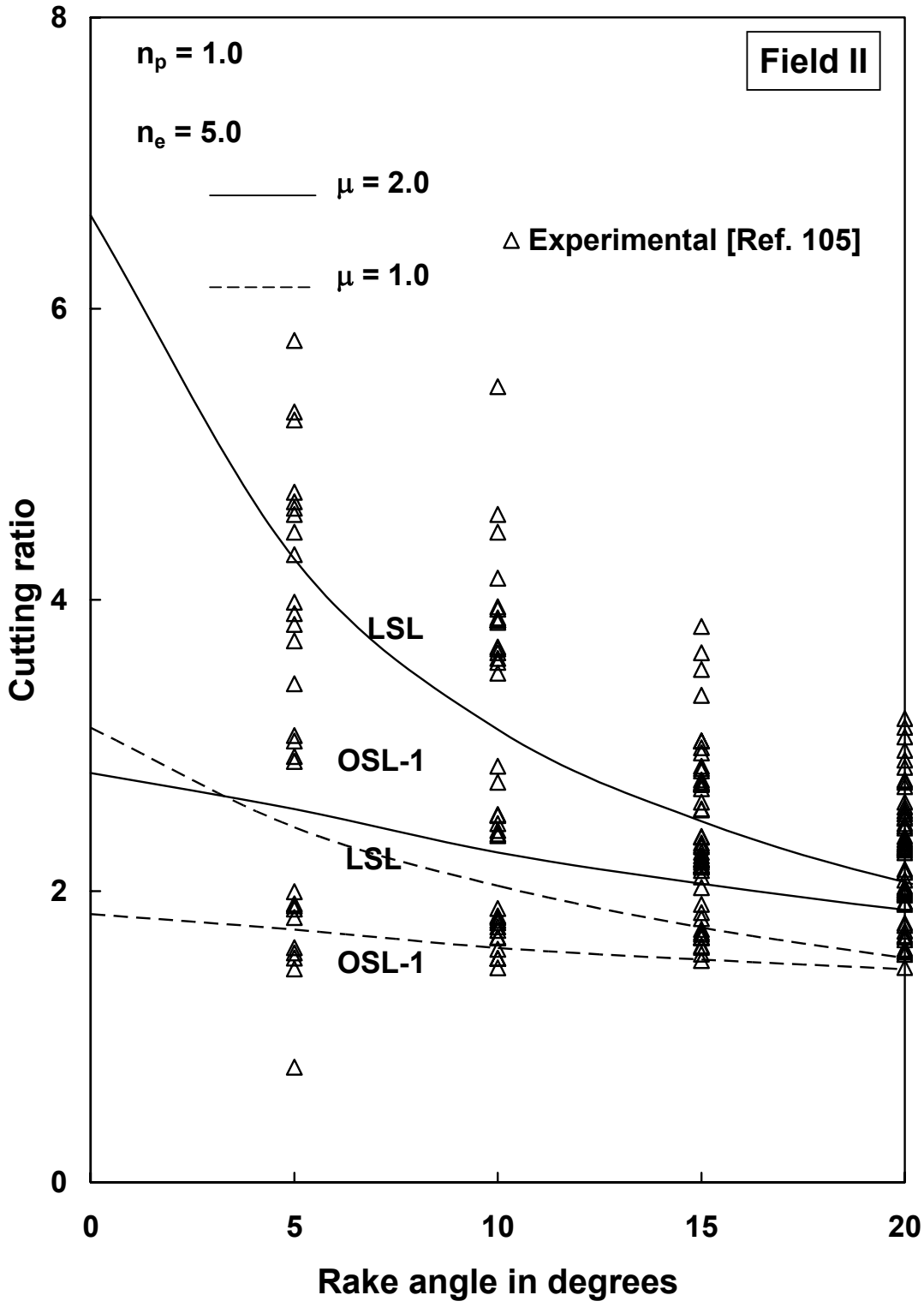

Fig. 4.7: Variation of cutting ratio with rake angle

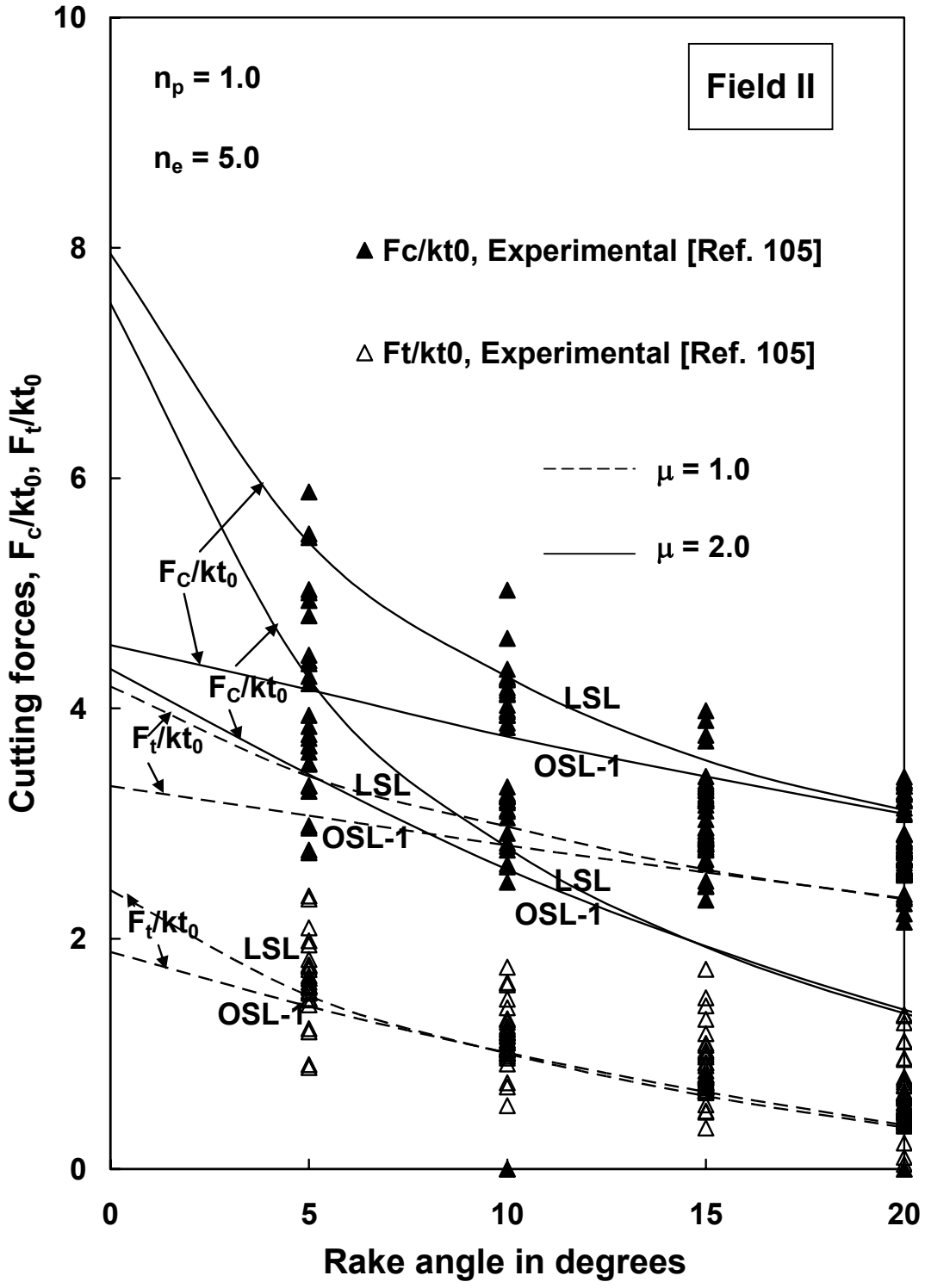

Fig. 4.8: Effect of rake angle on cutting and thrust forces.

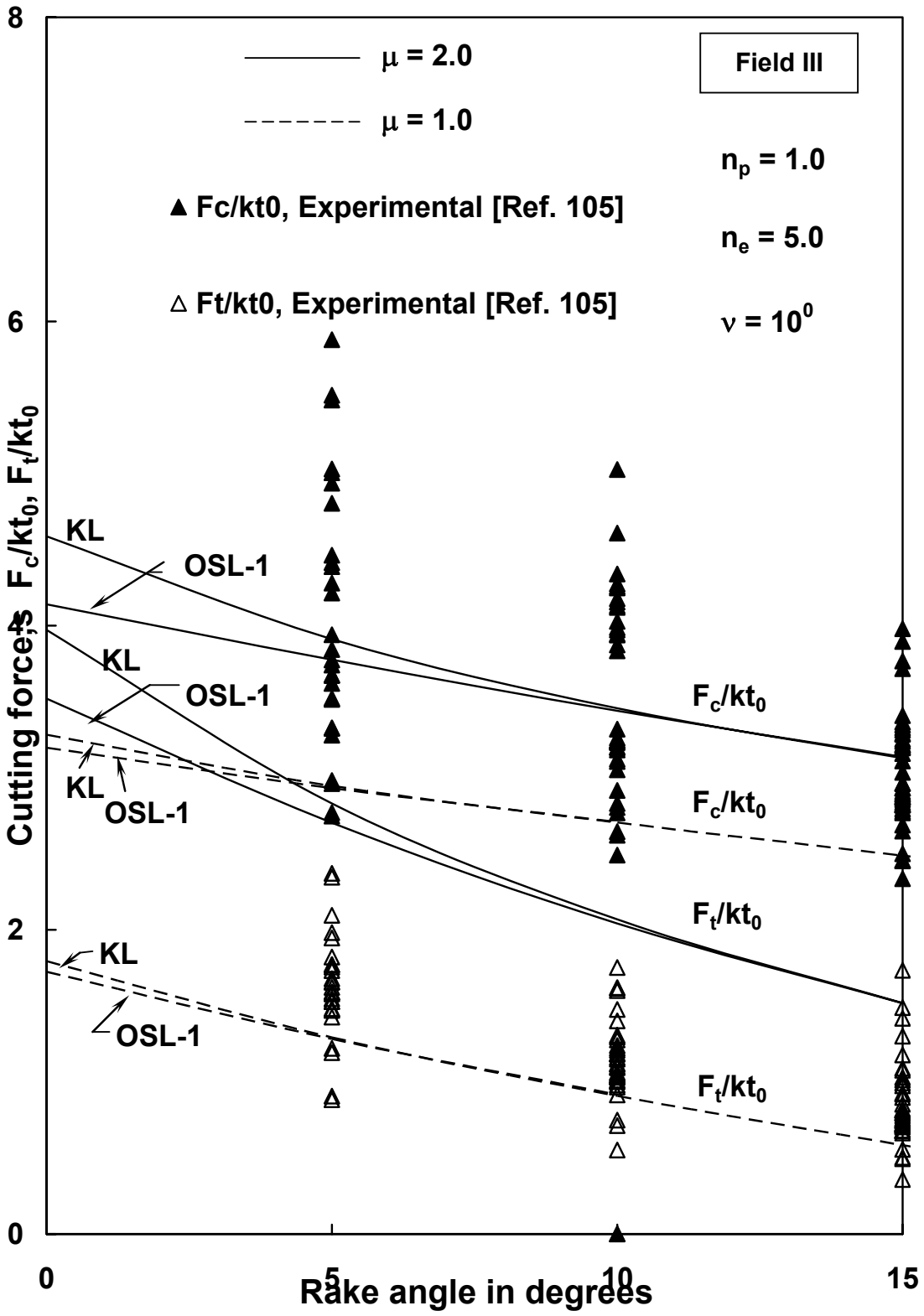

Fig. 4.9: Effect of rake angle on cutting and thrust forces

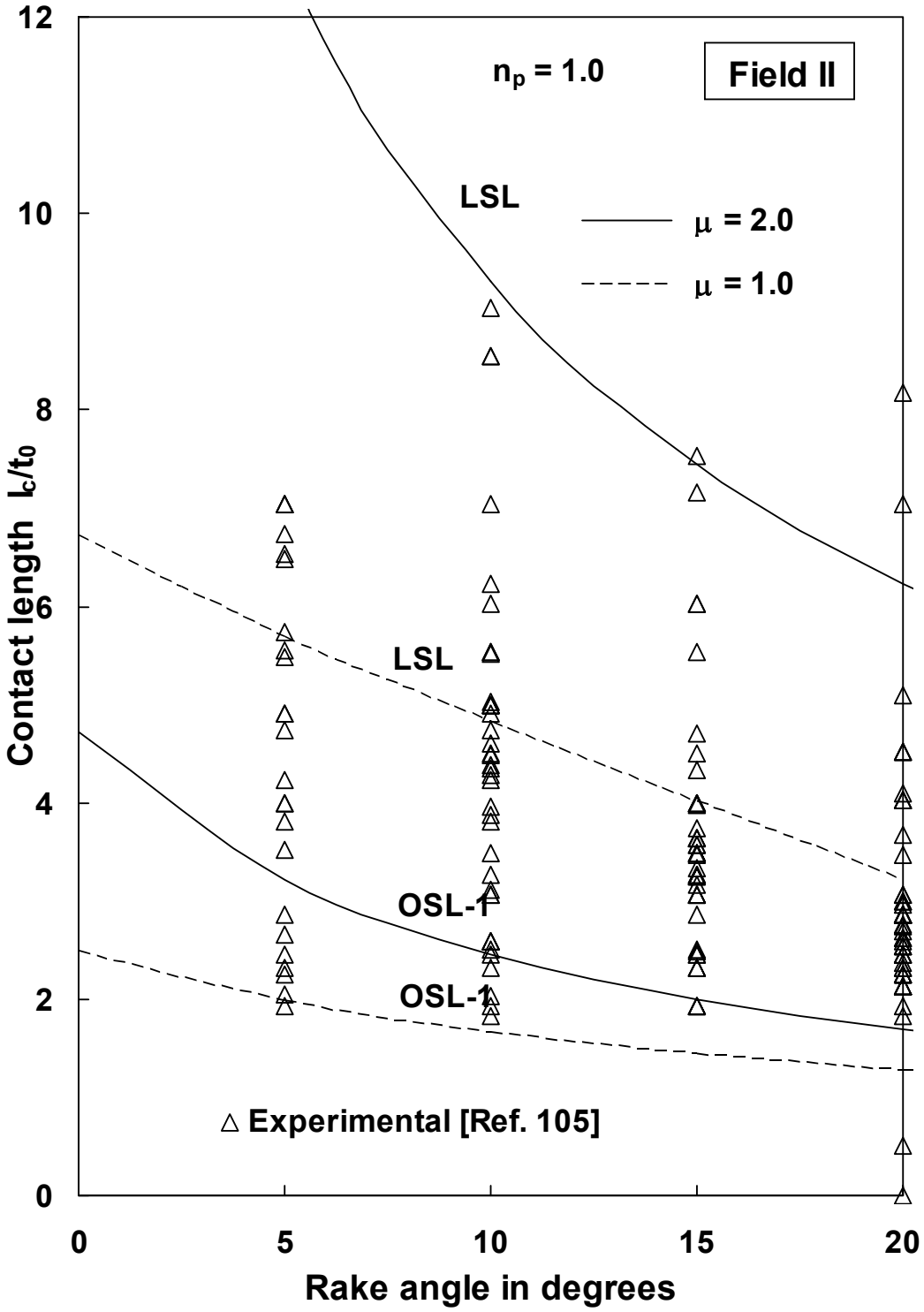

Fig. 4.10: Variation of contact length with rake angle.

The variation of average Coulomb coefficient of friction on the rake face with rake angle as calculated from the contact stresses is shown in Fig. 4.12. The figure indicates that the friction coefficient is not uniquely determined by the rake angle γ, but may have a range of allowable values for any particular value of γ.

Theoretical contact stress distribution along the natural contact length is shown in figures 4.14 (Field II) and in 4.15 (Field III) for a tool with 10^0 rake angle. The n_e value for these cases were obtained by matching the slopes of the normal stress distribution curves in the elastic and plastic contact zones. The variation agrees qualitatively with those determined experimentally by other investigators [52,64].

4.5 Conclusions

Two slipline field solutions for orthogonal machining are presented by introducing elastic effects into the analysis of chip formation and by assuming adhesion friction at chip/tool interface. The friction law assumed was that suggested by Maekawa et al [65]. The fields are analysed by the matrix operational procedure developed by Dewhurst and Collins [89] and Dewhurst [92,93] assuming a linear relation between the angular range of α - and β - lines in the secondary deformation zone. The range of validity of the proposed solutions is examined using Hill's overstressing criterion [45].

For both the fields extreme values of cutting and thrust forces and cutting ratio are found to be associated with the corresponding chip streaming solutions. It is seen that the machining parameters for any given rake angle and friction coefficient are not uniquely determined but lie within a range as dictated by the overstressing criterion.

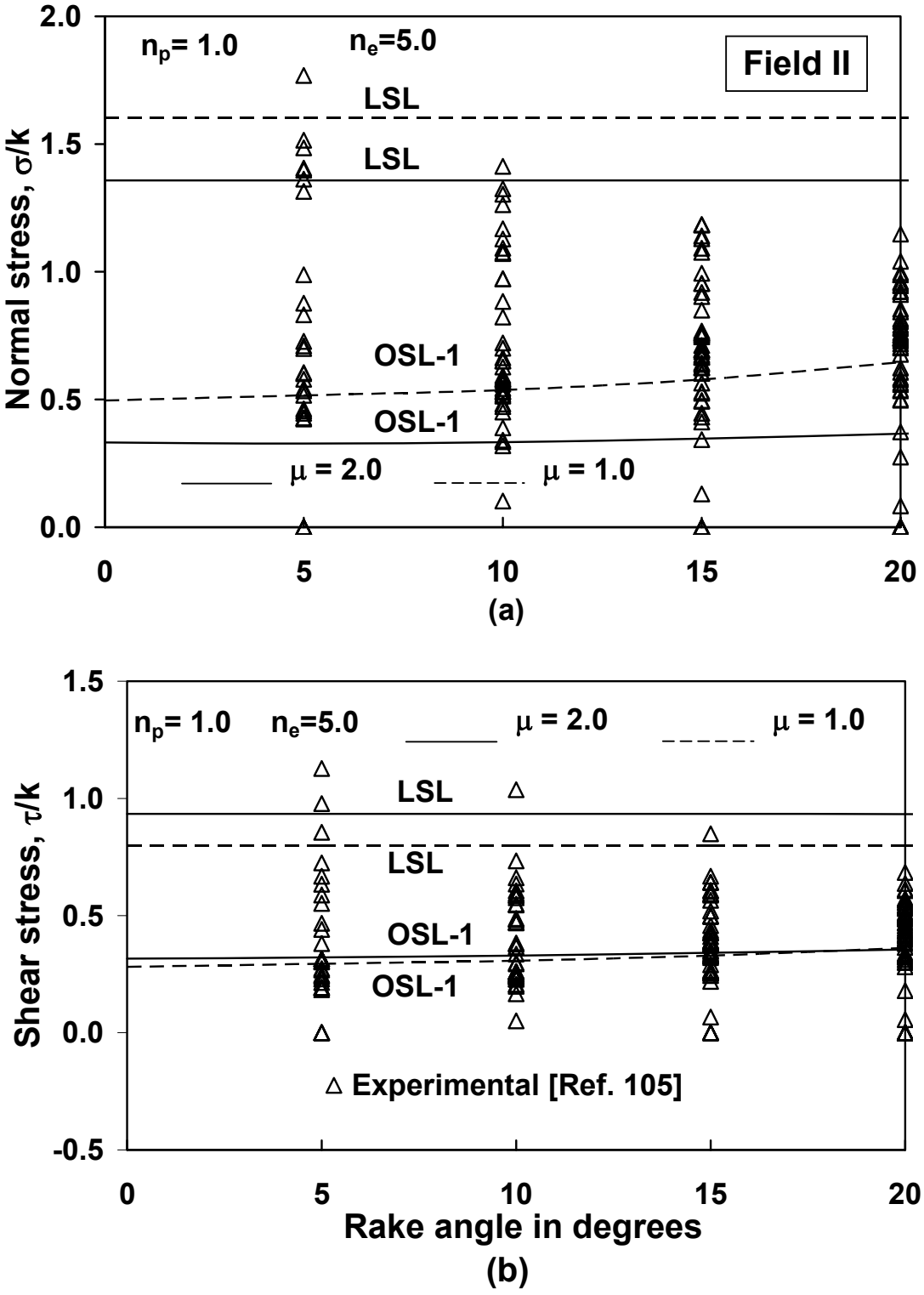

Fig. 4.11: Variation of chip-tool contact stresses with rake angle (a) Average normal stress (b) Average shear stress.

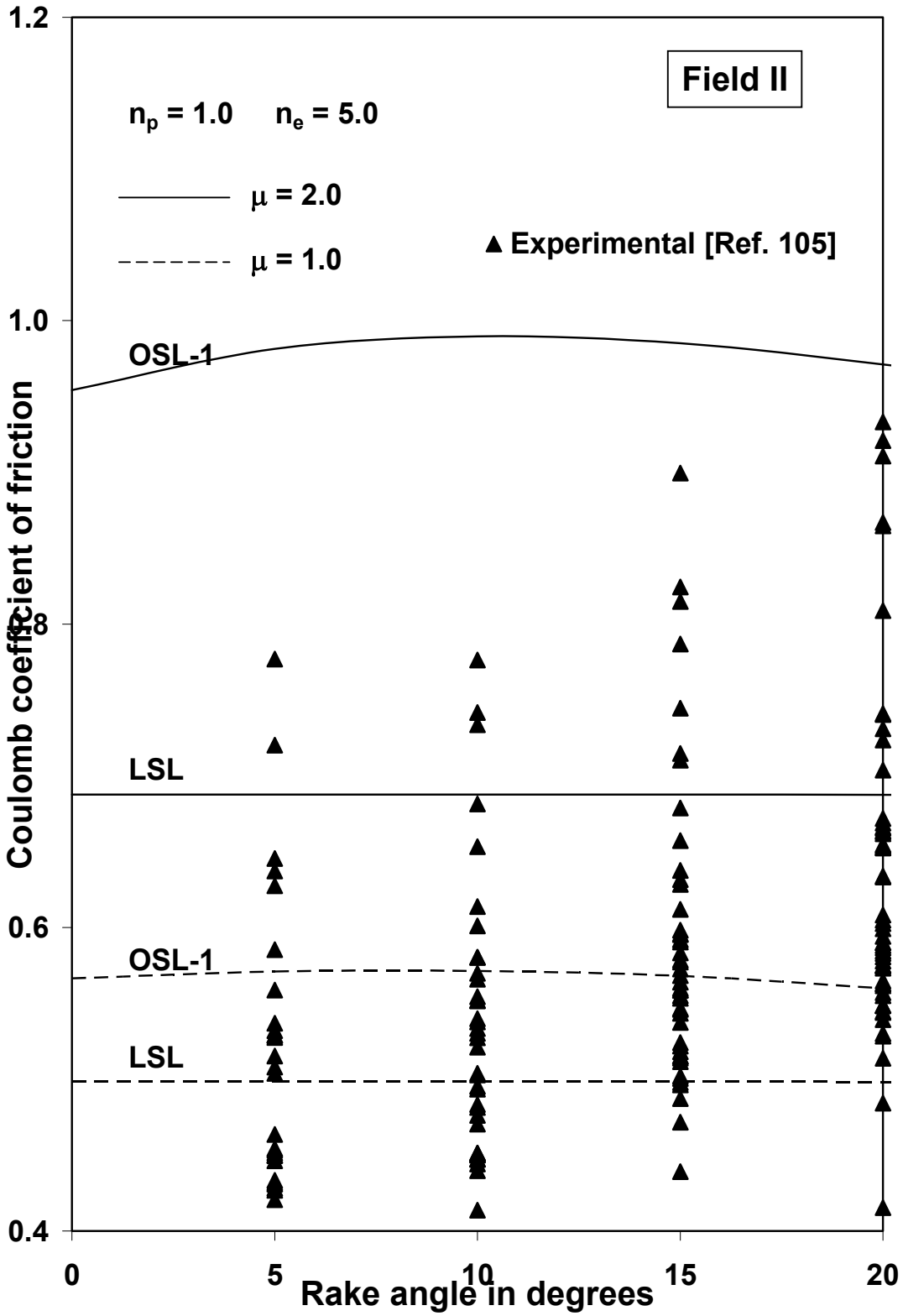

Fig. 4.12: Effect of rake angle on average Coulomb coefficient of friction.

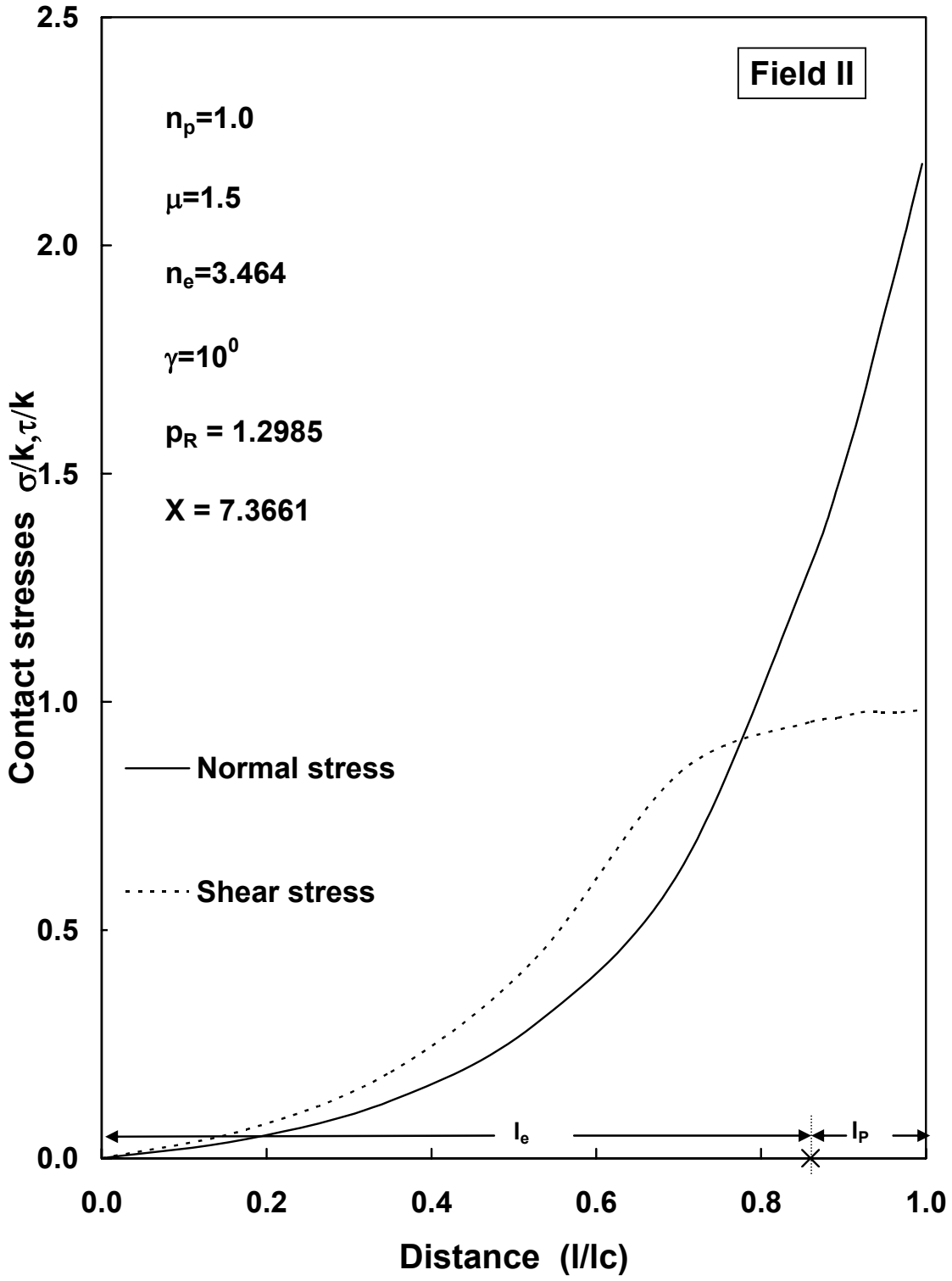

Fig. 4.13: Distribution of contact stresses at the chip-tool interface.

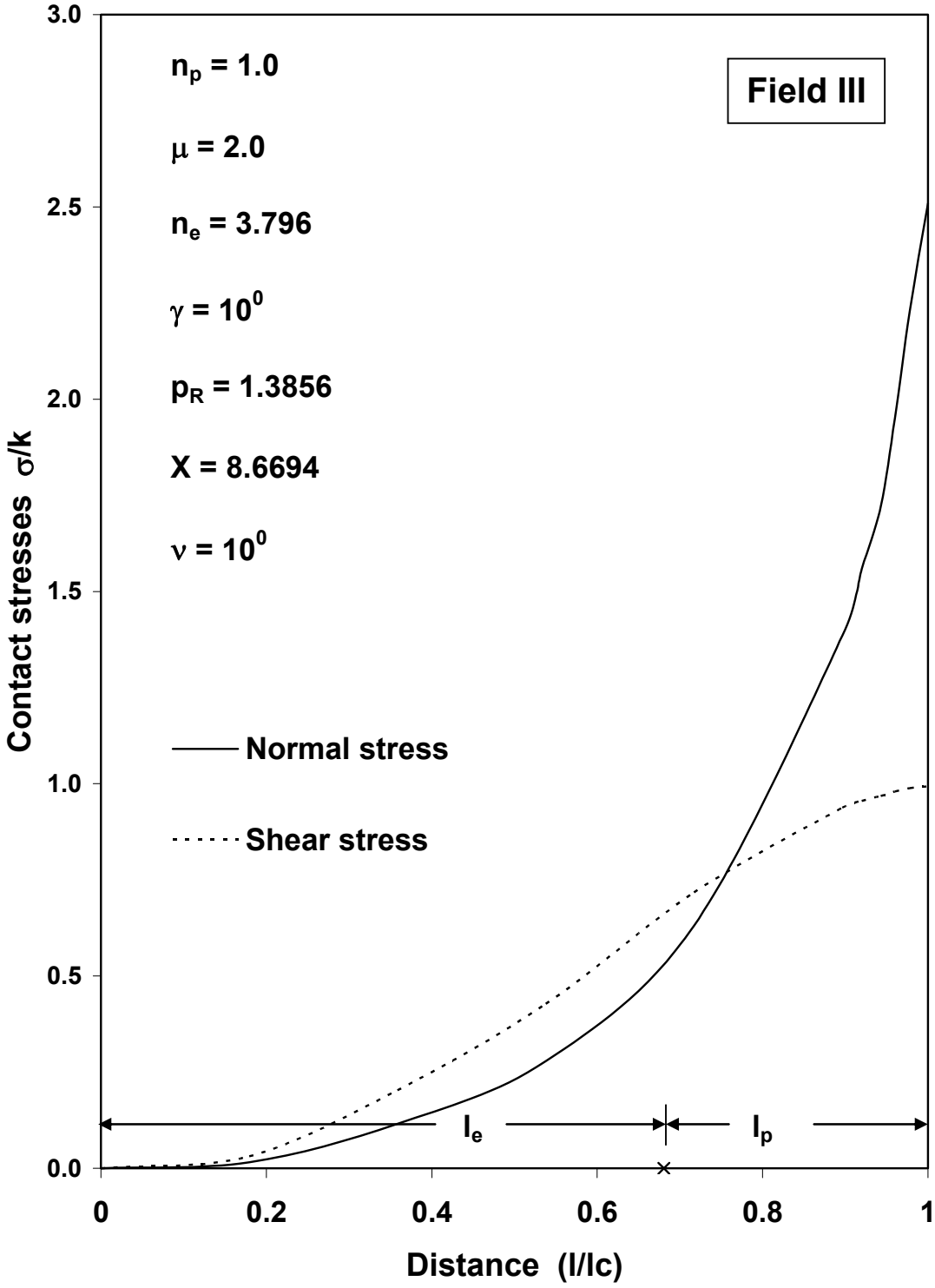

Fig. 4.14: Distribution of contact stresses at the chip-tool interface.

Rake angle and rake friction are the two most important variables in metal machining that influence machining parameters. The cutting forces, the cutting ratio and the contact length increase as the rake the angle decreases and the coefficient of friction increases.

The exponent n_e of normal pressure distribution in the elastic contact region is found to have only marginal influence on the machining parameters. For computational purpose, the value of n_e in general can be chosen arbitrarily. A unique value of n_e, however, is calculated if it is assumed that the slopes of the normal pressure distribution curves in the elastic and plastic contact zones have the same value at R (Fig. 4.1 and Fig. 4.2).

The predicted values of machining parameters from the present analysis are found to agree well with the experimental observations with those obtained by Eggleston et al [105] from orthogonal cutting tests.

4.6 Plotting of some slipline fields and Hodographs

In the subsequent sections the slipline field networks plotted graphically as discussed earlier (section 3.6) for the sets of input friction parameters and rake angle (n_e=5, n_p=1, μ=1, γ=10^0), (n_e=5, n_p=1, μ=2, γ=10^0) and (n_e=5, n_p=2, μ=1, γ=10^0) are presented in figures 4.15-4.17 for Field II. Similar slipline field networks are also presented for Field III for the sets of input friction parameters, rake angle and fan angle ν (n_e=5, n_p=1, μ=1, γ=10^0, ν = 5^0), (n_e=5, n_p=1, μ=2, γ=10^0, ν = 10^0) and (n_e=1.735 (SLA), n_p=1, μ=1, γ=10^0, ν = 10^0) in figures 4.18-4.20.

-ooOoo-

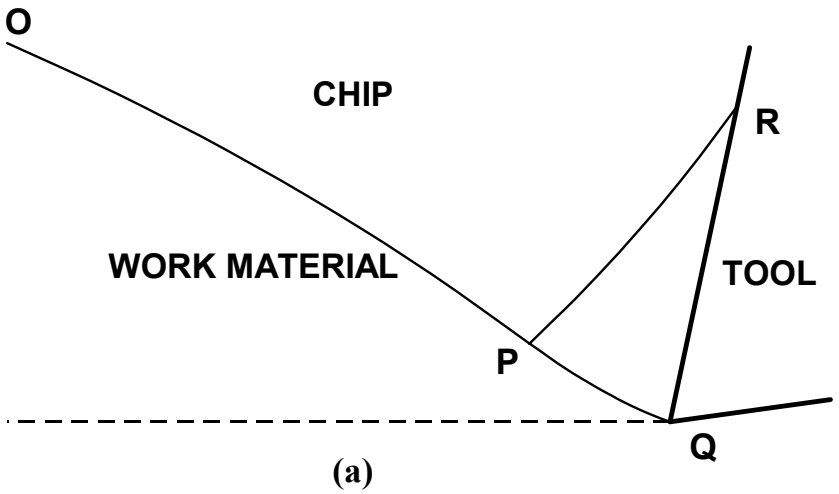

(a)

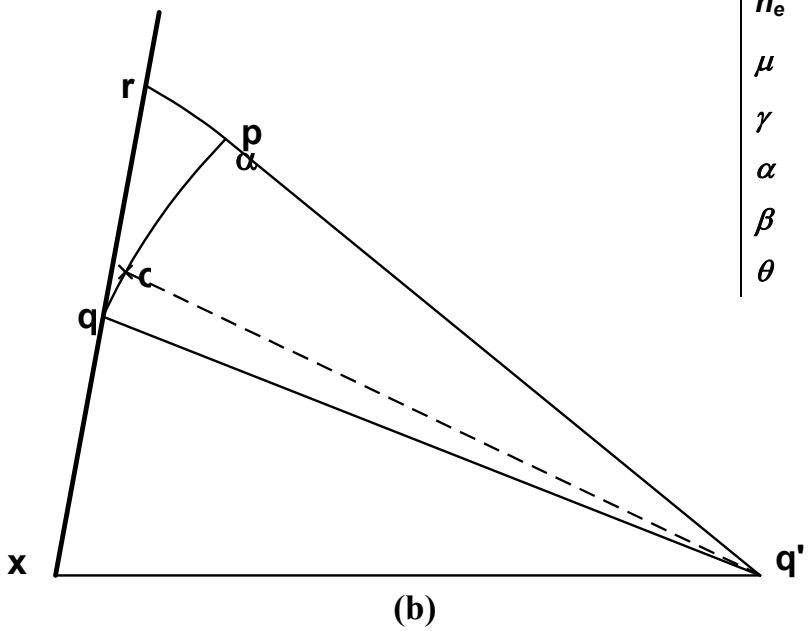

(b)

n_p	1.0
n_e	5.0
μ	1.0
γ	10^0
α	11^0
β	18.4^0
θ	14.15^0

(c)

Fig. 4.15: Graphical plotting of Field II (a) Slipline field (b) Hodograph (c) Table of input/output values.

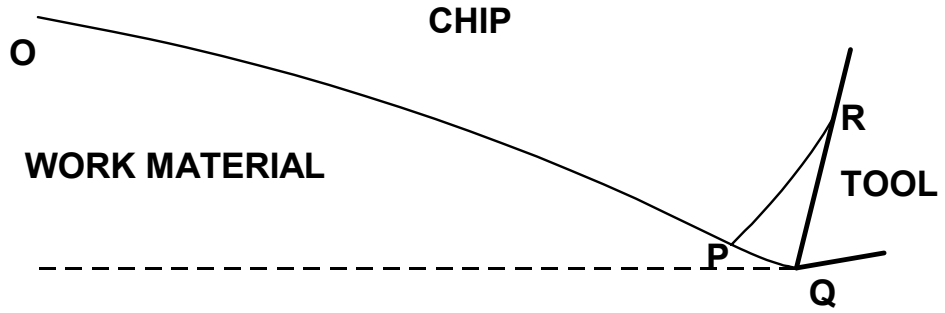

(a)

n_p	1.0
n_e	5.0
μ	2.0
γ	10^0
α	14^0
β	22.4^0
θ	22.0^0

(c)

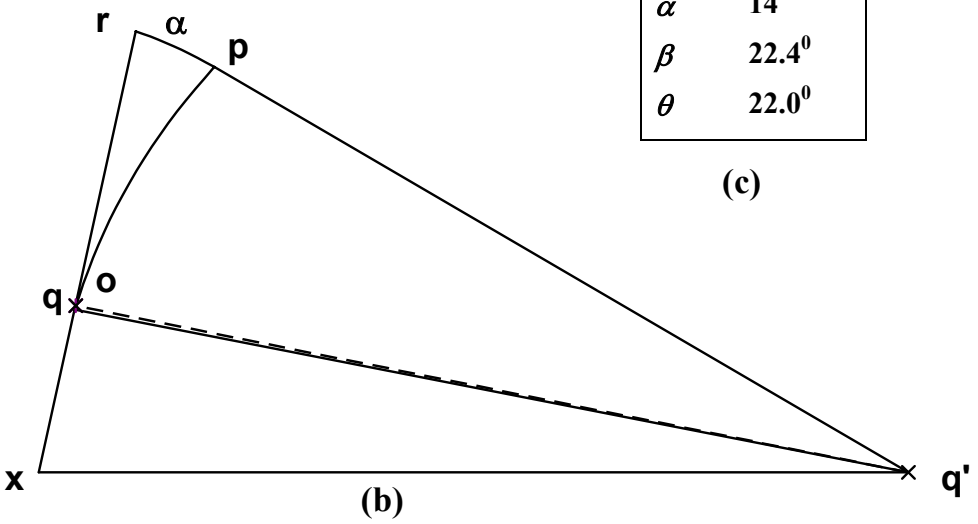

(b)

Fig. 4.16: Graphical plotting of Field II (a) Slipline field (b) Hodograph (c) Table of input/output values.

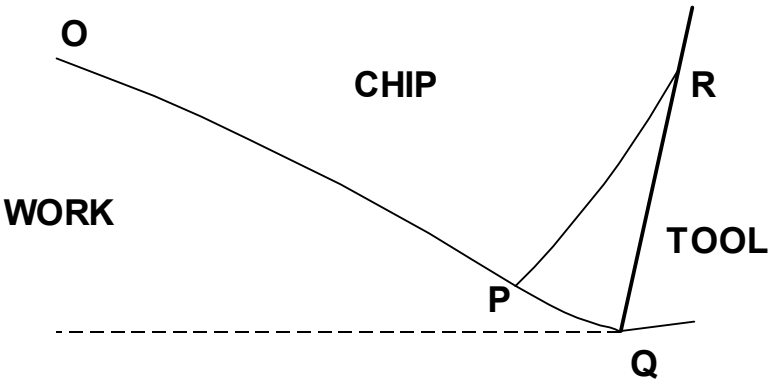

(a)

n_p	2.0
n_e	5.0
μ	1.0
γ	10^0
α	14^0
β	27.3^0
θ	12.0^0

(c)

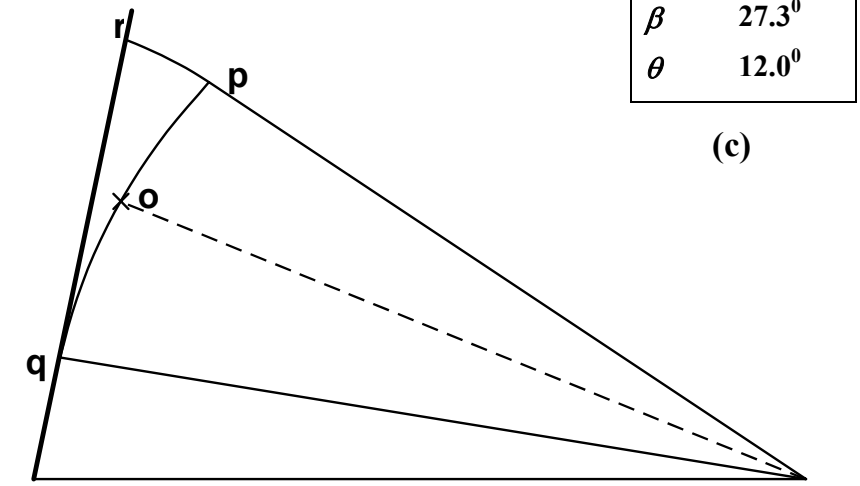

(b)

Fig. 4.17: Graphical plotting of Field II (a) Slipline field (b) Hodograph (c) Table of input/output values.

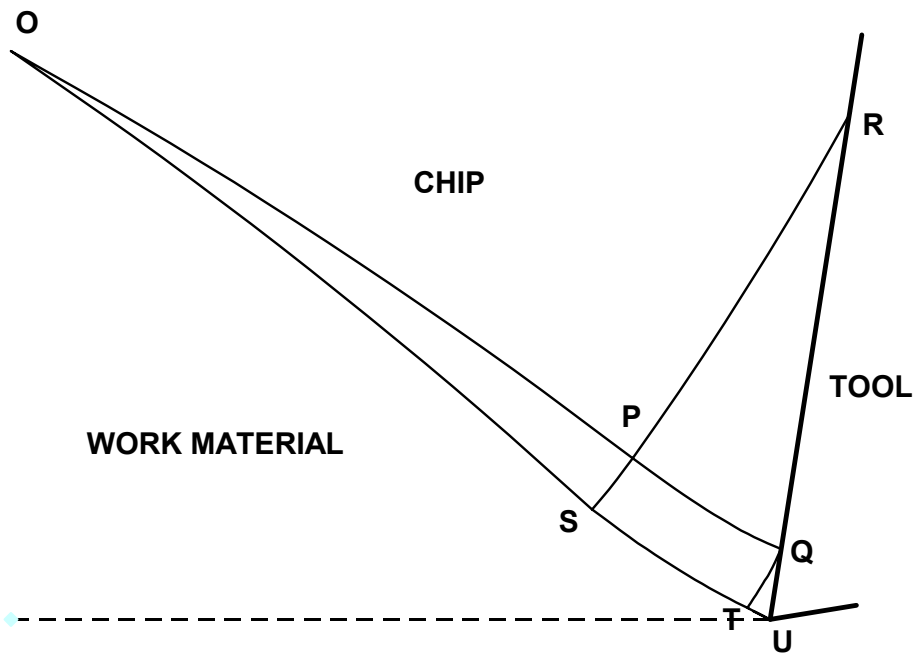

(a)

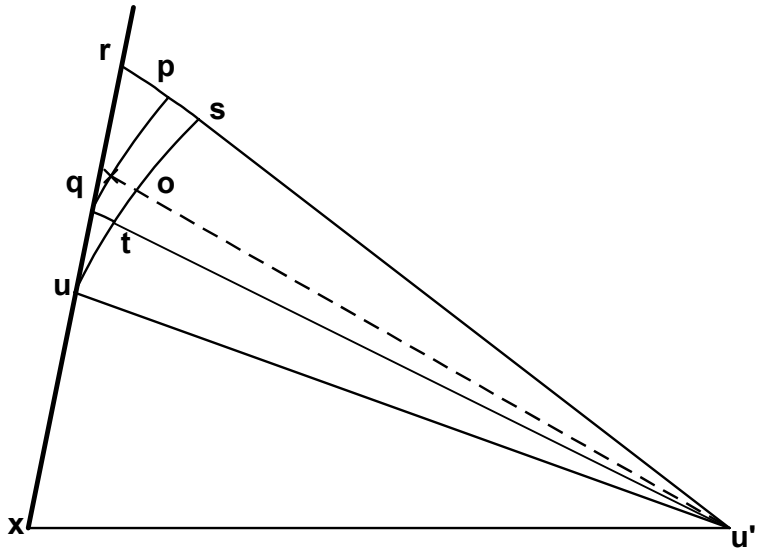

(b)

n_p	1.0
n_e	5.0
μ	1.0
γ	10^0
α	7^0
ν	5^0
β	10^0
ζ	4.5
θ	8.2^0

(c)

Fig. 4.18: Graphical plotting of Field III (a) Slipline field (b) Hodograph (c) Table of input/output values.

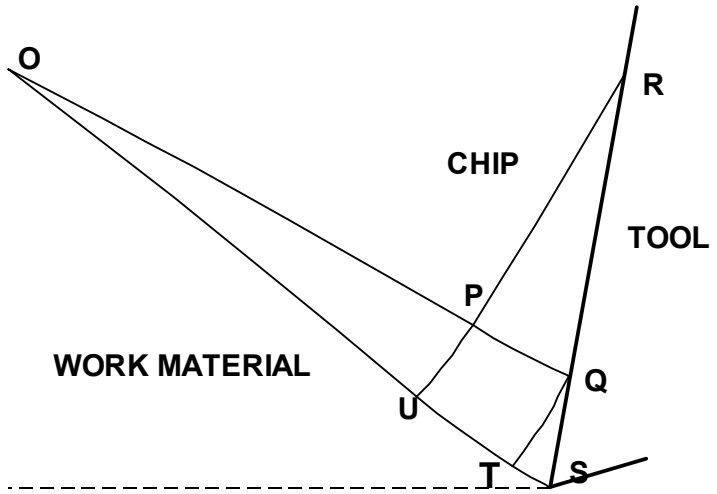

(a)

n_p	1.0
n_e	5.0
μ	1.0
γ	10^0
α	7^0
ν	10^0
β	5^0
ζ	15.2^0
θ	3^0

(c)

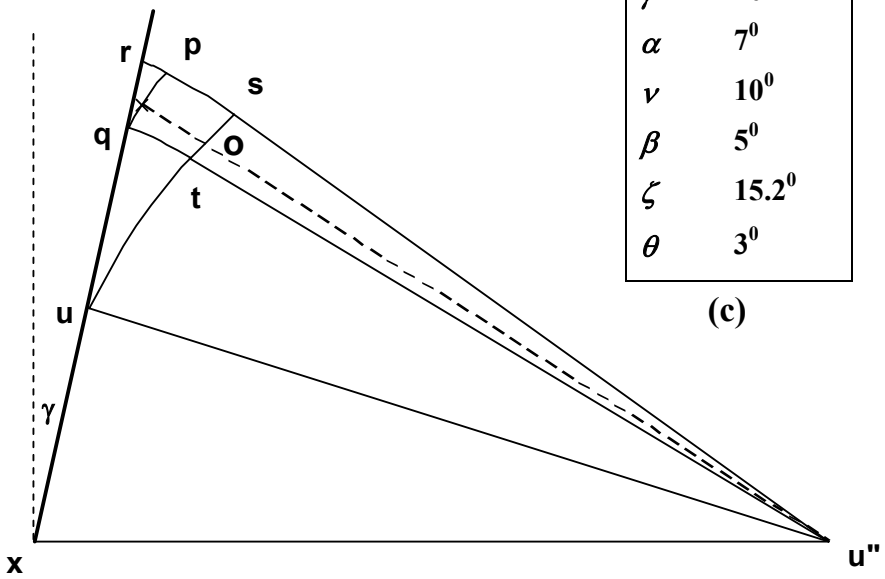

(b)

Fig. 4.19: Graphical plotting of Field III (a) Slipline field (b) Hodograph (c) Table of input/output values.

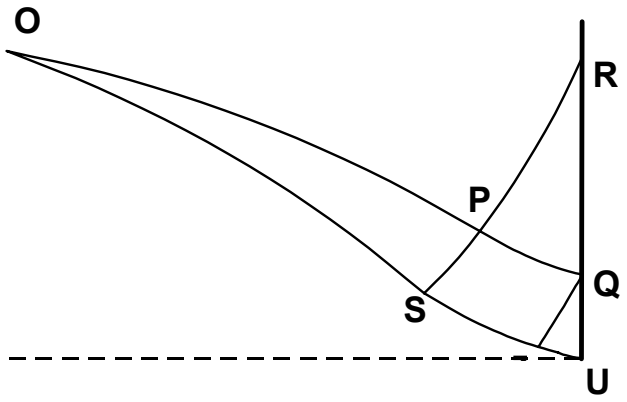

(a)

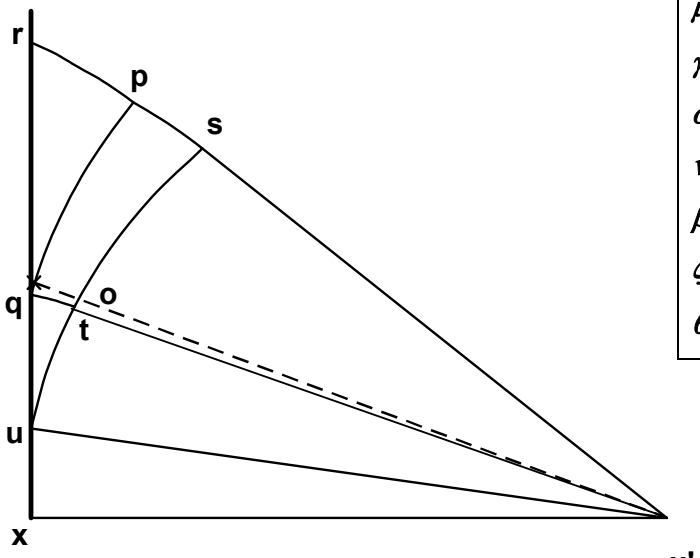

(b)

n_p	1.0
n_e	1.735
μ	1.0
γ	0^0
α	12^0
ν	10^0
β	20^0
ζ	13.7^0
θ	22^0

(c)

Fig. 4.20: Graphical plotting of Field III (a) Slipline field (b) Hodograph (c) Table of input/output values.

Chapter 5

CHAPTER 5

SLIPLINE FIELD MODELING OF ORTHOGONAL MACHINING FOR A WORN TOOL WITH ELASTIC EFFECTS AND ADHESION FRICTION AT CONTACT REGIONS:

5.1 Introduction

The importance of quantitatively estimating the technological performance of machining operations such as tool life, forces, power and surface finish attracts growing attention from the international machining research community due to the ever increasing applications of machining technologies in a wide variety of modern industries. This performance information is required for the selection and design of machine tools and cutting tools, as well as the optimization of cutting conditions for the efficient and the effective use of machining operations, so that the product quality and the operational safety in automated machining systems is assured. The machining performance is known to vary significantly with the progression of overall tool wear, including major flank wear, crater wear, minor flank wear, nose wear and groove wear at minor cutting edge. This is because the tool wear formed at different tool faces alters the original tool geometry/configuration thus resulting in unexpected machining performance. Of all the above types of tool wear, the flank wear has attracted maximum attention, since the amount of flank wear is often used in determining the tool life. In addition, the mechanism of wear development is more accurately modeled for flank wear than for crater wear.

A number of analytical and experimental techniques have been employed to study the progression of tool wear and its effect on machining performance during metal

machining. Attempts have been made to estimate the extent of tool wear from the measurement of surface roughness, cutting temperature and noise and sound signals generated during machining [28]. Tool wear and breakage have also been estimated from the vibration signals, the variation in motor current, the motor power consumption and the spindle speed [28]. But it is reported that the signal processing methods based on the force and the acoustic emission are more reliable and sensitive than other methods [28]. In stead of the cutting forces, the force ratios have been used in some cases to predict tool wear since, it is believed that the error in tool wear prediction arising out of noise present in the measurement of cutting forces is minimized by this procedure [29,30,66]. The method called *sensor fusion*, where a number of sensory systems are used simultaneously have also been attempted to provide the desired information reliably in some areas [107]. Attempts have also been made to detect flank and crater wear from the measurement of static and dynamic components of cutting forces [108] or by using a hybrid machining simulator based on the predictive machining theory and the neural network modeling [111].

The first analytical study on the *ploughing process* in metal cutting seems to have been carried out by Albrecht [94] to explain the large variation in the apparent coefficient of friction on tool/chip contact area with rake angle. Modeling of tool forces for worn tools taking account of flank wear effects has been reported by Elanayar and Shin [109] and for a tool with edge radius by Manjunathaiah and Endres [110]. More recently, the effect of tool flank wear on orthogonal cutting process has been studied by Wang et. al. [87] assuming a thin shear zone model. Flank wear and its effect on tool life has been the focus of study of a number of Russian investigators such as Zorev and Loladze and their co-workers as may be seen from references [1] and [84].

Considerable attention has also been devoted to the analysis and simulation of the machining process in the presence of tool wear using Finite Element Technique (FEM) as may be seen from the bibliography prepared by Mackerle [80]. More recently tool wear in orthogonal cutting has been estimated with acceptable accuracy using an empirical wear model from the temperature and stresses on the tool face predicted by the FEM simulation [112].

The first slipline field solution for orthogonal cutting for a worn tool with flank wear was proposed by Shi and Ramalingam [85]. The solution was *unique* and it was shown by these authors that the cutting geometry is completely determined by specifying the rake angle and tool-chip interface friction. The static admissibility condition in this solution was satisfied using a chip breaker constraint. A slipline field for ploughing has also been proposed by Waldorf, Devor and Kapoor [113] assuming a small stable build-up of material in contact with the cutting edge and a raised prow ahead of the cutting edge. More recently slipline field solutions for an edge-radiused tool have been suggested by Fang [103].

The major shortcoming of the above proposed fields is that the chip formation in these studies is assumed to take place under conditions of constant friction stress ($\tau = mk$). This is contrary to the observations made by other investigators which suggest that interface friction in metal machining is characteristically adhesion where the friction force stems from the shear fracture of the bonded asperities [61-65]. Measurement of contact stress distributions at the chip/tool interface using split tool dynamometers [50-52] or photo-elastic tools [47-49] are in agreement with this view. The solutions also do not take account of the existence of the zone of elastic contact beyond region of plastic contact which is observed in the above experimental studies.

In the present investigation slipline field solutions are proposed for a tool with finite flank wear land assuming adhesion friction at rake and flank faces. The friction law assumed is that suggested recently by Maekawa et al [65] (refer to equations 3.1 and 4.1) The solutions take account of the existence of an elastic contact region within the natural contact zone. The fields are analyzed by the matrix operational procedure developed by Dewhurst and Collins [89] and Dewhurst [92,93] and are constructed by assuming a linear relation between the angular range of $\alpha-$ and $\beta-$ lines within the secondary shear zone. Contribution of flank wear to the cutting and thrust forces is studied. It is shown that even a small amount of wear on the tool flank has significant effect on the tool-chip interface friction coefficient. It is demonstrated that though the cutting forces increase, the peak normal stress at the tool tip for a worn tool is less than that for a sharp tool. The results from the theoretical analysis are also compared with experiment.

5.2 Slipline field solutions

Two slipline field solutions for metal machining with tools with flank wear are shown in Fig. 5.1 (Field IV) and 5.2 (Field V) with their associated hodographs.

Referring to Fig. 5.1(a) it may be seen that the field consists of the primary shear zone *OQDF*, secondary shear zones *PQR* and *QCB*, two center fan fields *OGF* and *QCD* and the pre-deformation zone *OGH* with its free surface *OH* inclined to the horizontal at angle φ given by the equation,

$$\varphi = \frac{\pi}{4} - \left(\phi_R + \gamma + \alpha + \psi_1 - \theta\right) \tag{5.1}$$

where ϕ_R is the friction angle at *R*, γ is the tool rake angle, α and θ are the field angles as shown in Fig. 5.1(a) and ψ_1 is the fan angle of the center fan field *OGF*. This is calculated from the hydrostatic pressure p_R at R using the relation

$$\psi_1 = \frac{1}{2}\left[p_R + 2(\alpha + \theta) - 1.0\right] \tag{5.2}$$

It is easily verified that for flank wear land l_f = 0, the present field reduces to that suggested by Kudo [58].

Referring to the hodograph (Fig. 5.1(b)) it may be seen that the material suffers velocity discontinuities of magnitudes ρ_1 and ρ_2 on crossing the initial boundary *FD* and the final boundary *OQ* respectively of the primary deformation zone. Hence, *de* and *qp* are segments of concentric circles in the hodograph with radii ρ_1 and ρ (= $\rho_1 + \rho_2$). Within *OGH* the material moves as a rigid block in a direction parallel to the free surface *HO* and within *QCB* parallel to the flank surface *QB*. *OPR* defines the rigid-plastic chip boundary. It is assumed that the material on leaving *OPR* undergoes rigid body rotation forming a curled chip of constant curvature. Hence hodograph curves *op* and *pr* are geometrically similar to their slipline images *OP* and *PR* respectively and that *OP* is a circular arc of radius (ρ / ω) where, ω is the angular velocity of chip curl. As shown in Chapter 4, the column vector σ in the power series expansion of the radius of curvature of the base slipline *RP* is given by the equation (refer to equation 4.2)

$$\sigma = -\left(\frac{\rho}{\omega}\right) AF_{\beta\phi_Q} \rho \bar{c} \tag{5.3}$$

where *AF* is the adhesion friction operator that constructs the field between the straight rough surface *xqr* and the hodograph curve *qp* consistent with the friction law stated in equation (4.1) and $\bar{c}$ is column vector representing a circle of unit radius. In the above equation ϕ_Q (= $\phi_R + \alpha - \beta$) is the friction angle at *Q* and β is the angular range of *qp*.

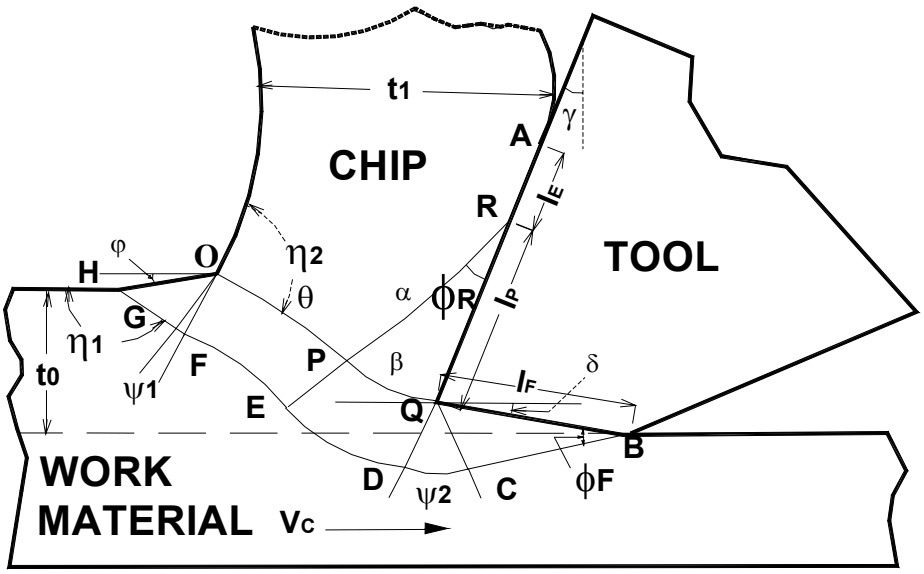

(a)

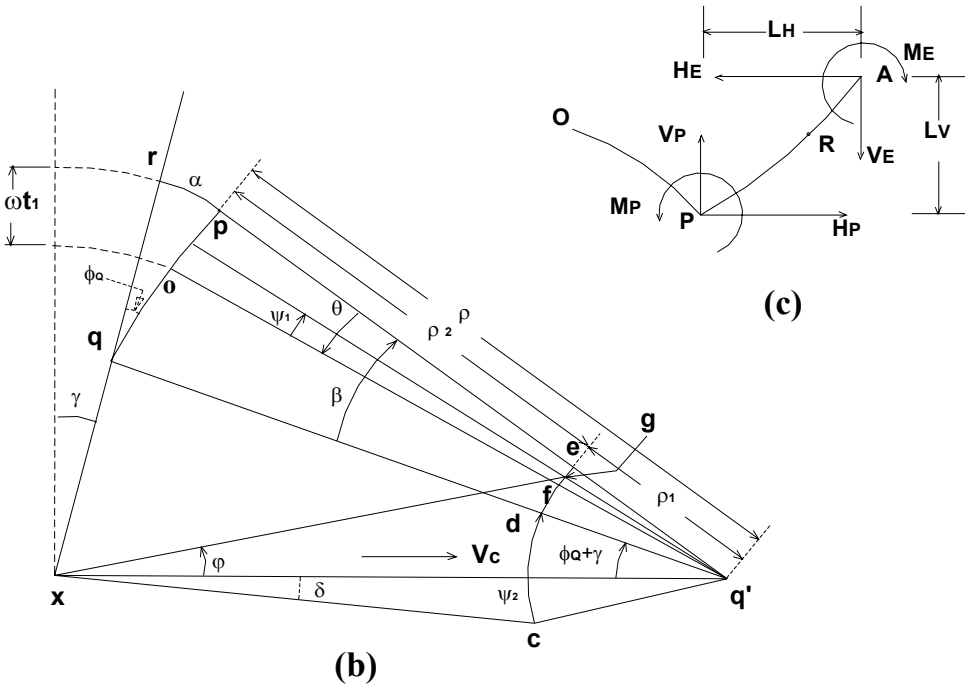

Fig. 5.1: Field IV (a) Slipline field (b) Hodograph (c) Forces and moment On the chip.

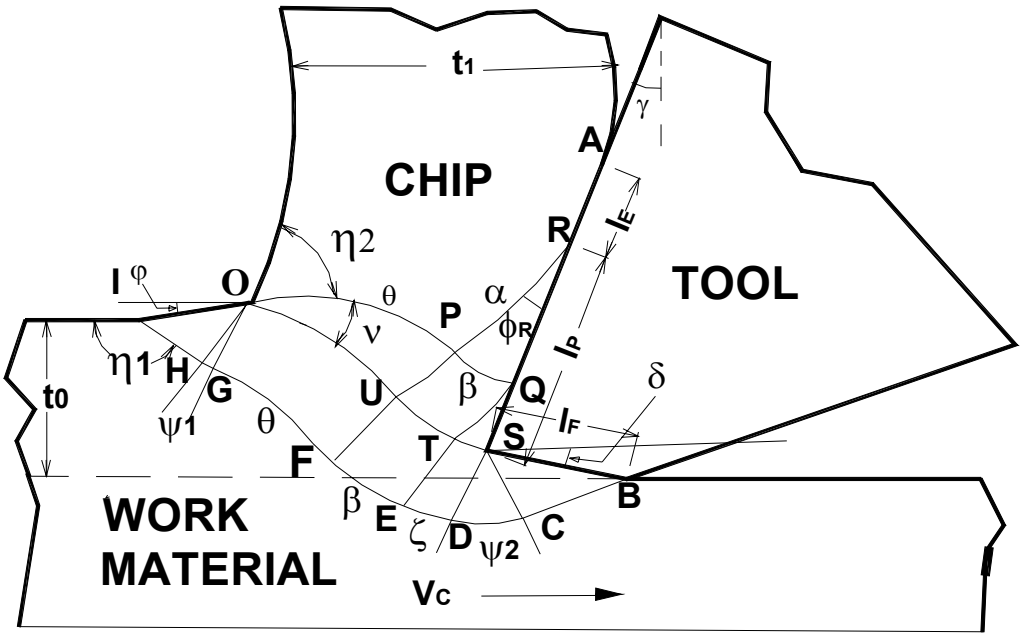

(a)

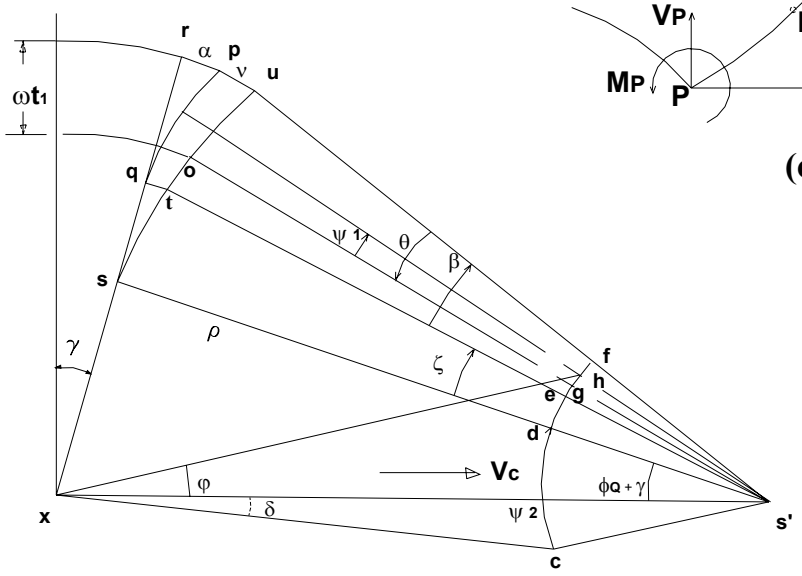

(b)

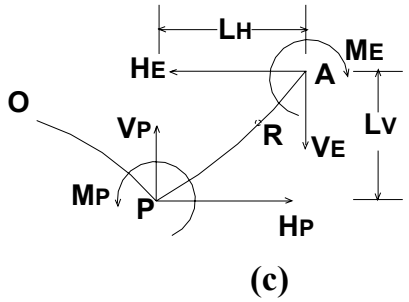

(c)

Fig. 5.2: Field V (a) Slipline field (b) Hodograph (c) Forces and moment on the chip.

Field V shown in Fig. 5.2 (a) is very similar to Field IV except that a singular field *OPU* now separates the chip from the primary shear zone. With reference to it's hodograph (Fig 5.2(b)) it is also verified that all velocity boundary conditions are satisfied. The inclination angle φ of the free surface *IO* with horizontal for this field is given by equation

$$\varphi = \frac{\pi}{4} - \left(\phi_R + \alpha + \upsilon + \gamma + \psi_1 - \theta\right) \tag{5.4}$$

where, $$\psi_1 = \frac{1}{2}\left[p_R + 2\left(\alpha + \theta + \upsilon\right) - 1.0\right] \tag{5.5}$$

In the above equations ν is the angular range of the center fan *OPU* as shown in the above figure.

The matrix equations yielding the radii of curvature of sliplines *OP* and *PR* for this field are derived in Chapter 4. These may be written as (refer to equations (4.8) and (4.9).

$$OP = -\left(\frac{\rho}{\omega}\right) s_\xi \left(P_\upsilon^* + Q_\upsilon^* R_\upsilon A F_{\zeta\phi_Q}\right)\bar{c} \tag{5.6}$$

$$RP = -\left(\frac{\rho}{\omega}\right) A F_{\beta\phi_U} \left(P_\upsilon^* + Q_\upsilon^* R_\upsilon A F_{\zeta\phi_Q}\right)\bar{c} \tag{5.7}$$

where, $$\xi = \beta - \theta \tag{5.8}$$

5.3 Method of solution

Field IV and Field V shown in figures 5.1 and 5.2 respectively are of "direct" type and are characterized by five degree of freedom defined by the field angles α, θ, ψ_2, δ and the hydrostatic pressure p_R at *R*. The fields therefore can be constructed if these five field variables are known. The five equations from which these five variables are determined may be written as

$$F_1 = H_P - H_E = 0 \tag{5.9}$$

$$F_2 = V_P - V_E = 0 \tag{5.10}$$

$$F_3 = M_P - M_V + H_E L_V - V_E L_H = 0 \tag{5.11}$$

$$F_4 = \sin\delta - \sqrt{2}\sin\varphi \sin\phi_B = 0 \tag{5.12}$$

$$F_5 = \cos(2\phi_B) - \left[1 - e^{-\left(\mu\left(p_B + \sin(2\phi_B)\right)\right)^{n_p}}\right]^{\frac{1}{n_p}} = 0 \tag{5.13}$$

where, ϕ_B and p_B are the friction angle and the hydrostatic pressure at *B* respectively (Fig. 5.1(a) and Fig. 5.2(a)), H_P , V_P and M_P are the forces and moment at the rigid-plastic chip boundary, H_E , V_E and M_E are the elastic forces and moment calculated assuming exponential stress distribution in the elastic contact zone (equation 4.10), L_H and L_V are the horizontal and vertical distances of *A* from *P* as shown in Fig. 5.1(c) and Fig. 5.2(c)) and δ is the inclination of the flank wear land with the horizontal.

Equations (5.9)-(5.11) are written down from the requirement of the static admissibility condition of the chip, equation (5.12) states that the ratio (ρ_I / V_C) calculated from the lower and upper triangles of the hodographs (Fig. 5.1(b) and Fig. 5.2(b)) have the same value $\left(\left(\rho / V_C\right) = \left(\sin\varphi / \sin\left(\frac{3\pi}{4}\right)\right) = \left(\sin\delta / \sin\phi_B\right)\right)$ and equation (5.13) ensures that adhesion friction condition also obtains on the flank wear land *QB*.

ϕ_B and p_B in equations (5.12) and (5.13) are related to the field angles in the two slipline fields by the following equations:

Field IV:

$$\phi_B = \psi_2 + \delta + \beta - \left(\phi_R + \alpha + \gamma\right) \tag{5.14 (a))}$$

$$p_B = p_R + 2\left(\alpha + \beta + \psi_2\right) \tag{5.14(b))}$$

Field V:

$$\phi_B = \psi_2 + \delta + \beta + \zeta - \left(\phi_R + \alpha + \gamma + \upsilon\right) \tag{5.15 (a)}$$

$$p_B = p_R + 2\left(\alpha + \beta + \upsilon + \zeta + \psi_2\right) \tag{5.15 (b)}$$

where, p_R is the hydrostatic pressure at *R*..

Equations (5.9)-(5.11) for the present fields were solved using the algorithm developed by Powell [104] to determine the field variables θ (angular range of slipline curve *OP*), p_R (hydrostatic pressure at *R*) and *X* (ratio of elastic to plastic contact lengths). The procedure was similar to that followed for solution to equations (4.11) in Chapter 4. These optimized field parameters were then used to compute φ, ϕ_B and p_B from equations (5.1), (5.2) and (5.14) for Field IV or from equations (5.4), (5.5) and (5.15) for Field V and then determine ψ_2 and δ by solution to equations (5.12) and (5.13). As these equations are non-linear these were solved by the algorithm developed by Powell [104]. δ and ψ_2 were assumed to be correctly estimated when sum of the square of the residuals was less than 10^{-10} .

In this manner all the field variables for both the fields could be computed. These data were then used to construct the slipline fields and hodographs and calculate the machining parameters. The program incorporated Hill's inequalities [45] to check for the overstressing of the chip at the rigid vertex at *O* and that of the work piece at the rigid vertex *H* (or *I*). With reference to Fig. 5.1(a) and Fig. 5.2(a) these inequalities may be written as ,

$$-\frac{1}{2} + \cos\left(\eta_2 - \frac{\pi}{4}\right) \le \frac{p_0}{2k} \le \frac{1}{2} + \left(\eta_2 - \frac{\pi}{4}\right) \tag{5.16(a)}$$

and $$\eta_1 \ge \frac{3\pi}{4}\ ,\ \varphi \ge 0 \tag{5.16(b)}$$

The programme also checked for tool flatness both in the slipline fields and

hodographs (due to the simplification, $\beta = m_0\alpha$) . The programme was terminated when either the vertex angle η_1 at O was overstressed or when the friction angle at the tool tip became negative. For the complete range of solutions studied, the vertex angle η_2 was never found to be overstressed.

5.4. Results and discussion

The predicted variation of peak tool-tip pressure with rake angle as computed from the present analysis is shown in figure 5.3 for slipline Field IV and in Fig. 5.4 for slipline Field V. For prescribed friction parameters the tool-tip pressure for both the fields increased with angular range α of the base slipline PR and was maximum when α was maximum and was such that the vertex angle η_1 at H (I for Field V) became overstressed (equation 5.16 (b)). Referring to these figures it may be seen that the peak tool tip pressure for a sharp tool is much higher compared to that for a worn tool with a finite flank wear land and this is in agreement with the results of the photo-elastic analysis reported by Chandrasekharan et al [115]. The figures also indicate that the peak pressure for a worn tool is only marginally influenced by the tool rake angle. For both the fields the effect of the size of the flank wear land on peak pressure was also found to be similar. It may also be seen that for a given tool rake angle and friction condition , the peak pressure predicted by Field V is higher than that predicted by Field IV.

In Fig. 5.3 and Fig. 5.4 the peak tool-tip pressure for a sharp tool as computed from the present analysis is compared with that calculated from Loladge's equation [115]

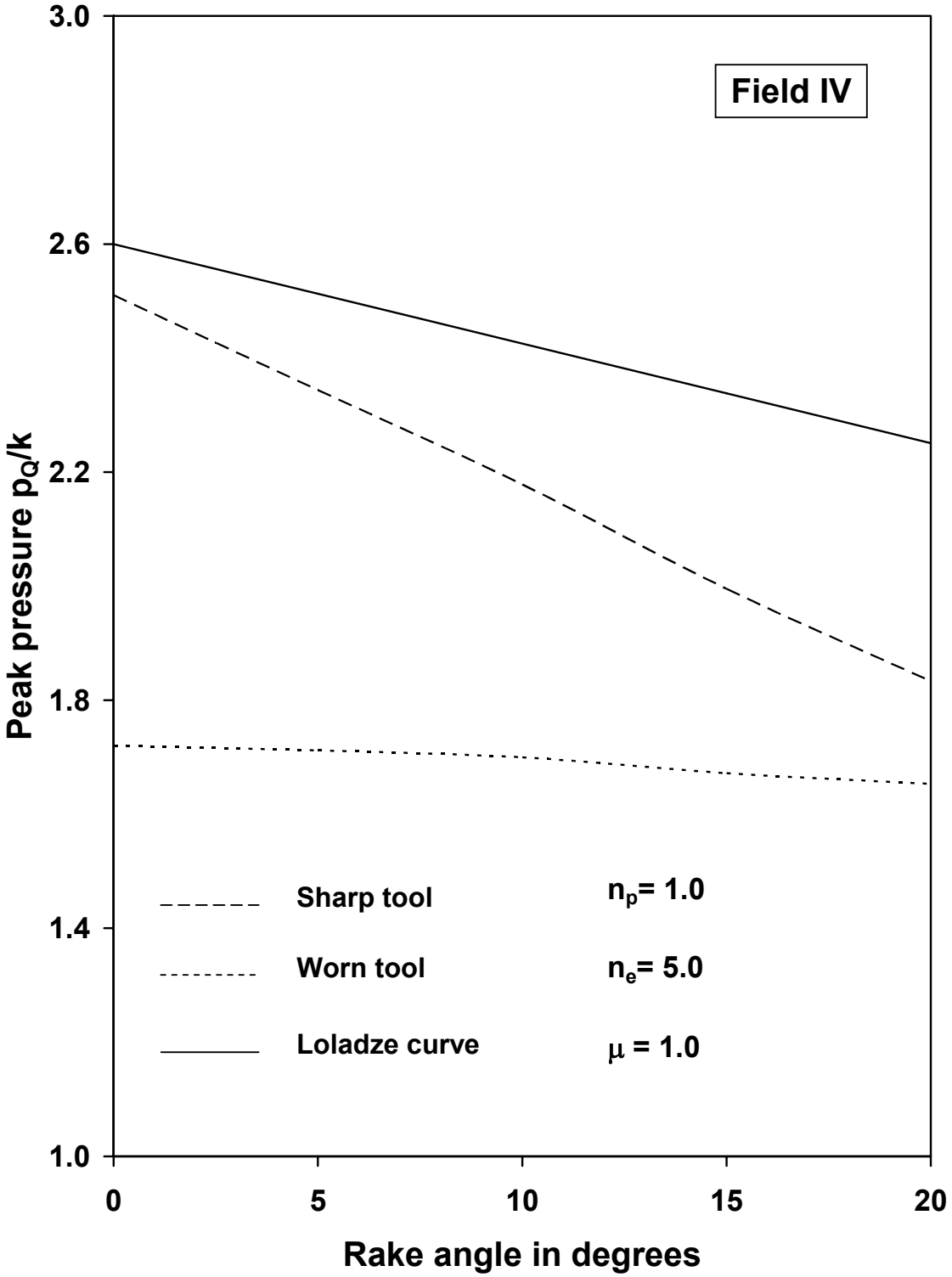

Fig. 5.3: Variation of peak tool-tip pressure with rake angle.

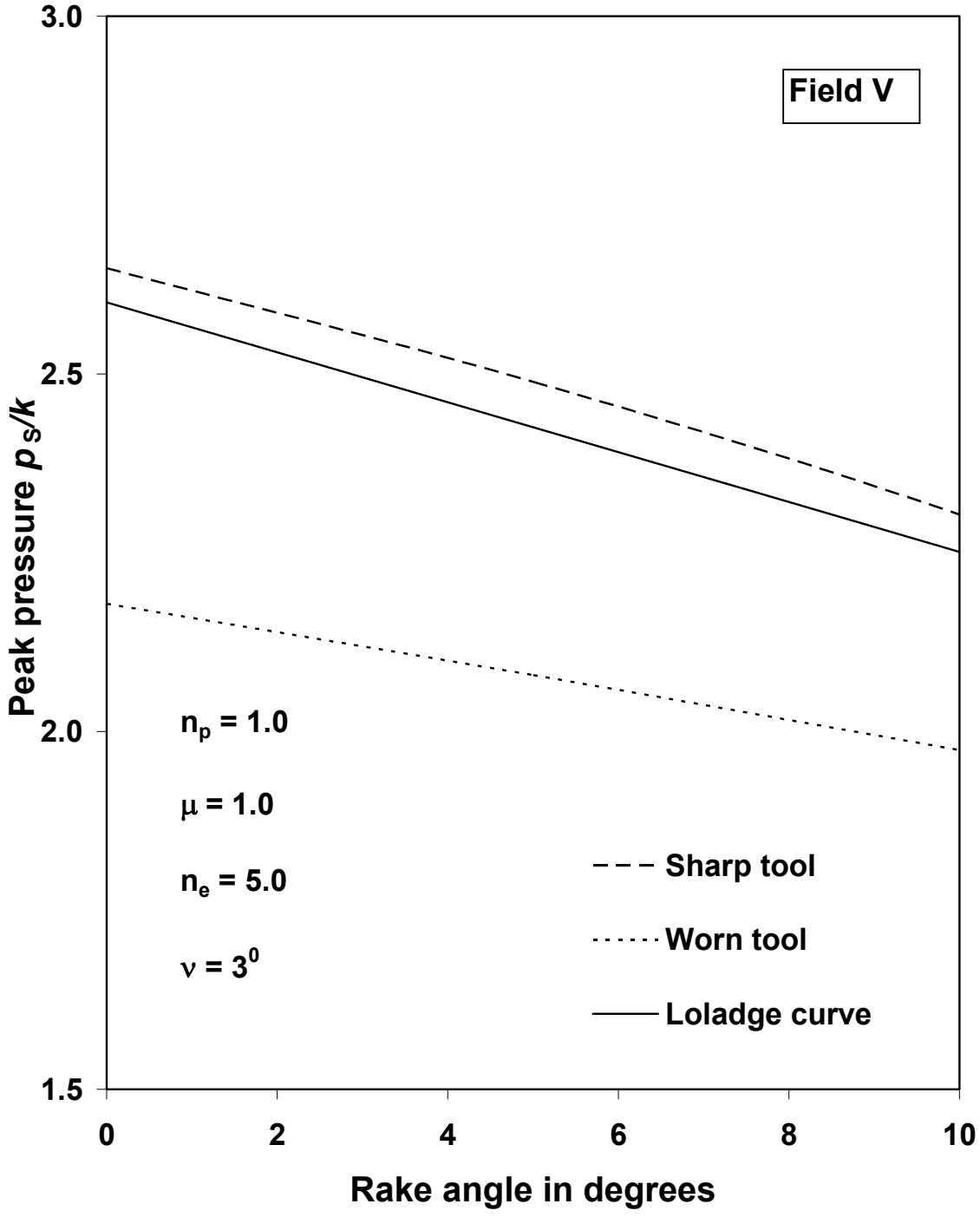

Fig. 5.4: Variation of peak tool-tip pressure with rake angle.

$$\frac{p}{2k} = 1.3 - \gamma \tag{5.17}$$

where, γ is the tool rake angle. The figures indicate that while the peak pressure calculated from equation (5.17) is of the same order as that calculated from Field V (Fig. 5.2) it may deviate considerably from that calculated from Field IV (Fig. 5.1).

The results of computation of cutting and ploughing forces are shown graphically in Fig. 5.5 and Fig. 5.6 for Field IV and Field V respectively where these are plotted against the non-dimensional flank wear parameter (l_f / t_0). The results refer to the field geometries for which the vertex angle η_1 at O is overstressed (limit (OSL-1)). The figures indicate that the ploughing, cutting and thrust forces vary linearly with flank wear and that the thrust forces increase more rapidly than the cutting forces. Both these observations are in agreement with those reported by Shi and Ramalingam [85].

The variation of force ratio (F_t / F_c) with flank wear for the two fields are illustrated in figures 5.7-5.10 where the theoretical results are compared with the experimental observations of Kobayashi et al [66] and Choudhury et al [30]. The results shown in figures 5.7-5.8 demonstrate the effect of μ on force ratio (n_p=1) while, those presented in figures 5.9-5.10 show the effect of n_p (μ =1). Referring to these figures it may be seen that for any given value of (l_f / t_0), the force ratio is not uniquely determined but may have a range of allowable values. For Field IV this range is bounded by Lee and Shaffer's limit (LSL) and the overstressing limit (OSL-1) and for Field V by the modification to Lee and Shaffer's solution as suggested by Kudo [58] (Kudo limit KL) and the overstressing limit (OSL-1). The figures also demonstrate that increasing either μ or n_p decreases the force ratio and the solution

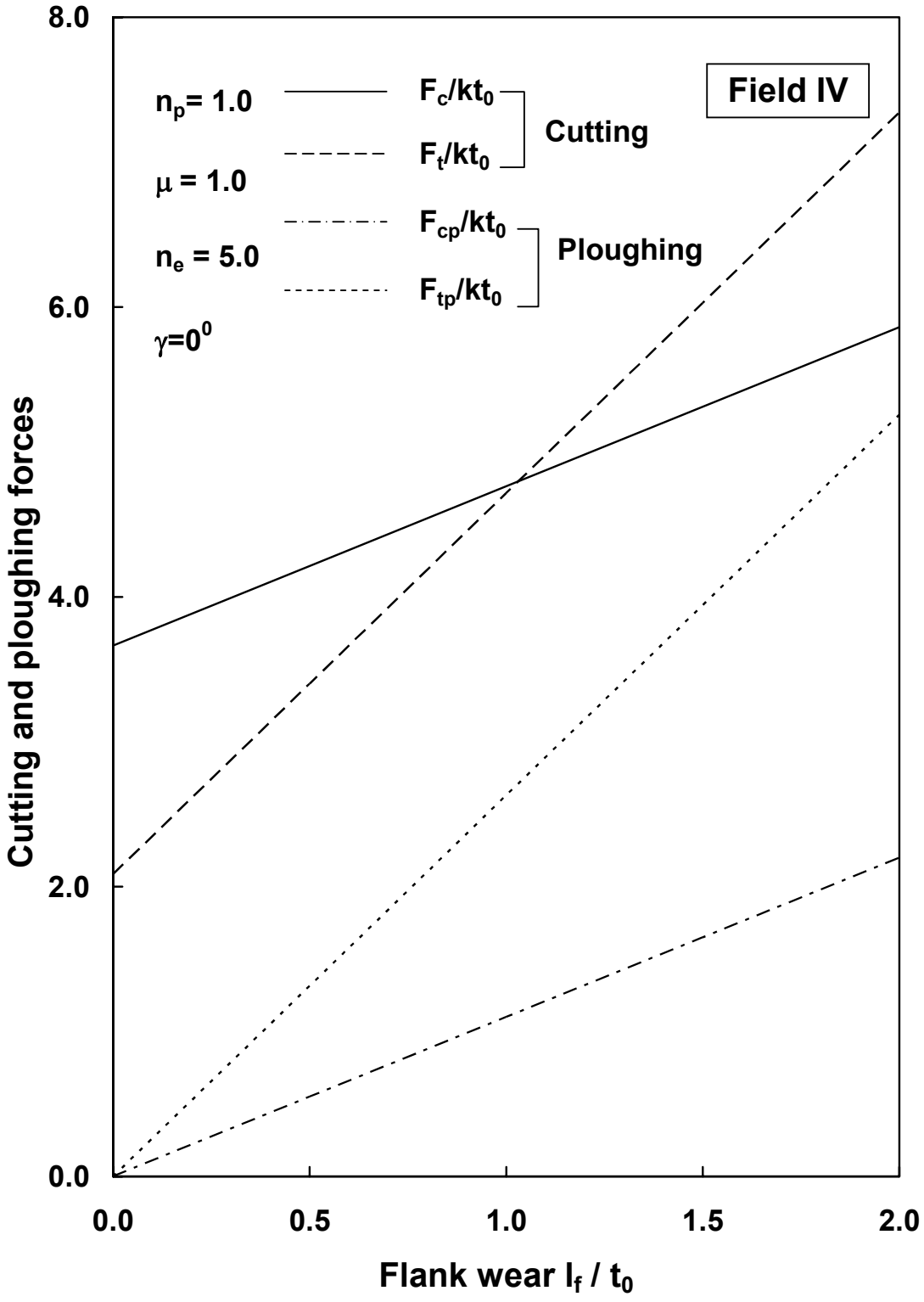

Fig. 5.5. Effect of flank wear on cutting and ploughing forces.

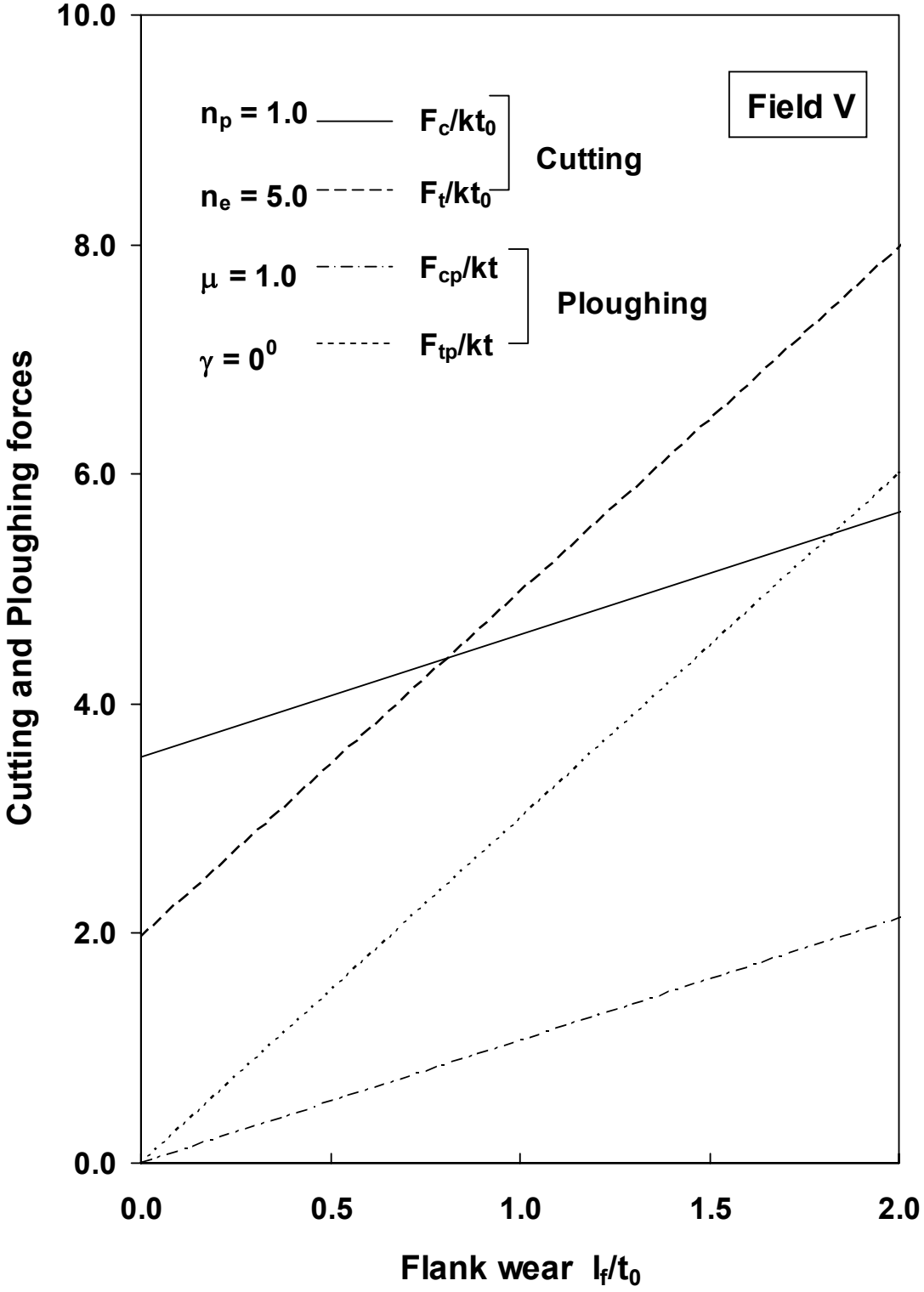

Fig. 5.6: Effect of flank wear on cutting and ploughing forces.

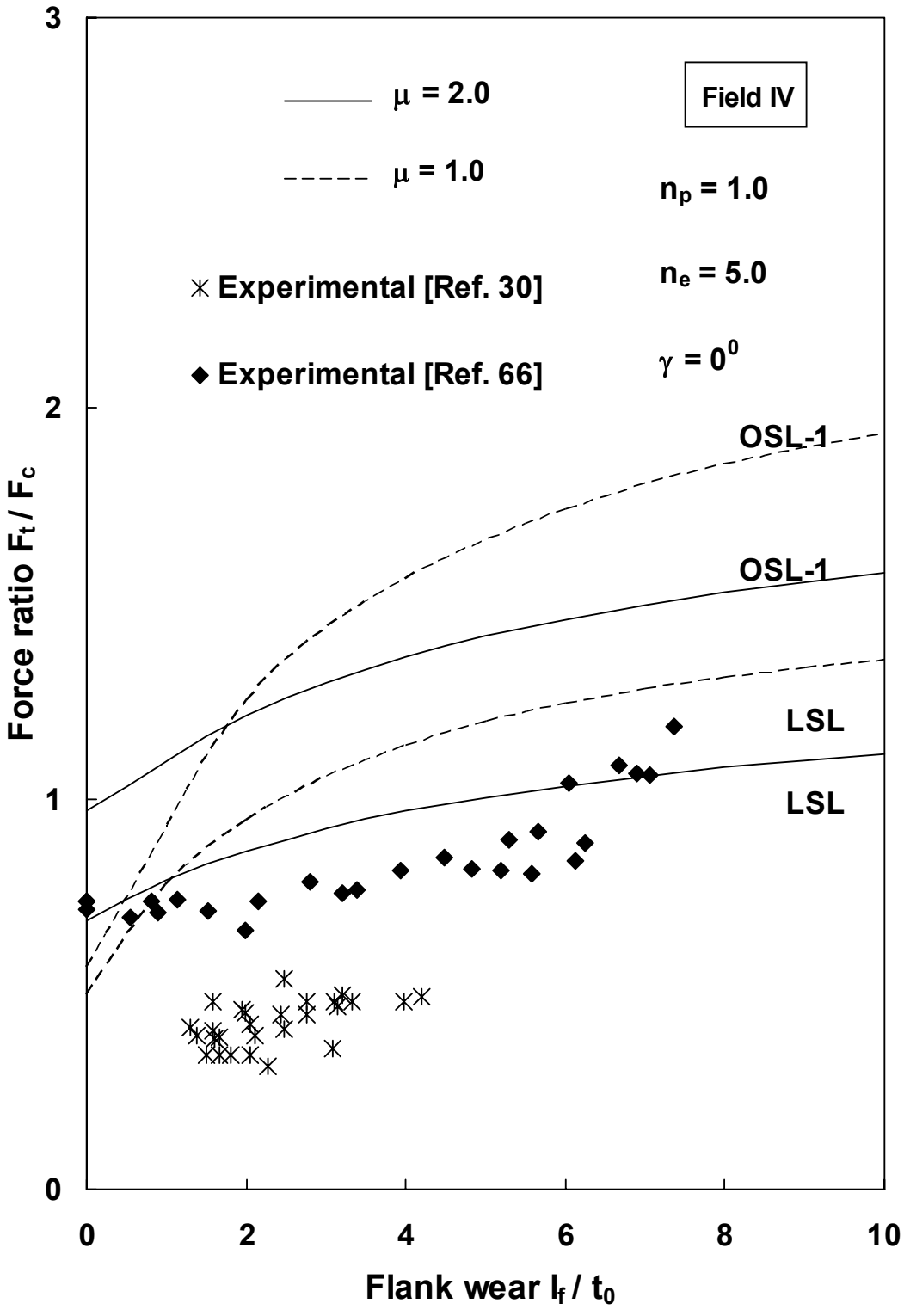

Fig. 5.7: Effect of flank wear on force ratio (OSL-1: Overstressing limit, LSL: Lee and Shaffer limit)

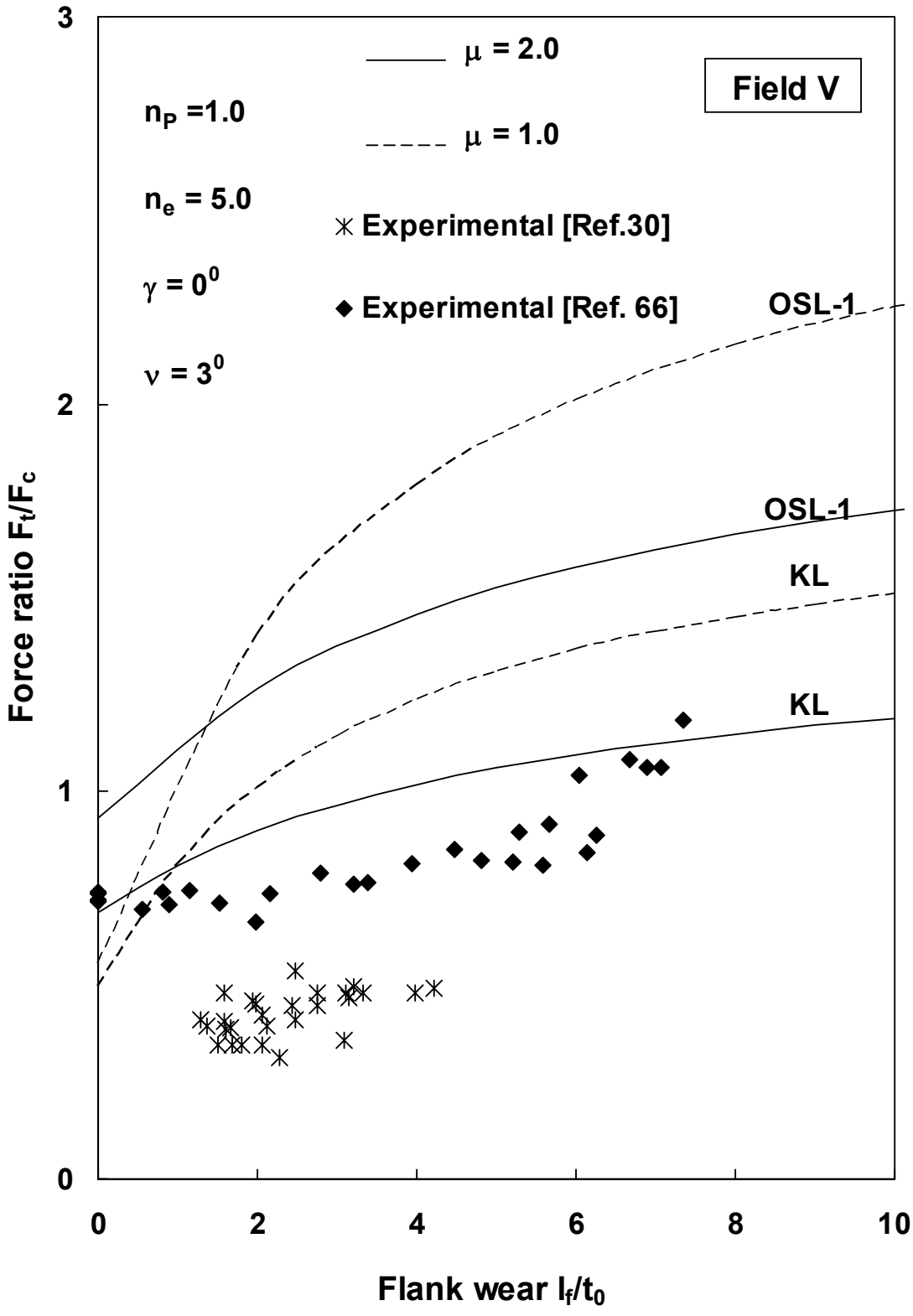

Fig. 5.8: Effect of flank wear on force ratio.

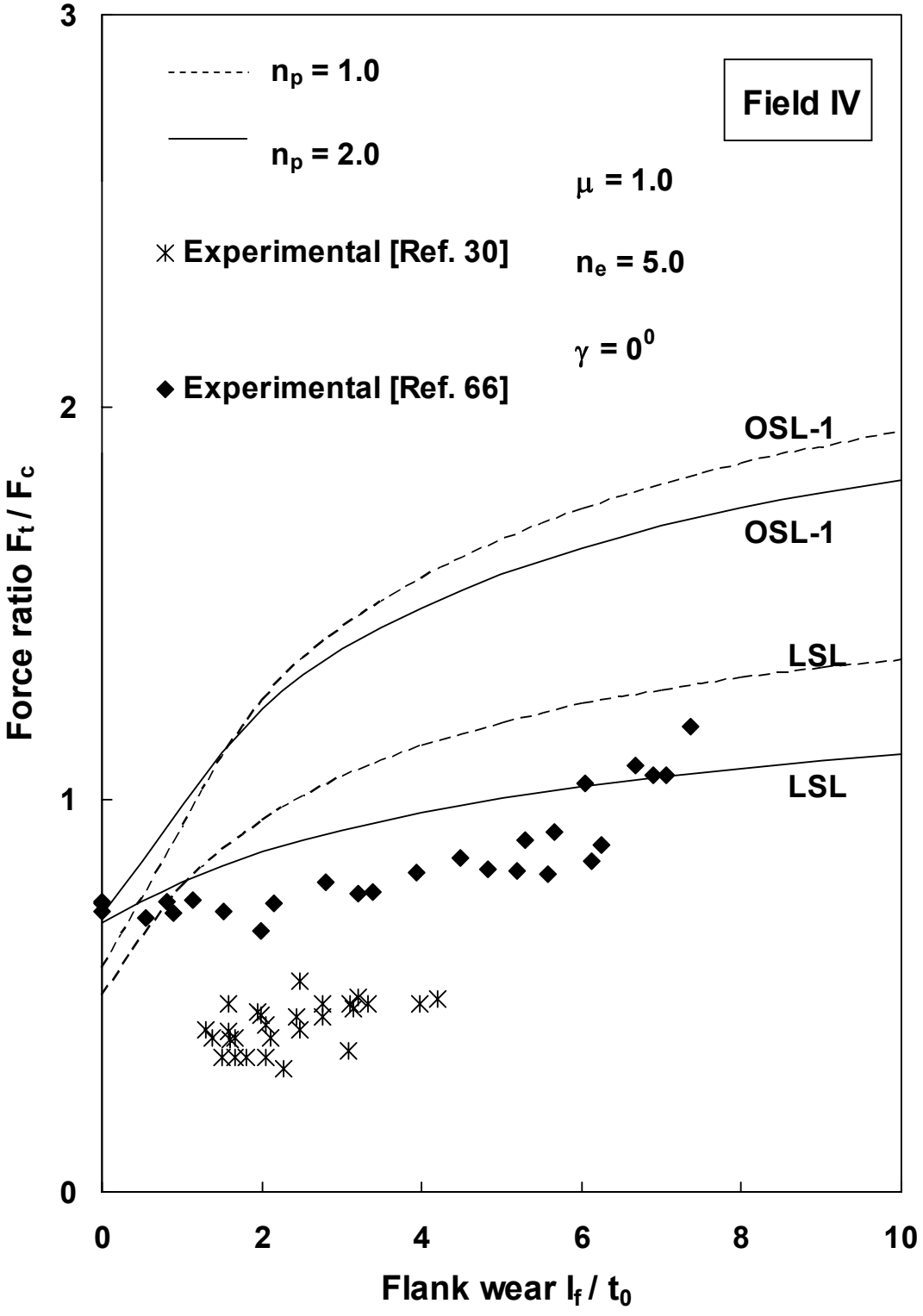

Fig. 5.9: Effect of flank wear on force ratio.

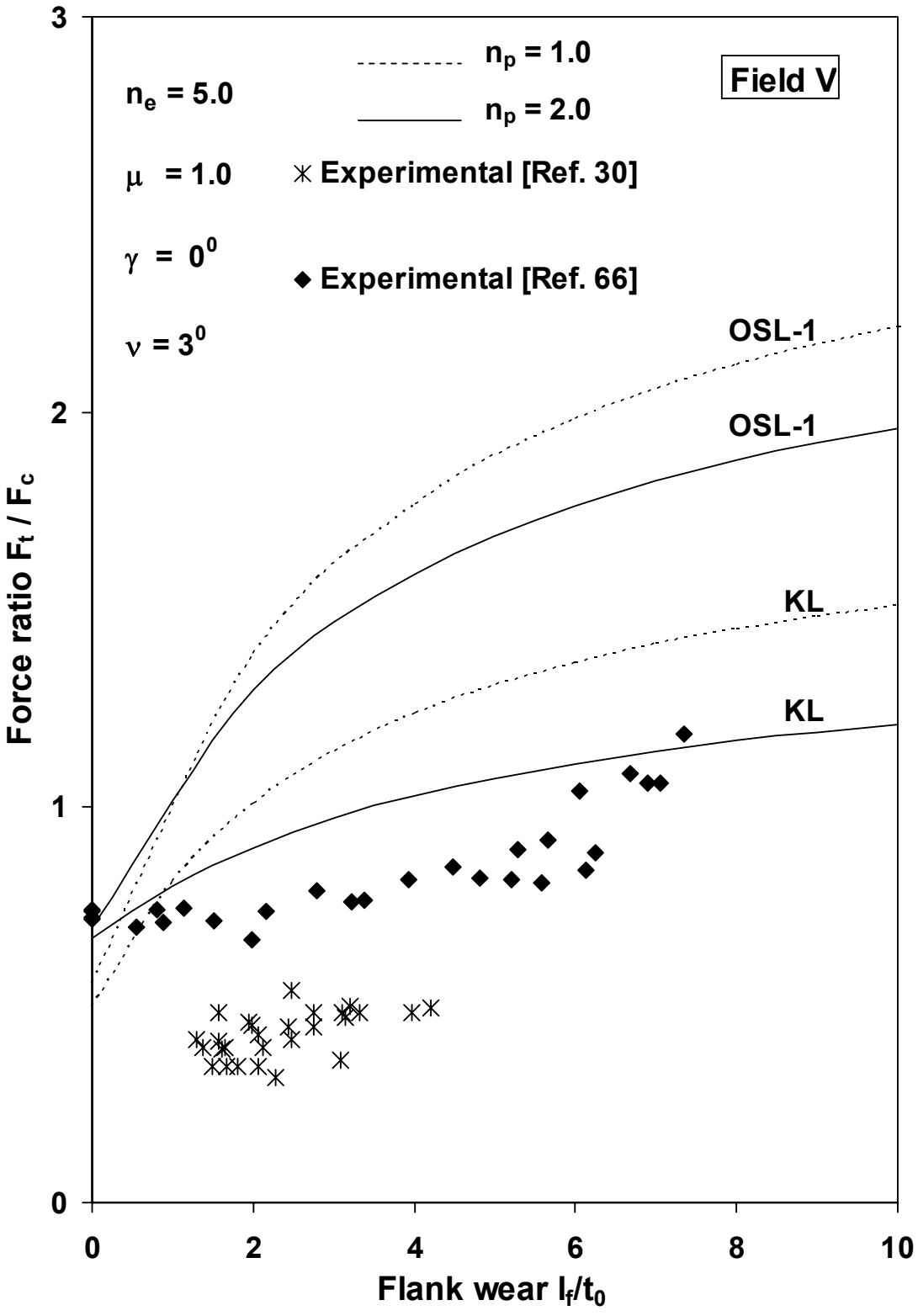

Fig. 5.10: Effect of flank wear on force ratio.

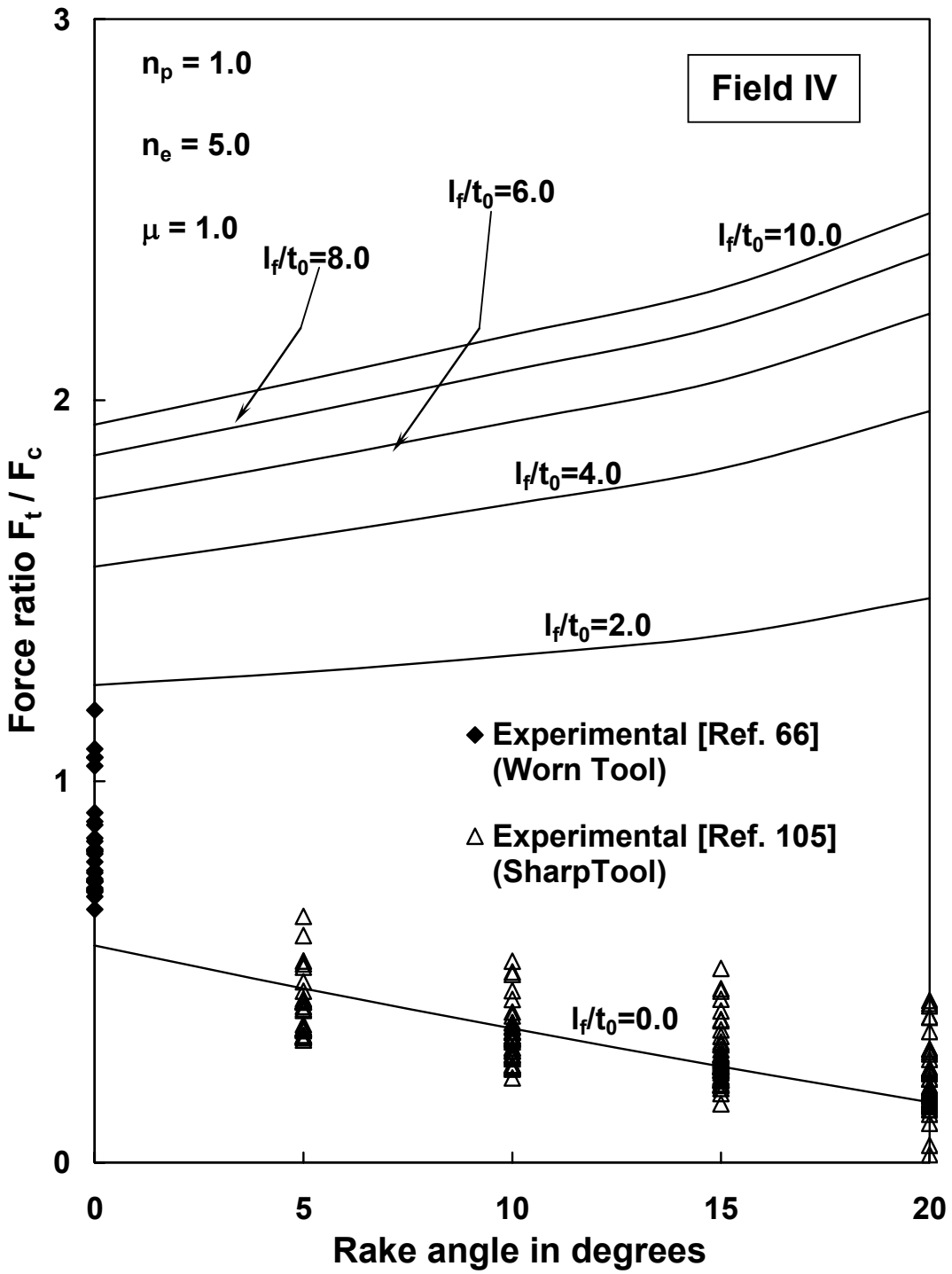

Fig. 5.11: Variation of force ratio with rake angle for sharp and worn tools.

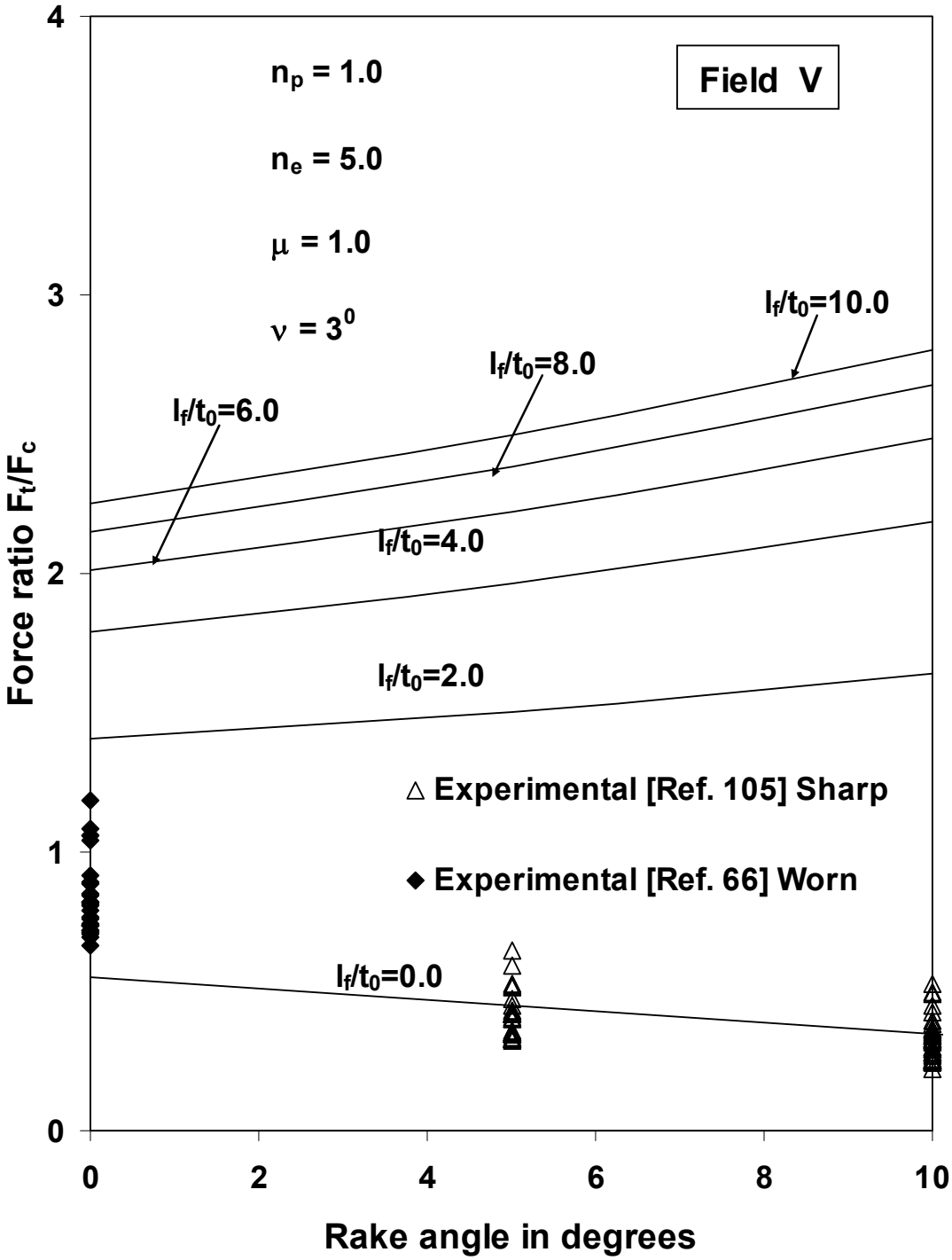

Fig. 5.12: Variation of force ratio with rake angle for sharp and worn tools.

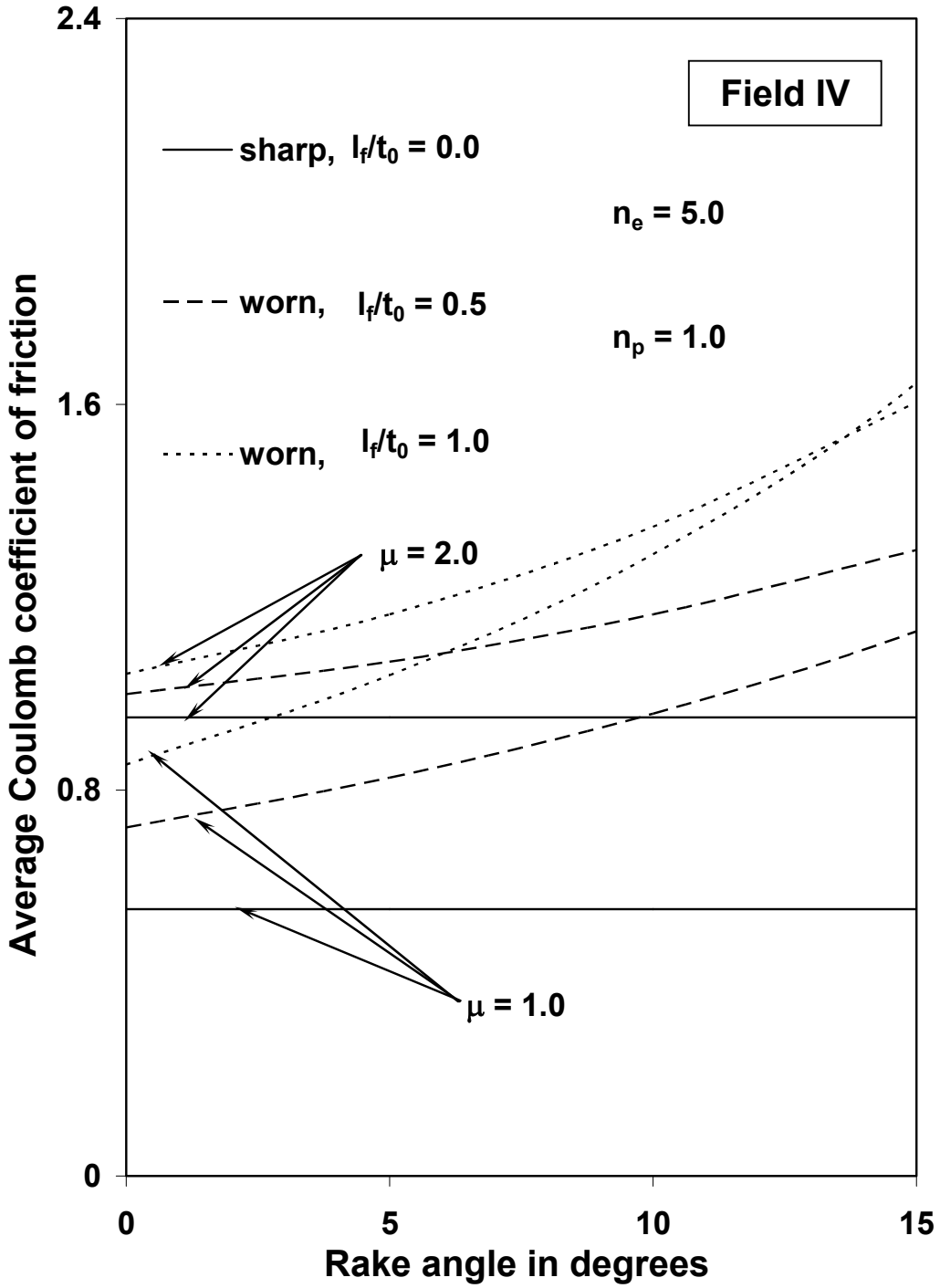

Fig. 5.13: Variation of average Coulomb coefficient of friction with rake angle for sharp and worn tools.

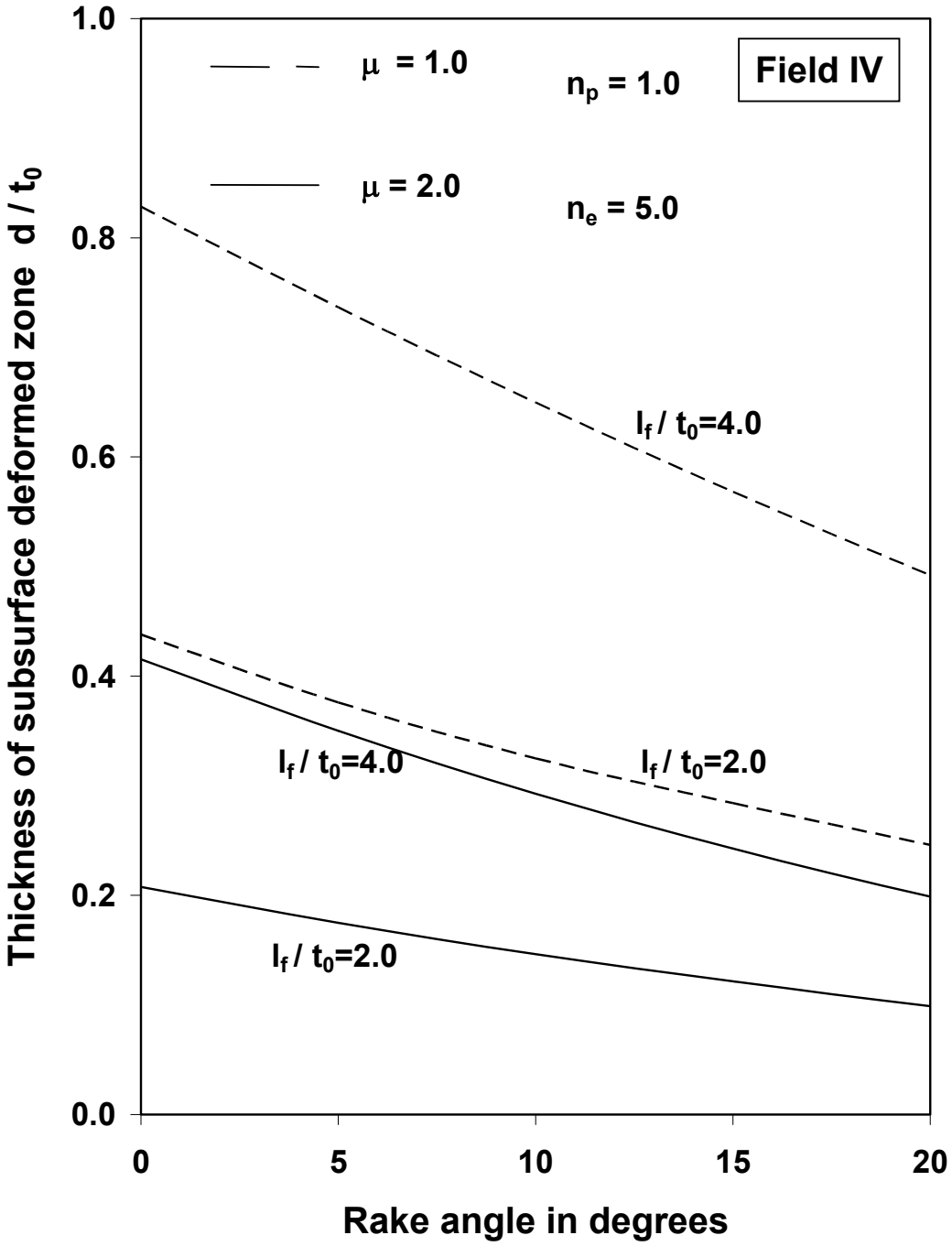

Fig. 5.14: Effect of rake angle on thickness of subsurface deformation zone.

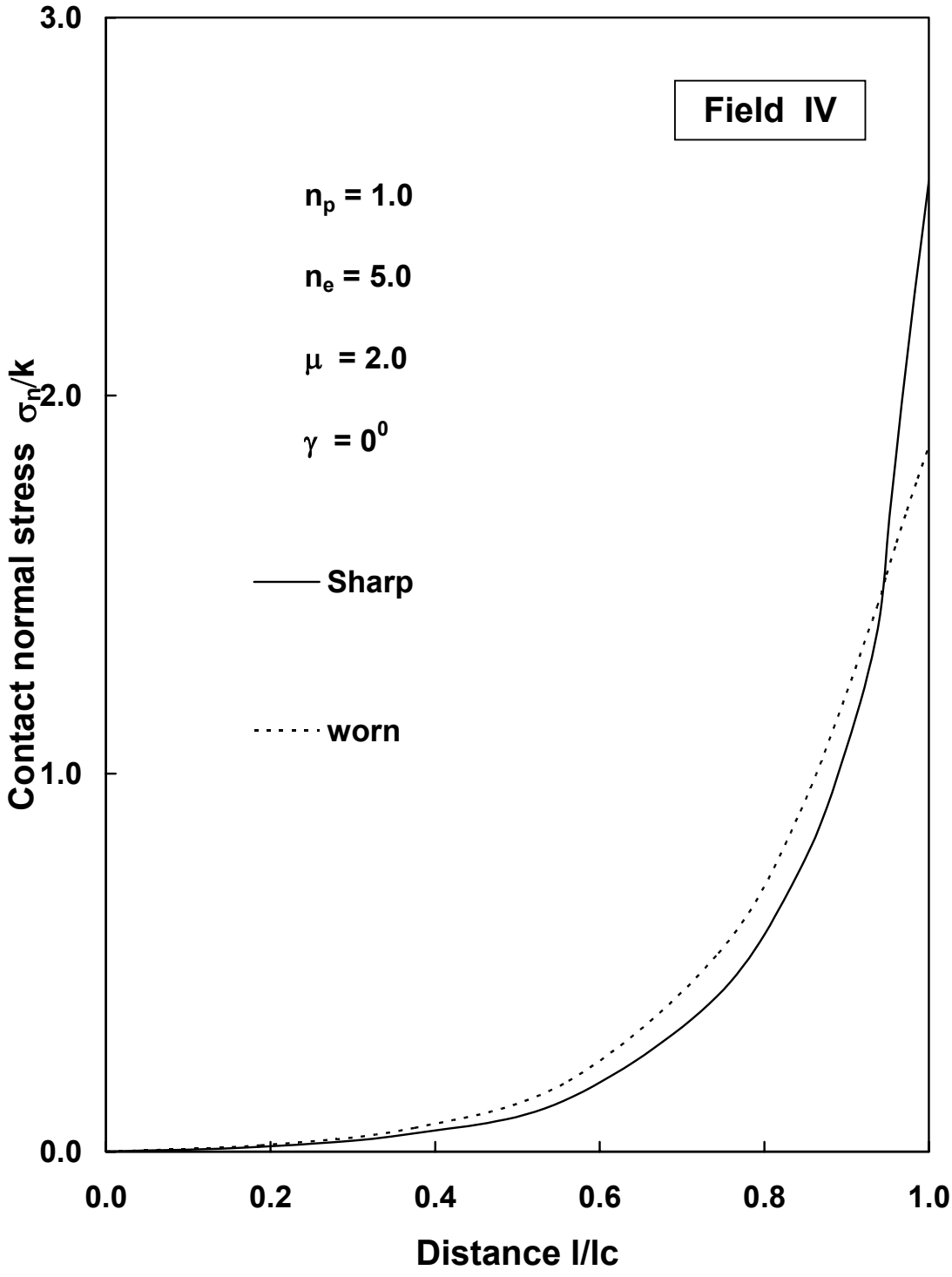

Fig. 5.15: Distribution of contact normal stress at chip-tool interface for sharp and worn tools.

range though the absolute values of the forces may increase [66]. It may further be observed that the experimental results do not compare well with the present theoretical values. This may be due to the fact that friction parameters μ and n_p in these experiments were probably higher than the μ and n_p values used in the present theoretical calculations. However the nature of variation exhibited by the above set of experimental results are similar to that predicted by the slipline field theory.

It may be seen that the force ratio for a sharp tool as calculated from the present slipline field analysis decreases with rake angle and this observation compares favorably with the experimental results especially at lower rake angles (figures 5.11 and 5.12) [105]. However, the presence of even a small flank wear land (low (l_f/t_0) value) is found to reverse this trend. The same observations are also found to be true for the average Coulomb coefficient of friction at chip-tool interface calculated from cutting and thrust forces (Fig. 5.13). In earlier studies of friction process in metal cutting especially by Finnie and Shaw [64] and by Kobayashi and Thomsen [66] this increase in μ with γ was thought to be a characteristic of the machining process itself. It must be emphasized that in these studies the tool was assumed to be perfectly sharp. In fact Albrecht [94] had pointed this out as early as in 1960 that this rather anomalous behavior is a consequence of tool wear. This observation is now verified by slipline field analysis.

The variation of subsurface deformation zone thickness (d / t_0) with rake angle is presented in Fig. 5.14. The thickness of the plastically deformed layer appears to increase with increase in the length of the flank wear land l_f and decrease with interface friction coefficient μ.

Theoretical normal stress distribution for a worn tool with 0^0 rake angle is shown in Fig. 5.15 where it is compared with that for a sharp tool. The results agree qualitatively with those of photo-elastic analysis by Chandrasekharan et al [115].

5.5. Conclusions

Slipline field solutions for a tool with flank wear are proposed assuming rake and flank face friction to be governed by the adhesion friction law proposed by Maekawa et al [65]. The fields are similar to that suggested by Shi and Ramalingam [85] and are analyzed by assuming a region of elastic contact beyond the zone of plastic contact such that the elastic forces in this zone together with the forces in the rigid-plastic chip boundary keep the chip in equilibrium. The validity of the proposed solutions is examined using Hill's overstressing criteria [45].

The results of the theoretical analysis indicate that the peak tool tip pressure for a sharp tool decreases with rake angle and is much higher than a worn tool with a finite flank wear land. It is further observed that the peak pressure for a worn tool is only marginally influenced by the tool rake angle and the size of the flank wear land.

The ploughing, cutting and thrust forces vary linearly with flank wear and that the thrust forces increase more rapidly than the cutting forces. The results also demonstrate that increasing the friction coefficient μ decreases the force ratio (F_t / F_c). It is further seen that the force ratio and the average Coulomb coefficient of friction at chip-tool interface for a sharp tool decrease with rake angle. But the presence of a small flank wear land may reverse the trend. The thickness of plastically deformed layer appears to increase with increase in the length of the flank wear land l_f and decrease with interface friction coefficient μ. The results of

theoretical normal stress distribution at chip-tool interface for worn and sharp tools agree qualitatively with experiment.

5.6. Plotting of some slipline fields and Hodographs

In the subsequent sections the slipline field networks graphically plotted for Field IV for the set of input values of (n_e=5, , n_p=1, μ=1, γ=0^0, l_f / t_0 =2) , (n_e=5, n_p=1, μ=1, γ=0^0, l_f / t_0 =10) and (n_e=5, , n_p=1, μ=2, γ=10^0, l_f / t_0 =10) are presented in figures 5.16-5.18. Similarly for Field V they are plotted for the set of input values (n_e=5, n_p=1, μ=1, γ=0^0, ν=10^0 l_f / t_0 =1) , (n_e=5, n_p=1, μ=1, γ=10^0, ν=3^0, l_f / t_0 =1) and (n_e=5, n_p=2, μ=1, γ=10^0, ν=3^0, l_f / t_0 =1) and are presented in figures 5.19-5.21.

-ooOoo-

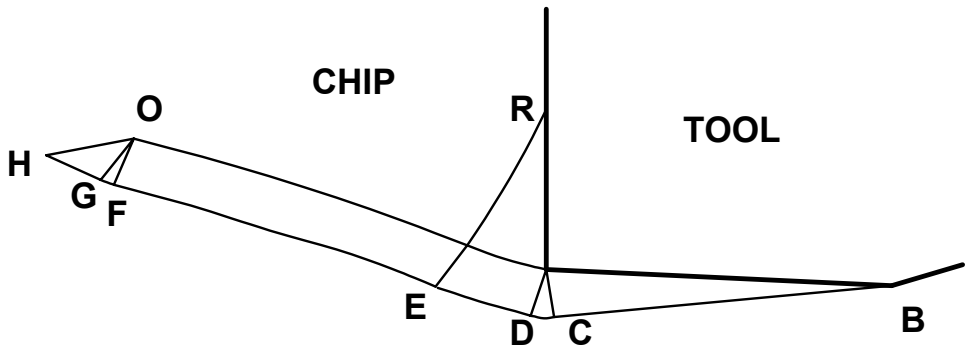

(a)

n_p	1	ϕ_R	19.8^0
n_e	5	ϕ_Q	14.4^0
μ	1	ϕ_B	13.4^0
γ	0^0	δ	3.6^0
l_f/t_0	2	ψ_1	13^0
α	8^0	φ	13.9^0
β	13.4^0	ψ_2	21.4^0
θ	9.7^0		

(c)

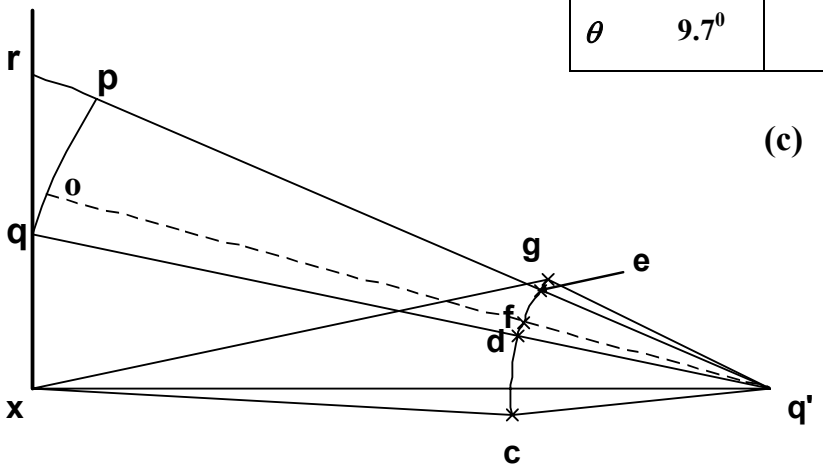

(b)

Fig. 5.16: Graphical plotting of Field IV (a) Slipline field (b) Hodograph (c) Table of input/output values.

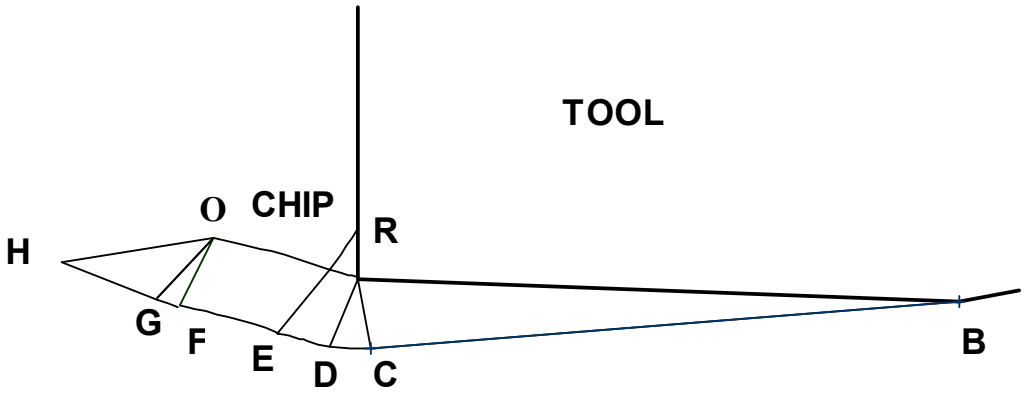

(a)

n_p	1	ϕ_R	19.8^0
n_e	5	ϕ_Q	14.4^0
μ	1	ϕ_B	10.6^0
γ	0^0	δ	3.6^0
l_f/t_0	10	ψ_1	13^0
α	8^0	φ	13.9^0
β	13.4^0	ψ_2	21.4^0
θ	9.7^0		

(c)

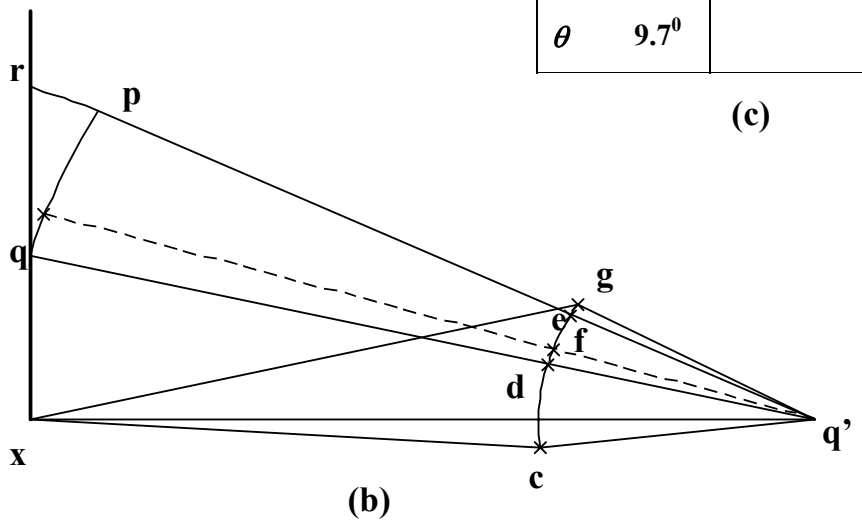

(b)

Fig. 5.17: Graphical plotting of Field IV (a) Slipline field (b) Hodograph (c) Table of input/output values.

n_p	1	α	8^0	ϕ_B	4^0
n_e	5	β	4.8^0	δ	3.6^0
μ	2	θ	9.7^0	ψ_1	13^0
γ	10^0	ϕ_R	9^0	φ	13.9^0
l_f/t_0	10	ϕ_Q	7.2^0	ψ_2	19.9^0

(c)

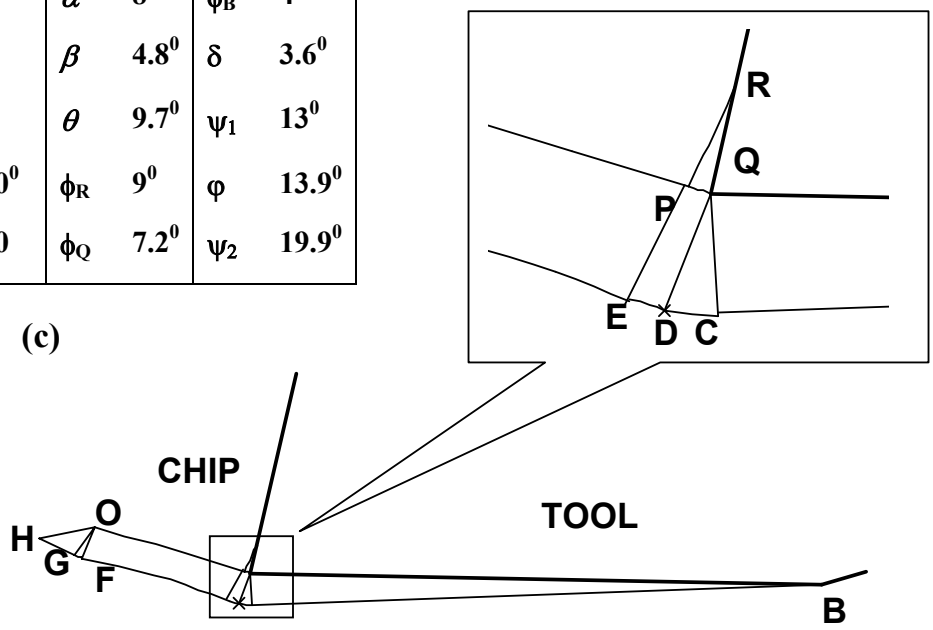

(a)

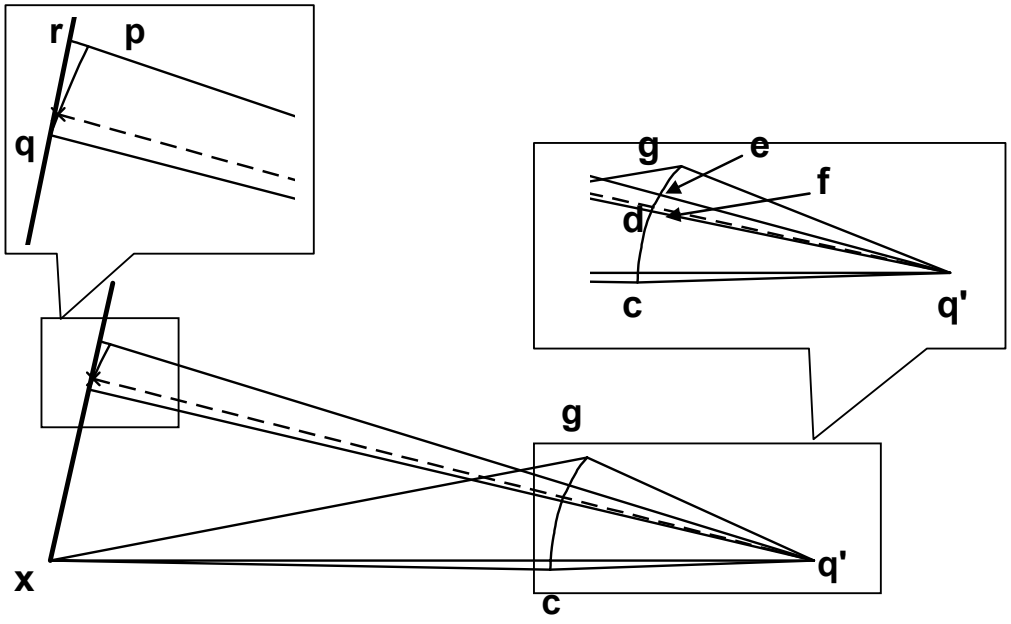

(b)

Fig. 5.18: Graphical plotting of Field IV (a) Slipline field (b) Hodograph (c) Table of input/output values.

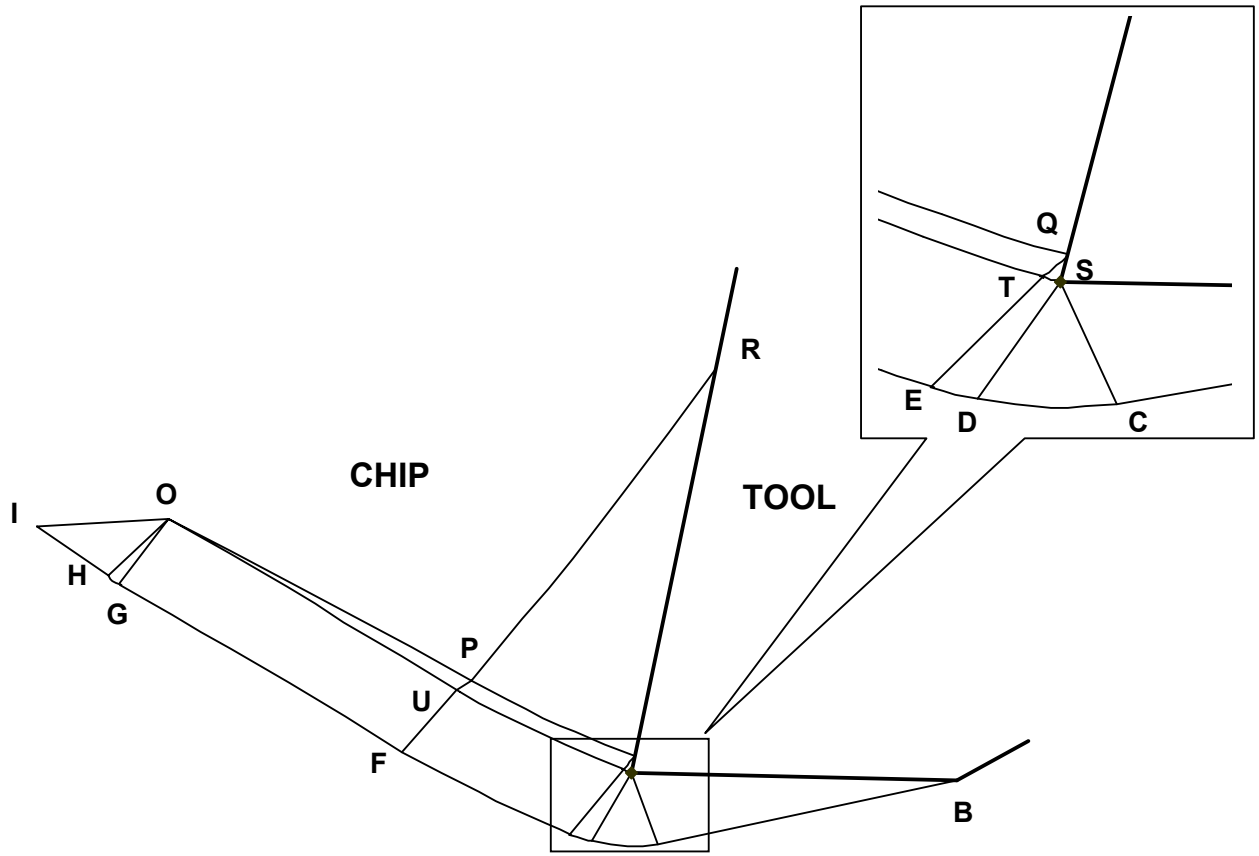

Fig. 5.19 (a) Graphical plotting of slipline field [Field V]

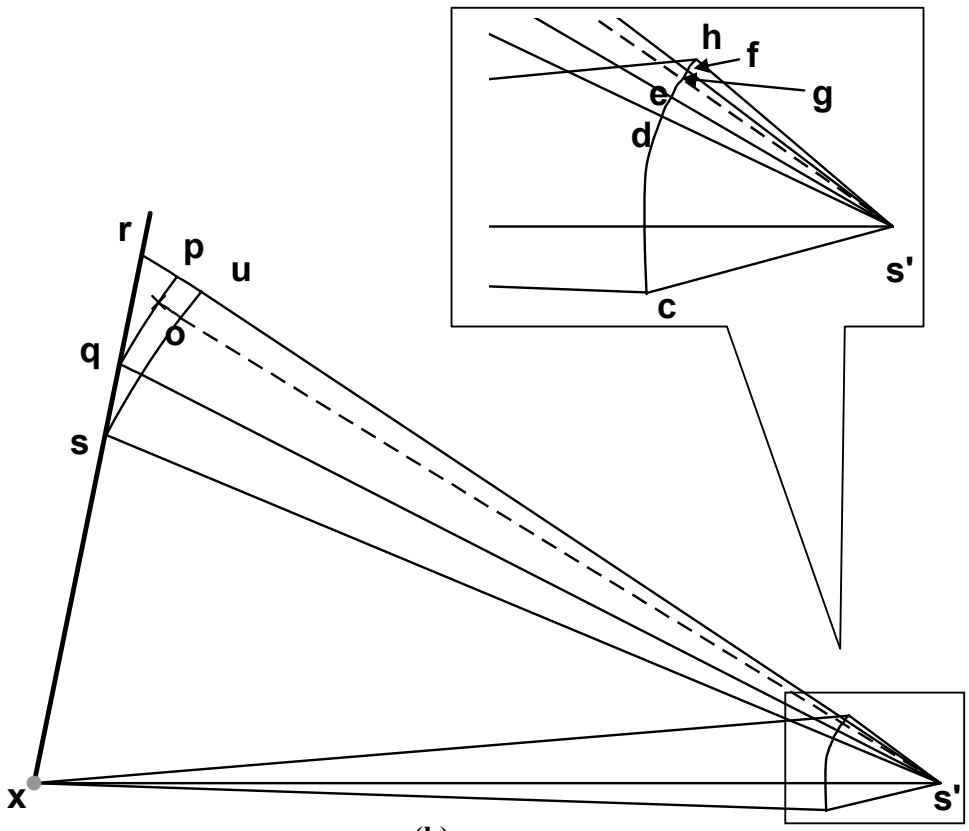

(b)

n_p	1
n_e	5
μ	1
γ	10^0
l_f/t_0	1
α	4^0
β	6.8^0
ν	3^0
ζ	4.6^0
θ	4.3^0
ϕ_R	18.8^0
ϕ_Q	16^0
ϕ_S	14.4^0
ϕ_B	16.5^0
δ	1.3^0
ψ_1	10.2^0
φ	3.3^0
ψ_2	39.6^0

(c)

Fig. 5.19: Graphical plotting of Field V (b) Hodograph (c) Table of input/output values.

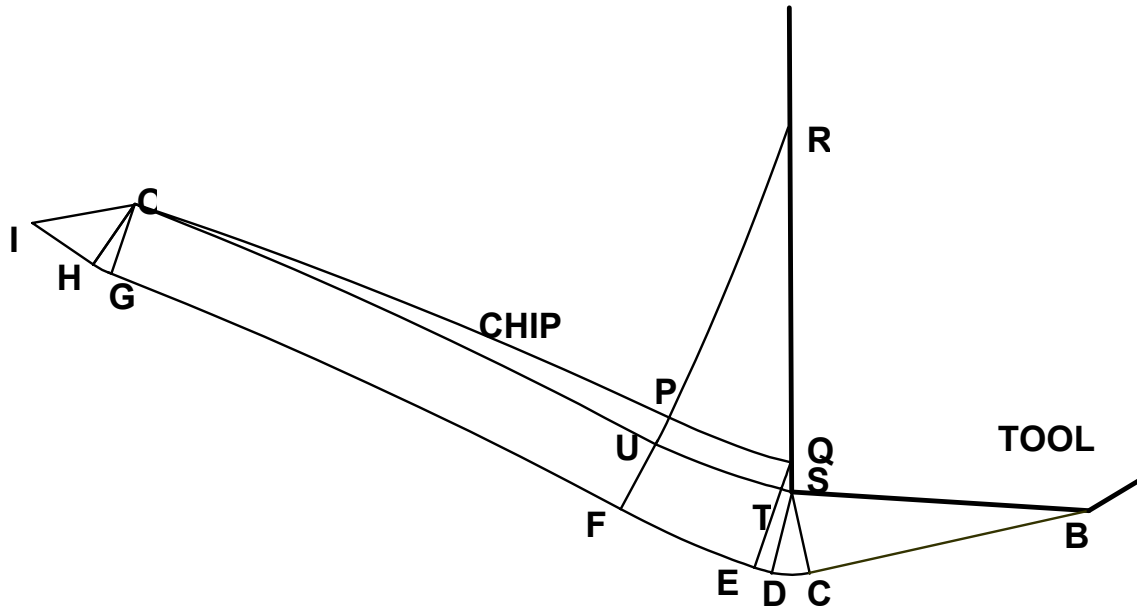

Fig. 5.20(a): Graphical plotting of slipline field [Field V]

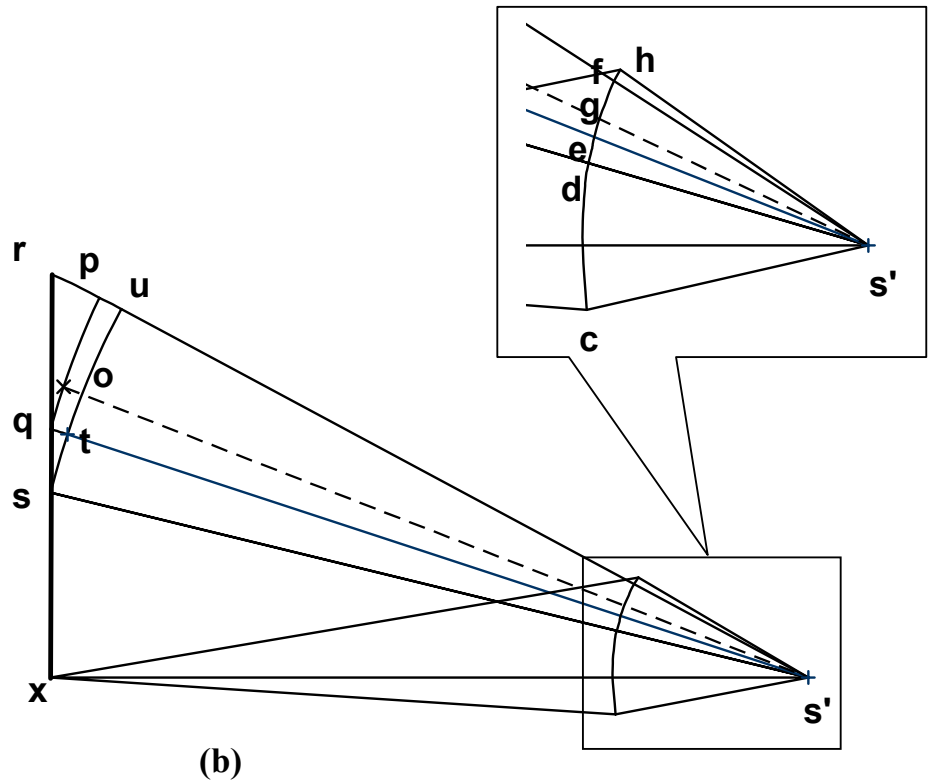

n_p	1
n_e	5
μ	1
γ	0^0
l_f/t_0	1
α	6^0
β	10.7^0
ν	3^0
ζ	4.6^0
θ	6.9^0
ϕ_R	19.2^0
ϕ_Q	17^0
ϕ_S	15.2^0
ϕ_B	14.3^0
δ	3.6^0
ψ_1	13.1^0
φ	10.5^0
ψ_2	24.5^0

(c)

Fig. 5.20: Graphical plotting of Field V (b) Hodograph (c) Table of input/output values.

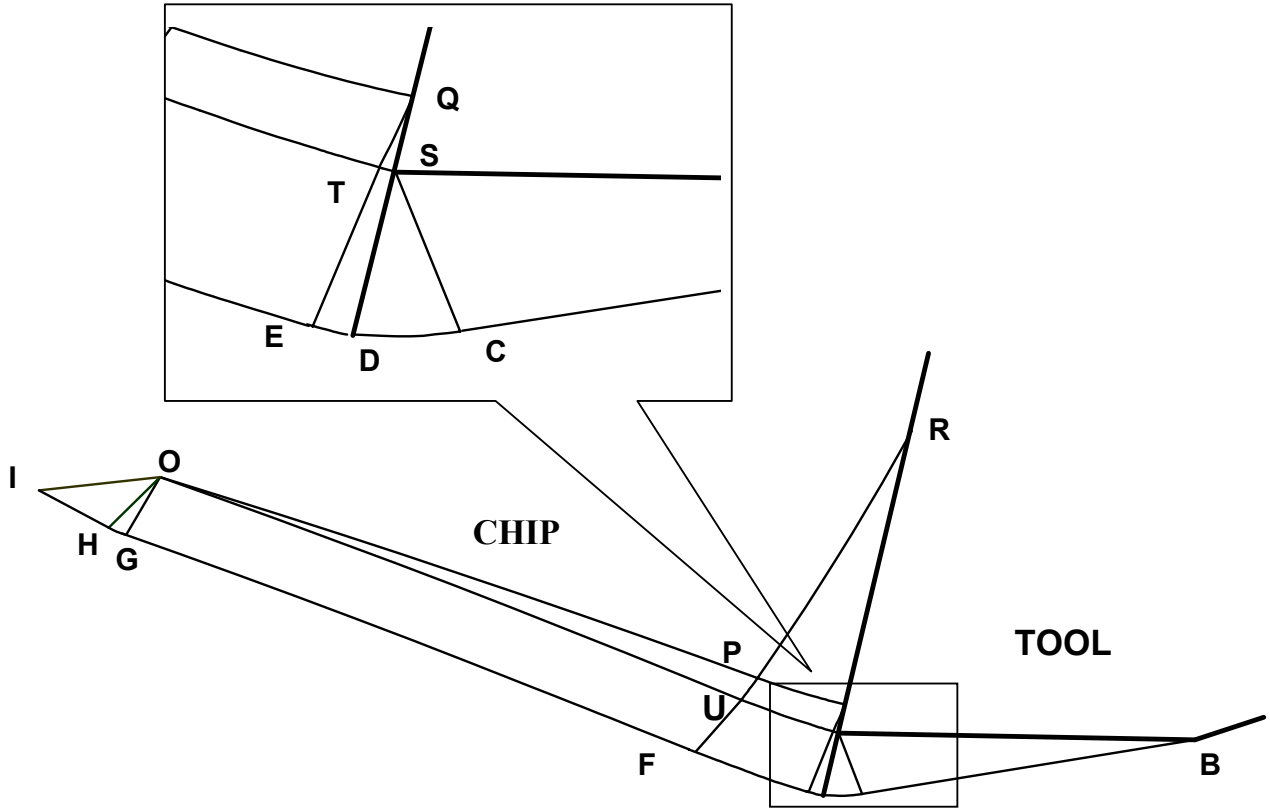

Fig. 5.21 (a): Graphical plotting of slipline field [Field V]

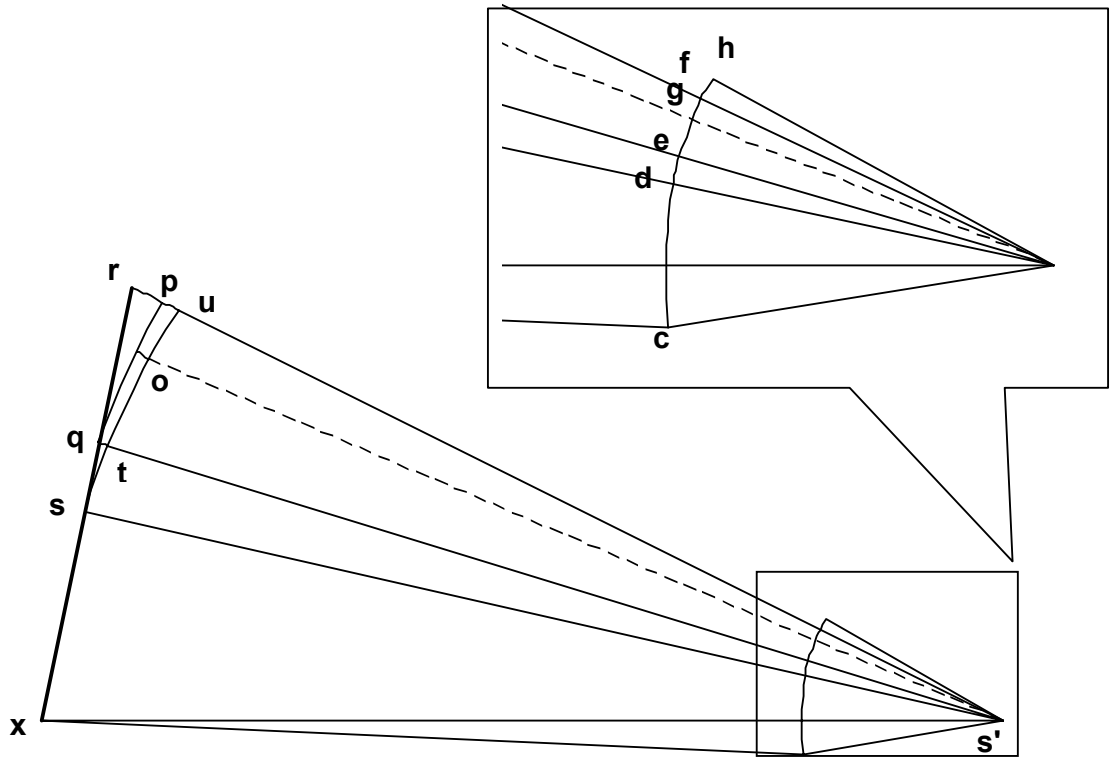

(b)

n_p	2
n_e	5
μ	1
γ	10^0
l_f/t_0	1
α	6^0
β	12.3^0
ν	3^0
ζ	4.6^0
θ	4.6^0
ϕ_R	12^0
ϕ_Q	5.7^0
ϕ_S	4.1^0
ϕ_B	13.6^0
δ	2.3^0
ψ_1	11.6^0
φ	6.9^0
ψ_2	25.4^0

(c)

Fig. 5.21: Graphical plotting of Field V (b) Hodograph (c) Table of input/output values.

Chapter 6

CHAPTER 6

SLIPLINE FIELD ANALYSIS OF FREE-CHIP MACHINING WITH ADHESION FRICTION AT CHIP-TOOL AND WORK-TOOL CONTACT REGIONS

6.1 Introduction

Free-chip machining may be defined as a metal cutting operation carried out without any externally imposed forces on the chip such as those due to a groove/obstruction type chip breaker or when the elastic effects on chip formation are neglected. In this metal removal process therefore, the resultant force and moment acting on the field boundary separating the rigid chip from the plastically stressed region are taken to be zero. During free-chip machining the chip produced may be distinguished qualitatively into two types:

a) Chips of small radius promoted by gradual reduction of rake friction with distance from the cutting edge, and

b) Straight chips promoted by a short contact of uniform friction.

It has been observed that curled chips are produced when cutting at low speeds or when the tool-chip interface friction is low as in cutting with a coolant, where as chip streaming or straight chip formation is a consequence of cutting at high speeds or when the tool-chip interface friction is high as in dry cutting.

Slipline field solutions for free-chip formation involving chip streaming has been proposed in the past by Lee and Shaffer [56], Kudo [58] and those involving chip curling by Dewhurst [73], Childs [78]and more recently by Maity and Das [79], Fang and Jawahir [100] and Fang [101-103]. In all these solutions, however, the tool is assumed to be perfectly sharp. Hence, these solutions

apply only to the beginning of a cutting operation by a new tool or by a freshly ground tool. In practice a tool wears out both on the face and flank as cutting progresses developing either a crater on the face or a wear land on the flank or both or even an edge radius. The slipline field solutions mentioned above do not address to this situation.

In this chapter slipline field solutions are proposed for free-chip machining with a worn tool with a finite wear land at tool flank. These solutions are obtained by modifying the solutions proposed earlier by Lee and Shaffer [56] and by Kudo [58] along the lines suggested by Shi and Ramalingam [85] and take account of both chip streaming and chip curling. Results are computed when the interfacial friction condition is assumed to be governed by the adhesion friction law suggested by Maekawa et al.[65] (equation 4.1). Range of validity of the proposed solutions is examined using Hill's overstressing criteria [45]. Variation of cutting and thrust forces with tool wear and the interface friction condition is studied. The results from the theoretical analysis are also compared with experimental results reported in literature.

It must be mentioned here that a primary requirement for the worn tool solutions is that the hydrostatic pressure at the free surface intersection point between the chip and the work material should not be less than one. Hence, the well-known Dewhurst field [73] can not be modified to yield solutions to the problem under consideration.

6.2 Slipline field solutions

Slipline field solutions for 'free-chip machining' for cutting with a worn tool with a finite flank wear land are shown in figures 6.1, 6.2 and 6.3 (Field VI, Field VII and Field VIII respectively) along with their associated hodographs.

Field VI (Fig. 6.1 (a)) is obtained when Lee and Shaffer's solution [56] is modified to account for the presence of a finite flank wear land. Referring to this figure it may be seen that the field consists of the pre-deformation zone *OGI*, the primary deformation zone *OQDG*, the center fan *DQC* and secondary shear zones *PQR* and *CQB* in contact with the tool face and flank respectively. Referring to the hodograph indicated in Fig 6.1 (b) it may also be seen that all velocity boundary conditions are satisfied: namely, rigid translation of the material within *OGI* parallel to the free surface *IO*, translation within *CQB* parallel to the flank wear land *QB* and translational motion parallel to the tool face *QR* within the secondary shear zone *PQR*.

Field VII shown in Fig. 6.2 is a modification of Field VI and incorporates the center fan *OPU* between the rigid chip and the primary deformation zone The field has two secondary shear zones *PSR* and *TQS* in contact with the tool face and the third *CQB* in contact with the tool flank. Referring to it's hodograph (Fig. 6.2(b)) it is also verified that all velocity boundary conditions are satisfied. The fan angles of the two center fans *OPU* and *OGH* have the same value as the hydrostatic pressure within *OPR* and *OIH* are equal.

The slipline fields illustrated in figures 6.1 and 6.2 account for formation of straight chips. The solution shown in Fig. 6.3 (Field VIII) applies when the chip on leaving the deformation zone undergoes rigid body rotation forming a chip of constant curvature (chip curl). Referring to Fig. 6.3 it may be seen that the chip boundary is defined by two identical circular arcs *PR* and *PO* of equal angular span α. This ensures that the force and moment equilibrium condition of the chip is satisfied [58]. The field is associated with the normal stress that decreases continuously from *R* to *Q* while the shear stress increases. It is assumed that the shear

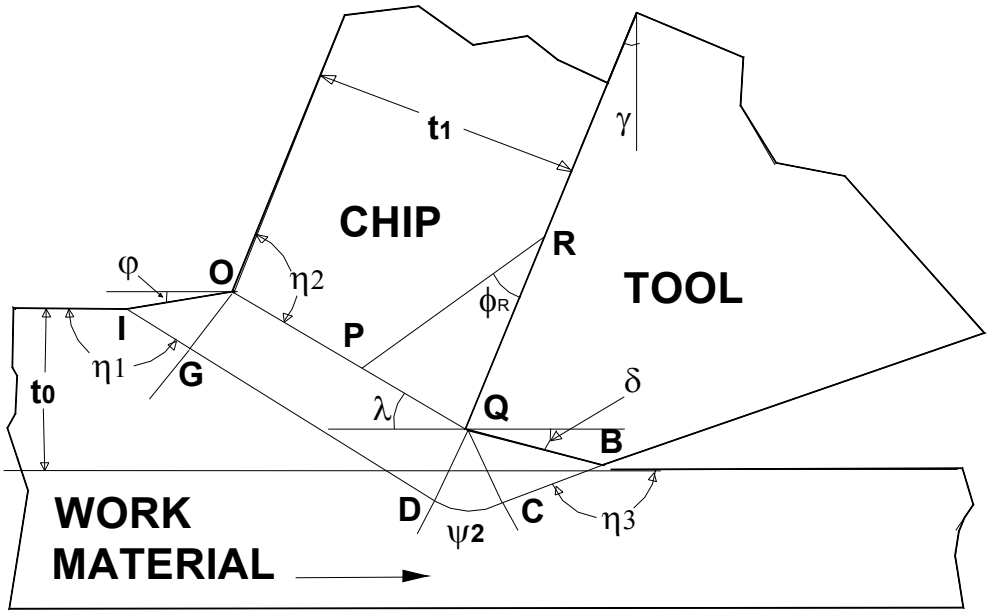

(a)

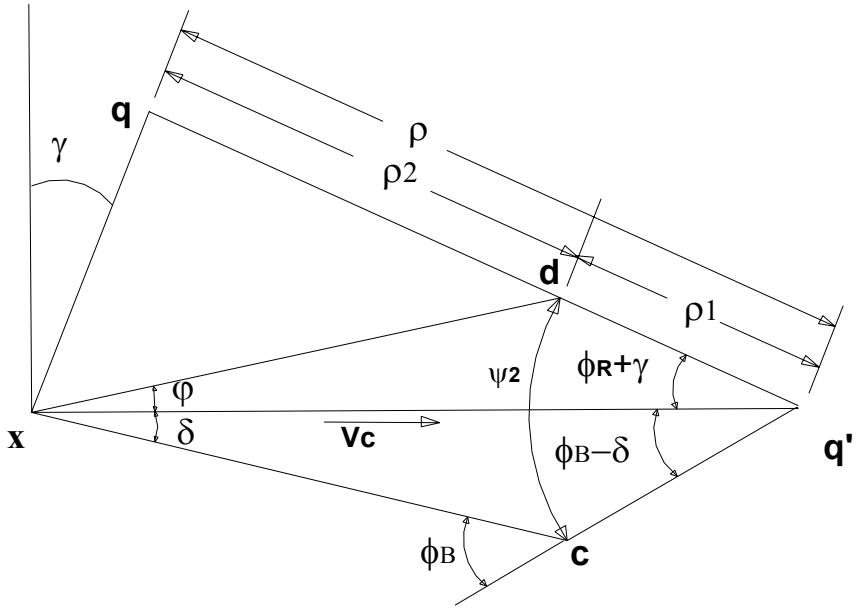

(b)

Fig. 6.1: Field VI (a) Slipline field (b) Hodograph

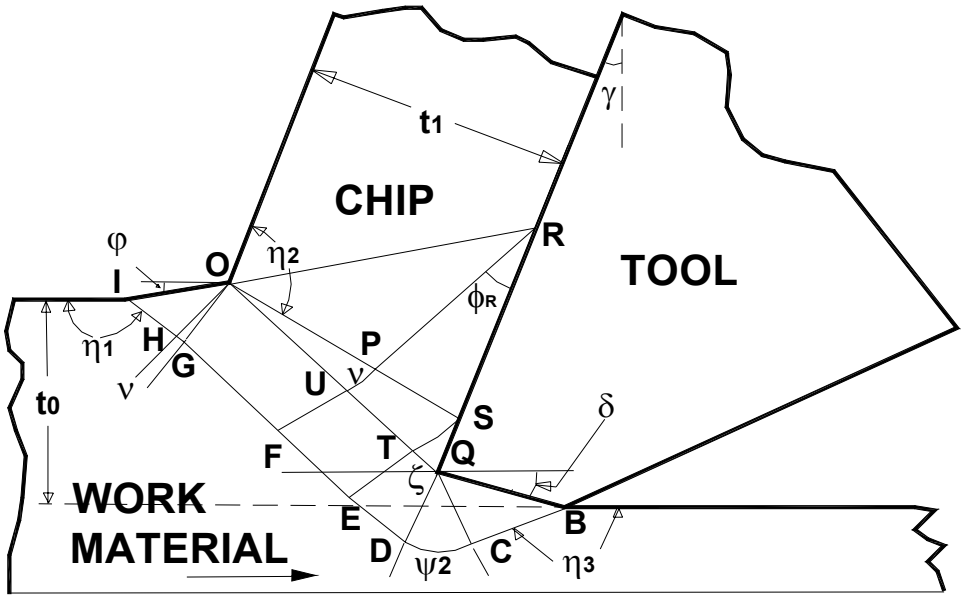

(a)

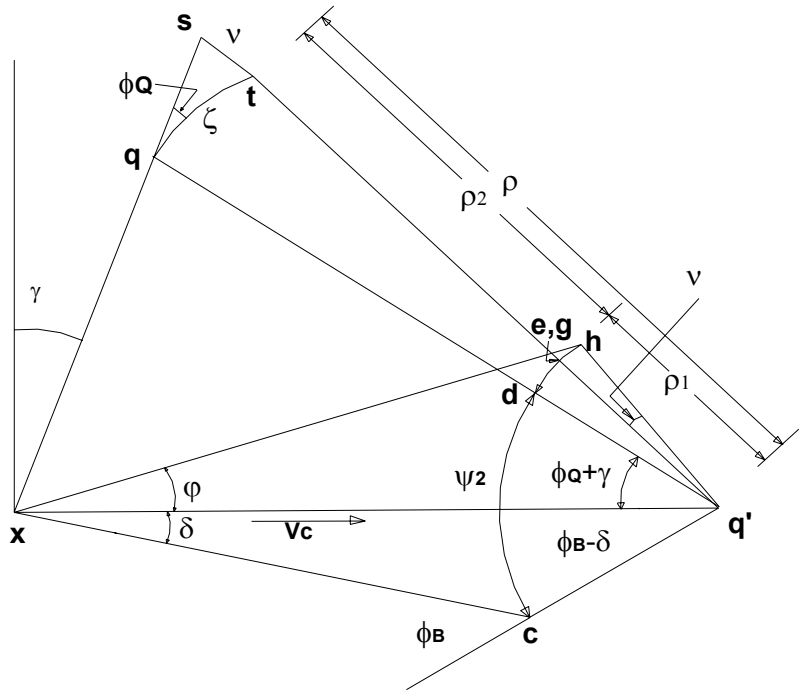

(b)

Fig. 6.2: Field VII (a) Slipline field (b) Hodograph

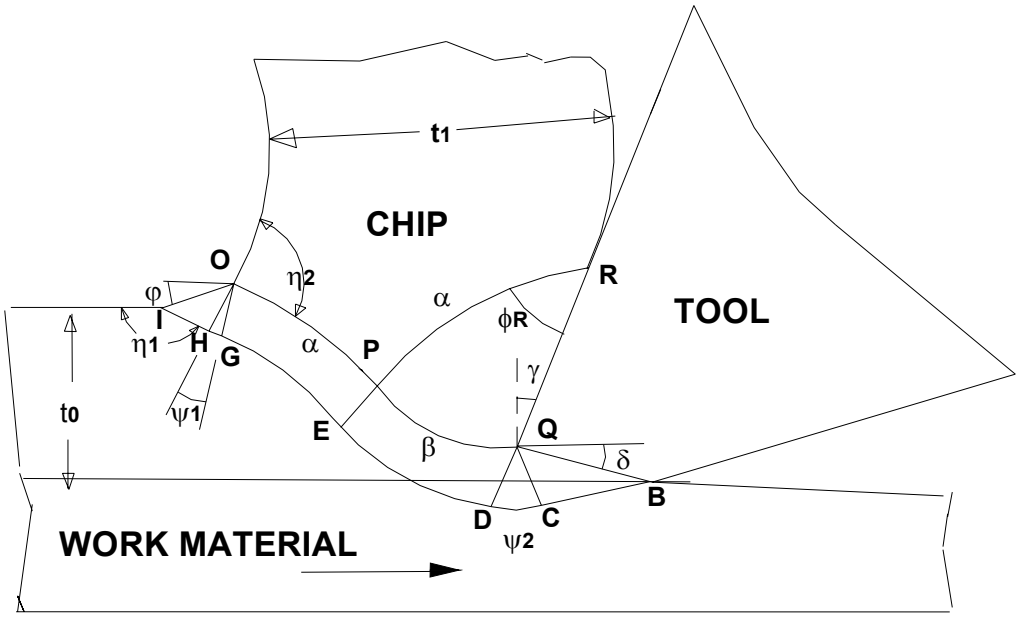

(a)

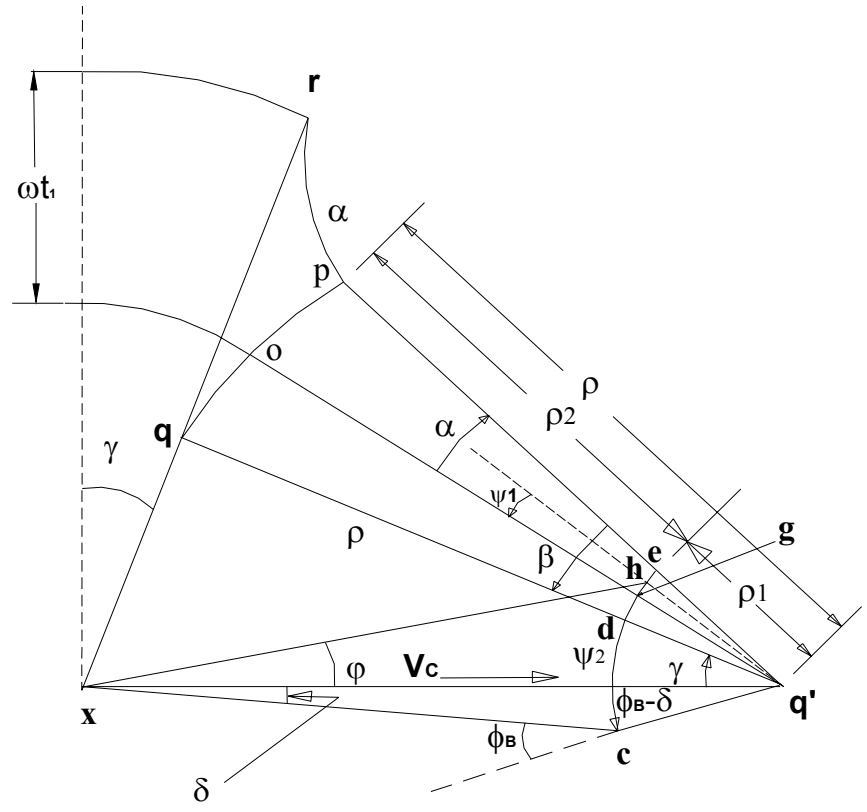

(b)

Fig. 6.3: Field VIII (a) Slipline field (b) Hodograph

stress attains the limiting value k of the yield stress in shear of the chip material at Q so that the slipline PQ meets the tool face orthogonally at this point.

This requires that

$$\phi_R = \alpha + \beta$$

and $$\phi_Q = 0$$

where, ϕ_R and ϕ_Q are the friction angles at R and Q respectively, α is the angular span of the slipline curve RP and β is the angular span of PQ.

In the presence of flank wear, the primary shear line OPQ in Kudo's original solution [58] "opens up" giving rise to the primary shear zone $OQDG$. The field consists of centre fan fields OHG and QDC, the pre-deformation zone IOH and secondary shear zones PQR and CQB. The hydrostatic pressure p_O at O is given by the relation [58]

$$\frac{p_O}{k} = 1 + \frac{2(\alpha - \sin\alpha)}{\cos\alpha + \sin\alpha - 1} \tag{6.1}$$

Hence, the angular range ψ_1 of the centre fan field OHG is written as

$$\psi_1 = \frac{\alpha - \sin\alpha}{\cos\alpha + \sin\alpha - 1} \tag{6.2}$$

It is shown in Appendix III that the field angle α and the friction angle ϕ_R in this field are related by the equation

$$\alpha = \frac{\pi}{4} + \phi_R - \cos^{-1}\left(\frac{(1 - \sin\phi_R)}{\sqrt{2}}\right) \tag{6.3}$$

Thus, the friction condition at R in this solution is dictated by the value of α only.

6.3 Method of solution

The slipline fields shown in figures 6.1-6.3 are of "direct type". Hence, these fields can be constructed when the unknown field angles ψ_2 and δ are

determined. Two conditions also exist from which these angles can be evaluated. These may be stated as,

a) The ratio (ρ_1 / V_C) calculated from the upper and the lower triangles in the hodographs must have the same value.

b) The normal stress σ_n and the shear stress τ on the flank wear land *QB* must be compatible with the assumed friction law.

These conditions yield (refer to equations (5.12)-(5.13))

$$\sin\delta - \sqrt{2}\sin\varphi\sin\phi_B = 0 \tag{6.4}$$

$$\cos\left(2\phi_B\right) - \left[1 - e^{-\left(\mu\left(p_B + \sin\left(2\phi_B\right)\right)\right)^{n_p}}\right]^{\frac{1}{n_p}} = 0 \tag{6.5}$$

Where, δ is the inclination of the flank wear land *QB* with the horizontal, φ is the inclination of the free surface *IO* with the horizontal and ϕ_B , p_B are respectively the friction angle and the hydrostatic pressure at B . In formulating equation (6.5), it is assumed that the friction at tool flank is governed by the adhesion friction law stated by equation (4.1).

For each of the above fields φ , ϕ_B and p_B are functions of the field angles. These functional relations are expressed by the following equations:-

Field VI:-

$$\varphi = \frac{\pi}{4} - \left(\phi_R + \gamma\right) \tag{6.6 (a)}$$

$$\phi_B = \psi_2 + \delta - \left(\phi_R + \gamma\right) \tag{6.6 (b)}$$

$$p_B = 1.0 + 2\psi_2 \tag{6.6 (c)}$$

Field VII:-

$$\varphi = \frac{\pi}{4} - \left(\phi_R + \gamma + 2\upsilon\right) \tag{6.7 (a)}$$

$$\phi_B = \psi_2 + \delta - \left(\phi_R + \gamma + \upsilon - \zeta\right) \tag{6.7 (b)}$$

$$p_B = 1.0 + 2\left(\upsilon + \zeta + \psi_2\right) \tag{6.7 (c)}$$

Field VIII:-

$$\varphi = \frac{\pi}{4} - \left(\phi_R + \gamma + \psi_1 - 2\alpha\right) \tag{6.8 (a)}$$

$$\phi_B = \psi_2 + \delta - \gamma \tag{6.8 (b)}$$

$$p_B = 1.0 + 2\left(\psi_1 + \psi_2 + \phi_R - 2\alpha\right) \tag{6.8 (c)}$$

where, ψ_1 is given by equation (6.2) and $\beta = \phi_R - \alpha$.

For inputs of friction parameters μ , n_p and the hydrostatic pressure p_R (=1), the FORTRAN programme developed for construction of Field VI and Field VII first evaluated ϕ_R from the adhesion friction condition at *R* (equation (4.1)). For Field VIII, ϕ_R for any given value of α was calculated directly using equation (6.3). For each of the above fields the programme then determined ψ_2 and δ by solutions to equations (6.4) and (6.5) and using the relations as stated by equations (6.6), (6.7) and (6.8) according as whether it was Field VI, Field VII or Field VIII. As equations (6.4) and (6.5) are non-linear these were solved by the algorithm developed by Powell [104]. ψ_2 and δ for each field were assumed to be correctly estimated when the sum of the squares of the residuals were less than 10^{-10} . These optimized ψ_2 and δ values were then used to construct the fields and to evaluate the cutting and thrust forces on the flank wear land. For Field VIII the construction was carried out using the step-by-step procedure as explained in [95]. For Field VI and Field VII the construction was carried out using the matrix method.

6.4 The range of validity of the fields

For the above slipline field solutions to be valid it is necessary to demonstrate that the material outside the assumed limits of the deforming zone remains rigid. This imposes limits on the allowable values of the field angles so that the rigid vertices at I , O and B are not overstressed (figures 6.1-6.3).

Following the work of Hill [45] it can be shown that the rigid vertex at I in the above fields is not overstressed if $\eta_1 \left(= \frac{3\pi}{4} + \varphi \right) \geq \frac{3\pi}{4}$ so that the inequality

$$-\frac{1}{2} - \left(\eta_1 - \frac{\pi}{4} \right) \leq \frac{1}{2} \leq \frac{1}{2} + \left(\eta_1 - \frac{3\pi}{4} \right) \tag{6.9}$$

is always satisfied . Thus valid solutions from the above fields are obtained only if φ is positive. This requires that $\left(\phi_R + \gamma \right) \leq \frac{\pi}{4}$ for Field VI, $\left(\phi_R + \gamma + 2\upsilon \right) \leq \frac{\pi}{4}$ for Field VII and $\left(\phi_R + \gamma + \psi_1 - 2\alpha \right) \leq \frac{\pi}{4}$ for Field VIII (equations (6.6 (a)), (6.7 (a)) and (6.8 (a)) respectively.

Similarly it can be demonstrated that the vertex angle η_2 at O in figures (6.1) and (6.2) is not overstressed if

$$-\frac{1}{2} + \cos\left(\eta_2 - \frac{\pi}{4} \right) \leq \frac{1}{2} \leq \frac{1}{2} + \left(\eta_2 - \frac{\pi}{4} \right), \quad \frac{\pi}{4} \leq \eta_2 \leq \frac{3\pi}{4} \tag{6.10}$$

For these two fields $\eta_2 = \left(\frac{\pi}{2} + \phi_R \right)$ and $0 \leq \phi_R \leq \frac{\pi}{4}$. Hence left and right hand side inequalities of equation (6.10) are always satisfied for all values of ϕ_R and γ.

For Field VIII, Hill's inequalities at O are written as,

$$-\frac{1}{2} + \cos\left(\eta_1 - \frac{\pi}{4} \right) \leq \frac{1}{2} + \frac{\alpha - \sin\alpha}{\cos\alpha + \sin\alpha - 1} \leq \frac{1}{2} + \left(\eta_2 - \frac{\pi}{4} \right) \qquad 6.11(a))$$

and $\eta_2 \geq \frac{\pi}{4}$ (6.11(b))

For this case the field angle α was found to lie between 0 and 12 degrees corresponding to friction angle ϕ_R values between 0 and $\frac{\pi}{4}$ (equation (6.3)) and for all combinations of rake angle and friction conditions equations (6.11) were found to be always satisfied.

It may be seen that the vertex angle $\eta_3 \left(= \pi - \left(\phi_B - \delta\right)\right)$ at *B* in the above fields is not overstressed if

$$-\frac{1}{2} - \left(\frac{\pi}{4} - \left(\phi_B - \delta\right)\right) \leq \frac{p_B}{2} \leq \frac{1}{2} + \left(\frac{3\pi}{4} - \left(\phi_B - \delta\right)\right) \quad (6.12)$$

For Field VI, $p_B = 1 + 2\psi_2$ where, $\psi_2 = \left(\phi_R + \gamma\right) + \left(\phi_B - \delta\right)$ (Fig. 6.1(b)). As $(\phi_R + \gamma)$, $\left(\phi_B - \delta\right) \leq \frac{\pi}{4}$, $\psi_2 \leq \frac{\pi}{2}$. Hence, equation (6.12) is always satisfied.

For Field VII, $p_B = 1 + 2\left(\upsilon + \zeta + \psi_2\right)$. Also $\psi_2 = \left(\left(\phi_Q + \gamma\right) + \left(\phi_B - \delta\right)\right)$ (Fig. 6.2(b)). Hence, $\left(\psi_2 + \upsilon + \zeta\right)$ $\left(= \left(\left(\phi_R + \gamma + 2\upsilon\right) + \left(\phi_B - \delta\right)\right)\right)$ is always less than $\frac{\pi}{2}$. Thus, η_3 is never overstressed.

For Field VIII, $p_B = 1 + 2\left(\phi_R + \psi_2 + \psi_1 - 2\alpha\right)$ and $\psi_2 = \left(\phi_B - \delta + \gamma\right)$ (Fig. 6.3(b)). As $\left(\phi_R + \gamma + \psi_1 - 2\alpha\right)$ and $\left(\phi_B - \delta\right)$ are both less than $\frac{\pi}{4}$ (equation (6.8(a)), equation (6.12) is never violated and the material remains rigid at *B*.

6.5 Results and Discussion

The variation of non-dimensional cutting and ploughing forces with flank wear (l_f / t_0) as computed from these slipline fields are presented in figures 6.4-6.6. In all the three cases the ploughing forces vary linearly with flank wear and that the

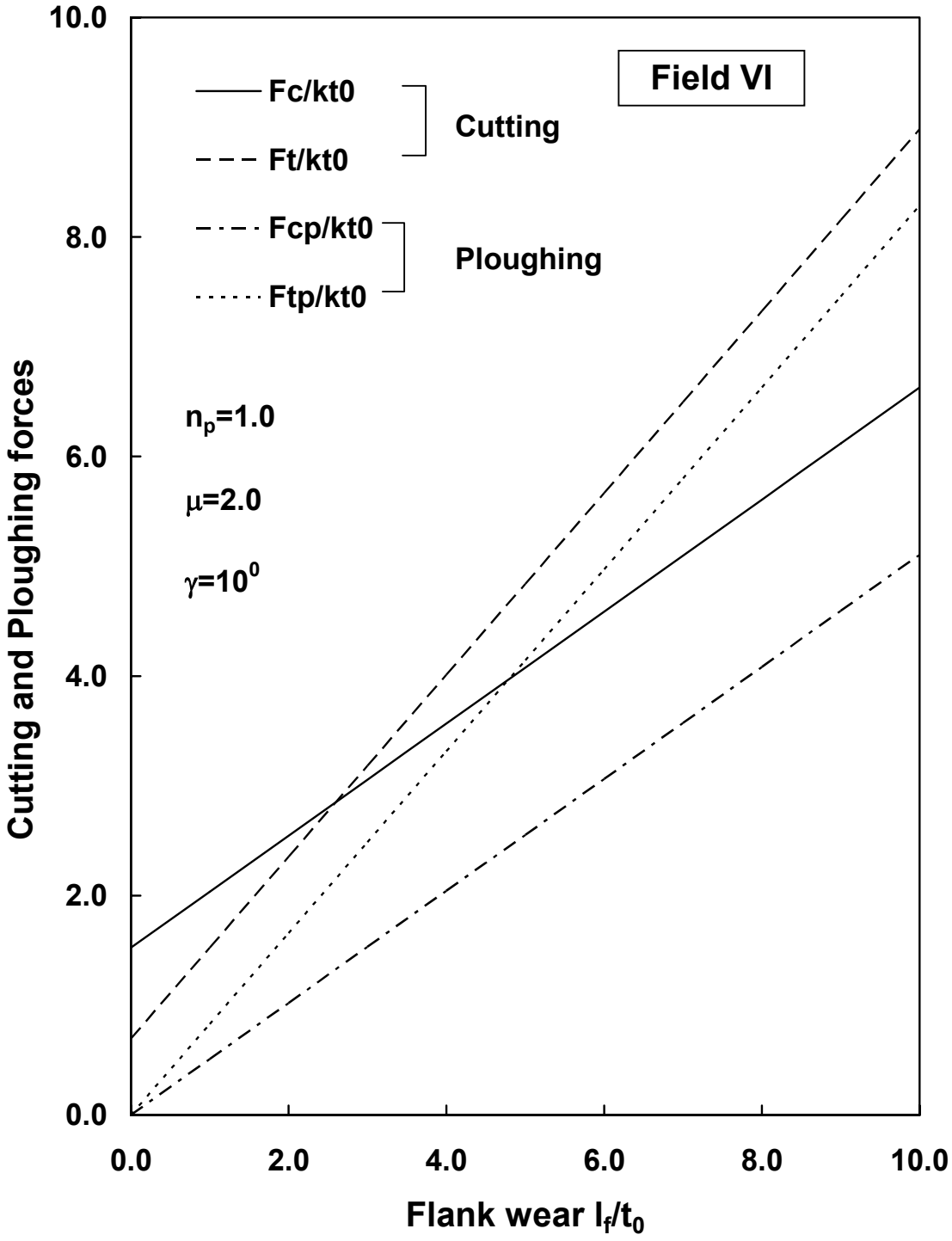

Fig. 6.4: Effect of flank wear on cutting and ploughing forces.

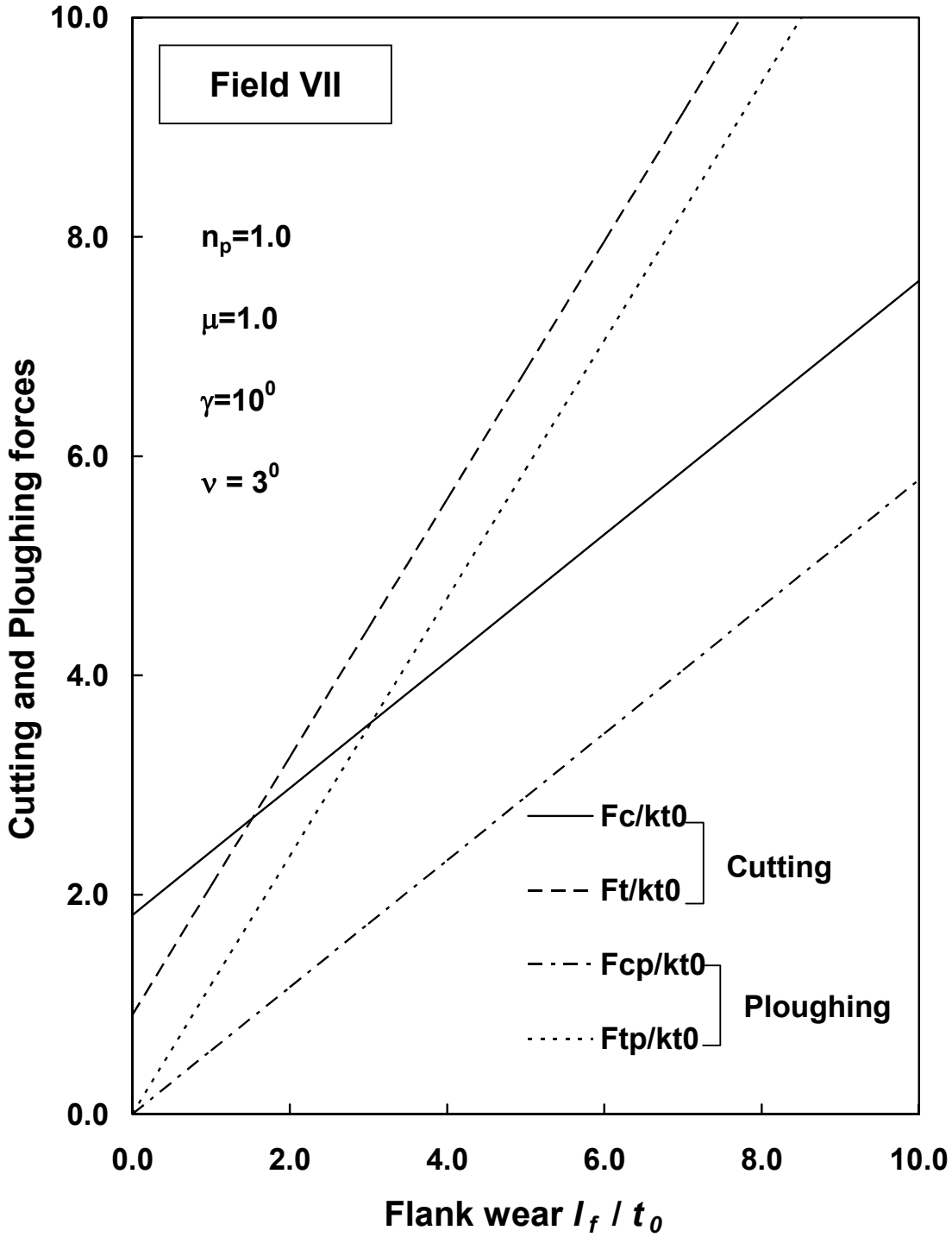

Fig. 6.5: Effect of flank wear on cutting and ploughing forces.

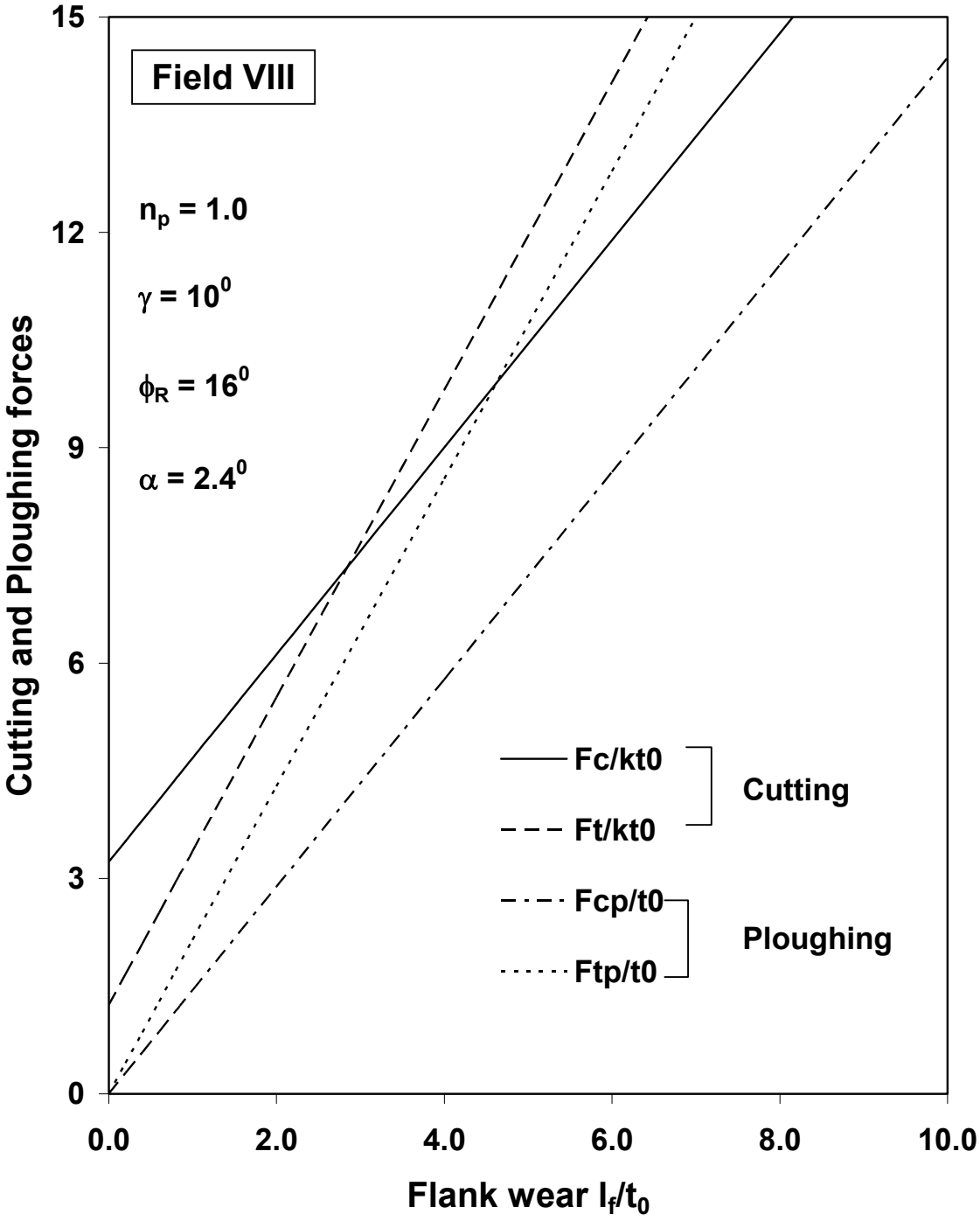

Fig. 6.6: Effect of flank wear on cutting and ploughing forces.

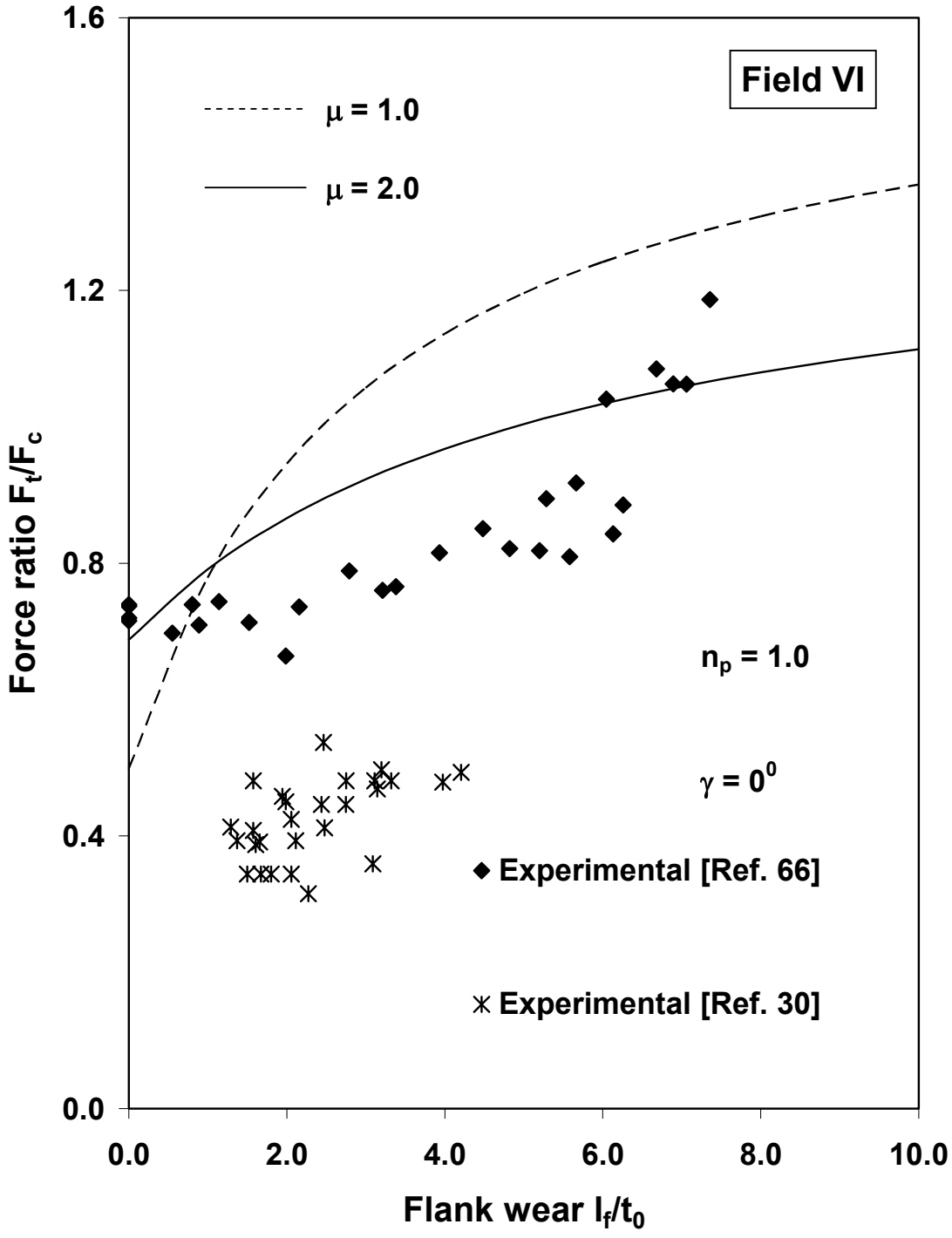

Fig. 6.7: Effect of flank wear on force ratio.

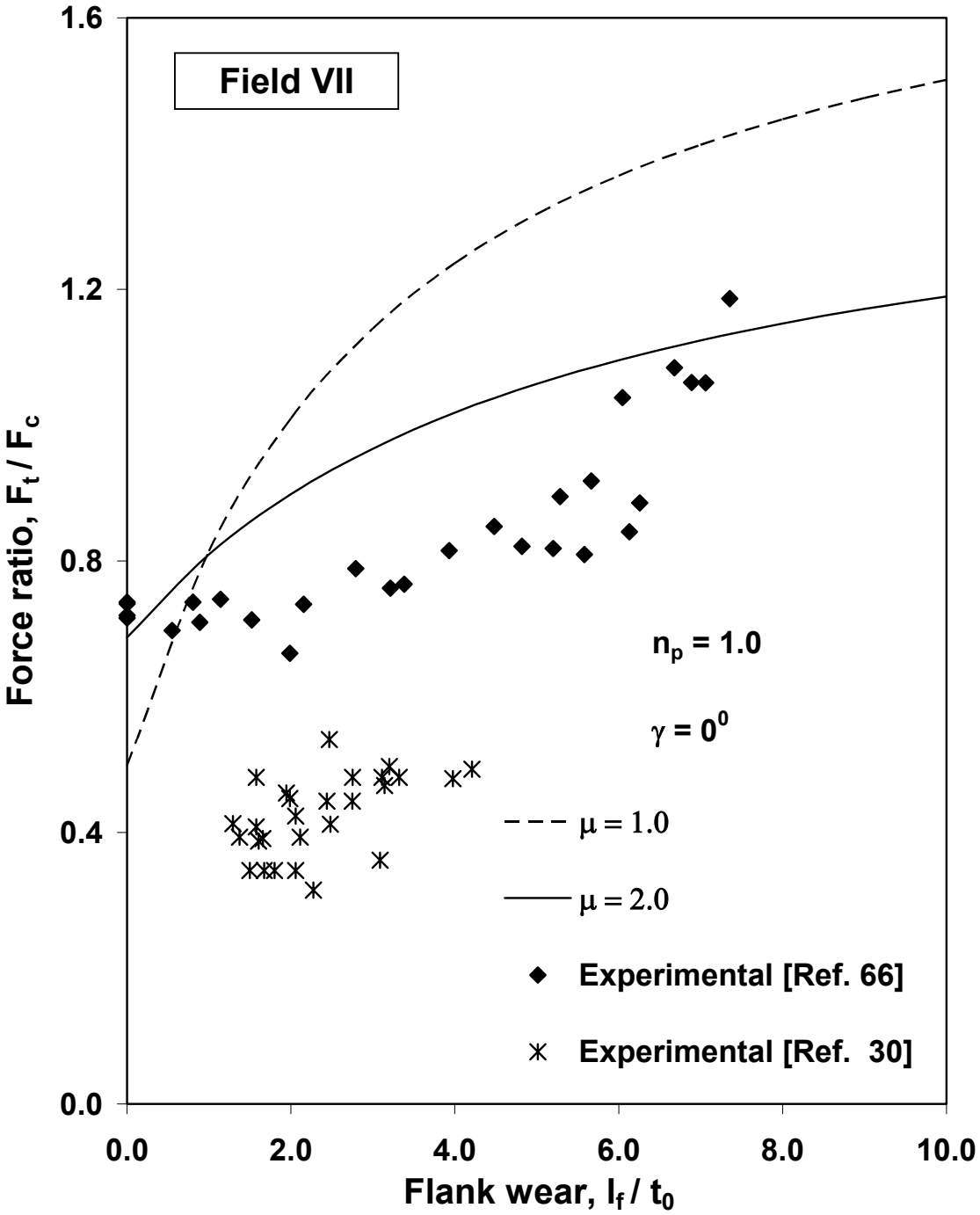

Fig. 6.8: Effect of flank wear on force ratio.

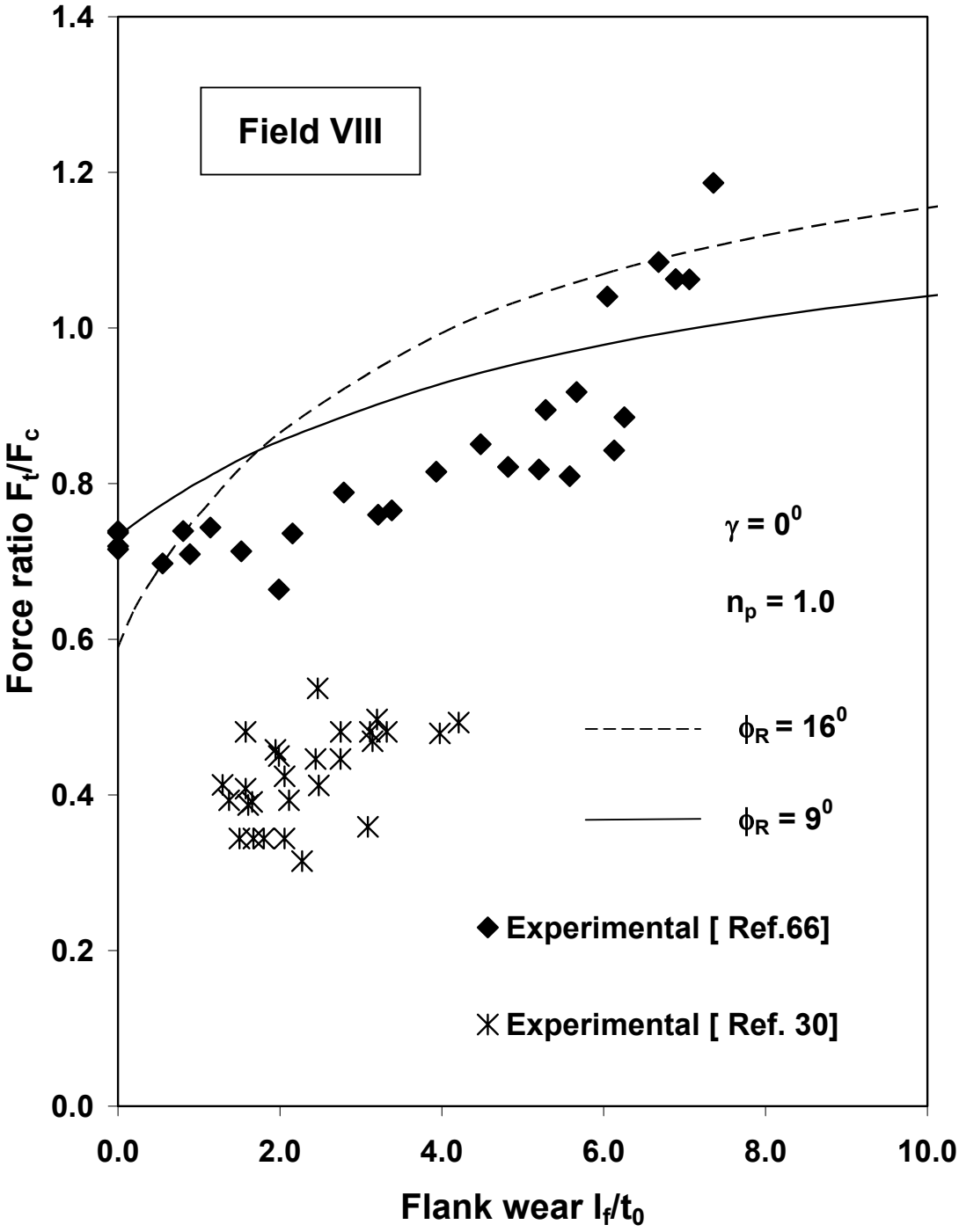

Fig. 6.9: Effect of flank wear on force ratio.

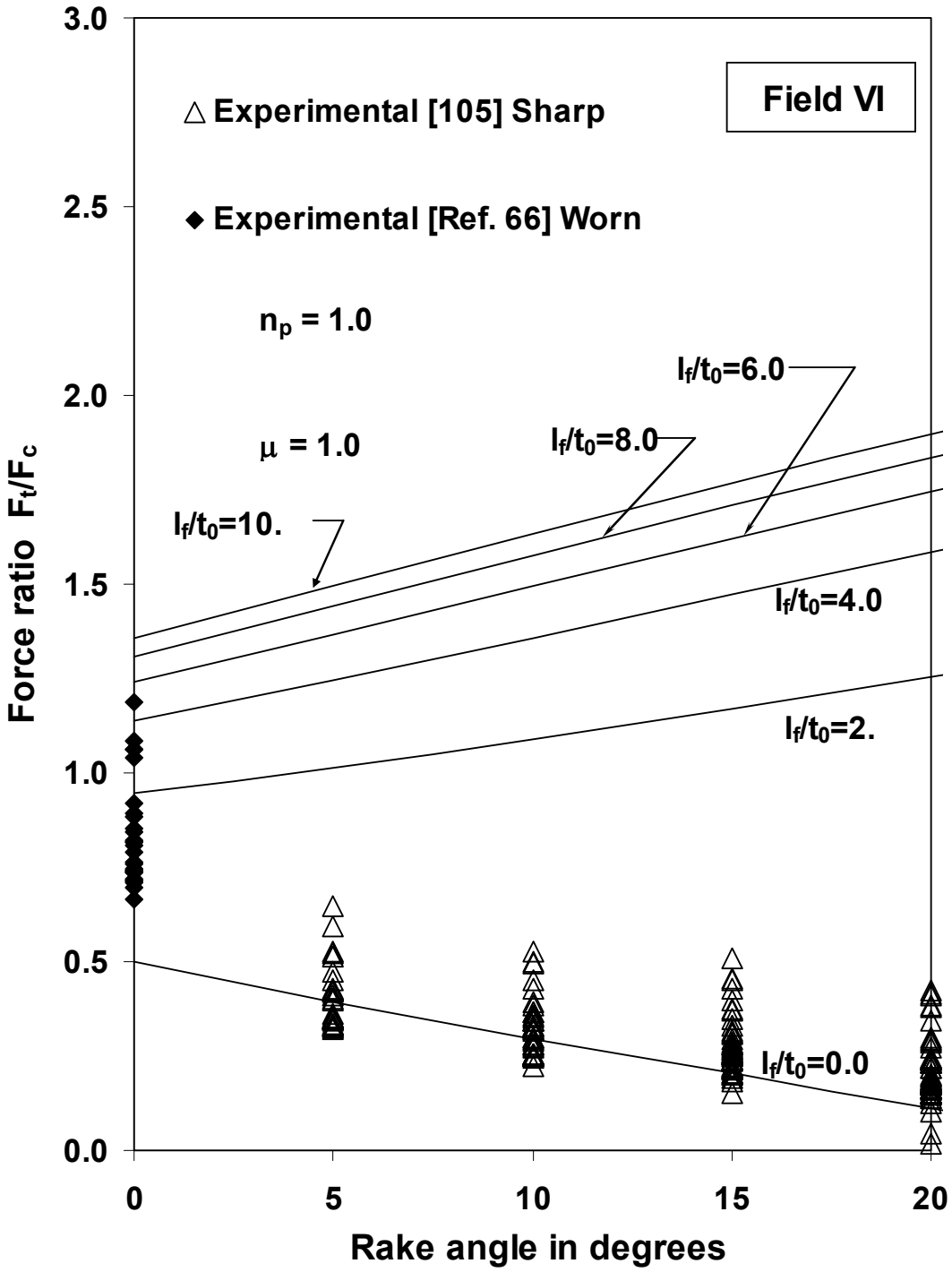

Fig. 6.10: Variation of force ratio with rake angle for sharp and worn tools

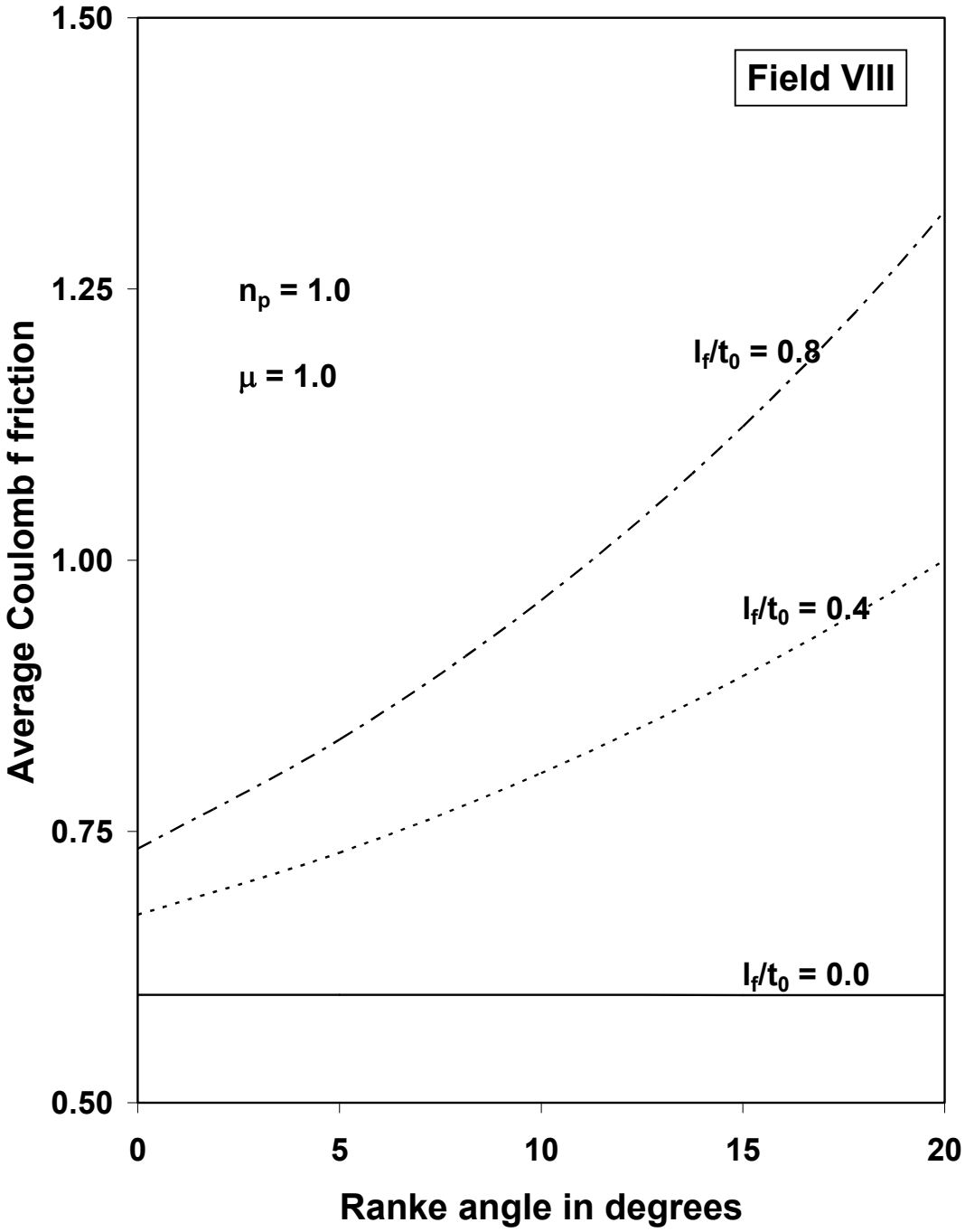

Fig. 6.11: Variation of average Coulomb coefficient of friction with rake angle for sharp and worn tools

thrust forces are found to increase more rapidly than the cutting forces, which is in agreement with the observations reported in chapter 5. The cutting and thrust forces from field VIII, however are found to be much greater than those computed from the other two fields for the same value of flank wear (l_f / t_0). The variation of the force ratio (F_t / F_c) with flank wear also indicates the same trend as was reported in chapter 5 (figures 6.7-6.9). It is also observed that the force ratio for a sharp tool (Field VI) decreases with rake angle and this in agreement with the experimental results reported by Eggleston et al [105]. In the presence of flank wear, however, this ratio increases (refer to figures 5.11 and 5.12)

The variation of average coefficient of friction with rake angle as computed from field VIII is illustrated in Fig. 6.11. For a sharp tool the average friction coefficient is almost independent of rake angle. The trend is reversed in the presence of even a small flank wear land.

6.6 Conclusions

Slipline field solutions are proposed for free-chip machining with a worn tool with a finite wear land at the tool flank. The solutions for chip streaming are obtained by modifying the solutions proposed earlier by Lee and Shaffer [56] and Kudo [58] along the lines suggested by Shi and Ramalingam [85]. Results are computed when the interfacial friction condition is assumed to be governed by the adhesion friction law suggested by Maekawa et al [65]. For the case of free machining involving a curled chip, solutions are obtained by defining the rigid-plastic chip boundary by two identical circular arcs of equal angular span. The validity of the proposed solutions is examined using Hill's overstressing criteria [45].

For all the fields the ploughing, cutting and thrust forces are found to vary linearly with flank wear and that the thrust forces increase more rapidly than the

cutting forces. The results also demonstrate that increasing the friction coefficient μ decreases the force ratio (F_t / F_c). It is further seen that the force ratio and the average Coulomb coefficient of friction at chip-tool interface for a sharp tool decrease with rake angle but the presence of a small flank wear land may reverse this trend.

6.7 Plotting of some slipline fields and hodographs

In the subsequent sections the slipline field network graphically plotted for Field VII for the set of input values of (n_p=1, μ =1, γ=10^0, l_f / t_0 =1) is presented in figures 6.12. Similarly for Field VIII these are plotted for the set of input values (n_p=1, μ =1, γ=20^0, l_f / t_0 =1,α=2.4) and (n_p=1, μ =1, γ=20^0, l_f / t_0 =1,α=1.0). These are presented in figures 6.13-6.14.

-ooOoo-

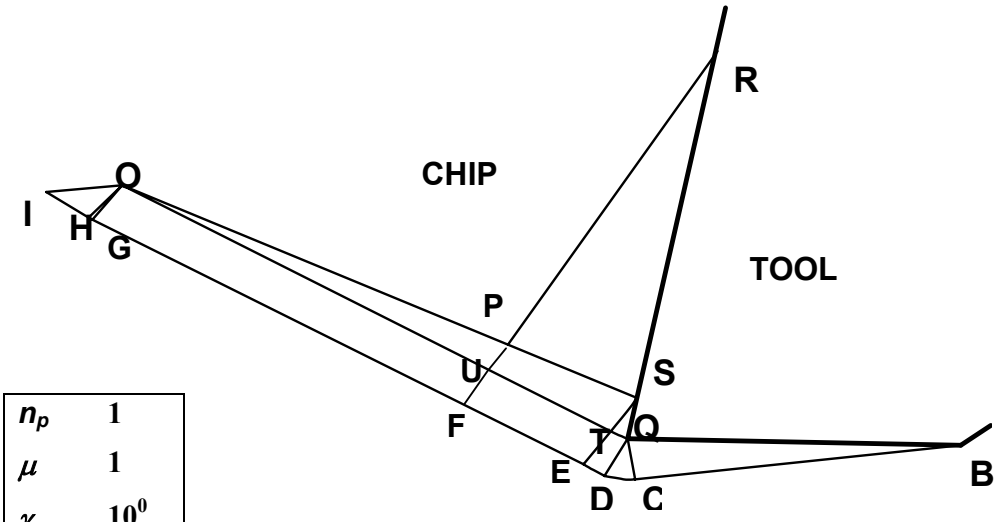

(a)

n_p	1
μ	1
γ	10^0
l_f/t_0	1
ϕ_R	18.5^0
δ	1.5^0
φ	6.5^0
ψ_2	33.1^0

(c)

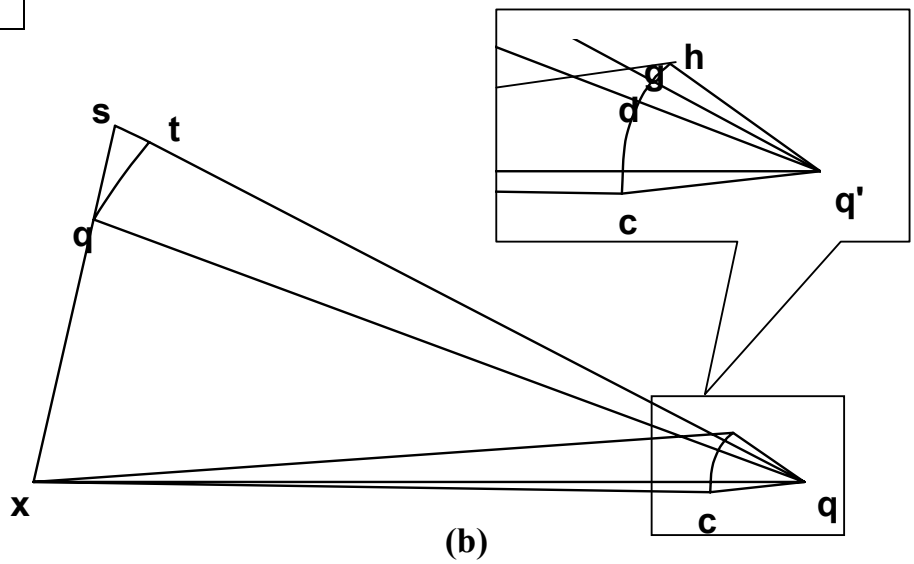

(b)

Fig. 6.12: Graphical plotting of Field VII (a) Slipline field (b) Hodograph (c) Table of input/output values.

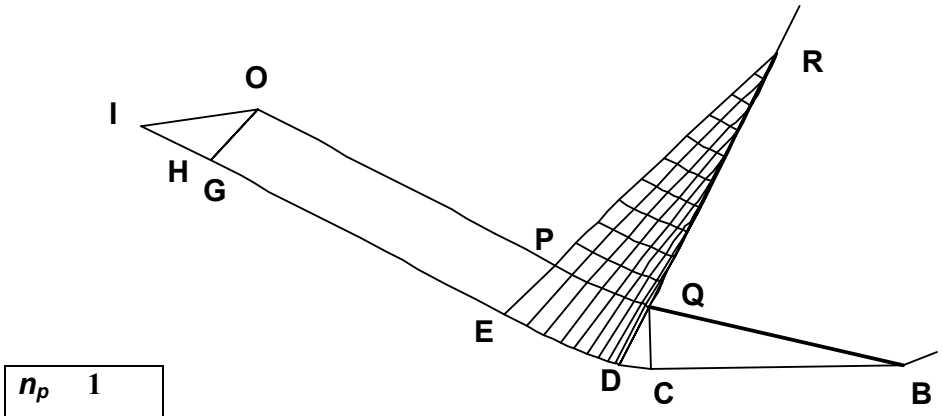

(a)

n_p	1
μ	1
γ	20^0
l_f/t_0	1
α	2.4^0
β	16.1^0
ϕ_R	18.5^0
δ	17.7^0
φ	11.2^0
ψ_2	20.7^0

(c)

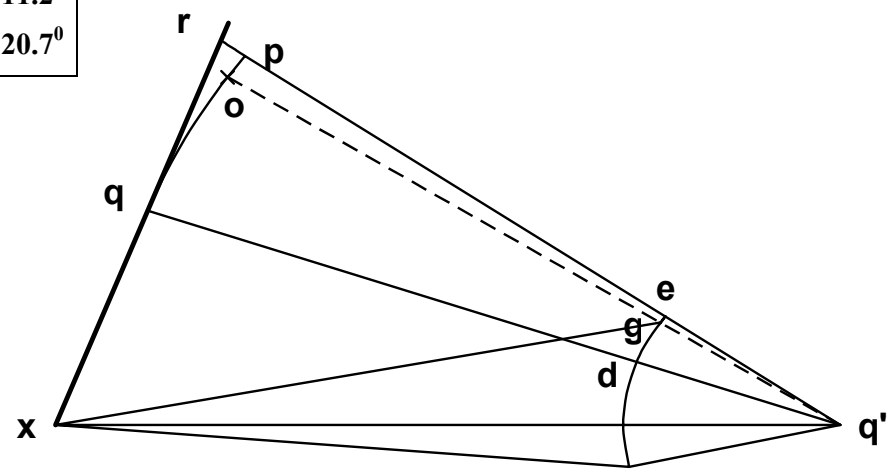

(b)

Fig. 6.13: Graphical plotting of Field VIII (a) Slipline field (b) Hodograph (c) Table of input/output values.

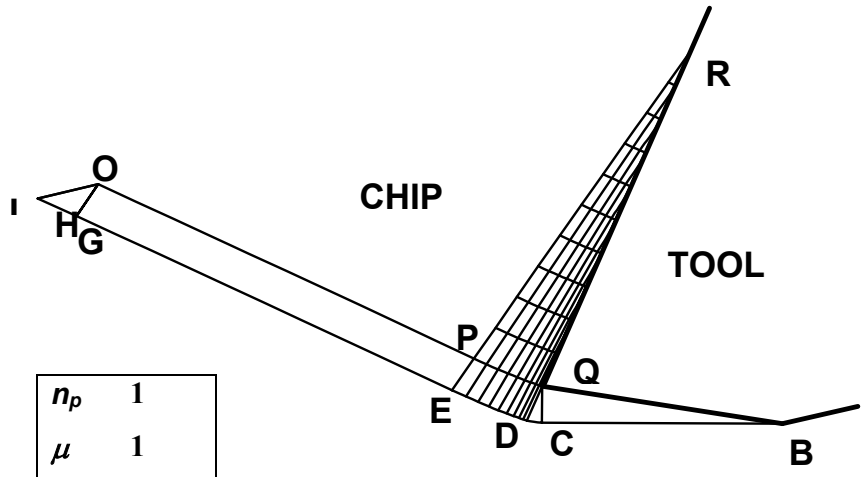

(a)

n_p	1
μ	1
γ	20^0
l_f/t_0	1
α	1^0
β	9.6^0
ϕ_R	10.5^0
δ	4.4^0
φ	16.2^0
ψ_2	26.1^0

(c)

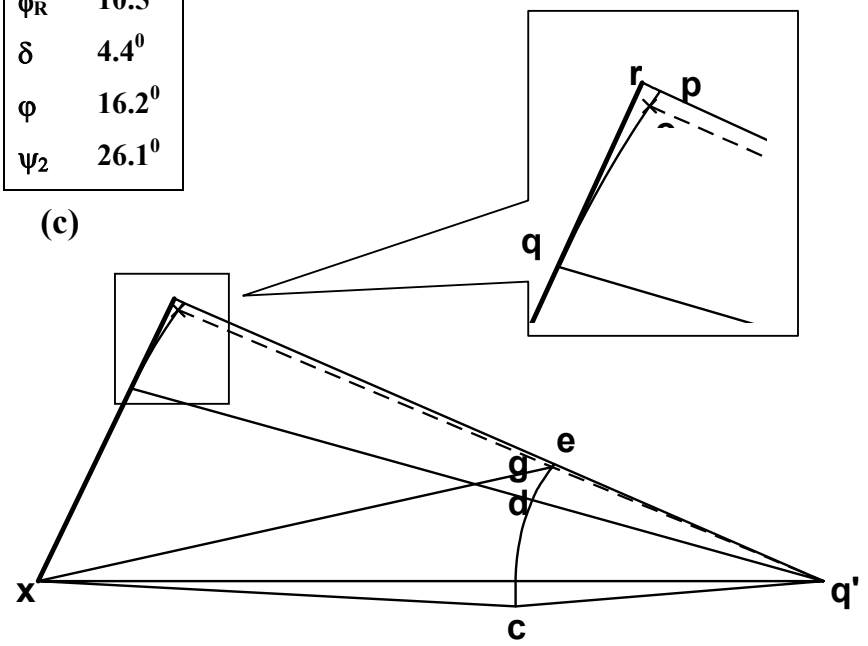

(b)

Fig. 6.14: Graphical plotting of Field VIII (a) Slipline field (b) Hodograph (c) Table of input/output values.

Chapter 7

Chapter 7

Experimental validation

7.1 Introduction

Although machining process came into use in industry at the very beginning of the Industrial revolution in the late 18th century, virtually no technological/mathematical representations capable of describing the physics or mechanics of the machining process came into being for over 200 years. Efforts in this direction began in the early stage by the use of experimental data as the basis for modeling. This resulted in a number of empirical models, the most successful amongst which was the one suggested by Taylor [1] ($VT^n = c$) on the basis of his wholly factory based research programme at 'Midvale Steel Works' in the beginning of 20th century. This trend picked up in thirties and forties, during which period, investigations were mainly undertaken to set up empirical equations for cutting forces and tool life in terms of the variables such as speed, feed and depth of cut (Kronrnberg [38], Woxen [116],). After fifties, however, attention was mostly directed towards having a deeper understanding of the mechanics of the machining process and on the basis of that knowledge to establish predictive models. Experimental investigations carried out during that period were mainly intended for the validation of such theoretical models. An exhaustive volume of experimental data of machining parameters such as cutting force, thrust force, contact length, and

cutting ratio was given by Eggleston et al [105] in late fifties. Trend in the experimental investigations changed radically in 60's with the introduction of digital computer technology, which brought digitally controlled machine tools into the field of machining. The strength of this new modeling technology was its ability to propose hybrid models by combining experimental data with predictive machining theories. In addition computers were used for simulating the ongoing performance of machining operation (dynamic modeling). However, in view of the lack of reliable sensors and difficulties associated with signal processing techniques, these efforts so far have proved to be less productive. That may be the reason why analytical models based on classical theories of plasticity have once again caught the attention of researchers of present times for deeper understanding of the machining process.

This chapter describes the experimental investigation carried out in the present study for the purpose of validating the theoretical results. Machining parameters such as cutting ratio, cutting forces, radius of chip curvature and chip-tool contact length were determined from orthogonal cutting tests on steel using sharp and worn tools with finite flank wear land and results are compared with those obtained from slipline field analysis.

7.2 Experimental Procedure

Orthogonal cutting tests were conducted on commercially available mild steel bars using freshly ground HSS tools with 10% cobalt on a heavy-duty HMT copier lathe (Fig. 7.1). Before commencing the tests, these bars were first turned all through to a uniform diameter by a skin pass. For carrying out the cutting tests each bar was supported at one end by a three-jaw self-centering chuck and at the other end

by a revolving center. Tests were conducted on these bars using both sharp and worn tools. Tool geometry and cutting conditions used in these tests are shown in Table 7.1. For tests with worn tools artificial flank wear land having five degrees negative inclination were ground on the flank face of these tools using a surface grinder having 1 μm accuracy. The size of this wear land was measured by a '*Axiotech*' reflected

Table 7.1: Tool geometry and test conditions.

Sharp tool			
***Rake angle*, degrees**	**0**	**10**	**20**
***Clearance angle*, degrees**	**12**		
Cutting speed, rpm	**151**	**245**	
***Feed,* mm/rev**	**0.049**	**0.098**	**0.196**
Worn tool			
***Rake angle*, degrees**	**15**	**20**	**25**
***Clearance angle*, degrees**	**12**		
Cutting speed, rpm	**250**		
***Feed,* mm/rev**	**0.05**	**0.06**	**0.10**
Flank wear land, mm	**0 to 1.55**		

light microscope (*Zeiss* make) with 50*X* magnification (Fig. 7.2) supported by a '*Vedio Pro32*' colour image analysis system (*Version 4.070*). The thickness of the chip after each test was also measured by the same microscope. The magnified images of some of these chips are shown in Fig. 7.3. The width of the chip was maintained at 1 mm in all tests. The chip curvature was measured on a tool maker's microscope (*Zeiss* make, accuracy 1.0 μm (Fig. 7.4))

Fig. 7.1 : Experimental set up

Fig. 7.2 : ***Photograph of reflected light microscope***

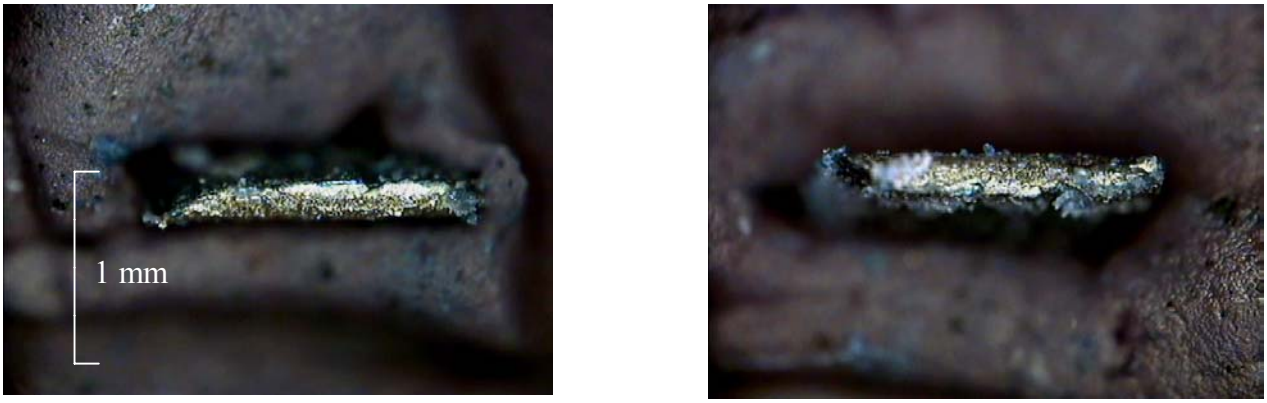

Fig. 7.3 : ***Magnified images of chip cross section***

Fig. 7.4 : ***Photograph of Tool Maker's microscope***

Table 7.2 : Experimental results (Sharp tool)

Exp No	γ Deg	t_0 mm	V_c m/min	d mm	F_C Kgf	F_t Kgf	R mm	t_1/t_0	l_f/t_0	λ Deg	F_C/kt_0	F_T/kt_0
1	0	0.049	17.7	1.02	23.53	10.59	9.78	3.490	4.050	16.0	3.41	1.54
2	0	0.098	17.7	0.92	41.52	14.57	1.93	3.656	4.067	15.3	3.30	1.16
3	0	0.196	17.7	1.02	69.41	32.75	2.19	2.731	2.712	20.1	2.69	1.27
4	0	0.049	28.6	1.11	21.08	11.35	1.35	4.163	5.370	13.5	4.33	2.33
5	10	0.098	17.7	1.02	37.06	10.59	2.08	2.582	5.063	22.2	2.61	0.74
6	10	0.196	17.7	1.02	59.02	18.04	5.16	3.048	3.860	18.9	3.01	0.92
7	10	0.049	28.7	0.97	15.67	5.15	2.19	3.231	3.616	17.9	3.01	0.99
8	20	0.049	17.7	1.02	15.69	5.10	2.24	4.871	3.149	11.7	4.80	1.56
9	20	0.098	17.7	1.02	29.41	9.61	2.65	2.707	4.072	21.7	2.63	0.86
10	20	0.196	17.7	1.02	50.20	16.27	2.97	2.388	2.271	24.7	2.34	0.76
11	20	0.049	28.6	1.02	19.80	6.27	2.36	4.088	4.450	14.1	4.00	1.27
12	0	0.049	12.0	1.55	28.26	12.65	3.53	4.347	3.357	13.0	6.43	2.88
13	0	0.098	11.9	1.775	27.27	11.49	2.38	3.058	3.887	18.1	5.28	2.23
14	0	0.196	11.9	1.8	69.11	34.11	2.68	2.845	5.985	19.4	4.90	2.42
15	0	0.049	19.6	1.65	15.15	6.79	2.47	4.503	6.734	12.5	7.09	3.18
16	0	0.098	19.5	1.8	36.33	17.67	1.96	2.993	5.853	18.5	5.15	2.51
17	0	0.196	19.6	1.6	81.88	47.63	3.86	3.862	7.226	14.5	5.73	3.33
18	10	0.049	12.1	1.65	14.06	6.55	3.27	3.388	2.552	17.0	5.16	2.40
19	10	0.098	12.0	1.89	25.50	9.84	5.22	2.180	6.341	26.1	4.02	1.55
20	10	0.196	12.0	1.85	61.51	23.03	2.07	2.973	5.310	19.4	5.22	1.95
21	10	0.049	20.9	1.7	15.41	6.59	2.36	2.558	7.881	22.4	4.09	1.75
22	10	0.098	22.1	1.55	28.13	13.03	2.50	2.881	5.380	20.0	4.13	1.91
23	10	0.196	22.2	1.45	61.10	27.59	3.60	2.798	7.416	20.6	3.77	1.70
24	20	0.049	12.0	1.7	15.65	6.12	3.37	3.224	2.416	18.1	5.12	2.00
25	20	0.098	12.0	1.89	26.24	10.69	9.67	2.333	4.728	25.3	4.11	1.67
26	20	0.196	12.0	1.9	43.58	16.00	2.73	2.265	2.470	26.0	4.08	1.50
27	20	0.049	19.6	1.7	15.88	7.06	3.83	4.014	2.556	14.4	6.35	2.82
28	20	0.098	22.1	1.55	27.48	11.10	3.32	3.497	3.535	16.6	5.06	2.04
29	20	0.196	22.1	1.6	46.63	20.50	4.22	2.534	2.416	23.2	3.72	1.63

Table 7.3 : Experimental results (Worn tool)

Exp No.	γ Deg	l_f mm	V_c m/min	t_0 mm	F_c Kgf	F_t Kgf	t_1 mm
1	15	0.000	50.3	0.05	31.9	36.1	0.158
2	15	0.000	50.3	0.05	16.7	12.6	0.154
3	15	0.000	50.3	0.05	16.4	12.4	0.133
4	15	0.000	50.3	0.05	16.9	12.6	0.161
5	15	0.000	50.3	0.05	17.1	12.9	0.151
6	15	0.000	50.3	0.05	16.9	12.8	0.148
7	15	0.000	50.3	0.05	16.9	12.9	0.148
8	15	0.000	50.3	0.05	16.2	12.9	0.184
9	15	0.447	50.3	0.05	37.3	40.4	0.264
10	15	0.597	50.3	0.05	39.0	44.1	0.300
11	15	2.419	50.3	0.05	49.3	42.9	0.329
12	15	0.000	50.3	0.06	21.4	16.1	0.181
13	15	0.000	50.3	0.06	14.7	10.3	0.181
14	15	0.296	50.3	0.06	24.3	24.0	0.209
15	15	0.317	50.3	0.06	16.9	16.5	0.144
16	15	0.369	50.3	0.06	27.2	28.8	0.160
17	15	0.604	50.3	0.06	24.4	27.7	0.135
18	15	0.768	50.3	0.06	49.6	58.9	0.147
19	15	0.784	50.3	0.06	50.1	67.4	0.146
20	15	0.967	50.3	0.06	64.0	100.3	0.149
21	15	1.115	50.3	0.06	56.4	78.0	0.246
22	15	1.557	50.3	0.06	34.3	27.0	0.305
23	15	0.000	50.3	0.10	19.2	11.3	0.217
24	15	0.436	50.3	0.10	36.9	37.9	0.208
25	15	0.519	50.3	0.10	51.0	52.2	0.227
26	15	0.688	50.3	0.10	55.8	59.7	0.213
27	15	1.095	50.3	0.10	50.0	67.4	0.202
28	20	0.000	50.3	0.05	46.9	57.2	0.163
29	20	0.000	50.3	0.05	14.7	11.3	0.118
30	20	0.000	50.3	0.05	13.1	8.6	0.224
31	20	0.575	50.3	0.05	41.8	47.9	0.220
32	20	0.636	50.3	0.05	47.6	54.2	0.220
33	20	0.000	50.3	0.06	18.4	12.2	0.166
34	20	0.000	50.3	0.06	15.4	9.3	0.164
35	20	0.182	50.3	0.06	20.5	17.5	0.172
36	20	0.251	50.3	0.06	19.5	19.5	0.134
37	20	0.410	50.3	0.06	18.1	17.5	0.132
38	20	0.410	50.3	0.06	31.8	37.6	0.144
39	20	0.570	50.3	0.06	39.9	46.6	0.125
40	20	0.582	50.3	0.06	31.7	34.5	0.151
41	20	0.859	50.3	0.06	58.2	72.5	0.116
42	20	1.008	50.3	0.06	31.7	34.6	0.140
43	20	0.000	50.3	0.10	16.9	8.8	0.249
44	20	0.214	50.3	0.10	34.6	27.1	0.171
45	20	0.340	50.3	0.10	22.3	18.1	0.209
46	20	0.416	50.3	0.10	34.0	40.6	0.168
47	20	0.747	50.3	0.10	30.6	33.9	0.193
48	20	0.995	50.3	0.10	48.2	57.9	0.184
49	25	0.000	50.3	0.05	56.2	78.8	0.097
50	25	0.000	50.3	0.05	10.0	6.0	0.109
51	25	0.000	50.3	0.05	10.0	5.8	0.120
52	25	0.000	50.3	0.05	10.0	6.2	0.116
53	25	0.000	50.3	0.05	10.4	6.1	0.136
54	25	0.000	50.3	0.05	10.5	6.3	0.119
55	25	0.000	50.3	0.05	8.3	5.7	0.128
56	25	0.607	50.3	0.05	40.3	51.5	0.225
57	25	0.718	50.3	0.05	36.5	39.5	0.244
58	25	0.000	50.3	0.06	19.0	12.5	0.145
59	25	0.000	50.3	0.06	14.6	8.7	0.186
60	25	0.175	50.3	0.06	15.0	14.1	0.127
61	25	0.244	50.3	0.06	23.5	21.4	0.140
62	25	0.303	50.3	0.06	27.4	28.8	0.129
63	25	0.315	50.3	0.06	19.7	20.1	0.121
64	25	0.573	50.3	0.06	32.2	33.9	0.125
65	25	0.720	50.3	0.06	39.8	51.9	0.117
66	25	1.171	50.3	0.06	45.6	48.7	0.125
67	25	1.389	50.3	0.06	73.3	106.9	0.151
68	25	0.000	50.3	0.10	17.6	8.7	0.233
69	25	0.102	50.3	0.10	20.7	12.3	0.175
70	25	0.286	50.3	0.10	24.7	23.4	0.259
71	25	0.489	50.3	0.10	34.5	36.3	0.303
72	25	0.664	50.3	0.10	41.6	43.0	0.180
73	25	0.911	50.3	0.10	61.5	124.5	0.249

For measurement of tool-chip contact length, the tool face was first made horizontal by placing the tool on a tilting device. The contact length was then assessed by observing the length over which the chip material adhered to the rake face of the tool.

The cutting and thrust forces in the above tests were measured using a three-component digital lathe-tool-dynamometer (Syscon make) of 0-500 Kgf range. The least count of the dynamometer was 1 Kgf. Data collected from the above experiments are presented in Tables 7.2 and 7.3. Data presented in Table 7.2 refer to experiments using sharp tools and those in Table 7.3 refer to experiments with worn tools.

The cutting velocity V_c in the above tables has been calculated from the machine rpm N using the formula

$$V_c = \frac{\pi DN}{1000} \tag{7.1}$$

where, D is the mean test bar diameter. The shear plane angle λ has similarly been estimated from the relation

$$\tan\lambda = \frac{\cos\gamma}{(t_1/t_0) - \sin\gamma} \tag{7.2}$$

The yield stress k in shear of the chip material equal to the net shear force on the shear plane divided by the shear plane area was determined from the equation

$$k = \frac{(F_c\cos\lambda - F_t\sin\lambda)\sin\lambda}{t_0} \tag{7.3}$$

This value of k was then used to calculate the non-dimensional cutting and thrust forces.

All tests were conducted dry and the values of cutting and thrust forces were recorded after cutting process got stabilized. For greater reliability ten readings of each force component was taken for each cutting test. The data of force components presented in Tables 7.2 and 7.3 corresponding to any given feed value is the mean of these ten readings. Similarly, the chip thickness t_1 used for calculation of cutting ratio and shear plane angle λ was the mean of five chip thickness readings taken at five different locations of the chip. In case of machining with worn tools, the size of the flank wear land was measured using the reflected light microscope before and after each test. The mean of these two values was taken for calculating (l_f / t_0). Photographs of the rake and flank faces taken with the help of the reflected light microscope are depicted in Fig. 7.5 which clearly shows the sticking of the work material onto the rake and flank faces of the tool.

7.3 Results and discussion

The machining parameters determined from the above cutting tests are compared with those predicted from the slipline field analysis in figures 7.6-7.19. The theoretical results presented in these figures have been computed from the slipline field analysis for values of n_p=1 and μ=1,2.

Referring to these figures it may be seen that there is an excellent agreement between theory and experiment especially at low rake angles when machining with a sharp tool is considered. Thus cutting ratios (figures 7.6-7.8), average shear plane angle (Fig. 7.9) and cutting forces (figures 7.10-7.12) determined from the above cutting tests are found to lie within the solution range predicted by the slipline field theory for γ = 0 and 10 degrees. Agreement in respect of chip curvature (Fig. 7.13) and contact

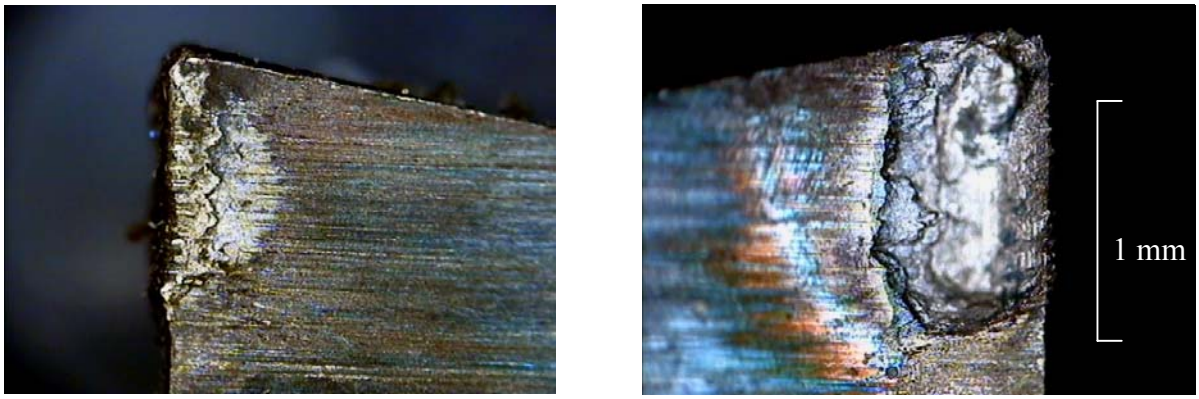

(a) (b)

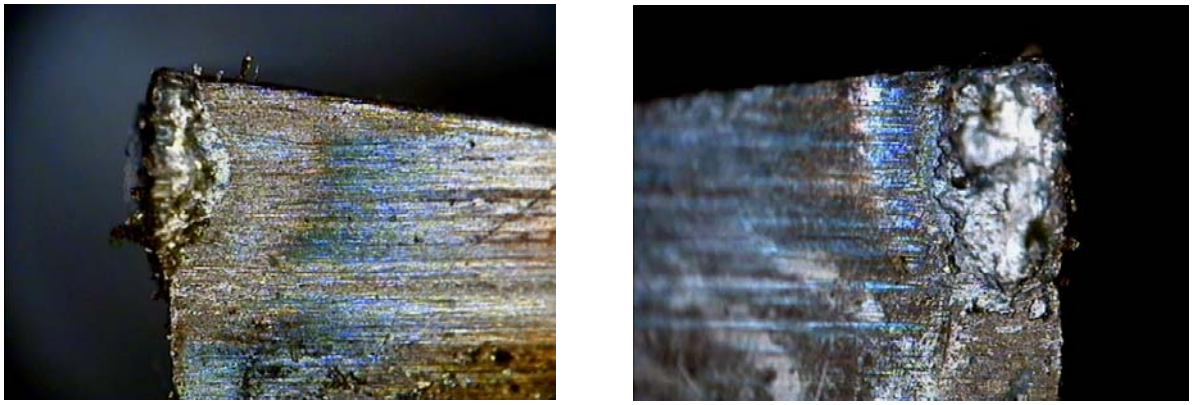

(c) (d)

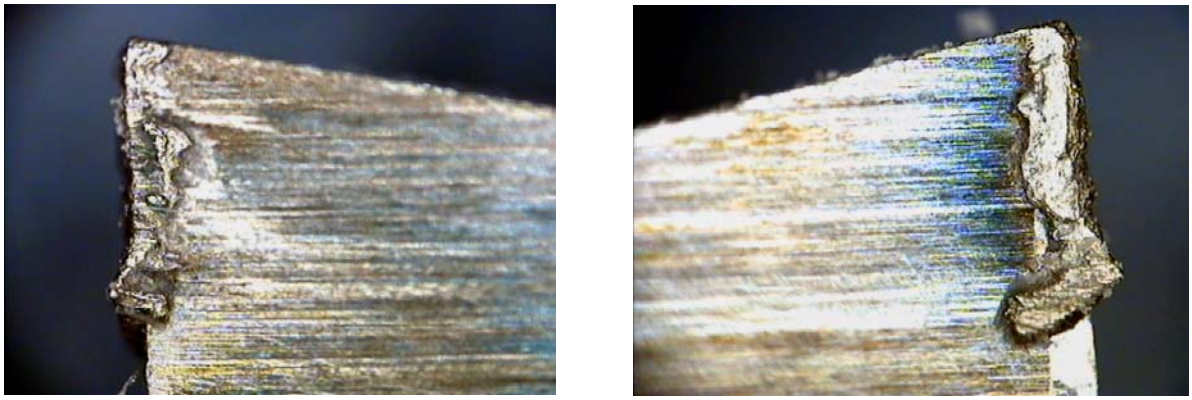

(e) (f)

Fig. 7.5 : Photographs showing adhesion of steel on HSS tools at rake face[(a),(c),(e)] and at flank wear land [(b),(d),(f)]

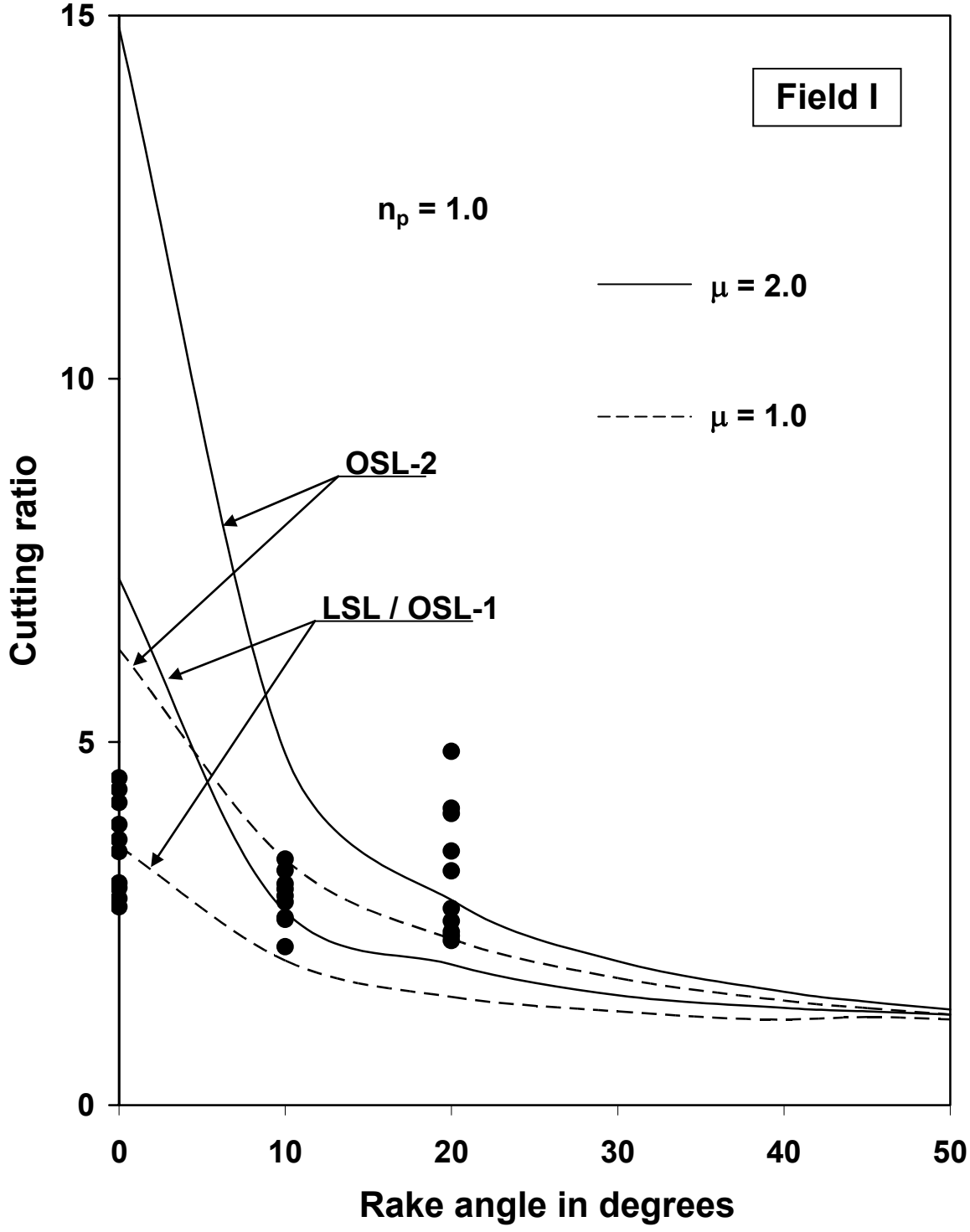

Fig. 7.6: Variation of cutting ratio with rake angle: Comparison with experimental data.

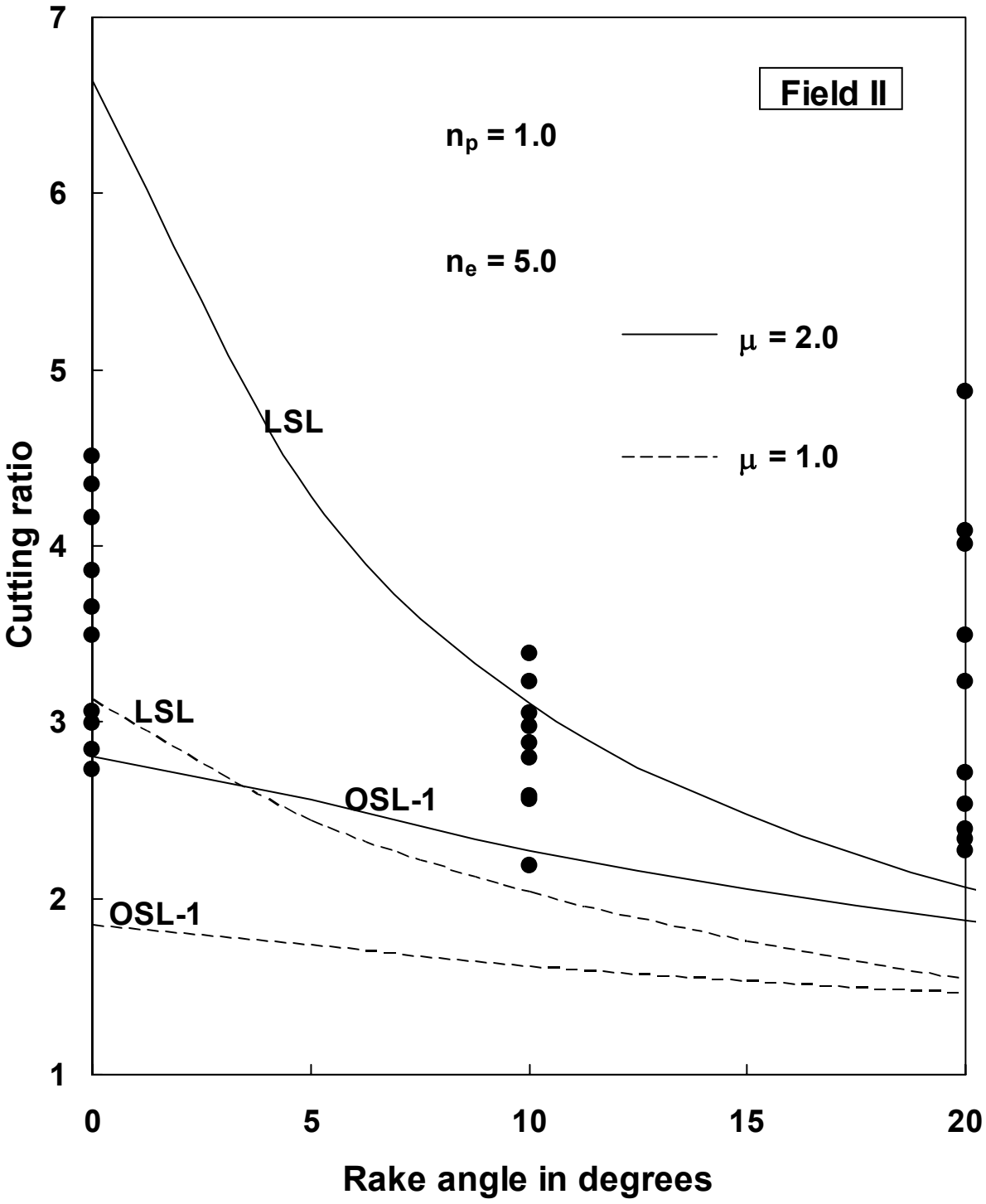

Fig. 7.7 Variation of cutting ratio with rake angle: Comparison with experimental data.

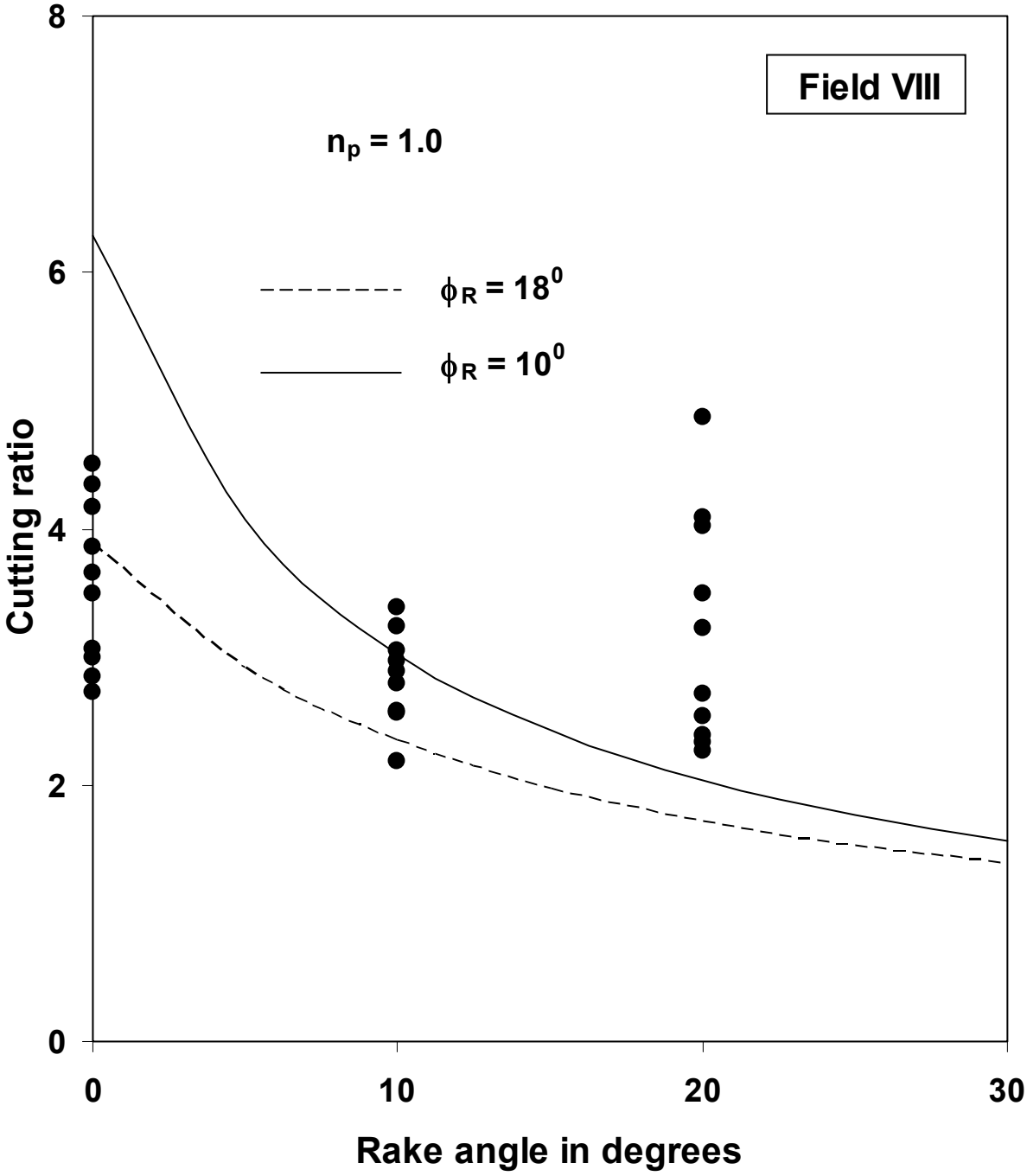

Fig. 7.8: Variation of cutting ratio with rake angle: Comparison with experimental data.

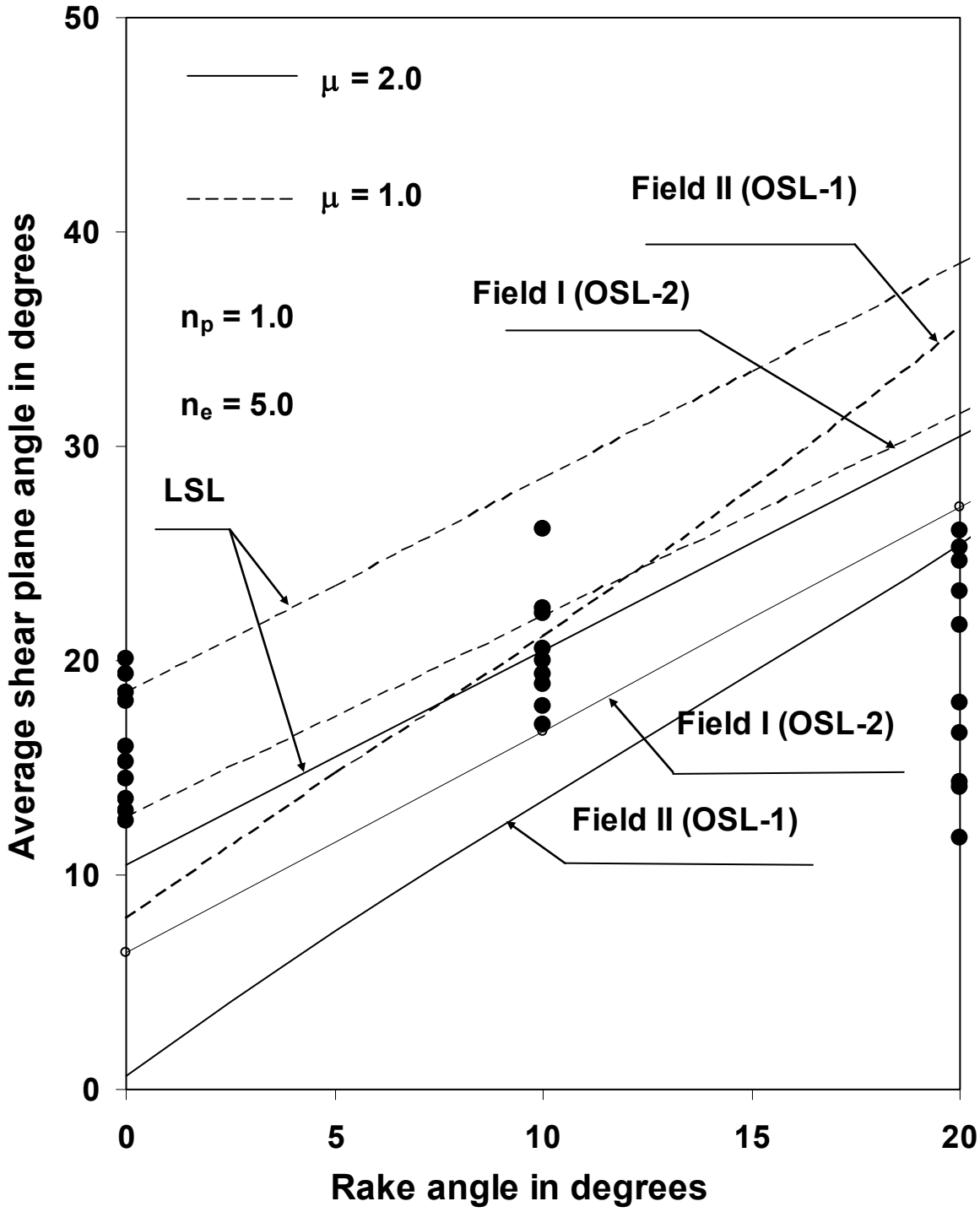

Fig. 7.9 Variation of average shear plane angle with rake angle: Comparison with experimental data.

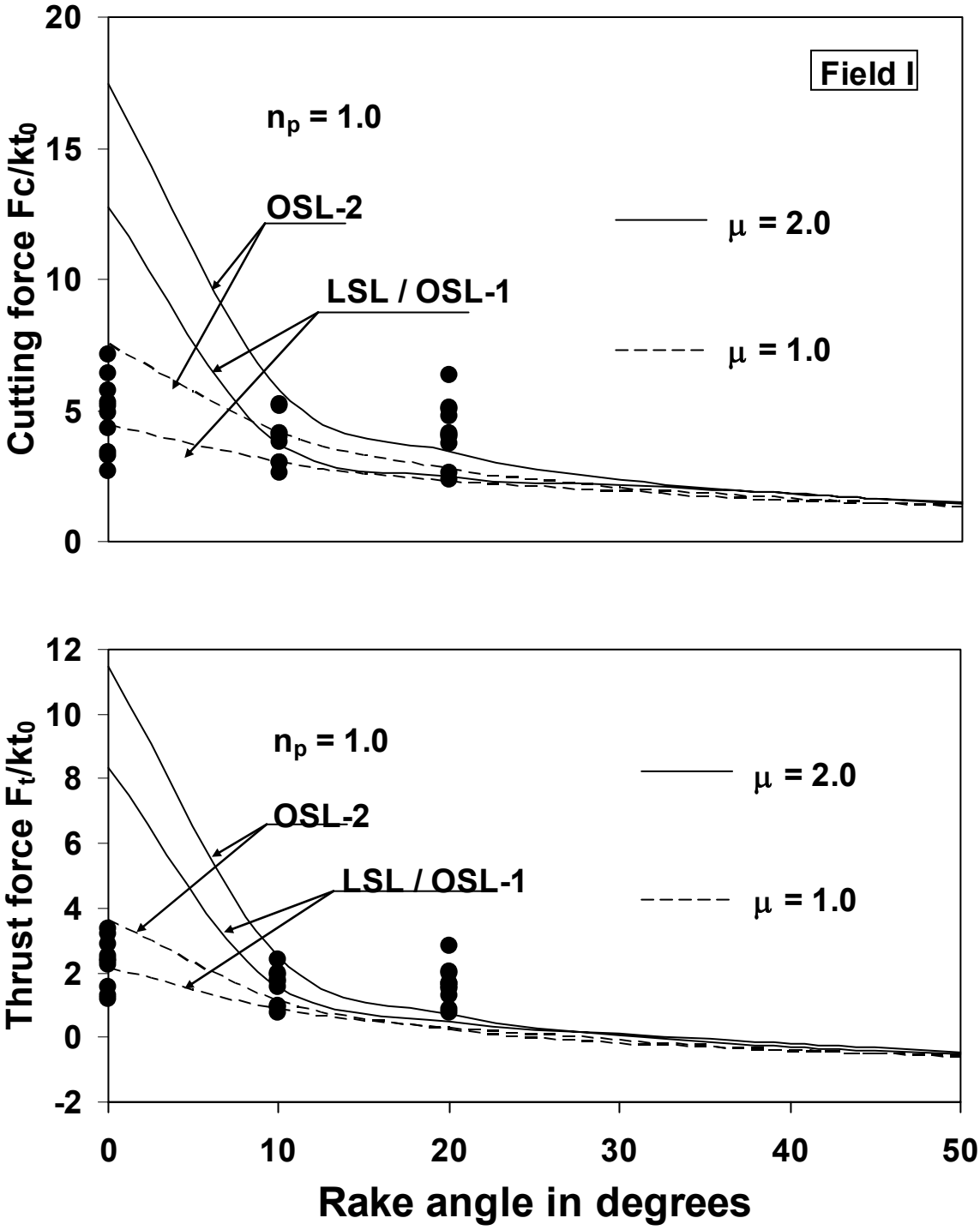

Fig. 7.10: Variation of cutting and thrust forces with rake angle: Comparison with experimental data.

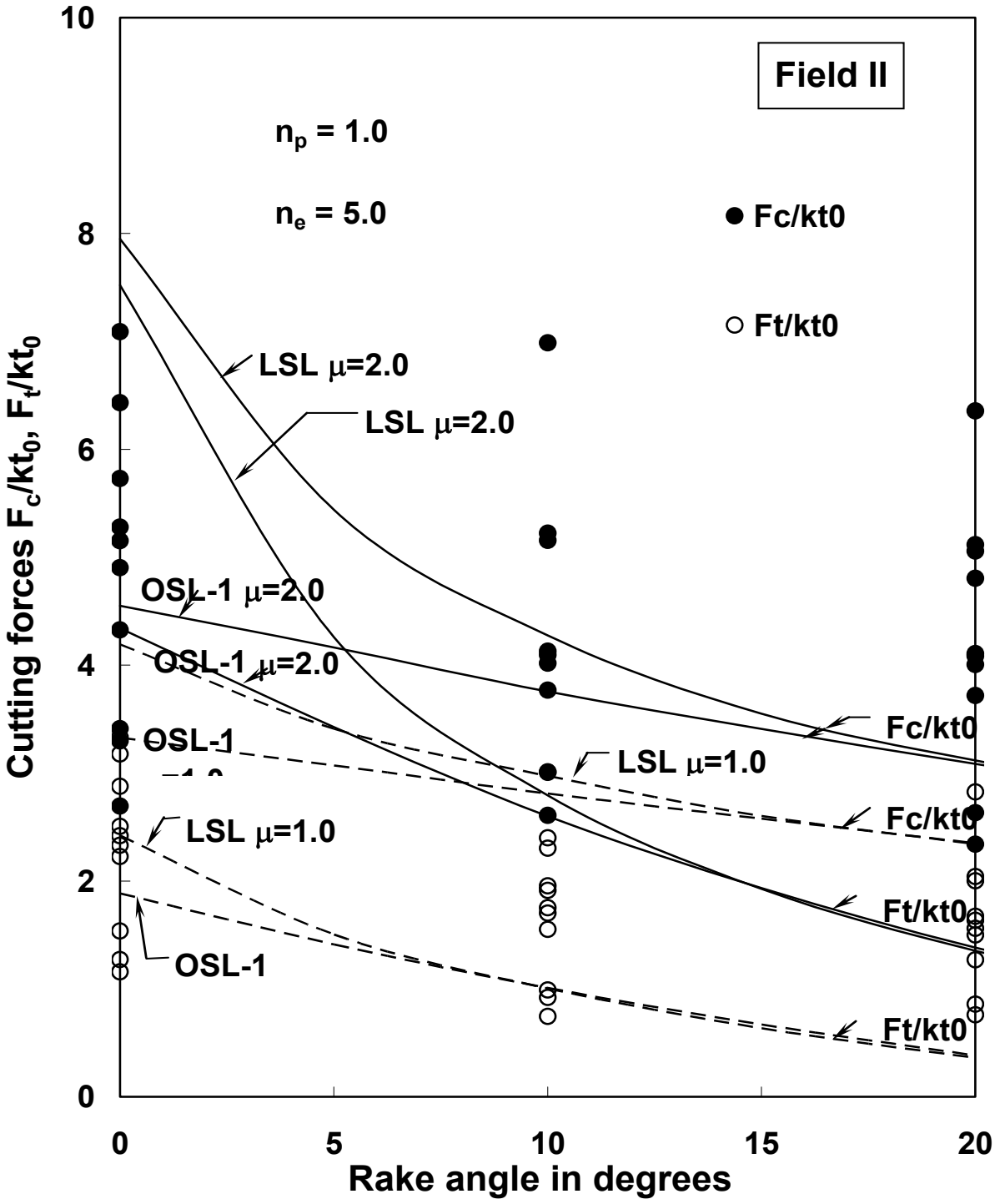

Fig. 7.11: Variation of cutting and thrust forces with rake angle: Comparison with experimental data.

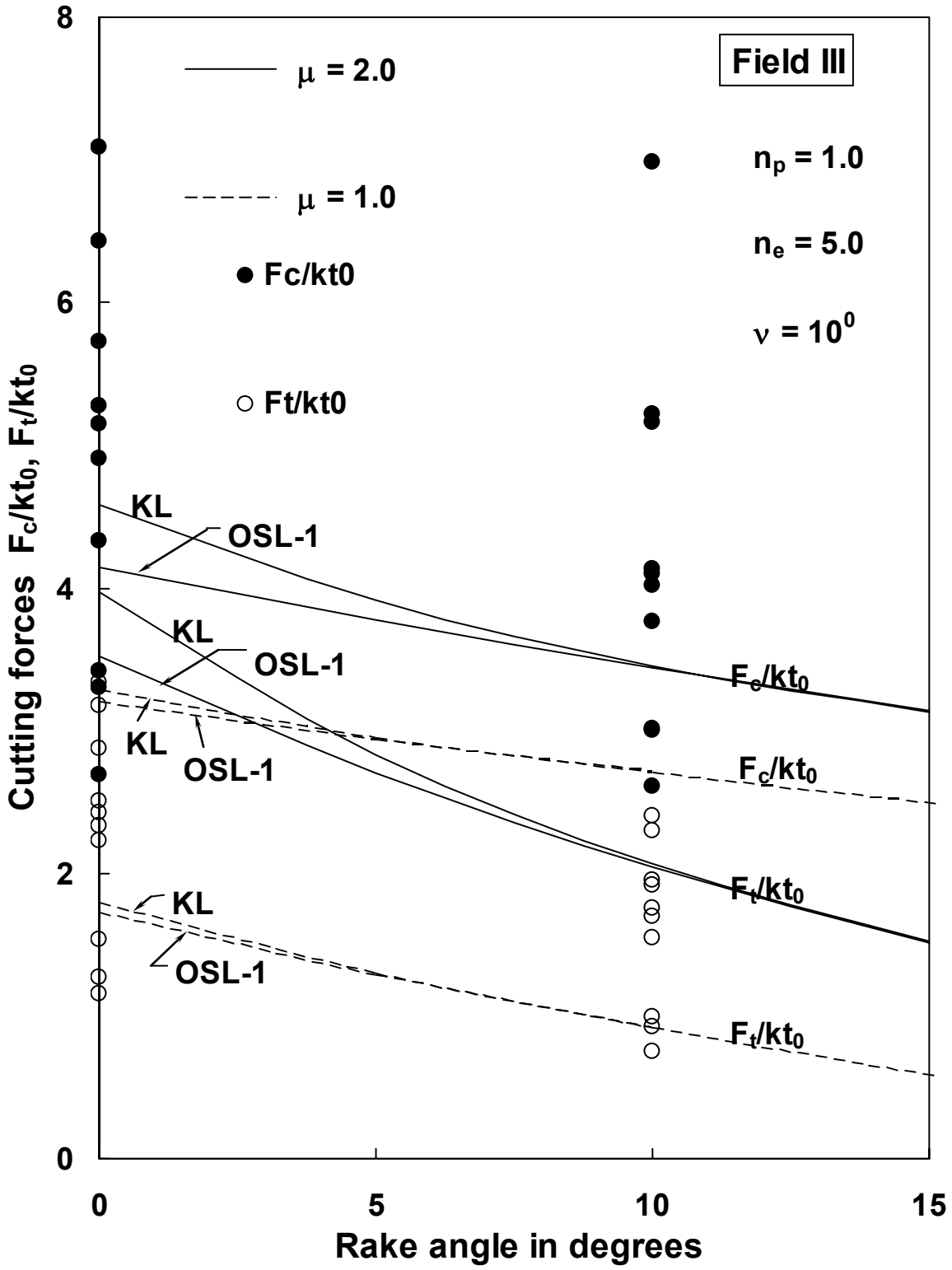

Fig. 7.12: Variation of cutting and thrust forces with rake angle: Comparison with experimental data.

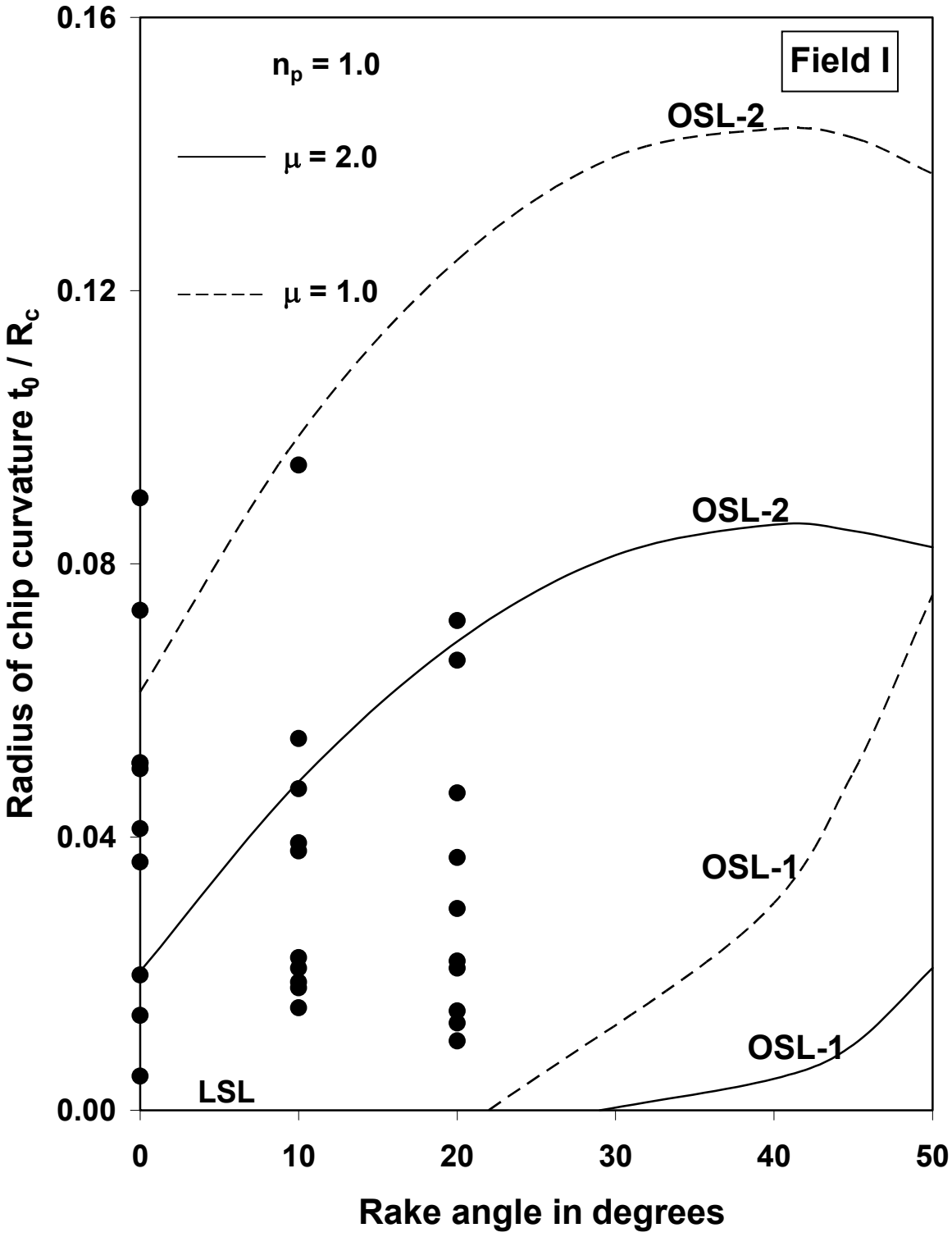

Fig. 7.13: Variation of radius of chip curvature with rake angle: Comparison with experimental data.

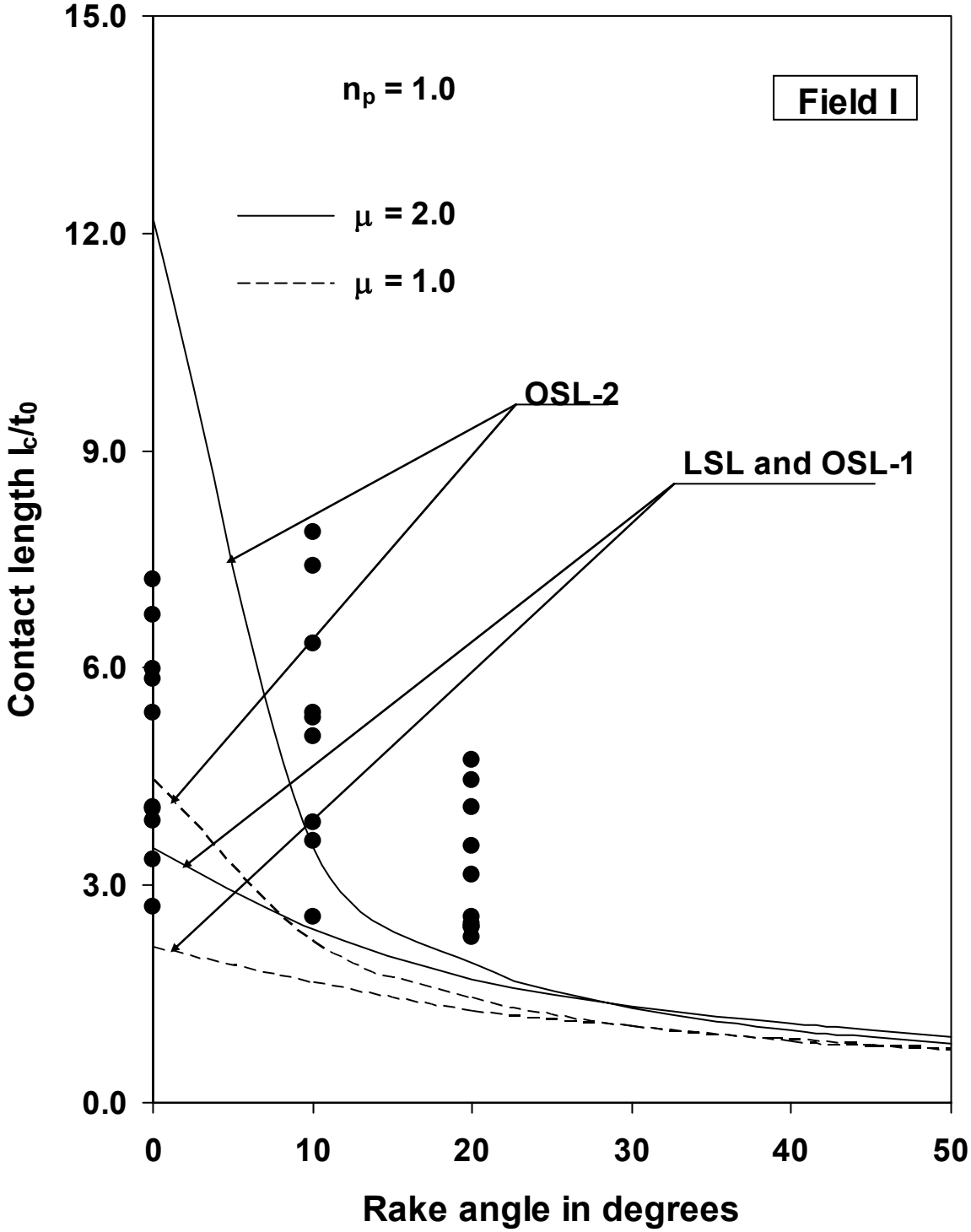

Fig. 7.14: Variation of contact length with rake angle: Comparison with experimental data.

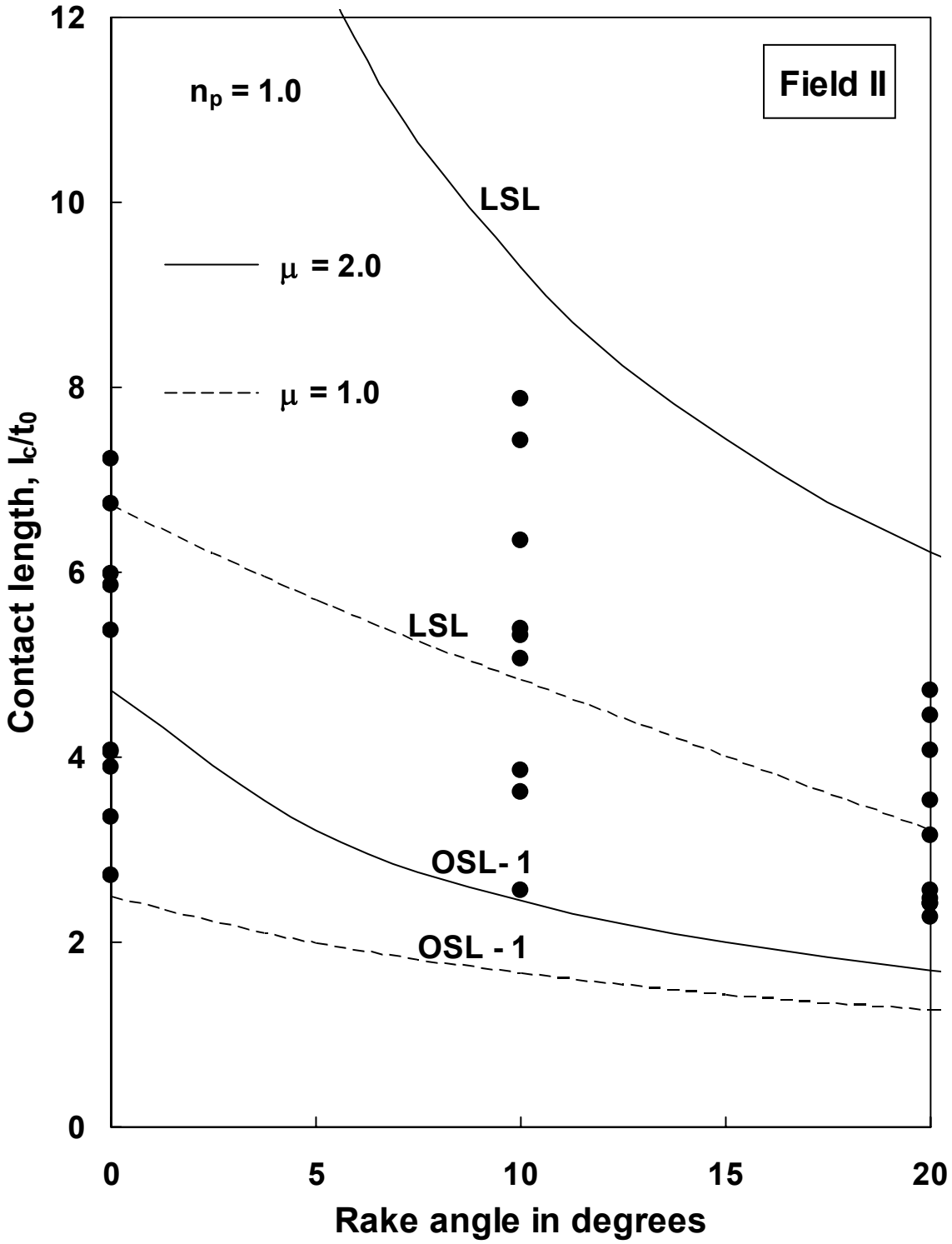

Fig. 7.15: Variation of contact length with rake angle: Comparison with experimental data.

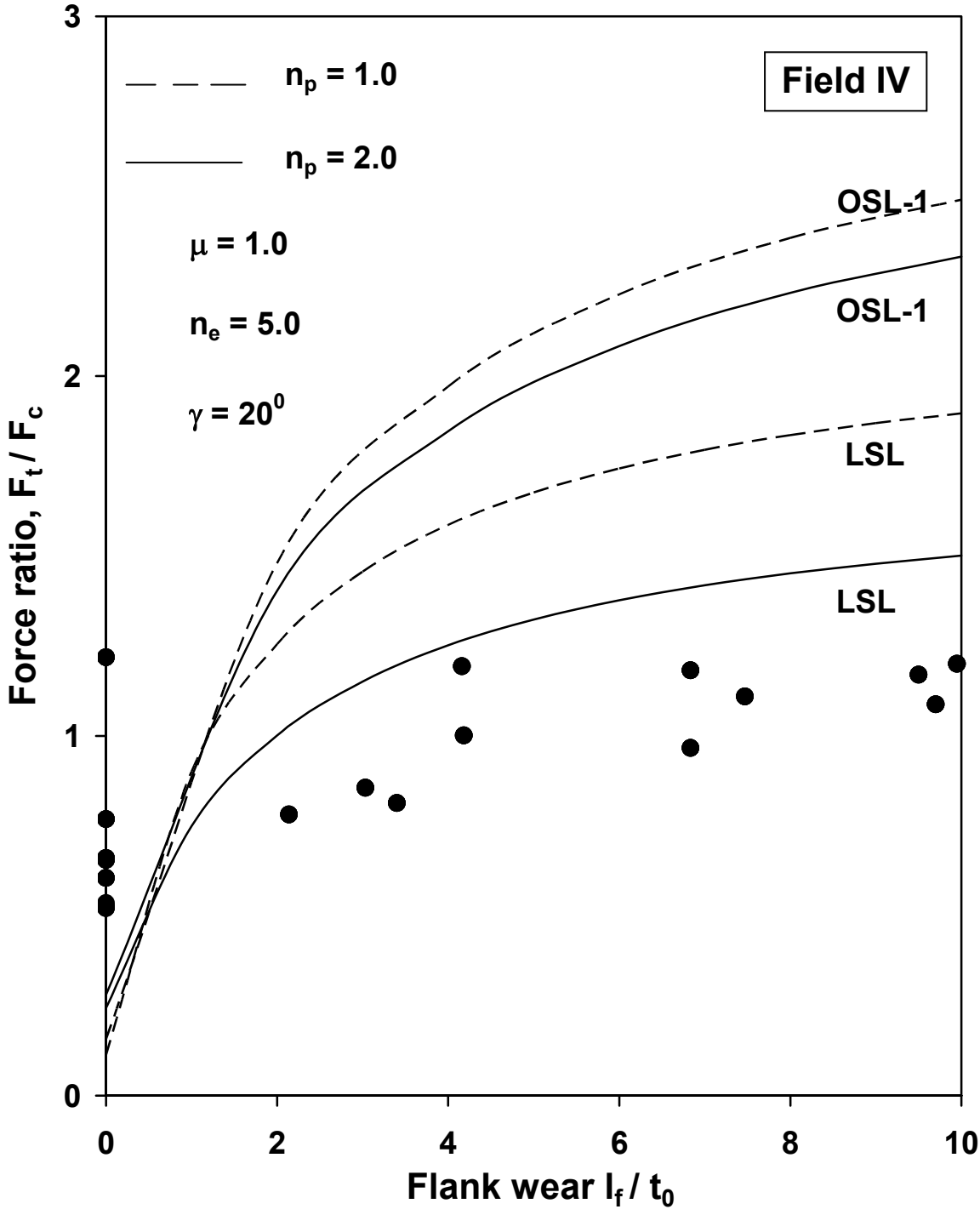

Fig. 7.16: Variation of force ratio with flank wear: Comparison with experimental data.

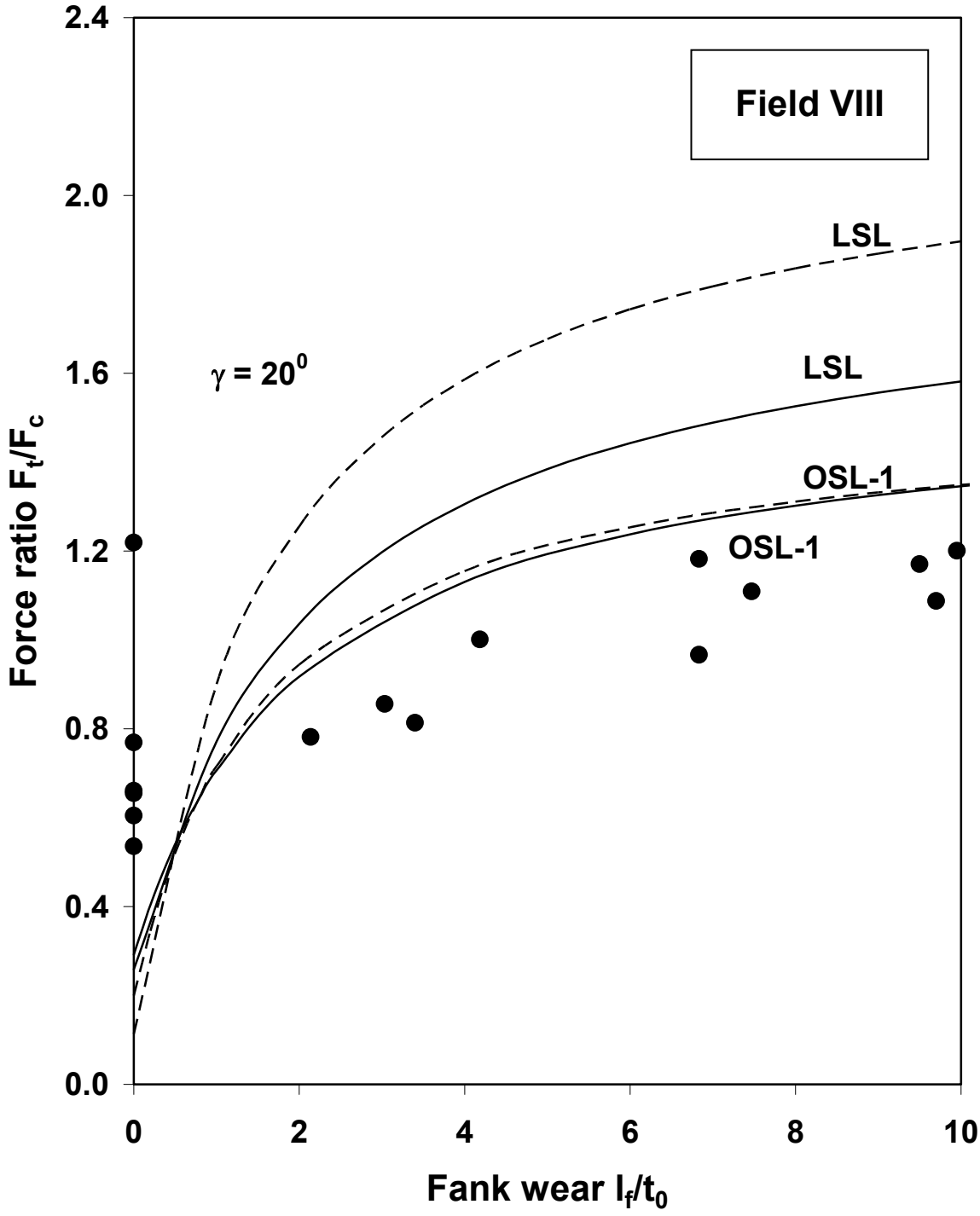

Fig. 7.17: Variation of force ratio with flank wear: Comparison with experimental data.

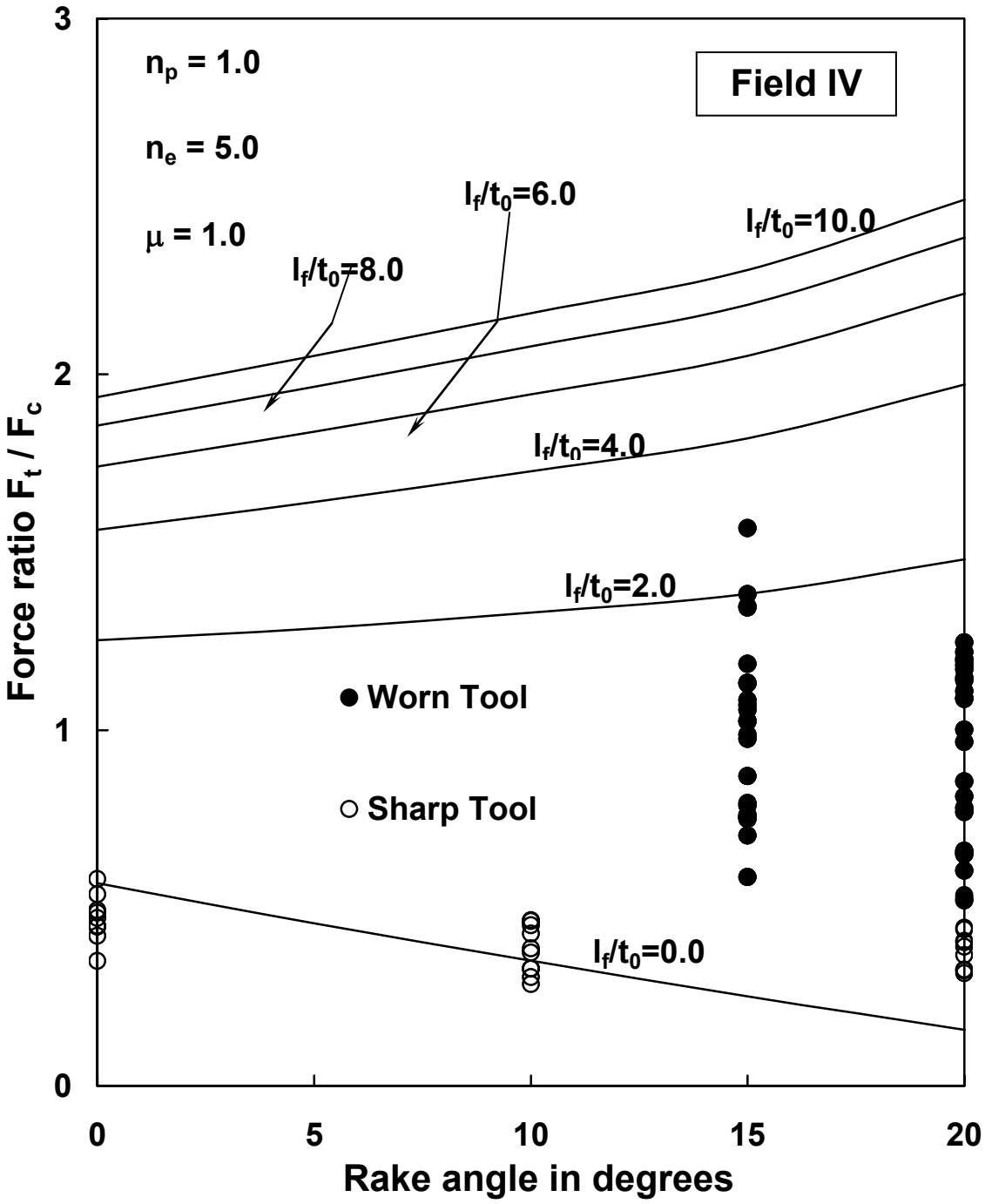

Fig. 7.18: Variation of force ratio with rake angle: Comparison with experimental data.

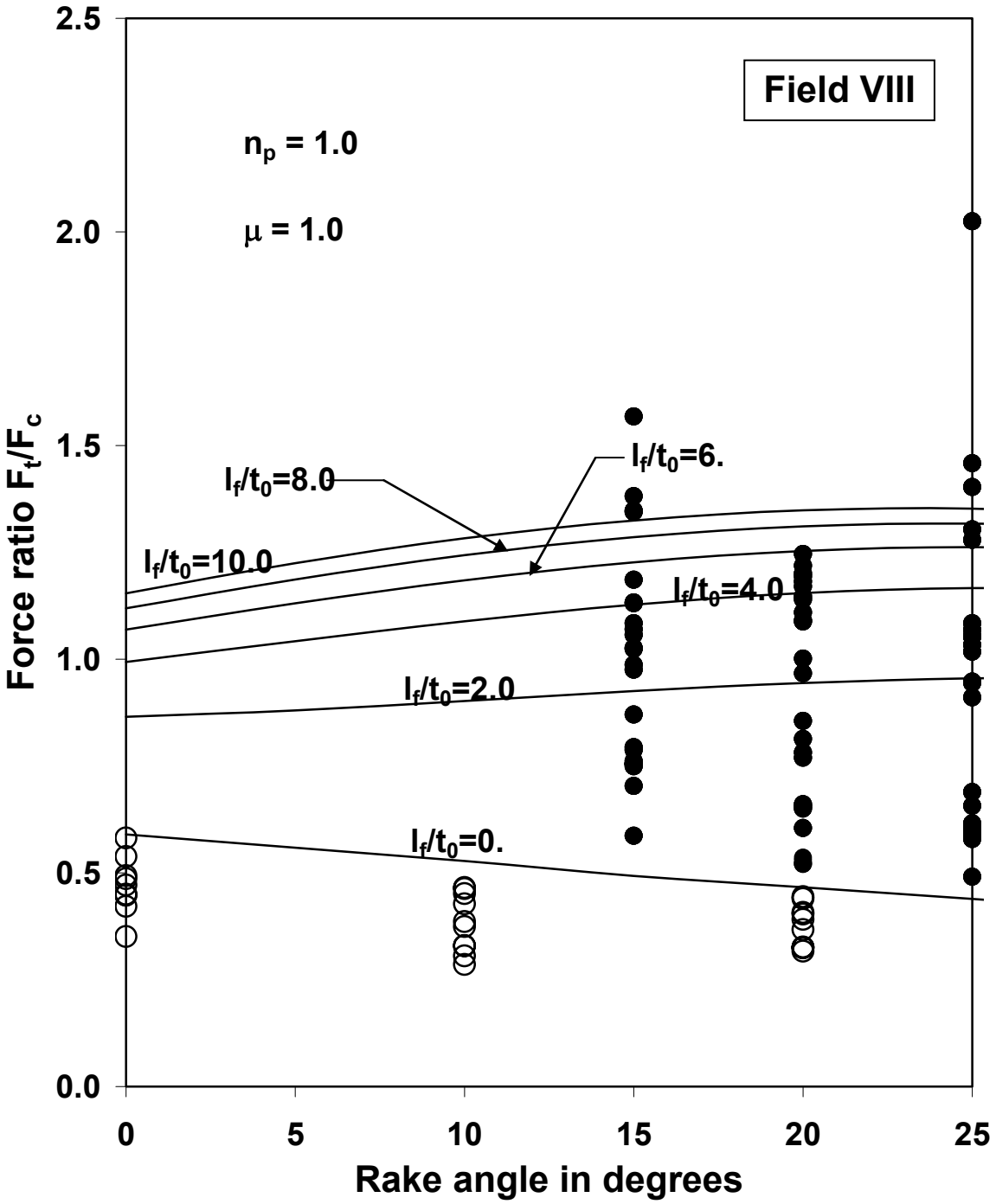

Fig. 7.19: Variation of force ratio with rake angle: Comparison with experimental data.

length (figures 7.14-7.15) is also similar. However, the contact length calculated from Field II is found to show better correlation with experiment than that calculated from Field I. This may be because in the analysis of Field II the presence of elastic contact length is taken into account.

The force ratios computed from Field IV and Field VIII are compared with those obtained from cutting tests with worn tools in Fig. 7.16 and Fig. 7.17 respectively. In both cases the experimental results are found to lie outside the solution range predicted by the slipline field analysis. This may be due to the fact that μ and n_p values for these tests were different from those for which the above theoretical results were calculated. However, the force ratio calculated for a sharp tool from the slipline field analysis shows good agreement with experiment at rake angles between 0 and 20 degrees (Fig. 7.18 and Fig. 7.19).

7.4 Conclusions

Sticking of work material on the rake and flank face clearly indicates that adhesion friction phenomenon predominates over abrasion at these contact regions. The machining parameters such as cutting force, thrust force, force ratio, shear plane angle, chip radius of curvature show good correlation between theory and experiment at low rake angles and for machining with a sharp tool. The agreement, however, is not so good when machining with a tool with a wear land.

-ooOoo-

Chapter 8

CHAPTER 8

CONCLUSIONS

In the present investigation a class of slipline field solutions for the chip forming process are presented for machining with sharp and worn tools with the assumption of adhesion friction at the contact regions on tool face and flank. The friction law assumed was that suggested by Maekawa et al [65]. The slipline fields analyzed are similar to those suggested earlier by Kudo [58], Dewhurst [73] and Lee and Shaffer [56] and results are computed with and without the assumption of the existence of an elastic contact region. The solutions are obtained by the matrix operational procedure developed by Dewhurst and Collins [89] and Dewhurst [92,93] assuming a linear relation between the angular range of α- and β- lines in the secondary shear zone. The results of the analysis indicate that the machining process is not uniquely defined in the sense that the machining parameters are not uniquely determined by the tool rake angle and tool-chip interface friction condition, but may have a range of allowable values. The allowable range of these solutions for any given rake angle is examioned using Hill's overstressing criterion [45].

For slipline field shown in Fig 3.1(a) (Field I) the allowable solution range was found to be limited by OSL-2 and LSL at lower rake angles and between OSL-2 and OSL-1 at higher rake angles. For slipline fields shown in Fig. 4.1(a) (Field II) and Fig. 5.1(a) (Field IV) the vertex angle η_2 was never overstressed and the allowable solution range for all rake angles was found to lie between LSL and OSL-1. For solutions of Fig. 4.2(a) (Field III) and Fig. 5.2(a) (Field V), KL and OSL-1 defined the allowable solution range for all rake angles. Thus under similar conditions of friction and

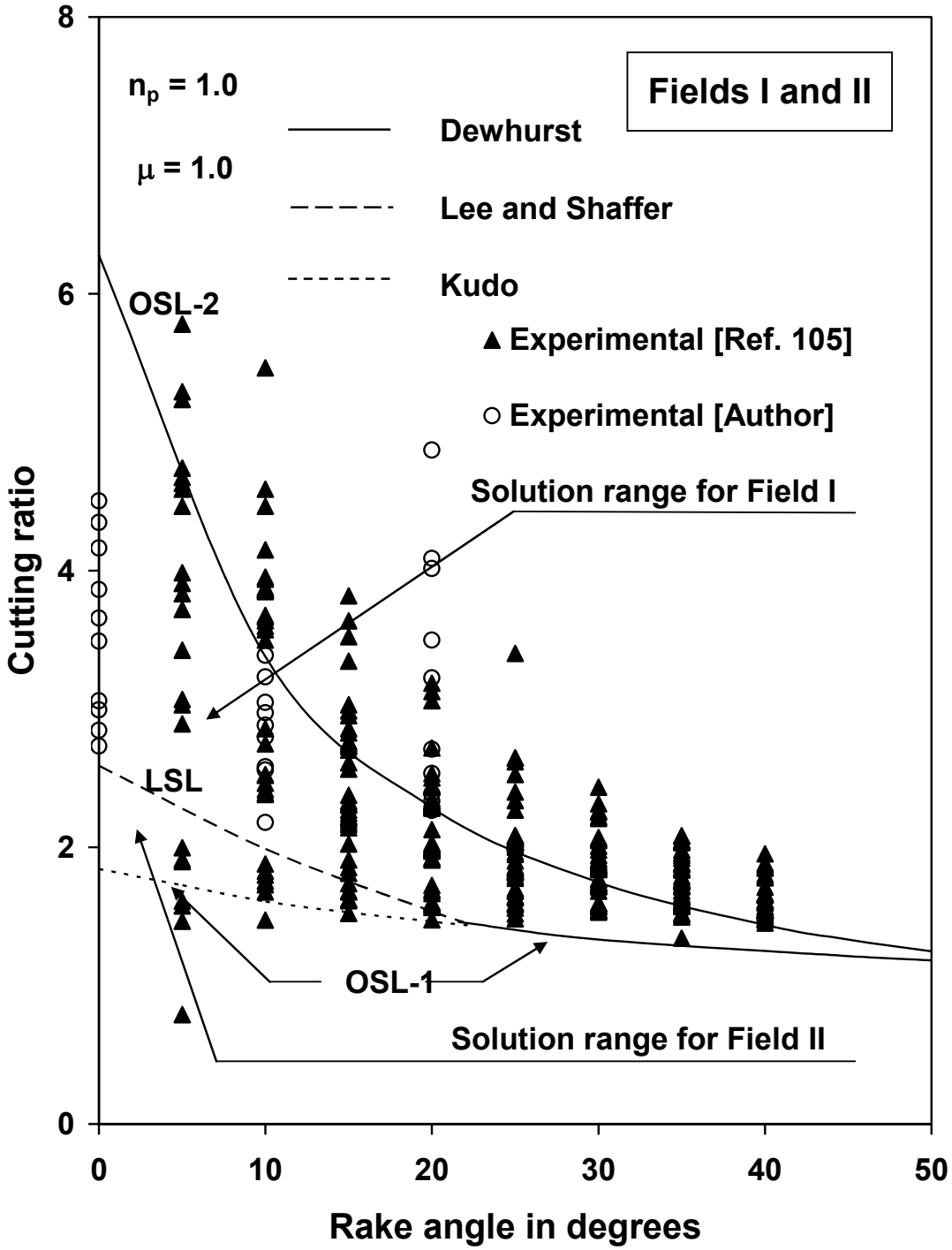

Fig. 8.1: Variation of cutting ratio with rake angle showing smooth transition between solutions of the Fields I and II.

tool/work material combination a smooth transition takes place at low rake angles from Field I (Fig. 3. 1(a)) to Field II (Fig. 4.1(a)) as shown in Fig. 8.1.

Rake angle, rake friction and the constant n_p (equation 3.1) are found to be the most important variables that influence the machining parameters. Cutting forces and cutting ratio decrease as rake angle increases but increase as μ increases. It is seen that the average normal and shear stresses on the tool face increase as rake angle increases. This is because the tool-chip contact length decreases as rake angle increases. The computed results show that the friction coefficient is not uniquely determined but has a range of allowable values for any particular value of rake angle.

The exponent n_e of normal pressure distribution in the elastic contact region is found to have only marginal influence on the machining parameters. For computational purposes, the value of n_e in general can be chosen arbitrarily. A unique value of n_e, however, is calculated if it is assumed that the slopes of the normal pressure distribution curves in the elastic and plastic contact zones have the same value at elastic-plastic transition point.

The results of the analysis indicate that the peak tool tip pressure for a sharp tool decreases with rake angle and is much higher compared to that for a worn tool with a finite flank wear land. It is further observed that the peak pressure for a worn tool is only marginally influenced by the tool rake angle and the length of the flank wear land.

The ploughing, cutting and thrust forces vary linearly with flank wear and that the thrust force increases more rapidly than the cutting force. The results also demonstrate that increasing either the interface friction coefficient μ or the exponent of contact stress distribution n_p decreases the force ratio (F_t / F_c). It is further seen that the

force ratio for a sharp tool decreases with rake angle. But the presence of a small flank wear land may reverse this trend.

The value of the average friction coefficient μ at chip-tool interface for a sharp tool is found to decrease marginally with rake angle. The μ value however, increases with rake angle if the tool wears out developing a flank wear land. The results of theoretical normal stress distribution at chip-tool interface for worn and sharp tools agree qualitatively with experiment.

The predicted values of machining parameters from the present analysis are found to agree well with the experimental observations of Eggleston et al [105], Kobayashi et al [66] and Choudury et al [30] and also with those obtained from orthogonal cutting tests by the author.

Scope for future work:

Incorporation of adhesion friction condition into slipline field analysis may be extended to tools with more complex geometries such as tools with nose radius and tools with restricted contact length. Solutions may also be obtained for the tools with step/groove type chip breakers.

-ooOoo-

Bibliography

1. Bhattacharya A., Book- Metal cutting theory and practice, New Central Book Agency (P) ltd (India), 1984

2. Boothroyd G. and Knight W. A., Book-Fundamentals of machining and machine tools (Manufacturing Engineering and material processing), Marcel Dekker, NewYork, 1998.

3. Pfeifer T. and Wiegers L., Reliable tool wear monitoring by optimized image and illumination control in machine vision, Measurement, Vol. 28, 2000, p 209-218

4. Yao Y. L. and Fang X. D., Assessment of chip formation patterns with tool wear progression in machining via neural networks, Int. J. of Mach. Tools and Manufacture., Vol.-31, 1991, p 89-102.

5. Ham I., Fundamentals of tool wear, ASTME, Paper no. MR-68-617

6. Giusti F. and Santochi M., Development of a fiber optic sensor for in process measurement of tool flank wear, Proc. 20th Int. Machine tool design and Research Con., 1979, p. 351-360.

7. Wong Y. S., Nee A. Y. C., Li X. Q. and Residorf C., Tool condition monitoring using laser scatter pattern, J. of Mat. Proc. Tech., 63, 1997, p 205-210.

8. Jeon J. U. and Kim W. Optical flank wear monitoring of cutting tools by image processing, Wear, Vol. 127, 1988, p 207-217.

9. Uehara K. New attempts for short time tool life testing, Ann. CIRP, Vol. 22, 1973, p 23-24.

10. Uehara K., Kumagai S., Mitsui H. and Takeyama H., Relationship between the size of wear particles and the mechanisms of tool wear in metal cutting, Ann. CIRP, Vol. 23, 1974, p 13-14.

11. Bath M. and Sharp R., In-process control of lathes improves accuracy and productivity, Proc. 9th Int. Mach. Tool Des. and Res. Conf., 1968, p 1209-1221.

12. Stoferle T. H. and Bellmann B., Continuous measuring of flank wear, Proc. 16th Int. Mach, Tool Des. and Res. Conf., 1975, p 573-578.

13. Danai K. and Ulsoy A. G., A dynamic state model for on-line tool wear estimation in turning, J. of Eng. for Industry, Vol. 109, 1987, p 396-399.

14. Akgerman N. and Frisch J., The use of cutting force spectrum for tool wear compensation during turning, Proc. 12th Int. Mach. Tool Des. and Res. Conf., 1971, p 517-526.

15. Filippi A. De. and Ippolito R., Adoptive control in turning: cutting forces and tool wear relationship for P10, P20, and P30 carbides, Ann. CIRP, Vol. 17, 1969, p 377-385.

16. Lindstrom B. and Lindberg B., Measurement of dynamic cutting forces in the cutting process, A new sensor for in-process measurement, Proc. 24th Int. Mach. Tool Des. and Res. Conf., 1983, p 137-147.

17. Kannatey-Asibu E. and Dornfeld D. A., A study of tool wear using statistical analysis of metal cutting acoustic emission, Wear, 76(1982)247-261.

18. Emel E. and Kannatey-Asibu E. Tool failure monitoring in turning by pattern recognition analysis of AE signals, J. of Eng. for Ind., Vol. 110, 1988, p 137-145.

19. Kamarthi S. V., Kumara S. R. T. and Cohen P. H., Flank wear estimation in turning through wavelet representation of acoustic emission signal, Trans. ASME., Vol. 122, February 2000, p 12-19.

20. Pandit S. M. and Kashou S., Variation in friction coefficient with tool wear, Wear, Vol. 84, 1983, p 65-79.

21. Weller E. J., Schrier H. M. and Weichbrodt B., What sound can be expected from a worn tool?, J. of Eng. for Ind., August 1969, p 525-534.

22. Zakaria A. A. and El Gomayel B. M., On the reliability of the cutting temperature for monitoring tool wear, Int. J. of Mach. Tool Des. Res., Vol. 15, 1975, p 195-208.

23. Solaja V. and Vukaija D., Identification of tool wear rate by temperature variation of carbide tip, Ann. of CIRP., Vol. 22, 1973, p 5-6.

24. Stephenson D. A., Tool-work thermocouple temperature measurements- Theory and implementation issues, Trans. ASME, Vol. 115, Nov. 1993, p 423-437.

25. Leshock C. E. and Shin Y. C., Investigation of on cutting temperature in turning by a tool-work thermocouple technique, Trans. ASME., Vol. 119, Nov 1997, p 502-508.

26. Liao Y. S., Development of a monitoring technique for tool change purpose in turning operations, Proc. 26th Int. Mach. Tool Des. and Res. Conf., 1974, p 251-257.

27. Venkatesh V. C. and Satchidanandam M., A discussion of tool life criteria and total failure causes, Ann. of CIRP, Vol. 29, 1980, p 19-22.

28. Das S., Roy R. and Chattopadhyay A. B., Evaluation of wear of turning carbide inserts using neural networks, Int. J. of Mach. Tools and Manufacture., Vol.-36, No. 7, 1996, p-789-797.

29. Yellowley I. and Lai C. T., Use of force ratios in the tracking of tool wear in turning, J. of Eng. for Ind., Vol. 115, August 1993, p 370-372.

30. Choudhury S. K. and Kishore K. K., Tool wear measurement in turning using force ratio, Int. J. of Mach. Tools & Manufacture, 2000, Vol.-40, PP 899-909.

31. Ravindra H. V., Srinivasa Y. G. and Krisnamurthy R., Modeling of tool wear based on cutting forces in turning, Wear 169(1993)25-32.

32. Park J. J. and Ulsoy A. G., On-line flank wear estimation using an adaptive observer and computer vision part 1: Theory, ASME J. of Eng. for Ind., Vol. 115, Feb. 1993, p 30-36.

33. Park J. J. and Ulsoy A. G., On-line flank wear estimation using an adaptive observer and computer vision part 2: Experiment, ASME J. of Eng. for Ind., 1993 Vol. 115, Feb, p 37-43.

34. Dimla D E Jr, Lister P M and Leightia, Neural network solution to the tool condition monitoring problem in metal cutting – A review of methods, Int. J. of Mach. Tools & Manufact., 1997, Vol.-34, No 4, p 591-601.

35. Tarng Y. S., Hseih Y. W. and Hwang S. T., Sensing tool breakage in face milling with a Neural network, Int. J. of Mach. Tools & Manufacture, 1994, Vol.-34, No 3, p 341-350.

36. Astakhov K. P. and Shvets S., The assessment of plastic deformation in metal cutting, J. of Mat. Proc. Tech., Vol. -146, no. -2, Feb. 2004, p 193-202.

37. Purushottaman S. and Srinivasa Y. G., A procedure for training an artificial neural network with application to tool wear monitoring, Int. J of Prod. Res., 1998, Vol.-36, No-3, p 635-651.

38. Kronenberg M., Machining science and application, Theory and practice for operation and development of machining process, Pergmon Press, 1966.

39. Oxely P. L. B. and Hasting S., Minimum work as a possible for determining friction conditions at tool/chip interface in machining, Phil. Trans. R. C., Lond., 1976, p 565-584.

40. Tresca H., Memoire surle rabtoge, des Metaux, Bulletin de La Societed, Encouragement pour 1' Industrie Nationale, 1873.

41. Coker E. G.and Chakko K. C., An account of some experiments on the action of cutting tools, Proc. Inst. of Mech. Eng., April, 1922, p 567-621.

42. Piispanen V., Theory of formation of Metal chips, , J of Appl. Phy.,Vol. 19, No. 10, , 1948, p 876-881.

43. Rosenberge A. M. and Eremin A. N., Elements of theory of process of metal cutting, Mashgiz, Moscow, 1956.

44. Kececioglu D., Shear strain rate in metal cutting and its effect on shear flow stress, Trans. ASME., Vol. 80, No. 1, Jan 1958, p 158.

45. Hill R., On the limits set by plastic yielding to the intensity of singularities of stress., J. of Mech. and Phy. of Solids., 2, 1954, p 278-285.

46. Chawla B. S., Biswas C. K., and Das N. S., An analysis of strain in chip breaking using slipline field theory with adhesion friction at chip/tool interface, In press.

47. Chandrasekaran H., Kapoor D.V., Photoelastic analysis of tool-chip interface stresses., J. of Eng. for Ind., 87 (11), 1965, p 495-502.

48. Bagchi A. and Write P. K., Stress analysis in machining with use of saphire tools, Proc. of Roy. Soc. London., A 409, 1987, p 99-113.

49. Kattwinkel W., *Untersuchungen an Schneiden Speanender Werkzeuge mit Hiflfe der spannungsoptic***,** *Industr. Anzeiger***,** 1957, 37, p 29-33.

50. Kato S. Yamaguchi K., Yanda M., Stress distribution at the interface between tool and chip in machining., ASME J. of Eng. for Ind., 94 (5), 1972, p 683-89.

51. Barrow G., Graham W., Kurimoto T. and Leong Y. F., Determination of rake face stress distribution in orthogonal machining, Int. J. of Mach. Tool Des. Res., Vol. 22, 1982, p 75-85.

52. Childs T.H.C., Mahdi M. I., On the stress distribution between the chip and tool during metal cutting., Ann. of CIRP, Vol. 38/1, 1989, p 55-58.

53. Buryta D, Sowerby R. and Yellowley I., Stress distribution on the rake face during orthogonal machining, Int. J. of Mach. Tools and Manufact., Vol. 34(5), 1994, p 721-739.

54. Lee L C, Liu X D and Lam K Y, Determination of stress distribution on the tool rake face using a composite tool, Int. J. of Mach. Tools & Manufact., Vol. 35, No. 3, 1995, p 373-382.

55. Ernst H, and Merchant M. E., Chip formation, friction and high quality machined surfaces, Trans. ASME, Vol. 29, 1941, p 229-378.

56. Lee E. H., Shaffer B. W., The theory of plasticity applied to a problem of machining, J. of App. Mech., 18, 1951, p 405-413.

57. Zorev N. N., Interrelationship between shear processes occurring along tool face and on shear plane in metal cutting., Proc. Conf. Int. Res. Prod. Eng., ASME, New York, 1963, p 42.

58. Kudo Hideaki., Some new slip-line solutions for two dimensional steady state, Int. J. of Mech. Sc., Vol. 7, 1965, p 43-55.

59. Burwell J. T. and Strang C. D., On the empirical laws of adhesive wear, J. of Appl. Phy., Vol. 23, 1952, p 18-28.

60. Chao B. T. and Trigger K. J., Controlled contact cutting, Tran. ASME, Series B, Vol. 81, 1959, p 139-151.

61. Bowden F. P. and Tabor D., The friction and lubrication of solids, Clarendon Press, Oxford, England, 1950.

62. Trent E. M., Metal cutting and tribology of seizure I – Seizure in metal cutting, Wear 128(1988) 29-45.

63. Trent E. M., Metal cutting and tribology of seizure II – Movement of work material over the tool in metal cutting, Wear 128(1988) 47-64.

64. Finnie I., Shaw M.C., Friction process in metal cutting, 1956, Tran. ASME 78 P- 1649-57.

65. Maekawa K., Kitagawa T., and Childs T.H.C., Friction characteristics at chip-tool interface in steel machining, 1997. 23rd Leeds Lyon Symposium in Tribology.

66. Kobayashi S. and Thomsen E. G., The role of friction in metal cutting, J. of Eng. for Ind., 1960, Vol. 82, p 324.

67. Wright P. K. and Tangaraj A., Correlation of tool wear mechanisms with new slip-line fields for cutting, Wear, 75(1982) 105-122.

68. Challen J. M. and Oxley P. L. B., An explanation of the different regimes of friction and wear using asperity deformation models, Wear, 1979, Vol. 53, p 229-243.

69. Vieregge G., Zerspannung der Eisenwerk Stoffe Stahl-Eiesen-Bucher,Band 16, Verlag,Stahlesian, Dusseldorf, 1959.

70. Usui E., Shirakashi T., On the art of cutting metals, ASME Pub. PED-7, 1982, p 13.

71. Merchant M. E., Mechanics of metal cutting II, Plasticity conditions in orthogonal cutting, J. of Appl. Phys., Vol. 16, 1945, p. 318-324.

72. Hill R., The mechanics of machining a new approach, J. Mech. Phys. Solids, 1954, Vol. 3, p 47-53.

73. Dewhurst P., On the non-uniqueness of machining process., 1978, Proc. of Roy. Soc. London , A360 p 587-610.

74. Ota T.,Shindo A. and Fukoaka H., An investigation of the theories of orthogonal machining, Tran. of Jap. Soc. Mech. Engineers., 1958, Vol. 24. p 484-493.

75. Low A. H., Effects of initial conditions in metal cutting, N E L Report no. 49, 1962.

76. Dewhurst P., The effects of chip breaker constraints on the mechanics of the machining process, Ann. CIRP 28(1), 1979, p 1-5.

77. Petryk H., On slip line solutions for steady-state and self-similar problems with stress free boundaries, Archs Mech., 1978, Vol. 31, p. 861

78. Childs T. H. C., *Elastic effects in metal cutting chip formation*, 1980, Int. J of Mech. Sc, 22 p 457-466.

79. Maity K.P. and Das N.S., A class of slip-line field solutions for metal machining with slipping and sticking contact at the chip-tool interface, 2001, Int. J of Mech. Sc., 43, p 2435-52.

80. Mackerle J., Finite-element analysis and simulation of machining: a bibliography (1976-1996), J. of Mat. Proc. Tech., 1999, Vol. 86, p17-44

81. McAdams H. T. and Rosenthal P., Forces on worn cutting tool, J. of Eng. for Ind., Vol. 83, 1961, p 505.

82. Thomsen E. G., McDonald A. G. and Kobayashi S., Flank friction studies with carbide tools reveal sub-layer plastic flow, J. of Eng. for Ind., Vol. 84, 1962, p 53.

83. Okashi M. and Sata T., Friction on the relief face of cutting tools, Scientific Papers, Inst. Phys. Chem. Research, Tokyo, Vol. 52(No. 1493), 1958, p. 216

84. Zorev N. N., Metal cutting mechanics, Paragamon Press, Oxford, 1966.

85. Shi T. and Ramlingam S., Slip-line solution for orthogonal cutting with a chip breaker and flank wear, Int. J. of Mech. Sc., Vol. 33, No. 9, 1991, p 689-704 .

86. Armarego E. J. A.and Brown, The metal cutting of metals, Prentice Hall, Englewood Cliffs, New Jersey, 1969.

87. Wang J., Huang C. Z. and Song W. G., The effect of tool flank wear on the orthogonal cutting process and it's practical implications, J. of Mat. Proc. Tech., Vol. 142, 2003, p338-346.

88. Maity K. P. and Das N. S., A class of slipline field solutions for metal machining with elastic contact, J. of Mat. Proc. Tech., Vol. 96, 1999, p 9-18.

89. Dewhurst P. and Collins I. F., A matrix methods for constructing slipline field solutions to a class of plain strain plasticity problems, Int. J. of Num. Meth. Eng., Vol. 7, 1973, p 357-378.

90. Venter R. D., Hewitt R. L. and Johnson W., An engineering approach to the matrix operator technique for slipline field construction,. North American Metal Working Research Conference VI, Florida USA, April 1978

91. Venter R. D., Hewitt R. L. and Johnson W., Application of matrix inversion technique to extrusion and drawing problems, ASME, Winter meeting, Dec 1978.

92. Dewhurst P., The Coulomb friction boundary value problem in plain-strain slipline field theory, Advanced Technology of Plasticity; II : 1984, p-1085-1090.

93. Dewhurst P., A general matrix operator for linear boundary value problems in slipline field theory, Int. J. for Numerical methods in Eng., Vol. 21, 1985, p 169-182.

94. Albrecht A. P., New developments in the theory of metal cutting process Part I-The ploughing process in metal cutting, ASME J. for Prod., Nov 1960, p 348.

95. Hill R., Mathematical Theory of plasticity, Oxford University Press, 1950.

96. Johnson W., Sowerby R. and Venter R. D., Book- Plain strain slipline fields for metal deformation processes, Pergamon Press, Oxford, 1982.

97. Johnson W., Sowerby R. and Haddow J. B.,Book- Plain strain slip line fields- Theory and Bibliography, Edward Arnold (Publishers) Ltd, London, 1986

98. Collins I. F., The algebraic-geometry of slipline fields with applications to boundary value problems, Proc. Roy. Soc., A 303, 1968, p 317-338

99. Ewing D. J. F., A series method for constructing plastic slipline fields, J. of Mech. Phys. Solids, Vol. 15, 1967, p 105.

100. Fang, N.; and Jawahir, I. S.; Analytical prediction and experimental validation of cutting force ratio, chip thickness and chip back flow angle in restricted contact machining using the universal slipline model, Int. J. of Mach. Tools & Manufacture., Vol. 42, 2002, p 681-694.

101. Fang, N.; Machining with tool-chip contact on the tool secondary rake face-Part I : a new slipline model. Int. J. of Mech. Sc., Vol. 44, 2002, p 2337-2354.

102. Fang, N.; Machining with tool-chip contact on the tool secondary rake face-Part II : analysis and discussion. , Int. J. of Mech. Sc., 44, 2002, p 2355-2368.

103. Fang, N.; Slipline model of machining with round edge tool Part I: New model and theory. J. Mech. Phys. and Solids, Vol. 51, 2003, p 715-742.

104. Powell, M. J. D.; A Fortran subroutine for solving systems of non-linear algebraic equations. 1970, In: Kuester, J. L; Mize, J. H.; Optimization techniques with FORTRAN. Mc-Graw Hill, New York , 1973.

105. Eggleston, D. M.; Herzog, R.; Thomsen, E. G.; Observations on the angle relationship in metal cutting. Tran. ASME., B-81, 1959, p 263-279.

106. Wanheim T., Friction at high normal pressures, Wear, 1973, 25, p 225-244

107. Diniz A. E., Liu I. I. and Dornfeld D. A., Correlating tool life, tool wear and surface roughness by monitoring acoustic emission in finish turning, Wear, 152 (1992) 495-407.

108. Youn J. W. and Yang M. Y., A study on the relationship between static/dynamic cutting force components and tool wear, Tran. ASME, J. of Manufact. Sc. Eng., Vol. 123, May 2001, p 196-204 .

109. Elanayar S. and Shin Y. C., Modeling of tool forces for warm tool: Flank wear effects, J. of Manufact. Sc. and Eng., Aug 1996, Vol. 118, p 359.

110. Manjunathaiah J. and Endes J., A new model and analysis of orthogonal machining with an edge radiused tool, J. of Manufact. Sc. and Eng, Aug 2000, Vol. 22, p 384-390.

111. Lee X. P. , Iyakaran K. and Nee A. Y. C., A hybrid machining simulator based on predictive machining theory and neural network modeling, , J. of Mat. Proc. Tech., Vol. 89, 1999, p 224-230.

112. Yen Y. C., Sohner J., Lilly B. and Alton T., Estimation of tool wear in orthogonal cutting using the finite element analysis, J. Mat. Proc. Tech., Vol. 146, No. 1, Feb. 2004, p 82-91.

113. Woldarf D. J., Dever R. E. and Kapoor S. G., Slip-line field for ploughing during orthogonal cutting, J. of Manufact. Sc. and Eng., Vol. 120-4, 1998, p 693-699.

114. Das N. S., and Dundur S. T., Slipline solutions for metal machining with adhesion friction and elastic effects at the chip-tool contact region, Proc. IMechE, J. of Eng. Manufact. Part B, Vol. 219 2005, p 57-72.

115. Chandrasekaran H. and Nagarajan R., Influence of flank wear on the stresses in a cutting tool, ASME J. of Eng. for Ind., Aug., 1977, p 566.

116. Woxen R. A., A theory and equation for tool life of lathe tools, IVA Hadlingar, Stockholm, 1932, p 119.

Appendix I

Determination of linear coefficient m_0 in the equation $\beta = m_0 \alpha$

Let σ_i and τ_i denote the normal stress and shear stress at any point i on the tool face QR with angular coordinates α_i and β_i (Fig. A1). Hence,

$$\frac{\sigma_i}{k} = p_R + 2(\alpha_i + \beta_i) + \sin 2(\phi_R + \alpha_i - \beta_i) \qquad \text{(A1)}$$

and

$$\frac{\tau_i}{k} = \cos 2(\phi_R + \alpha_i - \beta_i) \qquad \text{(A2)}$$

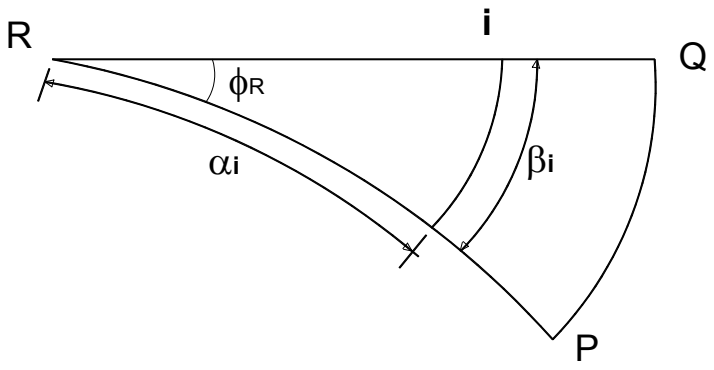

Fig. AI-1: Angular coordinates of any point on tool face

where, p_R and ϕ_R are respectively the hydrostatic pressure and friction angle at R. Substituting equations (A1) and (A2) in equation (1.5), we have,

$$\left[1 - e^{-\left(\mu\left(p_R + 2(\alpha_i + \beta_i) + \sin 2(\phi_R + \alpha_i - \beta_i)\right)\right)^{n_p}}\right]^{\frac{1}{n_p}} - \cos 2\left(\phi_R + \alpha_i - \beta_i\right) = 0 \qquad \text{(A3)}$$

For given values of μ and n_p equation (A3) may be solved numerically to determine the true value of β_i for any given value of α_i.

If the above non-linear relation between α_i and β_i is approximated by the linear relation [92,93]

$$\beta = m_0 \alpha$$

the error e_i between the true and approximate value may be expressed as

$$e_i = \beta_i - m_0 \alpha_i$$

when the calculation is carried out over n number of points on QR, the sum of the square of the errors is given as

$$\sum_{i=1}^{n} e_i^2 = \sum_{i=1}^{n} (\beta_i - m_0 \alpha_i)^2 \qquad \text{(A4)}$$

For best linear fit,

$$\frac{d \sum e_i^{\,2}}{dm_0} = 0$$

Hence,

$$m_0 = \frac{\sum_{i=1}^{n} \alpha_i^{\,2}}{\sum_{i=1}^{n} \beta_i \alpha_i} \qquad \text{(A5)}$$

At the origin R (Fig. A1), $\alpha_i = \beta_i = 0$ and equation (A3) reduces to

$$\left[1 - e^{-(\mu(p_R + \sin 2\phi_R))^{n_p}}\right]^{\frac{1}{n_p}} - \cos 2\phi_R = 0 \qquad \text{(A6)}$$

Equation (A6) is solved to determine ϕ_R for any given value of p_R.

The programme developed for determination of m_0 first evaluates ϕ_R by solution to equation (A6) by Newton-Rapson method. For ten known α_i values ($n = 10$) corresponding to ten discrete points on the slipline curve PR, the programme then

determine the corresponding β_i values by solution to equation (A3) and evaluates the linear coefficient m_0 using equation (A5).

-ooOoo-

Appendix II

Proof to show that the contact stresses and the aspect ratio for Lee and Shaffer's solution are independent of rake angle

Normal stress $\frac{\sigma_n}{k} = 1 + \sin 2\phi_R$

Shear stress $\frac{\tau}{k} = \cos 2\phi_R$

ϕ_R Calculated from equation (1.1) depends on μ and n_p only.

Hence, normal and shear stresses are independent of rake angle.

Considering triangle OQR we have

$$\frac{OQ}{\sin\left(\frac{\pi}{4} + \phi_R\right)} = \frac{RQ}{\sin\left(\frac{\pi}{4}\right)}$$

Hence, RQ = natural contact length $l_c = \left(\frac{OQ}{\cos\phi_R + \sin\phi_R}\right)$

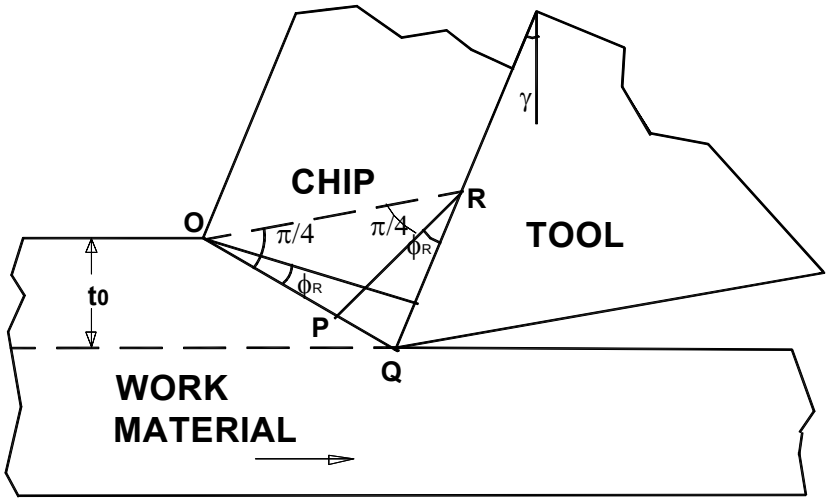

Fig. AII-1: Lee and Shaffer's solution

Chip thickness, $t_1 = OQ\cos\phi_R$

Aspect ratio, $\left(\frac{l_c}{t_1}\right) = \frac{1}{(\cos\phi_R(\cos\phi_R + \sin\phi_R))}$

Thus, aspect ratio is independent of rake angle

-ooOoo-

Appendix III

Derivation of relationship between α and ϕ_R for Field VIII

The figure shown in Fig. AIII-1 is that of the hodograph for Field VIII. The hodograph curve *pq* meets the tool face *qr* tangentially as corresponding slipline curve *PQ* meets the tool face *QR* orthogonally (Fig. 6.3 (a)). The curves *op* and *rp* are identical circular arcs of equal angular span α.

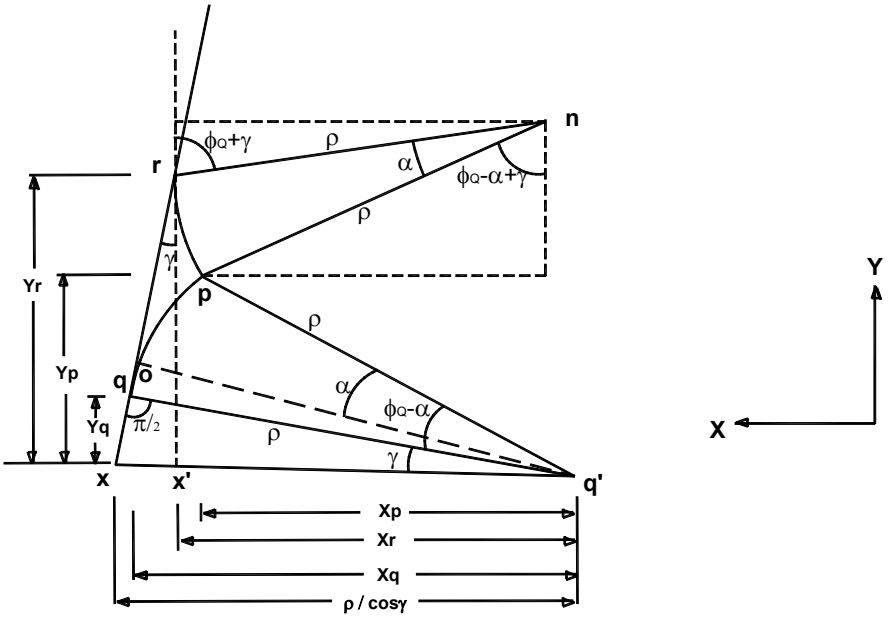

Fig. AIII-1; Hodograph for Field VIII.

With *q'* as origin, the coordinates of the points *q* , *p* , *n* and *r* in the above figure in the given coordinate system may be written as follows:

$$Xq = \rho\cos\gamma \qquad \text{(A-III (1a))}$$

$$Yq = \rho\sin\gamma \qquad \text{(A-III (1b))}$$

$$Xp = \rho\cos(\phi_R - \alpha + \gamma) \qquad \text{(A-III (2a))}$$

$$Yp = \rho\sin(\phi_R - \alpha + \gamma) \qquad \text{(A-III (2b))}$$

$$Xn = \rho\cos(\phi_R - \alpha + \gamma) - \rho\sin(\phi_R - \alpha + \gamma) \qquad \text{(A-III (3a))}$$

$$Yn = \rho\sin(\phi_R - \alpha + \gamma) + \rho\cos(\phi_R - \alpha + \gamma) \qquad \text{(A-III (3b))}$$

$$Xr = \rho\cos(\phi_R - \alpha + \gamma) - \rho\sin(\phi_R - \alpha + \gamma) + \rho\sin(\phi_R + \gamma) \qquad \text{(A-III (4a))}$$

$$Yr = \rho\sin(\phi_R - \alpha + \gamma) + \rho\cos(\phi_R - \alpha + \gamma) - \rho\cos(\phi_R + \gamma) \qquad \text{(A-III (4b))}$$

Referring to the right angled triangle *xrx'* we have

$$\frac{\sin\gamma}{\cos\gamma} = \frac{\dfrac{\rho}{\cos\gamma} - Xr}{Yr}$$

or $$Yr\sin\gamma = \rho - Xr\cos\gamma \qquad \text{(A-III (5))}$$

Substituting for *Xr* and *Yr* from equation (A-III (4)) in equation (A-III (5)) and simplifying we get

$$\cos\left(\phi_R - \alpha\right) - \sin\left(\phi_R - \alpha\right) + \sin\phi_R = 1 \qquad \text{(A-III (6))}$$

Equation (A-III (6)) may be solved to yield

$$\alpha = \frac{\pi}{4} + \phi_R - \cos^{-1}\left(\frac{1 - \sin\phi_R}{\sqrt{2}}\right) \qquad \text{(A-III (7))}$$

-ooOoo-

RESUME

Name	:	SURESH TOTAPPA DUNDUR
Designation	:	Q. I. P. Research Scholar Mechanical Engineering Department National Institute of Technology ROURKELA- 769 008 (India) Professor and Head Department of Industrial and Production Engineering Basaveshwar Engineering College BAGALKOT – 587 102 (India)
Academic qualifications	:	B. E. (Mech), Karnataka University Dharwad (India), 1984 M. Sc. (Engg), Sambalpur University, Jyoti Vihar, Burla (India), 1990

Papers Published:

1. Das N. S., and Dundur S. T., Slipline solutions for metal machining with adhesion friction and elastic effects at the chip-tool contact region, Proc. IMechE, J. of Eng. Manufact. Part B, Vol. 219 2005, p 57-72.

Papers communicated to International Journals:

1. Das N. S. and Dundur S. T., A slipline field analysis of free-chip orthogonal machining with adhesion friction at rake face.

2. Dundur S. T. and Das N. S., Slipline field modeling of orthogonal machining for a worn tool with elastic effects and adhesion friction at the contact regions

3. Dundur S. T. and Das N. S., Slipline field analysis of free-chip machining with a tool with flank wear.